

**STUDIES OF PULSE TIG WELDING PARAMETERS
ON MECHANICAL PROPERTIES OF DISSIMILAR
ALUMINUM ALLOYS AA6061 AND AA5083**

THESIS

**SUBMITTED TO DELHI TECHNOLOGICAL UNIVERSITY
FOR THE AWARD OF THE DEGREE OF
DOCTOR OF PHILOSOPHY
IN
MECHANICAL ENGINEERING**

By

PUSHP KUMAR BAGHEL



**DEPARTMENT OF MECHANICAL ENGINEERING
DELHI TECHNOLOGICAL UNIVERSITY
DELHI-110042 (INDIA)**

MARCH, 2018

**STUDIES OF PULSE TIG WELDING PARAMETERS
ON MECHANICAL PROPERTIES OF DISSIMILAR
ALUMINUM ALLOYS AA6061 AND AA5083**

By

PUSHP KUMAR BAGHEL

[Roll No. 2K11/Ph.D/ME/02]

**Submitted to Delhi Technological University in Partial
Fulfilments of the Requirement for the Degree of**

**DOCTOR OF PHILOSOPHY
IN
MECHANICAL ENGINEERING**



**DEPARTMENT OF MECHANICAL ENGINEERING
DELHI TECHNOLOGICAL UNIVERSITY
DELHI-110042 (INDIA)**

MARCH, 2018

© Delhi Technological University-2018
All rights reserved.



DELHI TECHNOLOGICAL UNIVERSITY, DELHI

DECLARATION

I hereby declare that the research work presented in this thesis entitled "**Studies of Pulse TIG Welding Parameters on Mechanical Properties of Dissimilar Aluminum Alloys AA6061 and AA5083**" is original and carried out by me under the supervision of Prof. D.S. Nagesh, Professor, Department of Mechanical Engineering, Delhi Technological University, Delhi, and being submitted for the award of Ph.D degree to Delhi Technological University, Delhi, India. The content of this thesis has not been submitted either in part or whole to any other university or institute for the award of any degree or diploma.

Pushp Kumar Baghel



DELHI TECHNOLOGICAL UNIVERSITY, DELHI

CERTIFICATE

This is to certify that the Ph.D. thesis entitled "**Studies of Pulse TIG Welding Parameters on Mechanical Properties of Dissimilar Aluminum Alloys AA6061 and AA5083**" being submitted by Mr. PUSHP KUMAR BAGHEL for the award of the degree of Doctor of Philosophy in Mechanical Engineering, to Delhi Technological University, Delhi, India, is a bonafide record of original research work carried out by him under my guidance and supervision. The work presented in this thesis has not been submitted to any other university or institution for the award of any degree or diploma.

Prof. D. S. NAGESH

Professor,
Department of Mechanical Engineering,
Delhi Technological University,
Delhi

Prof. R.S. MISHRA

Professor and DRC Chairman
Department of Mechanical Engineering
Delhi Technological University,
Delhi

Dedicated
To
My Parents

ACKNOWLEDGEMENTS

The work presented here would not have been possible without the help of many talented and learned people.

First and foremost I would like to thank my supervisor Prof. D.S. Nagesh, Professor, Delhi Technological University, Delhi, for extending his full support and encouragement. I deeply value invaluable suggestions and creative freedom, he provided to me. I also greatly benefitted from his experience and skills which he shared with me with utmost generosity. I highly appreciate the personal attention and interest which he showed towards my research work. I had the privilege to learn from him not just lessons of engineering but of life. I am thankful to the supervisor to help me to get access to all the necessary facilities in DTU including welding laboratory.

I wish to acknowledge the help and support from Prof. Reeta Wattal, which I received throughout the research work.

I express my gratitude to Prof. Vipin, Professor and Head for his constant encouragement.

I am thankful to my SRC committee members, Prof P.M Pandey, IIT Delhi, Prof Samsher, Prof. Uma Nangia, Delhi Technological University for their valuable suggestions. I also acknowledge the suggestions that I received from Prof Sunil Pandey, Professor, IIT Delhi for performing experiments.

I am also indebted to Prof. Sachin Maheswari, Professor, Department of MPAAE, Netaji Subhas Institute of Technology, Delhi for help and support provided during testing.

I am also thankful to Prof P.K Ghosh, Professor, IIT Roorkee for providing valuable suggestions in research work.

I would also like to thank Mr N.Yuvaraj, Mr Pravin Kumar Assistant Professor, Delhi Technological University, for his suggestion and support throughout the research work.

I sincerely thanks my lab mates and friends for their cooperation. I also thank the technical staff of welding laboratory, Mr. Vinay, Mr Ajay and Mr Tek Chand for all the help received during experimentation.

I would like to thank Mr Jitender Saraha, CEO, Ardent Engineers and Mr Raju, welder for the helping me in setup development.

I am deeply thankful to my family for their appreciation, patience and tolerance. The encouragement I received from my father and mother laid the foundation of this Ph.D thesis. I express special thanks to my sister Dr. Sarita Baghel, my brothers Utkarsh Baghel, Mayank and Dr. Shiv Kumar for their valuable assistance and suggestions during research work. I also exclusively thank my maternal uncle Mr. Omkar singh, for helping in setup.

Pushp Kumar Baghel

ABSTRACT

Aluminum is considered as most abundant metal in the earth crust and is third most common element which comprises of 8 % of earth crust. The consumption of aluminum is around 47.7 billion tonnes which is 40% of the total reserves of metal world wide. The global consumption of aluminum is expected to rise 6% in 2018. Due to increasing application of aluminum in industrial world. The demand for its welding not only similar alloys but dissimilar alloys increases. Welding of dissimilar aluminum poses several challenges to the designer and technologists as they are prone to hot cracking and porosity. These problems can be overcome using controlled heat input which is provided by Pulse TIG (Tungsten Inert Gas) welding. Due to pin point control of heat input, it is most commonly used process for welding aluminum alloys.

In this study an attempt has been made to weld dissimilar aluminum alloys AA5083-O and AA6061-T651. Weld was carried out on 6.35 mm plates and butt joint was successfully produced between two plates of length 150 mm using pulse TIG welding. A setup was prepared which automatically moves the welding torch and wire feed. The cost associated with the development of setup was very low around 300 USD as compared to the setup available in the market which is 1000 USD. The two special fixtures were designed and fabricated for holding the MIG wire feeder gun and for holding welding plates firmly together during welding.

Integrated Analytical Hierarchy process and Technique for order preference by similarity to ideal solution (AHP-TOPSIS) approach was used to select the best possible combination of filler alloy, electrode and shielding gas from available

alternates. The Extensive trails runs were conducted to develop the correct welding procedure for obtaining defect- free joints. The process parameters that can be varied and can have an effect on mechanical properties of the weld were identified. The range, within which those process parameters can be varied, were also found. Based on the central composited design, final experimentation was carried out to study the effect of process parameters on mechanical properties. 32 runs were conducted. Radiography was conducted and then samples for mechanical and metallurgical testing were taken out. Tensile test, impact test and micro-hardness were carried out to see the effect of process parameters on weld properties. Metallurgical testing was carried out using microstructural examination, energy dispersive X-ray spectroscopy analysis and corrosion studies.

The tensile strength, impact toughness and micro-hardness were all found to have improved over base material properties. The process parameters, particularly welding speed, was found to have significant effect on mechanical properties. Based on microstructural examination, significant grain refining is noticed in fusion zone which consist of soluble phase of Mg_2Si particles. The result of immersion test shows no crack initiation sites developed.

LIST OF PUBLICATIONS

Published Papers

- I. Baghel P K., Nagesh D S., ‘’Pulse TIG welding: Process, Automation and Control’’. Journal of Welding and Joining. 2017; 35(1): 43-48. <https://doi.org/10.5781/JWJ.2017.35.1.43>
- II. Baghel P K., Nagesh D S., ‘’ Multiattribute Assessment of Consumables for TIG Welding of Aluminum Alloys’’. International Journal of Manufacturing Engineering, 2016; Article ID 7291898, 9 pages. <http://dx.doi.org/10.1155/2016/7291898>

Paper Accepted

- I. Baghel P K., Nagesh D S., ‘’ Influencing and Analysis of TIG Welding Process on Mechanical Properties of Extruded Aluminum Parts’’ Transaction of Canadian Society of Mechanical Engineering.’’ 2017.
- II. Baghel P K., Nagesh D S., ‘’Some studies on mechanical properties and microstructural characterization of automated pulse TIG welding of dissimilar aluminum alloy’’. Indian Journal of Engineering and Material Science. 2017

TABLE OF CONTENTS

	<i>Page No.</i>
List of Figures	i
List of Tables	v
List of Abbreviations	vii
CHAPTER- 1 INTRODUCTION	1-26
1.1. Introduction to Aluminum Alloys	1
1.2. Classification of Aluminum Alloys	2
1.2.1 Wrought Alloy Designation System	2
1.2.2 Temper Designation System	3
1.3 Welding of Various Types of Aluminum Alloys	4
1.3.1 Welding of 1 xxx series	4
1.3.2 Welding of 2xxx series	4
1.3.3 Welding of 3xxx series	4
1.3.4 Welding of 4xxx series	5
1.3.5 Welding of 5xxx series	5
1.3.6 Welding of 6xxx series	5
1.3.7 Welding of 7xxx series	5
1.4 Aluminum Alloys chosen for this Investigation	6
1.4.1 Aluminum Alloy 5083-O	6
1.4.1.1 Applications of 5083-O	6
1.4.2 Aluminum Alloy 6061-T651	8
1.4.2.1 Applications of 6061-T651	8
1.5 Need for Welding of Different Grades of Aluminum Alloys	10
1.6 Application of Dissimilar Aluminum Alloy Joints of 5xxx and 6xxx series	11
1.6.1 Applications of Dissimilar Aluminum Alloy joint of 5083-O and 6061-T651	13
1.7 Challenges Associated with Welding of 5083-O and 6061-T651 Dissimilar Aluminum Alloy	14
1.8 Problems Related to Welding of 5083-O and 6061-T651 Aluminum Alloys	14
1.9 Uniqueness of Pulse TIG Welding	18

1.10	Introduction to Tungsten Inert Gas (TIG) Welding Process	18
1.10.1	Process Principle	19
1.10.2	TIG Welding Equipment	20
1.10.3	Advantages of TIG Welding Process	22
1.10.4	Disadvantages of TIG Welding Process	22
1.10.5	Applications of TIG Welding Process	23
1.11	Pulse TIG Welding Process	23
1.11.1	Advantages of Pulse TIG Welding Process	23
1.12	Motivation to Weld Dissimilar Aluminum Alloys	24
1.13	Organization of Thesis	24
CHAPTER-2:	LITERATURE REVIEW	27-53
2.1	Introduction	27
2.2	Studies on TIG Welding	28
2.2.1	TIG Welding of Different Metals other than Aluminum	28
2.2.2	TIG Welding of Aluminum Alloys	36
2.2.3	TIG Welding of Dissimilar Aluminum Alloys	43
2.3	Application of Design of Experiments in Welding	45
2.3.1	Factorial Design	45
2.3.2	Response Surface Methodology	47
2.4	Gaps in Research Work	51
2.5	Research Objectives	52
2.6	Benefits of Research	53
CHAPTER-3:	DEVELOPMENT OF EXPERIMENTAL SET-UP	54-63
3.1	Introduction	54
3.2	Problems Associated with Manual TIG Welding	54
3.3	Necessity for Automation in Pulse TIG Welding	55
3.4	Advantages of Automation in Pulse TIG Welding	55
3.5	Automation in Pulse TIG Welding Machine	55
3.5.1	Automatic Torch Movement	57
3.5.2	Custom Built Wire Feed System	57
3.6	Design and Fabrication of Fixture	59
3.7	Design and Fabrication of Welding Torch Holder	61

CHAPTER – 4: SELECTION OF WELDING CONSUMABLE USING MULTI- ATTRIBUTE DECISION MAKING APPROACH (MADM)	64-95
4.1 Introduction	64
4.2 Methodology Adopted	66
4.3 Filler Alloy	75
4.4 Electrode	80
4.5 Shielding Gas	84
4.6 Result	87
4.6.1 Computational Results for Selection of Filler Alloy	88
4.6.2 Computational Results for Electrode	90
4.6.3 Computational Results for Shielding Gas	92
4.6.4 Analysis of Ranking Results	94
CHAPTER – 5: METHODOLOGY AND EXPERIMENTATION	96-139
5.1 Introduction	96
5.2 Base Metal Grade Selection	97
5.3 Welding Machine	98
5.4 Process Parameters of Pulse TIG Welding which are Affecting the Mechanical Properties of Weld	99
5.5 Design of Experiment (DOE)-An Overview	100
5.5.1 Types of DOE	101
5.5.1.1 One Factor Design	101
5.5.1.2 Factorial Design	101
5.5.1.3 Response Surface Design	103
5.6 Selection of Design	104
5.7 Identifying the Important Process Parameters	105
5.8 Experimentation	105
5.8.1 Experimental Trails and Determination of Working Limits of Parameters	105
5.8.2 The Design of Experiments Matrix	109
5.8.3 Conducting the Experiments	111
5.9 Non-Destructive Testing of Weld	111
5.9.1 Visual Examination of the Weld	112
5.9.2 X-Ray Radiography of the Welds	113

5.10 Mechanical Testing of Welds	113
5.10.1 Tensile Testing of Welds	114
5.10.1.1 Transverse Tensile Testing of Weldments	114
5.10.1.2 Analysis of Tensile Testing	117
5.10.2 Micro-hardness Test	117
5.10.2.1 Vickers Micro-hardness Test	118
5.10.2.2 Analysis of Micro-hardness Test	120
5.10.3 Impact Testing of Welds	121
5.10.3.1 Charpy Impact Test	121
5.10.3.2 Analysis of Charpy Impact Test	123
5.10.4 Fractography of Fractured Surface of Impact Test Specimen	123
5.10.4.1 Analysis of Fractography	124
5.11 Recording of responses	126
5.12 Development of Mathematical Model	127
5.12.1 Checking the Adequacy of Developed Model	129
5.12.2 Comparison of Predicted and Experimentally Determined Mechanical Properties	132
5.12.3 Conformity of Test to Declare Validity of Mathematical Models	135
5.12.4 Residual Plots	135
CHAPTER- 6: RESULT AND DISCUSSION	140-178
6.1 Introduction	140
6.2 Tensile Strength	140
6.2.1 Effect of Peak Current on Tensile Strength	140
6.2.2 Effect of Base Current on Tensile Strength	141
6.2.3 Effect of Pulse Frequency on Tensile Strength	142
6.2.4 Effect of Pulse On Time on Tensile Strength	143
6.2.5 Effect of Welding Speed on Tensile Strength	144
6.2.6 Effect of Interactions of Parameters on Tensile Strength	145
6.3 Yield Strength	147
6.3.1 Effect of Peak Current on Yield Strength	147
6.3.2 Effect of Base Current on Yield Strength	148

6.3.3	Effect of Pulse Frequency on Yield Strength	149
6.3.4	Effect of Pulse On Time on Yield Strength	150
6.3.5	Effect of Welding Speed on Yield Strength	151
6.3.6	Effect of Interactions of Parameters on Yield Strength	152
6.4	Percent Elongation	154
6.4.1	Effect of Peak Current on Percent Elongation	154
6.4.2	Effect of Base Current on Percent Elongation	155
6.4.3	Effect of Pulse Frequency on Percent Elongation	156
6.4.4	Effect of Pulse On Time on Percent Elongation	157
6.4.5	Effect of Welding Speed on Percent Elongation	158
6.4.6	Effect of Interactions of Parameters on Percent Elongation	159
6.5	Micro-hardness	162
6.5.1	Effect of Peak Current on Micro-hardness	162
6.5.2	Effect of Base Current on Micro-hardness	162
6.5.3	Effect of Pulse Frequency on Micro-hardness	163
6.5.4	Effect of Pulse On Time on Micro-hardness	164
6.5.5	Effect of Welding Speed on Micro-hardness	165
6.5.6	Effect of Interactions of Parameters on Micro-hardness	166
6.6	Impact Toughness	168
6.6.1	Effect of Peak Current on Micro-hardness	168
6.6.2	Effect of Base Current on Impact Toughness	169
6.6.3	Effect of Pulse Frequency on Impact toughness	170
6.6.4	Effect of Pulse On Time on Impact Toughness	171
6.6.5	Effect of Welding Speed on Impact Toughness	172
6.6.6	Effect of Interactions of Parameters on Impact Toughness	173
6.7	Summary	175
6.7.1	Effect of Parameters on Mechanical Properties of Weld	175
6.7.2	Interaction Effect of Parameters on Mechanical Properties of Weld	177

CHAPTER- 7: METALLURGICAL TESTING OF WELDS **179-188**

7.1	Introduction	179
7.2	Energy Dispersive X-Ray Spectroscopy (EDS) Analysis	179

7.3	Microstructural Examination of Weld	180
7.3.1	Procedure of Microstructural Examination	181
7.4	Analysis of Microstructure and its Evolution	181
7.4.1	Microstructure of Base Metal	182
7.4.1.1	Microstructure of Base Metal 5083-O	183
7.4.1.2	Microstructure of Base Metal 6061-T651	183
7.4.2	Microstructure of Fusion Zone	184
7.4.3	Microstructure of Heat Affected Zone	185
7.4.3.1	Microstructure of Heat Affected Zone on 5083-O side	185
7.4.3.2	Microstructure of Heat Affected Zone on 6061-T651side	186
7.5	Immersion Test for Resistance to Pitting Corrosion	187
7.5.1	Procedure of Immersion Test	187
7.5.2	Result of Immersion Test	188
CHAPTER- 8: CONCLUSION AND SCOPE FOR FUTURE WORK		189-191
8.1	Conclusion	189
8.2	Scope for Future Work	191
REFERENCES		192-209

LIST OF FIGURES

<i>Figure No.</i>	<i>Title</i>	<i>Page No.</i>
1.1	Temper Designation System	3
1.2	Examples of usage of AA 5083 in various applications	7
1.3	Application of AA66061 in Industry	9
1.4	Engine Valve	11
1.5	Dissimilar Aluminum Alloy Wheel	11
1.6	BMW body frame	12
1.7	Audi A8 Body Structure	12
1.8	Jaguar XJ 2010 Model	13
1.9	Application of Dissimilar Aluminum Alloy AA5083-O and AA6061-T651 in Industry	13
1.10	Hydrogen Solubility in Aluminum	15
1.11	Cracking Sensitivity in 5xxx and 6xxx series Aluminum Alloys	16
1.12	Al-Mg Phase Diagram	16
1.13	Tube Breaking Under Stress Corrosion Cracking	17
1.14	TIG Welding Set-Up	19
1.15	DCEP Polarity	20
1.16	Torch Parts	21
3.1	Automatic TIG Set-Up	56
3.2	Air Cooled Torch	57
3.3	Torch Mounted on Trolley Moving on Dedicated Track	57
3.4	Custom Build Wire Feed System	58
3.5	Circuit Diagram of Custom Built Wire Feeder and Custom Build Wire Feeder for Pulse TIG Welding	58
3.6	Dimensional Drawing of Fixture	59
3.7	Fabricated Fixture	61
3.8	Dimensional Drawing of Welding Torch Holder	62
3.9	Fabricated Welding Torch Holder	63
4.1	TOPSIS Method	71
4.2	Flow Chart Depicting Integrated AHP-TOPSIS Methodology for Material Selection	74
4.3	Hierarchical Structure for Suitable Filler Selection	79
4.4	Hierarchical Structure for Electrode Selection	83

4.5	Hierarchical Structure for Selection of Shielding Gas	87
4.6	Histogram Depicting Ranking of Alternates of Filler	89
4.7	Pie-chart Depicting Ranking Percentage of Alternates of Filler Alloy	89
4.8	Histogram Depicting Ranking of Alternates of Electrode	91
4.9	Pie-chart Depicting Ranking Percentage of Alternates of Electrode	91
4.10	Histogram Depicting Ranking of Alternates of Shielding Gas	93
4.11	Pie-chart Depicting Percentage Ranking of Alternates of Shielding Gas	93
4.12	Plots for Best Consumable Material Selection	95
5.1	TRITON 220 AC/DC (Pulse TIG Welding Machine)	98
5.2	Current-Time Diagram during Pulse TIG Welding	99
5.3	Welded Plate	112
5.4	Radiography of Weld Joint 5083-O + 6061-T651	113
5.5	Universal Tensile Testing Machine	115
5.6	Drawing of Tensile Test Specimen according to ASTM E8 M04	116
5.7	Tensile Test Specimen as per Drawing	116
5.8	Fractured Tensile Specimen	116
5.9	Tensile Tested Specimens Showing Location of Fracture	116
5.10	Micro-hardness Tester Machine	119
5.11	Weldment Region of FZ and HAZ	119
5.12	Micro-hardness Profile	120
5.13	Impact Testing Machine	122
5.14	Drawing of Charpy Impact Test Specimen according to ASTM E23	122
5.15	Impact Test Specimen	123
5.16	Fractured Impact Test Specimen	123
5.17	SEM set up	124
5.18	SEM Fractography of Impact Test Samples a) TIG joint at 200µm b) TIG joint at 100µm c), d) TIG joint at 50µm.	125
5.19	SEM Fractographs of Failure Surface of Impact Specimens at a) 200µm b) 100µm c) 50µm.	125
5.20	Scatter Diagram for Responses a) Tensile Strength b) Micro-hardness c) Yield Strength d) Percent Elongation e) Impact Toughness	134

5.21	Plots for Checking Validity of a) Tensile Strength b) Yield Strength c) Percent Elongation d) Micro-hardness e) Impact Toughness	138
6.1	Effect of Peak Current on Tensile Strength	141
6.2	Effect of Base Current on Tensile Strength	142
6.3	Effect of Pulse Frequency on Tensile Strength	143
6.4	Effect of Pulse On Time on Tensile Strength	144
6.5	Effect of Welding Speed on Tensile Strength	145
6.6	Interaction Effect of Parameters on Tensile Strength i) P-B, ii) P-F, iii) P-T, iv) P-S, v) B-F, vi) B-T, vii) B-S, viii) F-T, ix) F-S, x) T-S	147
6.7	Effect of Peak Current on Yield Strength	148
6.8	Effect of Base Current on Yield Strength	149
6.9	Effect of Pulse Frequency on Yield Strength	150
6.10	Effect of Pulse On Time on Yield Strength	151
6.11	Effect of Welding Speed on Yield Strength	152
6.12	Interaction Effect of Parameters on Yield Strength i) P-B, ii) P-F, iii) P-T, iv) P-S, v) B-F, vi) B-T, vii) B-S, viii) F-T, ix) F-S, x) T-S	154
6.13	Effect of Peak Current on Percent Elongation	155
6.14	Effect of Base Current on Percent Elongation	156
6.15	Effect of Pulse Frequency on Percent Elongation	157
6.16	Effect of Pulse On Time on Percent Elongation	158
6.17	Effect of Welding Speed on Percent Elongation	159
6.18	Interaction Effect of Parameters on Percent Elongation i) P-B, ii) P-F, iii) P-T, iv) P-S, v) B-F, vi) B-T, vii) B-S, viii) F-T, ix) F-S, x) T-S	161
6.19	Effect of Peak Current on Micro-hardness	162
6.20	Effect of Base Current on Micro-hardness	163
6.21	Effect of Pulse Frequency on Micro-hardness	164
6.22	Effect of Pulse On Time on Micro-hardness	165
6.23	Effect of Welding Speed on Micro-hardness	166
6.24	Interactions Effects of Parameters on Micro-hardness i) P-B, ii) P-F, iii) P-T, iv) P-S, v) B-F, vi) B-T, vii) B-S, viii) F-T, ix) F-S, x) T-S	168
6.25	Effect of Peak Current on Impact Toughness	169
6.26	Effect of Base Current on Impact Toughness	170
6.27	Effect of Pulse Frequency on Impact Toughness	171

6.28	Effect of Pulse On Time on Impact Toughness	172
6.29	Effect of Welding Speed on Impact Toughness	173
6.30	Interaction Effect of Parameters on Impact Toughness, i) P-B, ii) P-F, iii) P-T, iv) P-S, v) B-F, vi) B-T, vii) B-S, viii) F-T, ix) F-S, x) T-S	175
7.1	EDS Analysis at Three Regions a) Regions adjacent to HAZ on AA6061 side, b) Regions adjacent to HAZ on AA5083 side, c) Fusion Zone	180
7.2	Optical Microscope	181
7.3	Sample after Polishing and Etching	182
7.4	Microstructure of AA5083-O at 200X	183
7.5	Microstructure of AA6061-T651 at 200X	183
7.6	Microstructure of Fusion Zone at 200X	184
7.7	Microstructure of HAZ at 5083-O side at 200X	185
7.8	Microstructure of HAZ at 6061-T651 side at 200X	186
7.9	Samples of Immersion Test before and after Test of Pitting Corrosion	188

LIST OF TABLES

<i>Table No.</i>	<i>Title</i>	<i>Page No</i>
4.1	Nine Point Intensity of Importance Scale	67
4.2	Random Index (RI) Values	69
4.3	List of Attributes for Selection of Filler Alloy	78
4.4	Welding Filler Alloy Identified for Joining Dissimilar Aluminum Alloy 5083-O and 6061-T651	79
4.5	List of Attributes for Electrode Selection	82
4.6	Electrode for Pulse TIG Welding of Dissimilar Aluminum Alloys 5083-O And 6061-T651	83
4.7	List of Attributes for Selection of Shielding Gas	86
4.8	Shielding Gas Alternates used for Pulse TIG Welding of 5083-O And 6061-T651 Aluminum Alloy	86
4.9	Consumable Material Weights	87
4.10	Alternates of Filler Alloy and their Properties	88
4.11	Alternates of Electrode and their Properties	90
4.12	Alternates of Shielding Gas and their Properties	92
4.13	Ranks Based on C Values	94
5.1	Chemical Composition (wt %) of Base Metal and Filler Metal	97
5.2	Mechanical Properties of Base Metal and Filler Metal	97
5.3	Physical Properties of Base Metal and Filler Metal	98
5.4	Trail Runs	106
5.5	Welding Parameters and their Upper and Lower Limits	108
5.6	Welding Parameters and their Levels	109
5.7	The Design Matrix	110
5.8	Constant Parameters	111
5.9	Design Matrix and Measured Response Values	126
5.10	Calculated Value of Coefficients for Five Responses	128
5.11	ANOVA Results for Testing Adequacy of Tensile Strength Model	130
5.12	ANOVA Results for Testing Adequacy of the Yield Strength Model	130

5.13	ANOVA Results for Testing Adequacy of the Percent Elongation Model	131
5.14	ANOVA Results for Testing Adequacy of the Micro-hardness Model	131
5.15	ANOVA Results for Testing Adequacy of the Impact Toughness Model	131
5.16	Comparison of R^2 , $R^2_{(adj)}$, $R^2_{(pred)}$ Values	132
5.17	Predicted and Experimentally Determined Mechanical Properties	133
5.18	Results of Conformity Test	135
7.1	Immersion Test for Testing Corrosion Resistance of Aluminum Alloy 5083-O and 6061-T651 Joint	187

S.No	Description of Abbreviation	
1.	Tungsten Inert Gas	TIG
2.	Direct Current Electrode Positive	DCEP
3.	Direct Current Electrode Negative	DCEN
4.	Megapascals	MPa
5.	US Dollar	USD
6.	Volts	V
7.	Ampere	A
8.	Hertz	Hz
9.	Degree Fahrenhiet	°F
10.	Degree Celcius	°C
11.	Electron Volt	eV
12.	Millimetre per minute	mm/min
13.	Alternating Current	AC
14.	American Society of Mechanical Engineers	ASME
15.	American Society of Testing Materials	ASTM
16.	Scanning Electron Microscope	SEM
17.	Energy Dispersive X-Ray Spectroscopy	EDS

Chapter 1
Introduction

INTRODUCTION

1.1 Introduction to Aluminum Alloys

Aluminum is considered as most abundant metal in the earth crust and is third most common element which comprises of 8 % of earth crust. It is normally found in oxide forms (Al_2O_3), i.e. bauxite, kaolinite, nephline and alunite. Aluminum and its alloys play a crucial and critical role in engineering material field. The ease of fabricability, excellent corrosion resistance and high strength combined with excellent combination of toughness and formability makes it suitable for widespread industrial application [1]. Due to the property of high strength to weight ratio it has found application in not only in aerospace industries but also in automobile industries. Some other applications are:

- Electrical conductors
- Transport
- Packaging
- Building and Architecture
- High Pressure Gas Cylinders
- Machined Components
- Ladders and Access Equipment
- Sporting Equipment
- Road Barriers and Signs
- Domestic and Office Furniture
- Lithographic Plates
- Marine Applications [1]

1.2 Classification of Aluminum Alloys

There are two principal classifications of aluminum alloys which are casting alloys and wrought alloys. About 85% of aluminum is used for wrought products as they have higher melting point and tensile properties than cast alloys. Wrought alloys are subdivided into two categories heat-treatable and non-heat treatable.

- Heat-treatable: They are those alloys which can be heated after welding to regain strength lost during welding process. Heat-treatable aluminum alloys develop their properties by solution heat treating and quenching followed by either natural aging or artificial aging. The heat-treatable alloys may also be annealed to attain maximum ductility.
- Non heat-treatable: The initial strength of these alloys depends primarily upon hardening effects of alloying elements such as silicon, copper, zinc, magnesium and manganese. These elements increase the strength either as dispersed phase or solid solution phase.

1.2.1 Wrought Alloy Designation system

Based on the composition of typical alloying elements like copper, magnesium, manganese, silicon, tin and zinc they are designated as:

- 1xxx –Pure Al (99% or greater)
- 2xxx- Al-Cu alloys
- 3xxx- Al-Mn alloys
- 4xxx- Al-Si alloys
- 5xxx- Al-Mg alloys

- 6xxx- Al-Mg-Si alloys
- 7xxx- Al-Zn alloys
- 8xxx- Al + Other Elements

First digit represents the principal alloying elements. Second digit represents variation of initial alloy. Third and fourth digit represents individual alloy variation. 1xxx, 3xxx, 4xxx, and 5xxx series are considered non-heat treatable alloys. 2xxx, 6xxx, 7xxx, 8xxx are considered heat treatable alloys.

1.2.2 Temper Designation system

The temper designation system is illustrated in figure 1.1

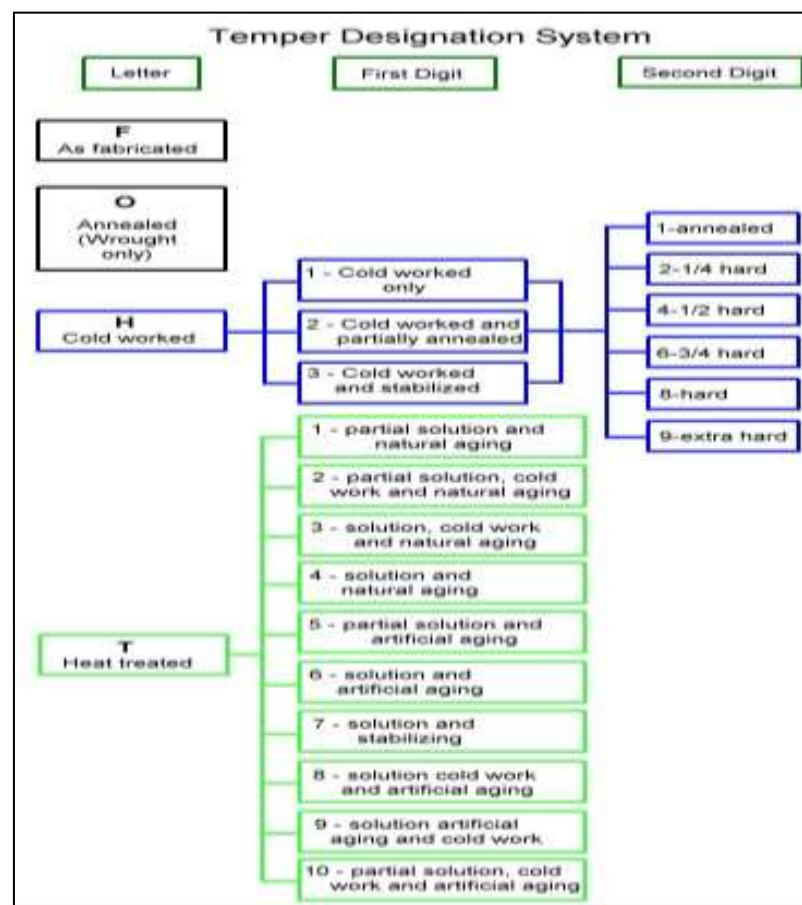


Figure 1.1: Temper Designation System[1]

1.3 Welding of Various Types of Aluminum Alloys

The various types of welding process used for joining aluminum alloys are Tungsten Inert Gas (TIG) Welding, Metal Inert Gas (MIG) Welding, Electron Beam Welding, Laser Beam Welding etc. MIG welding is used for joining thick sections and TIG welding is used for joining thin sections. For the welding of aluminum alloys the heat input plays a vital role. Therefore, care should be taken in the selection of suitable welding process parameters to get high quality welded joints. The improper weld process parameter selection may lead to major problems in welding of aluminum alloys [3].

1.3.1 Welding of 1xxx series

The 1-series alloys are generally considered as soft alloys and it is widely used in electrical and chemical applications. It is available as tubes, pipes, rod and wire form. This alloy consists of 99% aluminum and rest 1% is other metal. 0.12 % is the copper percentage which may be added to this metal. This alloy has low mechanical property, good workability, very good corrosion resistance and good electrical conductivity [3].

1.3.2 Welding of 2xxx series

This alloy consists of copper as major alloying element and it is heat-treated alloy used for specific applications. These alloys are very difficult to weld using arc welding process because they are very sensitive to hot cracking. Therefore, the welding of these alloys using arc welding process can be done by selecting correct filler material and proper weld process parameters [3].

1.3.3 Welding of 3xxx series

The 3 series alloys are also categorized as soft alloys. It may be available as sheet, plate, pipe and tube form. In this alloy manganese is the primary alloying element but copper or magnesium are also included often. This alloy has higher strength, excellent workability and fairly corrosion resistant [3].

1.3.4 Welding of 4xxx series

This alloy consists of silicon as major alloying element and it is available as heat treatable & non-heat treatable alloy and it is widely used as filler materials. These alloys are very much used as filler material for joining various series of aluminum alloys and care must be taken while welding of these alloys with other series alloys because they are very sensitive to crack formation [3].

1.3.5 Welding of 5xxx series

This alloy consists of magnesium as major alloying element and it possesses higher mechanical properties when compared to other non-heat treatable aluminum alloys. Hence, these alloys are widely used for structural applications. These alloys are also very crack sensitive to welding. Therefore, proper filler material and weld process parameters should be selected for the welding of these alloys [2, 3].

1.3.6 Welding of 6xxx series

This alloy consists of magnesium and silicon as major alloying elements and it is a heat treatable alloy. These alloys cannot be arc welded successfully without the filler material. Therefore, while welding these alloys with 4xxx series and 5xxx series alloys, proper consideration should be given for the selection of suitable filler material which reduces the weld metal crack sensitivity by diluting the percentage of Mg_2Si present in the base material [2, 3].

1.3.7 Welding of 7xxx series

This alloy consists of zinc, magnesium and copper as major alloying elements. These alloys are unsuitable for arc welding because of hot crack formation. The hot cracking is formed in the 7-series aluminum alloys due to the thermal stresses present during the welding and various degrees of solidification [3].

1.4 Aluminum Alloys Chosen for this Investigation

Since 5xxx and 6xxx series aluminum alloys like 5083 and 6061 are widely used in structural applications because of their higher mechanical properties. They are chosen in this investigation. The other considerations which were taken into account while selecting these two grades of aluminum alloys are:

- Properties of material suited for certain applications
- The Cost of material. Low cost of a material reduces the cost of manufacturing.
- Availability of material i.e. desired shape, size, quantity of material is available in the market
- Reliability of supply
- Service life of material i.e. Dimensional stability of material wear, corrosion, shorten life etc.
- Appearance of material i.e. color, surface texture etc.

1.4.1 Aluminum Alloy 5083-O

5xxx series alloys are non heat-treatable aluminum alloys which have magnesium as main alloying element. 'O' represents the alloy is in annealed condition as shown in designation system.

1.4.1.1 Applications of 5083-O

- Shipbuilding
- Rail Cars
- Vehicle Bodies
- Tip Truck Bodies

- Mine skips and cages
- Pressure vessels

Some exclusive examples are shown in figure 1.2

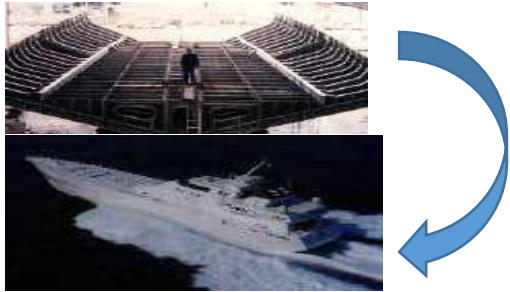



Shipbuilding	
The Foresmo bridge in northern Norway is an excellent example of the use of Al-Mg alloys for built up girders systems	
Rugged coal cars are provided by welded 5083 alloy plate construction	
Alloy 5083 was the work horse for the 125 ft. diameter spheres for shipboard transport of liquefied natural gas.	

Figure 1.2: Examples of usage of AA5083 in various applications (courtesy: Foresmo bridge in northern Norway)

1.4.2 Aluminum Alloy 6061-T651

These are heat treatable alloys which contain the combination of magnesium and silicon alloying elements. Magnesium silicate as a compound is formed due to the presence of magnesium and silicon. This magnesium silicate is responsible for imparting heat –treatability and medium strength to these alloys. These alloys are readily extruded and thus form a complementary system with the 5xxx sheet and plate alloys for structural applications.

1.4.2.1 Applications of 6061-T651

- Aircraft and aerospace components
- Marine fittings
- Transport
- Bicycle frames
- Camera lenses
- Drive shafts
- Electrical fittings and connectors
- Brake components
- Valves
- Couplings [1, 2]

Extruded Al-Mg-Si alloys, integrated stiffened bridge deck which are readily put in road ways in hours, Mag-Lev train developed in Europe and Japan, light weight aluminum space frames are some exclusive examples of application in industry as illustrated in figure 1.3.




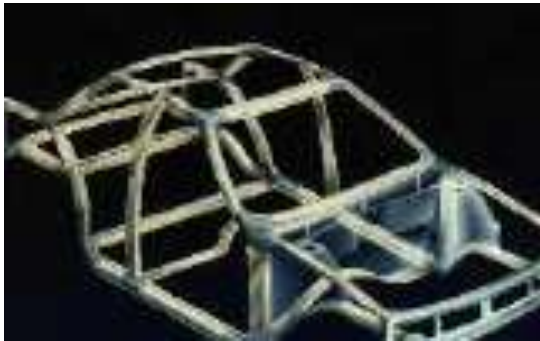

Extruded Al-Mg-Si alloys	
An integrated stiffened bridge deck shape usually produced by in 6061 aluminum alloy. They are often used as replacement of bridge decks which can be readily put in the roadway in hours.	
The new Mag-Lev trains in development in Europe and Japan employ bodies with 6061 and 6063	
Extruded Al-Mg-Si alloys may make up the entire frame of motorcycles or cars (illustration is of the Audi A-8 body)	
Light Weight aluminum space frames of 6061 aluminum alloy	

Figure 1.3: Application of AA6061 in Industry (Courtesy: Sapa Extrusion North America)

1.5 Need for Welding of Different Grades of Aluminum Alloys

Increasing application in industrial world has made the welding of aluminum and its alloys important. Due to increasing applications of aluminum need arises to have different properties from different parts of same weldments. In certain applications a part needs good corrosion resistance in one area and high temperature resistance in another. In other application like structures, one may need toughness or wear resistance in one area combined with high strength in another location. This brings about the need for joining dissimilar aluminum alloys. Some of the examples for need of different properties required within the weldment are:

- High strength to weight ratio property is required in airplanes, railroad cars, trucks and other transportation equipment.
- High resistance to corrosion and high thermal conductivity are important in equipment for chemical and petroleum industries; these properties combine with nontoxicity for food processing equipment.
- Striking appearance together with greater resistance to weathering and low maintenance requirements have led to widespread use in building of all types
- High reflectivity, excellent weathering characteristics, and light weight contributes to low handling and shipping costs.
- Various parts in automobile such as inner body panels, heat shields, structural parts, and body components are made from different aluminum alloy series. [2]

So, accordingly dissimilar welds will be required between different aluminum alloys in number of applications.

1.6 Application of Dissimilar Aluminum Alloy Joints of 5xxx and 6xxx Series

Due to higher physical and mechanical properties, the dissimilar joint of 5xxx and 6xxx series are commonly used in number of application. The applications are:

- i. Suspension rods, steering columns, gear box forks and drive shafts, as well as engine valves, in which the ability to join dissimilar materials means that the valve stem and head (figure 1.4) can be made of materials suited to their different duty cycles in service



Figure 1.4: Engine Valve (Courtesy: Electra engine valves California, USA)

- ii. Wheel assemblies using two aluminum alloys (figure 1.5) have made in which the butt or lap welds can be fabricated in wrought or cast material



Figure 1.5: Dissimilar Aluminum Alloy Wheel (Courtesy: Wheel assemblies using two aluminum alloys have been made by Hydro Aluminum in Norway)

iii. In BMW series the body frame (figure 1.6) is made of sheet aluminum of 5xxx series and extruded parts are made of 6xxx series aluminum alloys.

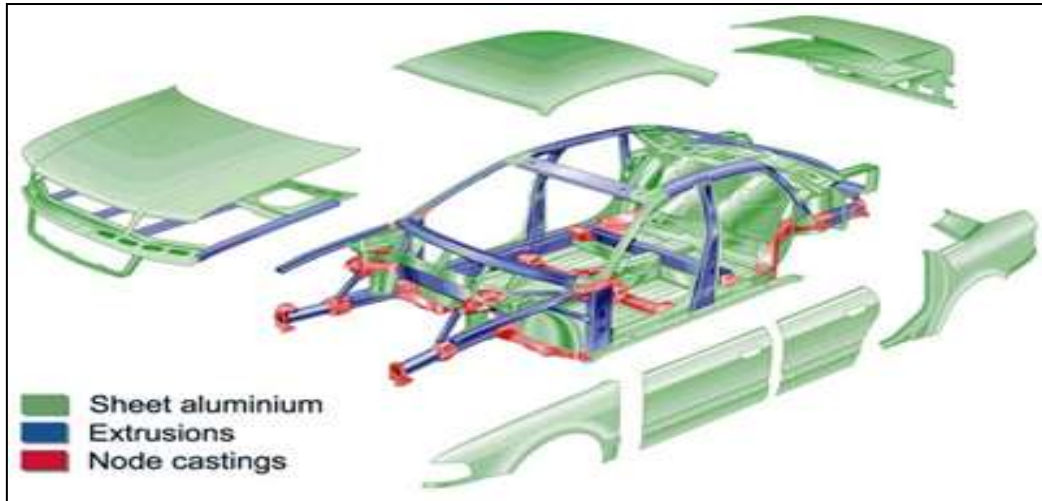


Figure 1.6: BMW Body Frame (Courtesy: Hydro Aluminum Deutschland GmbH, R&D, D-53014 Bonn, Germany)

iv. In Audi A8 series (figure 1.7) the combination of both 5xxx and 6xxx series aluminum alloys has been clearly seen

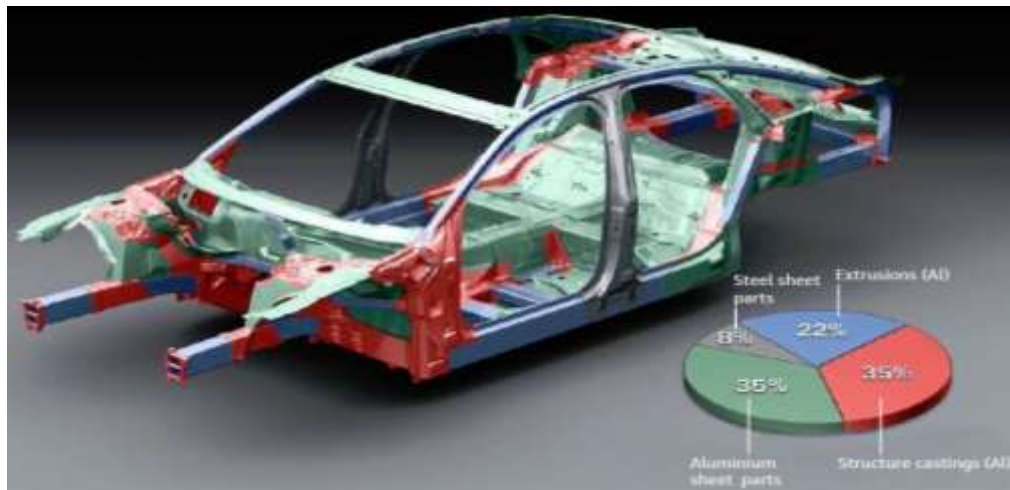


Figure 1.7: Audi A8 Body Structure (Courtesy: Doors and closures in Car Body Engineering, Bad Nauheim, Germany 2010)

v. In Jaguar XJ 2010 the door and front frame (figure 1.8) are made of 6xxx series alloys and the body sheet is made of 5xxx series aluminum alloys.

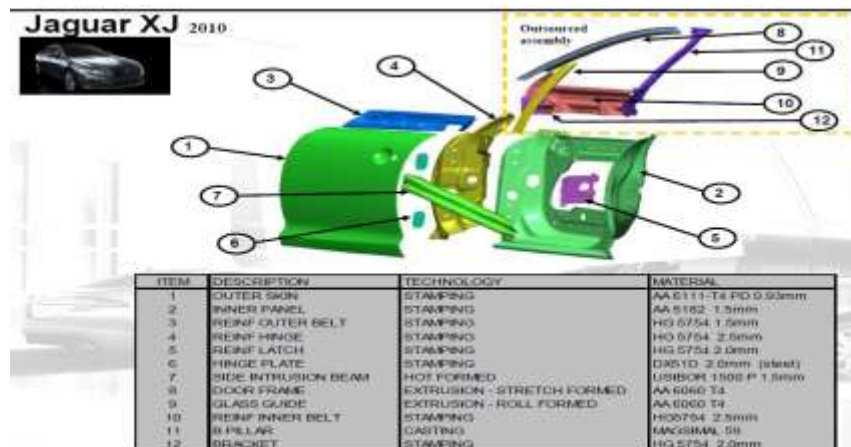


Figure 1.8: Jaguar XJ 2010 Model (Courtesy: Doors and Closures in Car Body Engineering, Bad Nauheim, Germany 2010)

1.6.1 Applications of Dissimilar Aluminum Alloy joint of 5083-O and 6061-T651

The application of dissimilar aluminum alloy is shown in figure 1.9




Single or multiple hull high-speed ferries, uses several Al-Mg alloys, 5083 and 5454 aluminum alloy is used as sheet and plate and 6xxx series aluminum alloys are used for extruded parts.	
Roof structures for arenas and gymnasiums are usually made of 6063 or 6061 extruded tube, and covered with 5xxx alloy sheet	
Welded 6061 extrusions combined with 5083 tubes make up the front and rear axle bodies for the BMW Model 5	

Figure 1.9: Application of Dissimilar Aluminum Alloy AA5083-O and AA6061-T651 in Industry

1.7 Challenges Associated with Welding of 5083-O and 6061-T651 Dissimilar Aluminum Alloy

The differences in the physical properties of 5083-O and 6061-T651 aluminum alloys is the primary challenge which has to be overcome to make the quality weld. The physical properties are:

- High difference of thermal conductivity- The heat produced by the arc flows more easily in the material with larger thermal conductivity. This can result in lack of fusion as excessive melting takes place on material with lower thermal conductivity.
- Coefficient of thermal expansion (CTE) of both welds- The wide difference between both coefficients of thermal expansion can cause the internal stresses set up in the IMC zone during any temperature change in the welding process.
- Melting temperature difference of two aluminum alloys.

1.8 Problems Related to Welding of 5083-O and 6061-T651 Aluminum Alloys

The problems related to welding of dissimilar aluminum alloys are:

A. Porosity:

- It arises from gas dissolved in the molten weld metal becoming trapped as it solidifies, thus forming bubbles in the solidified weld.
- The resulting porosity is greater in MIG than in TIG due to the high ratio of surface area to volume of the filler metal required for MIG.

- Porosity can be reduced using optimum parameters like small current and short arc length and welding speed. Higher the welding speed greater will be porosity.

The hydrogen solubility in aluminum is depicted in figure 1.10

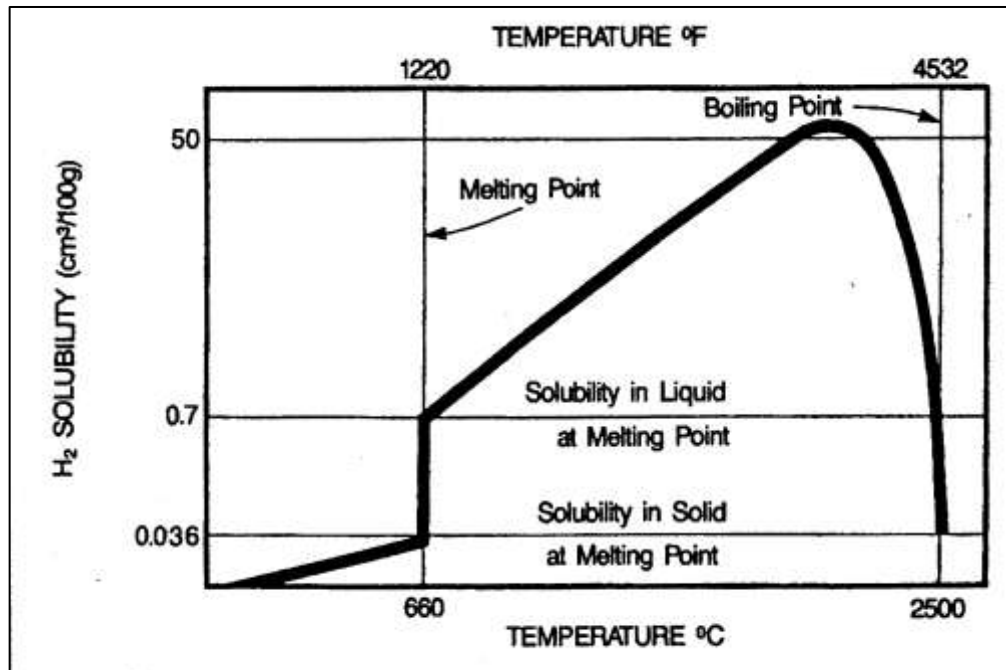


Figure 1.10: Hydrogen Solubility in Aluminum [3]

B. Hot Cracking

- Hot cracking is a high temperature cracking mechanism and is mainly a function of how metal alloy systems solidify
- Three things that can significantly influence the probability for hot cracking are susceptible base alloy chemistry, filler alloy and joint design
- Hot cracking can be reduced by selection of correct filler rod and reduction in amount of heat input.

The Alloy content Vs crack sensitivity is depicted in figure 1.11

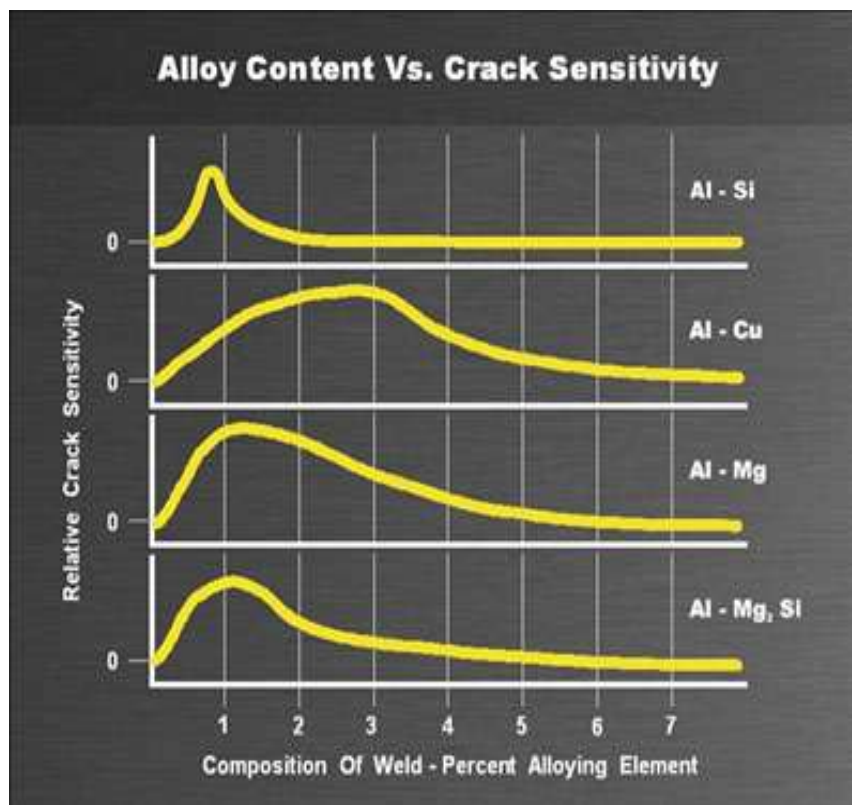


Figure 1.11: Cracking Sensitivity in 5xxx and 6xxx series Aluminum Alloys [3]

The Al-Mg phase diagram has been shown in figure 1.12

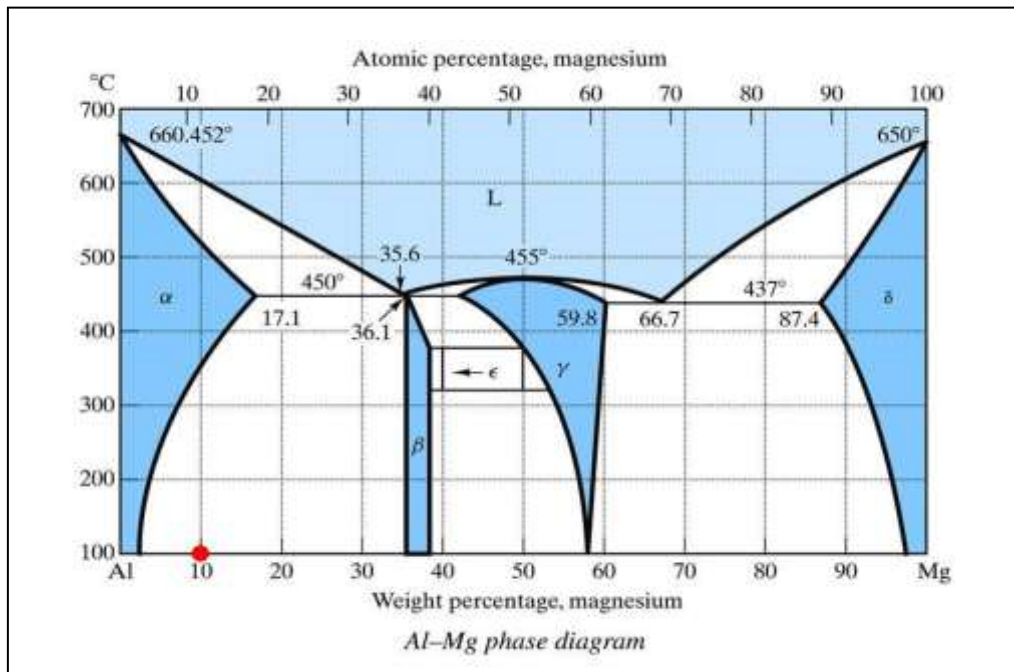


Figure 1.12: Al-Mg Phase Diagram [3]

C. Stress Corrosion Cracking (SCC)

- It is the cracking of metals caused by simultaneous effects of tensile stress in specific corrosive environment. For SCC to occur, three conditions must met: i) Susceptible microstructure, ii) Corrosive environment, iii) Tensile stress
- Alloys with relatively low magnesium contents such as 5052 and 5454 (2.5 % and 2.75 % Mg, respectively) has only mild chance of developing SCC at elevated temperature. In contrast, alloys with the magnesium contents more than 3 %, may develop susceptible structures as a result of heating or even after very long period of time at room temperature.
- The chance of SCC can be reduced by selecting proper welded-joint design and choice of welding parameters.

Tube breaking under stress corrosion cracking is depicted in figure 1.13.



Figure 1.13: Tube Breaking Under Stress Corrosion Cracking [3]

1.9 Uniqueness of Pulse TIG Welding

In area of joining process, TIG welding continues its top position due to its versatility and flexibility in adaptation. The superior weld quality obtained in TIG welding differentiates it with other competing and emerging joining process. But when pulsing character is attached to TIG welding, it makes it more advantageous as it reduces the heat input preventing certain problems. If the heat input is high following problems can occur or some advantages of pulse current over continuous current are:

- Passing of high heat during welding generally results in microstructural changes in weld bead and heat affected zone (HAZ) that affects the performance of material
- Excessive heat input during welding of non-heat treatable alloys results in large and equi-axed grains in weld bead.
- Broader HAZ is observed in high heat input process like TIG and MIG resulting in loss of strength over a larger section of parent metal.
- Welding between 5xxx and 6xxx series generally results in “hot short” cracks at bottom and toe which generally takes place due to residual heat which in turn caused due to excessive heat input.

1.10 Introduction to Tungsten Inert Gas (TIG) Welding Process

Tungsten Inert Gas (TIG) welding or Gas Tungsten Arc Welding (GTAW), is an arc welding process that uses a non-consumable tungsten electrode and an inert gas shield to protect the electrode, arc column and weld pool as illustrated in figure 1.14. The heat is generated by the electric arc which is maintained between electrode and metal part to be welded. The welding engineer has a choice of whether or not to add a filler

wire. Argon or helium is used as a shielding gas to provide the inert atmosphere to protect the weld from atmospheric contamination. The TIG process generates a pinpoint control of heat input resulting in narrow HAZ as compared to other arc welding processes. This process can be used for welding of wide range of materials which includes stainless steel, nickel alloys, aluminum alloys, magnesium, copper, gold. In addition to this dissimilar metals can be successfully welded by this process.

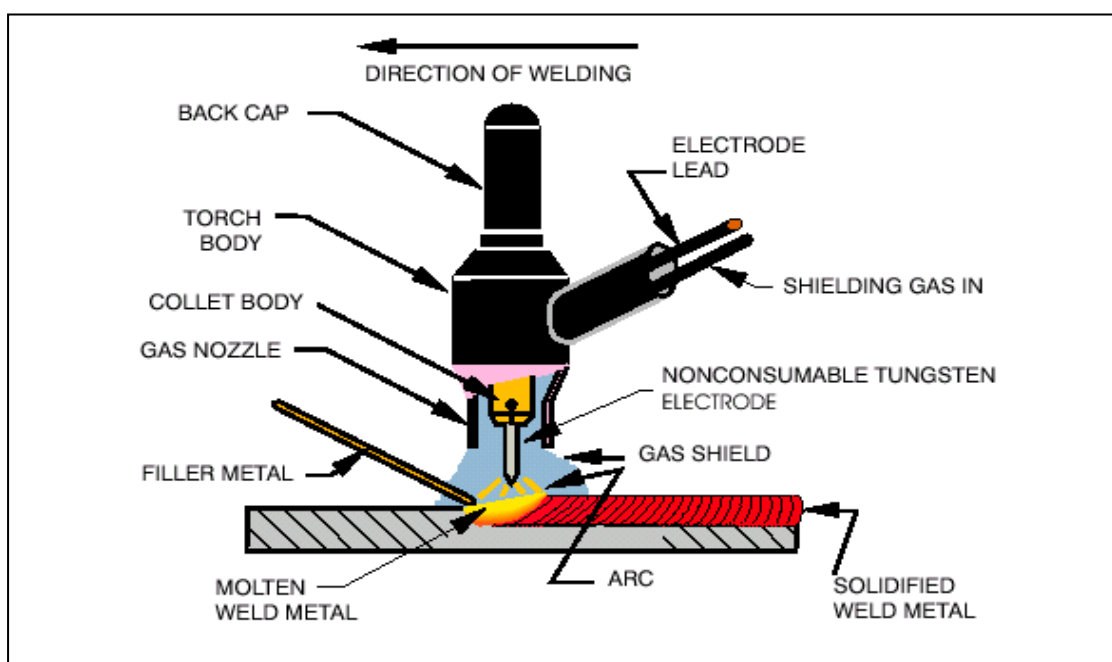


Figure 1.14 TIG Welding Set-Up [4]

1.10.1 Process Principle

The main equipment for TIG welding consists of power source, a welding torch, a supply of inert gas, a supply of filler wire and proper water cooling system.

Power Source: (V-I) characteristics of drooping type is used as power source. The direct current electrode positive (DCEP) or reverse polarity as shown in figure 1.15 is used for aluminum welding in which

- Torch is connected to the positive terminal.
- Work is connected to the negative terminal.
- Electrons flow from negative to positive, electrode is on negative side. Electrons are leaving the work.
- 70% of heat is on positive side and more into the electrode.
- Electrode has to be large
- Used for non-ferrous metals, as a cleaning form.

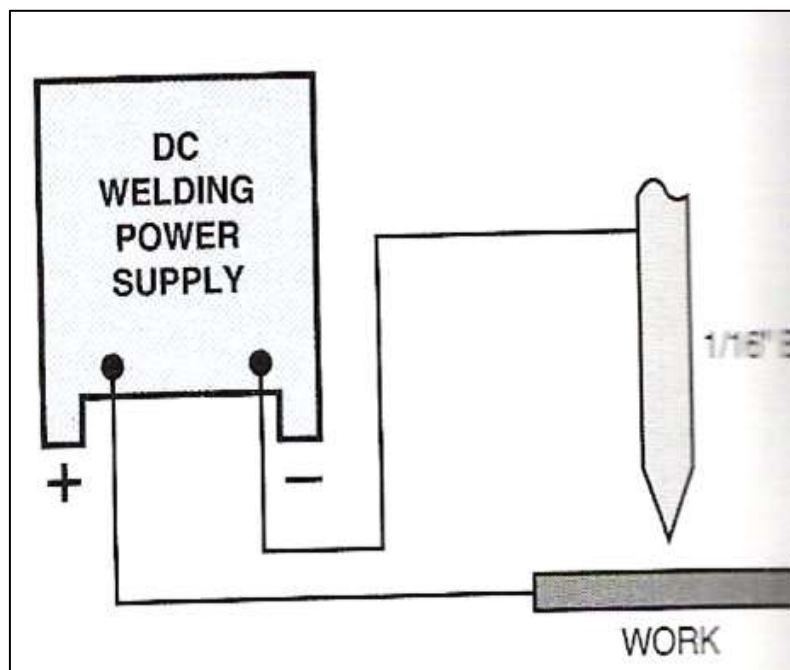


Figure 1.15: DCEP Polarity [4]

1.10.2 TIG Welding Equipment

- i. *Regulator*: Single stage or flow gages are the types used. The regulator regulates the gas pressure which depends on the type of gas being used, the size of the weld puddle, position, type of material etc

- ii. *Torch:* Two types of torch are used air cooled and water cooled. The air cooled is used when light duty or when water supply is not possible. Heavier gage wire is used with this type of torch. Water cooled torch carry more amperage through smaller gage wire. It requires cooling radiator or fresh water or drain.

Parts of torch head as shown in figure 1.16

- Torch body
- Collet (chuck)
- Collet body – Made of copper; the electrode fits inside and when the cap is tightened, it squeezes against the electrode and locks it in place.
- Torch cap – Locks the electrode on its position and prevents the escape of gas from the top of the torch
- Gas Nozzle –Directs the flow of shielding gas onto the weld puddle. Two type of nozzles are used; the one for light duty welding is made of ceramic material, and the one for heavy duty welding is a copper water cooled nozzle.

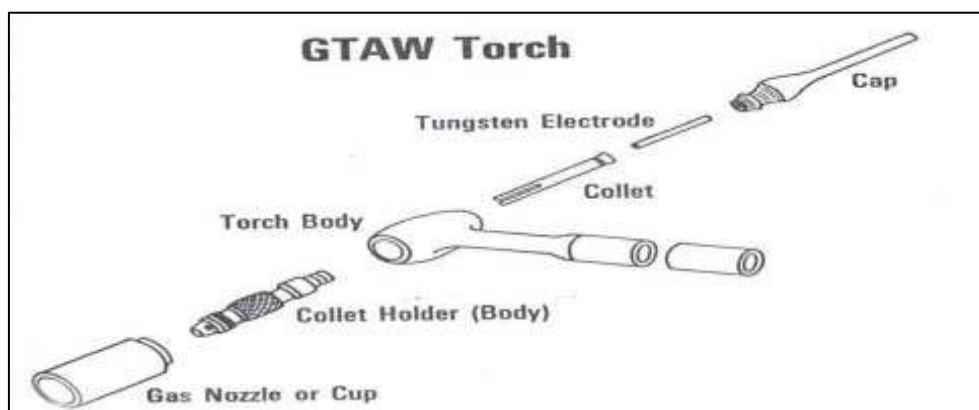


Figure 1.16: Torch Parts [4]

- iii. *Shielding Gases:* Argon and helium are two shielding gases commonly used.
- Argon: excellent arc starting, superior cleaning action, good arc stability, focused arc cone, lower arc voltages.

- Helium: Faster travel speeds, increased penetration, difficult arc starting, less cleaning action, low arc stability, flared arc cone, high arc voltages, higher flow rates, higher cost than argon.
- Argon/Helium mixture: Greater travel speeds over pure argon, higher penetration over pure argon, cleaning properties nearer to pure argon, better arc stability over pure helium, arc cone shape more focused than pure helium, arc voltages between pure argon and pure helium, increased flow rates than pure argon, more costly than pure argon.

1.10.3 Advantages of TIG Welding Process

- Concentrated Arc
 - Pin point control of heat input to the workpiece
 - Narrow heat affected zone
- Welds more metals and metal alloys than any other process
- High quality and precision
- Aesthetic weld beads
- No sparks or spatter
- No flux or slag
- No smoke or fumes

1.10.4 Disadvantages of TIG Welding Process

- Lower filler metal deposition rates
- Good hand-eye coordination a required skill
- Brighter UV rays than other processes

- Slower travel speeds than other processes
- Equipment costs tend to be higher than other processes

1.10.5 Applications of TIG Welding Process

- Weld more kinds of metals and metal alloy.
- Stainless steel, nickel alloys, titanium, aluminum, copper, brass
- Also can weld dissimilar metals to each other.
- Copper to Brass
- Stainless steel to mild steel

1.11 Pulse TIG Welding Process

This is modified version of TIG welding process in which pulse current alternates between a low or background level and peak level. Heating and fusion takes place during peak current period and weld pool cooling and solidification takes place between pulses as the heat is dissipated in the job during the background current period. This current pulsing leads to intermittent melting along the joint seam giving a series of discrete melt spots, which overlap each other. Pulse controls also adjust for the number of pulse per second and the percent of time spent at the peak amperage level which leads to control heat input and thus improves weld profile. DCEN is preferred current supply.

1.11.1 Advantages of Pulse TIG Welding Process

- Deeper penetration for given current
- Minimizes distortion, warpage (reduces thermal build-up) due to controlled heat input
- Thin sections: Full penetration, non burn-through
- Dissimilar thicknesses/metals are more easily joined

- Girth welds in horizontal pipe – same welding parameters in all positions
- Refines Fusion Zone grain structure

1.12 Motivation to Weld Dissimilar Aluminum Alloys

The aluminum and its alloys have always plays a vital role in engineering material field. The joining of dissimilar aluminum alloys has always presented the great challenge for designers and technologists. Lots of difficulties are associated with this joint process, which is mainly related to the presence of tenacious oxide layer, high thermal conductivity, high coefficient of thermal expansion, hot cracking, porosity and stress corrosion cracking. The motivation was provided by the desire to explore the frontiers of welding technology to minimize the defects in joining of aluminum and its alloys.

1.13 Organization of Thesis

Chapter One describes the brief introduction of aluminum and its alloys, their classification and designations are also discussed. It also describes the TIG Welding Process and its components in detail. The dissimilar grade of aluminum chosen for this investigation and the problems encountered in the welding of dissimilar aluminum alloy are briefly discussed.

Chapter Two describes the literature review of studies done on TIG welding. A brief survey is carried out on the welding of different materials other than aluminum using TIG welding. Survey is also carried out for TIG welding process on similar and dissimilar aluminum alloys. Further literature related to application of design of experiment in welding have been reviewed and presented. The research gap, research objectives and benefits of research are also presented in this chapter.

Chapter Three consists of a development of experimental setup. The automation for torch movement is done and the custom build wire feed system is made. The design and fabrication of fixture and torch holder have also been developed. The design is developed using SOLID WORKS 2017 software and fabrication is done using various machining operations. In addition to this work done in literature regarding automation in TIG welding systems has been given.

Chapter four Multi-Attribute decision making approach (MADM) has been explained and used in for selecting the welding consumable in this chapter. The optimum welding consumable like filler alloy, arc electrode and shielding gas has been determined from different alternates.

Chapter five deals with methodology and experimental analysis of dissimilar aluminum alloy joint of 5083-O and 6061-T651. The DOE approaches, trial runs for selection of a range of process parameters, Design matrix for experimentation and then mechanical testing and development of the mathematical model. The residual plots are also discussed in this chapter.

Chapter six presents the result and discussion of experimental analysis. The effect of various process parameters on mechanical properties of weld has been discussed. Apart from this the interaction effects of various process parameters on various mechanical properties are also presented.

Chapter seven provides the detailed study on metallurgical testing of welds. The Energy Dispersive X-ray analysis (EDS) results were discussed. The microstructural examination was also conducted for weld joint of 5083-O and 6061-T651. The microstructure pictures were taken at centre, at Heat Affected Zone (HAZ) at

magnification of 200X. The immersion test for resistance to pitting corrosion in fusion zone has also been analysed.

Chapter eight gives the conclusion of work presented in the above chapters and also includes the scope for future.

Chapter 2
Literature Review

LITERATURE REVIEW

2.1 Introduction

Now a days dissimilar Aluminum Alloys are largely employed in aerospace, shipbuilding, automotive and offshore structures etc due to their advantageous properties such as light weight, high specific strength and excellent corrosion resistant. The welding of these alloys is very difficult and one of the main reason is the application of local heat generated during welding which results in sharp temperature distribution and causes distortion. Therefore, the selection of suitable welding process and proper welding parameters are required to attain better quality joints. Hence pulse TIG welding is considered as the best welding process to weld similar and dissimilar aluminum alloys. In recent years, considerable research works were carried out to study and optimize pulse TIG welding process parameters for welding of different metals. A brief and selective review of the relevant available information collected is presented under the following broad headlines:

- *Studies on TIG welding*
 - i. TIG welding of different metals other than aluminum.
 - ii. TIG welding of aluminum alloys
 - iii. TIG welding of dissimilar aluminum alloys
- *Application of Design of Experiment (DOE) in welding*
 - i. Factorial Design
 - ii. Response Surface Methodology (RSM)

2.2 Studies on TIG welding

Pulse TIG welding which is one of the most well established processes gives not only best quality welds but also welds all metals of industrial use. Pulse TIG welding has successfully weld almost all metals required for normal fabrication. The literature available of TIG welding of different metals and alloy has been given in subsequent sections.

2.2.1 TIG Welding of Different Metals other than Aluminum

- Min et al. [5] studied the effect of heat input on the microstructure and mechanical properties of titanium alloy. The results indicates the increase in heat input resulted in an increase of width of HAZ and the grain coarsening of α -Mg in both the HAZ and FZ.
- Sudhakaran et al. [6] investigated the effect of welding process parameters on weld bead geometry and optimized the process parameters to maximize depth to width ratio for stainless steel using genetic algorithm. The results shows prediction of minimum depth to width ratio -0.18 and maximum depth to width ratio of 0.46.
- Balasubramanian et al. [7] developed the mathematical models to predict grain size and hardness of titanium alloy. The results shows the development of model which effectively predicts grain size and hardness.
- Yun et al. [8] performed the selection of optimal welding condition in root-pass of V-groove butt joint. Stainless steel of 7 mm thickness used as base metal. The observations shows the predicted values of bead width and height coming out to be 4.012 mm and 0.02 mm.

- Madadi et al. [9] performed the optimization of pulsed TIG cladding process of stellite alloy on carbon steel. Response surface methodology is the technique used for optimization. The results obtained shows welding current is significant parameter affecting hardness and dilution percent of weld.
- Lothongkum et al. [10] performed TIG pulse welding of 304L austenitic stainless steel in flat, vertical and overhead positions. The research revealed optimum conditions of parameters. Optimum welding speed was 3.4 mm/s at 55% on time. Controlling of ferrite content was also done i.e in the range of 3-12 % (v/v).
- Lothongkum et al. [11] studied the effects of pulse TIG welding parameters on delta-ferrite content, shape factor and bead quality in orbital welding of AISI 316L stainless steel plate. The optimum parameter conditions obtained are base current-61 A, pulse frequency of 5 HZ and pulse on time is 65%.
- Wang et al. [12] studied the transformation of Gamma (γ) phase in pulsed TIG weld metal of duplex stainless steel. The observations revealed that the finest grain size and highest content of γ phase obtained at 7°C. Further observations also shows the grain size and γ' (W) transformation is effected by pulse dc current.
- Reddy et al. [13] investigated the effect of the ratio of peak and background current durations on the fusion zone microstructure of pulsed current TIG welded Al-Li alloy. The optimum welding parameters obtained are; arc voltage of 15 volts, welding speed of 3.3 mm/s, pulse frequency of 2 Hz, heat input is 0.19 KJ/mm

- Balasubramanian et al. [14] performed the process parameter optimization of Pulse TIG of titanium alloy. Optimum parameters obtained were peak current at 80 A, base current at 40 A, pulse frequency at 6 Hz, pulse-on-time at 45%.
- Traidia et al. [15] obtained the optimal parameters for pulse TIG welding in partially and fully penetrated weld pools. The effects of gravity, electromagnetic forces, arc pressure and Marangoni effect are taken into account.
- Tsai et al. [16] investigated the fuzzy behaviour of pulsed TIG welds by using real-time root bead image feedback. The results obtained shows the development of fuzzy pulsed TIG which automatically adjusts the mean current in real time and achieve good welding quality.
- Babu et al. [17] determines the relationship of microstructure and mechanical properties of TIG weldments of Ti-6Al-4V which are made with and without current pulsing. The observations shows reduction in grain size with improved hardness, strength and ductility of the pulsed current weldments in as welded conditions.
- Balasubramanian et al. [18] predicts and optimizes the pulse TIG welding parameters to obtain sound weld pool geometry in titanium alloy using lexicographic method. Experimental results shows that front height, front width, back height, back width are greatly improved.
- Padmanaban et al. [19] studied the fatigue crack growth behavior of pulse TIG, friction stir and laser beam welded AZ31B magnesium alloy joints. The result shows greater resistance of fatigue crack growth exponent when welded with laser beam welding i.e 6% as compared to friction stir welded joints and 12 % compared to pulse current TIG welds.

- Babu et al. [20] studied the corrosion behavior of pulsed TIG weldments in power plant carbon steel. The observations revealed weld metal and heat affected zone have lower corrosion rate compared to base metal. Microstructure reveals presence of γFeMn_3 , FeO, FeN, Fe_3Si .
- Balasubramanian et al. [21] studied the effect of microstructure on impact toughness of pulsed current TIG welded α - β titanium alloy. The results obtained shows inverse relation of impact toughness with grain size. Further research shows pulsing current increases impact toughness upto particular frequency (6Hz).
- Huang et al. [22] performed the SVM-based fuzzy rules acquisition system for pulse TIG process. The results shows the optimum values SVM-FRAS without adaptive learning, SVM-FRAS with adaptive batch learning and SVM-FRAS with adaptive incremental learning, and RMS error are 1.33, 0.96 and 1.06mm
- Huang et al. [23] developed an adaptive inverse control method based on SVM-fuzzy rules acquisition system for pulsed TIG process. The overall simulation experiments for the TIG process shows the efficacy of the SVM-FRAS adaptive inverse control method.
- Tseng et al. [24] studied the effect of pulse TIG welding on residual stress of a stainless steel weldment. The results shows the residual stress of a 310 stainless steel weldment is found to be greater than for 304 stainless steel weldment.
- Balasubramanian et al. [25] optimized pulsed current parameters to minimize corrosion rate in TIG welded titanium alloy. The thickness of titanium alloy as base material is 1.6 mm. The results obtained shows minimum corrosion rate when optimized using genetic algorithm.

- Swaminadhan et al. [26] shows experimental investigations of weld characteristics for a single pass TIG welding with Stainless steel 304. The research obtained shows the value of front width for 2mm thick work piece with respect to 1mm thick workpiece for constant current and changing shielding gas flow increases by 20% and for 3mm piece with respect to 2mm workpiece increased by 21%.
- Kumar et al. [27] investigated the effect of heat input on the microstructure and mechanical properties of TIG welded AISI 304 stainless steel joints. The results obtained shows increase in heat input increases the fusion zone and heat affected zone. Grain coarsening is also increased with increasing heat input.
- Yan et al. [28] studied the microstructure and mechanical properties of 304 stainless steel joints by TIG, laser and laser-TIG hybrid welding. The results obtained shows full penetration joints without any defects were produced by TIG, laser and laser-TIG hybrid welding and δ -Fe phase and γ -Fe phases were observed in microstructure.
- Padmanaban et al. [29] influences the pulsed current weldments on mechanical and metallurgical properties of TIG welded AZ31B magnesium alloys. The optimum parameters obtained shows peak current of 210 A, base current of 80 A, pulse frequency of 6 Hz and pulse-on time of 50% showing higher tensile strength than their counter parts.
- Balasubramanian et al. [30] studied the effect of current pulsing on tensile properties of titanium alloy. The results obtained shows the effect of pulse frequency and peak current had two regions with initially increasing the tensile

properties and then decreasing the tensile properties irrespective of changes in base current and pulse-on-time.

- Balasubramanian et al. [31] studied the effect of pulsed current TIG welding on corrosion behavior of Ti-6Al-4V titanium alloy. The results obtained shows the improved grain refining due to current pulsing which further resulted in increase in corrosion resistance.
- Balasubramanian et al. [32] developed mathematical models to predict tensile properties of TIG welded Ti-6Al-4V alloy. The results obtained shows that mathematical model successfully predicts the tensile properties using TIG.
- Rose et al. [33] predicts and optimizes the pulse current TIG welding parameters to attain maximum tensile strength in AZ61A magnesium alloy. The results obtained shows the maximum tensile strength of 199.5 Mpa is obtained using optimum welding parameters of peak current 165.6 A, a base current of 83 A, pulse frequency of 6.24 Hz and pulse on time of 46.2%.
- Giridharan et al. [34] optimizes the pulse current TIG welding parameters for welding of AISI 304L stainless steel sheets. The results obtain shows the optimum values of pulse current is 211.4 A, for pulse current duration it is 537.65 ms and for welding speed it is 16.51 cm/min. Further the optimized weld bead parameters values for penetration is 3.4 mm, bead width is 9mm, aspect ratio is 2.57, bead area is 17.89 mm².
- Mallaiah et al. [35] investigated the effect of influence of grain refining elements on mechanical properties of AISI 430 ferritic stainless steel weldments. The results obtained in the form of optimum conditions are copper of 3g, titanium of 2g and Al at 1g.

- Rowe et al. [36] studied the hydrogen-induced cracking along the fusion boundary of dissimilar metal welds. The results shows that hydrogen-induced cracking was observed in high hardness martensite (400 to 550 HV) near the dissimilar metal fusion boundary between ER308, ER309LSi and ERNiCr-3 filler metals and A36 steel base metal and also it was revealed that cracking was observed in welds made with Ar-6% H₂ shielding gas, but not in welds made with pure argon shielding gas.
- Chen et al. [37] studied microstructure and mechanical property of rolled weld magnesium alloy AZ31. The results shows highest ultimate tensile strength of 252 MPa obtained when specimen is 7% rolled and the strength coefficient of 87.6% is obtained due to grain refinement in Heat affected zone.
- Fujii et al. [38] investigated the microstructure and mechanical property of rolled-welds magnesium alloy AZ31. The observations revealed the optimum combination of parametric values for a single pass deeper penetration requirement of weldment which are obtained at lower speed of 0.75mm/s, the welding current of 160 A and the electrode gap of 1mm under the He-0.4%O₂ shielding. The weld penetration reaches 9.4 mm which is much deeper for Ar-O₂ shielding gas.
- Padmanaban et al. [39] Studied the fatigue performance of pulsed current TIG, friction stir and laser beam welded AZ31B magnesium alloy joints.
- Munitz et al. [40] investigated the mechanical properties and microstructure of TIG welded magnesium AZ91D plates. The study yielded that Mg-AZ91D, 2-4mm plates can be successfully TIG welded. Further observations shows the

formation of continuous β -phase was formed on grain boundaries in the heat affected zone.

- Dong et al. [41] studied the improvement of arc joining of Al to steel and Al to stainless steel. The observations shows that aluminum can be joined to stainless steel by TIG welding with a flux-cored Zn based filler metal. A brief post weld heat treatment at 280 °C for 30 min doubles or triple joint strength.
- Padmanaban et al. [42] performed the optimization of Pulsed current TIG welding process parameters to attain maximum tensile strength in AZ31B magnesium alloy. The result showed that the maximum tensile strength of 188 MPa was obtained under optimum condition values of peak current of 210 A, base current of 80 A, pulse frequency of 6 HZ and pulse on time of 50%.
- Liu et al. [43] studied microstructure and mechanical properties of Mg-Li alloy after TIG welding. The results shows tensile strength of welded plate was 143.73 MPa. The fracture also occurred in the heat affected zone, which exhibits a mixed-mode fracture of ductile-brittle also segregation and enrichment of Aluminum and Ce are found at grain boundaries.
- Madadi et al. [44] studied the effect of pulse current on microstructure and wear resistance of stellite6/tungsten carbide claddings produced by TIG welding. The result shows increased current intensity level resulted in higher dilution and lower hardness, also current pulsing leads to finer and more homogenous solidification structures.
- Juang et al. [45] selected the optimum process parameters for optimization the weld pool geometry in TIG welding of stainless steel. Optimum results are, arc gap of 2.3 mm, flow rate of 8 l/min, welding current of 50 A and welding speed

of 15 cm/min. Experimental results have shown that the bead geometry parameters are greatly improved by using this approach.

- Li et al. [46] studied the law between the weld pool shape variations with the welding parameters under two TIG processes. The results shows that marangoni convection was considered to be the main factor controlling fluid flow in the liquid pool. Also this method allows for a wider range of welding parameters to obtain a narrow and deep weld pool.
- Shiri et al. [47] investigates the TIG welding of CP-copper to 304 stainless steel using different filler materials. The result findings indicate that Ni-Cu-Fe and Copper filler material can also be used for welding copper to 304 stainless steel. The results also reveals that using copper filler material, no macro and micro crack formed in the fusion zone.

Observation

1. Cracking could be avoided if pure argon is used as shielding gas.
2. Maneuvering the weld puddle significantly increases the joint strength.

2.2.2 TIG Welding of Aluminum Alloys

- Dongxia Yang et al. [48] studied the microstructural and mechanical property characterization of Er modified Al-Mg-Mn alloys Tungsten Inert Gas Welds. Microstructure characterization was performed by optical microscopy (OM), energy dispersive X-ray (EDX) and transmission electron microscopy (TEM). In addition, tensile and hardness test was conducted. Results indicate that ultimate tensile strength of the joints is 72% of the base metal. The characteristic equiaxed zone is obtained at the fusion boundary between the base metal and fusion

zone. Hardness test results indicate that the micro-hardness in the fusion zone is lower than that of base metal, due to the as-cast structure in this region. It is concluded that TIG welding is suitable welding procedure for joining the new type Er-containing aluminum alloy.

- M. Temmar et al. [49] investigated the effect of post-weld aging treatment on mechanical properties and metallurgical properties of 7075 aluminum alloy joints welded by TIG process. Hot cracking occurs in aluminum welds when high levels of thermal stress and solidification shrinkage are present while the weld is undergoing various degrees of solidification. The mechanical properties are found to be improved when joints are subjected to post weld aging treatment at 140°C.
- A. Kumar et al. [50] performed the optimization of magnetic arc oscillation process parameters on mechanical properties of AA 5456 aluminum alloy weldments using Taguchi method. Regression equations were developed to predict the quality characteristics within the selected range of parameters. Microstructures of all the welds are studied and correlated with mechanical properties.
- S. Malarvizhi et al. [51] studied the effect of welding process on AA2219 aluminum alloy joint properties. Butt joint were fabricated without filler wire using gas tungsten arc welding (GTAW), electron beam welding (EBW) and friction stir welding (FSW) processes. The effects of three welding processes on tensile, fatigue and corrosion behavior were studied. Microstructure analysis were also carried out using optical and electron microscopes. The results indicates that the FSW joints exhibit superior tensile and fatigue properties

compared to EBW and GTAW joints. It is also found that the friction stir welds show lower corrosion resistance than EB and GTA welds due to finer grains and uniform distribution of strengthening precipitates in weld metal of FSW joints.

- N. Karunakaran et al. [52] investigated the effect of pulsed current on temperature distribution, weld bead profiles and characteristics of gas tungsten arc welded aluminum alloy joints. Temperature distribution and weld bead profiles of constant current and pulsed current gas tungsten arc welded aluminum alloy joints were compared. The effect of pulse current on mechanical properties and microstructural features were investigated. The results indicated improved tensile strength with pulse current due to grain refinement occurring in the fusion zone.
- M. A. R. Yarmuch et al. [53] studied the behavior of variable AC polarity on Fusion region of 5083 aluminum alloys. They reported the increase of weld bead dimensions, notably penetration and width with increase of percentage of electrode positive polarity during the unbalanced square wave AC welding of aluminum alloys with GTAW process. This is contrary to conventional expectations which occurs primarily because of field emission characteristics of cathode.
- K. Subbaiah et al. [54] compared the mechanical properties of AA5083-H321 welded with tungsten inert gas and laser beam welding. The results indicated that low heat input of laser beam welding effectively reduced the size of fusion zone and heat affected zone compared to tungsten inert gas welding process. Further it was also noticed that evaporation of magnesium is less in LB welding as compared to TIG welding.

- M. El-Shennawy et al. [55] investigated the effect of Cu and Mg on similar and dissimilar welding of 7xxx series aluminum alloys. Both similar and dissimilar welded joints were made through various combinations of such alloys. Various mechanical properties were tested along with microstructural characterization. The research could explain the effects of alloying additions; Cu and Mg on weldability of Al-Zn-Mg-Cu based alloys. The results shows increasing Cu content to about 2.83 wt% with almost zero Mg showed the best tensile strength both in similar and dissimilar weld joints and vice versa. Increasing both Cu and Mg contents to 2.42 wt% and 2.53 wt% decreases the tensile strength.
- Biju S. Nair et al. [56] performed the TIG and pulse electron beam weld on AA2219 aluminum alloy and compared the mechanical properties of weldment of both the process. The research reported that direct current straight polarity in TIG with helium as shielding gas offers strong AA2219 joints, Consequently improved mechanical properties. Considerable reduction in heat input was achieved in pulsed EBW and subsequently results in high fusion zone hardness and strength because of fine grains, lowest copper segregation.
- Ratnesh K. shukla et al. [57] performed the comparative study of friction stir welding and tungsten inert gas welding process. The study shows the improved mechanical properties by FSW joint as compared to TIG welded joint due to lower heat input in FSW as compared to TIG.
- S.R. Koteswar Rao et al. [58] studied the mechanical and corrosion behavior of TIG welded AA2219 aluminum alloy using scandium fillers. Metallographic characterization was also studied which shows extensive grain refinement in

welds. The presence of scandium not only improved the mechanical properties but also resistance to cracking.

- A. Kumar et al. [59] performed the optimization of pulsed TIG welding process parameters on mechanical properties of AA5456 aluminum alloy weldments using taguchi method. Regression models and analysis of variance was employed to check the adequacy of developed models.
- Rajesh Manti et al. [60] studied the effect of pulse GTA parameters on microstructure and hardness of AA6061aluminum alloy. It is observed that current pulsing character in TIG welding produced finer grain structure of weld metal than continous current TIG welding. Further study reveals that an increase in pulse frequency refines the aluminum eutectic grain structure i.e using short pulse duration. Long pulse duration produces a coarser grain structure.
- A. kumar et al. [61] investigated the role of welding parameters of pulse TIG on mechanical properties of Al-Mg-Si alloy. Taguchi method was used to optimize. The results shows lower notch tensile strength and impact toughness than the parent metal due to interdendritic network microstructure features. An inverse relationship has been observed between the notch tensile strength and impact toughness.
- Rajesh Manti et al. [62] performed the pulse TIG welding of two Al-Mg-Si aluminum alloys. The research reports the influence of pulse TIG parameters on microstructure, hardness and tensile strength. The results revealed that the mechanical properties and microstructure are sensitive to microstructure of weld metal, which is affected by pulse parameters. Low frequency produces higher

strength and hardness under identical welding conditions. Further study shows the weld metal and HAZ strength were stronger than base metal.

- T. Senthil Kumar et al. [63] studied the role of pulse current parameters of tungsten inert gas welding on mechanical properties of AA6061 aluminum alloy. The study shows improved mechanical properties due to grain refinement occurring in the fusion zone when welded with pulse current parameters. Factorial design was used to predict the tensile properties. Peak current and pulse frequency are having directly proportional relationship with tensile properties of welded joints. However this is not the case of base current and pulse on time, both are inversely proportional to each other.
- S. Babu et al. [64] performed the optimization of pulsed current welding parameters of gas tungsten arc welding on AA6061 aluminum alloy using hooke and jeeves algorithm. The result indicates that peak current and base current are the most significant parameters which decides the fusion zone grain size and tensile strength of AA6061 aluminum alloy joint.
- V. Balasubramanian et al. [65] performed the study related to the role of pulsed current welding on mechanical properties of high strength aluminum alloy. Four different welding techniques were used to fabricate the joints: 1) Continuous current GTAW, 2) pulsed current GTAW, 3) continuous current GMAW, 4) pulsed current GMAW. The results revealed that finer and equi-axed grain structure is obtained in pulse GTA and pulse GMA welds.
- B. Wang et al. [66] developed the modeling based on rough set knowledge for pulsed GTAW welded aluminum alloy. The model obtained is easily understood

and revised. Experimental results obtained indicate that the method is effective and can be regarded as the basis of intelligent control of welding process.

- V. Balasubramanian et al. [67] investigated the effect of postweld aging treatment on fatigue behavior of pulsed current welded AA7075 aluminum alloy joints. Four different welding techniques were used to fabricate the joints: a) Continuous current GTAW, b) pulsed current GTAW, c) continuous current GMAW, d) pulsed current GMAW. Fatigue behavior of welded joints were studied. Current pulsing leads to grain refinement which in turn leads to increase fatigue life and endurance limit.
- Li. Laiping et al. [68] developed the model of weldig pool surface reflectance of pulse GTAW welded aluminum alloy. Based on the imaging characteristics of aluminum alloy welded pool, the surface reflectance model is built after analyzing arc intensity, filter system, welding pool shape and reflectance characteristics.

Observation

1. The main parameters of TIG welding which effects the bead geometry and mechanical properties are :
 - a) Peak current (A)
 - b) Base current (A)
 - c) Pulse duty cycle (%)
 - d) Pulse Frequency (Hz)
 - e) Welding speed (mm/min)

2. Direct Current Electrode Positive could also be used
3. Increased heat input is prime concern for researchers which results in various metallographic defects in welds.

2.2.3 TIG Welding of Dissimilar Aluminum Alloys

- Sayer et al.[69] compared the mechanical and microstructural behaviors of TIG and FSW welded dissimilar aluminum alloys AA2014 and AA5083. The study shows that both the welding has been applied successfully to dissimilar aluminum alloys with no visible porosity or macroscopic defects across the weld cross-section. Further study revealed that NZ possessed fine-equi-axed grains due to recrystallization, compared to increase size in TIG due to severe heat input.
- M.M. Mossman and J.C. Lippold [70] performed the weldability test of dissimilar combinations of 5000 and 6000 series aluminum alloys. They used sigma-jig weldability test to detect crack susceptibility of TIG welded for different combinations of sheet alloys. The results shows that the dissimilar combination of 5182/6111 exhibited the best resistance to weld solidification cracking
- C.C. Menzemer et al. [71] studied the microstructures of TIG welded joints made from 5xxx and 6xxx series dissimilar aluminum alloys. The Hot-short cracks were observed near the weld toe on the 6xxx series. Occurrence of eutectic melting or hot-short cracking suggests that local heat input was fairly large coupled with the existence of localized stress.

- Michinori Okubo et al. [72] studied the mechanical properties of Aluminum –based alloy joints by YAG laser beam, electron beam, metal inert gas arc, tungsten inert gas arc and friction stir welding. They butt welded different combination of base metals like A1050-H24, A2017-T3, A5083-O, A6061-T6 and A7075-T651. The results indicates that FSW welded specimen depicts higher mechanical properties as compared to TIG or MIG due to absence of melting.
- T Luijendijk et al. [73] performed the TIG welding of dissimilar aluminum alloys of the series 5xxx and 6xxx for different plate thicknesses. The results shows reduced strength in HAZ of metal . The study further shows that reduction in strength is smaller for solution hardened and strain hardened alloys, than for precipitation harden alloy.
- S. Jannet et al.[74] performed the comparative study of friction stir welding and fusion welding of 6061-T6 and 5083-O aluminum alloy based on mechanical properties and microstructure. The results obtained shows that tensile properties of joints AA5083-O and 6061-T6 aluminum alloy joints are influenced by welding process and post weld aging treatments. Grain refinement with fine distribution of precipitates is obtained in FSW joints compared to TIG welding which indicates improved strength and ductility in FSW joints compared to TIG.

Observation

1. The dissimilar joining of 5xxx and 6xxx series alloys exhibits best resistance to solidification cracking.
2. The reduction in strength is smaller for solution hardened and strain hardened alloys, than for precipitation harden alloy.

2.3 Application of Design of Experiments in Welding

Design of Experiment is one of the many problems-solving quality tools that can be used for various investigations such as finding the significant factors in a process, the effect of each factor on the outcome, the variance in the process, screening the parameters, and modeling the process. There are many DOE models to choose from however the best DOE model for given welding application depends on the cost of parts, time to conduct the DOE, number of input factors and input factor levels. Depending on this, many researchers have used factorial design, response surface design in welding. The brief literature is presented in subsequent section.

2.3.1 Factorial Design

- Harris and Smith [75] applied the factorial technique for weld quality prediction for plasma transferred arc (PTA) weld cladding process on mild steel. It was confirmed that all the process variables were acting as main parameters in controlling the deposit quality.
- Murti and Sunderesan [76] performed the optimization of friction stir welding of dissimilar materials using factorial design. The main aim was to determine the metallurgical and mechanical behaviour of the friction welded joints produced using optimum welding conditions. Three mathematical models were developed to relate the notched tensile strength (NTS) and shear energy to the process parameters, namely: friction pressure, friction time and forging pressure with different levels according to the two materials which formed the joint. It was reported that the statistical experimental design was useful for reducing the number of trials necessary to optimize the welding conditions for friction

welding. Also, the strength of the joint which was produced by using the optimized condition was in fair agreement with the predicted results.

- Arya and Parmar [77] investigated the controlling of distortion in robotic CO₂-shielded FCAW. A three level fractional factorial was used to develop mathematical models to predict angular distortion in 10 mm thick low carbon steel. It was concluded that the models developed were fairly accurate and can be usefully employed for controlling the angular distortion in automated welding lines using FCAW process.
- Zhou et al. [78] have utilized factorial experimentation to investigate the influence of joining parameters on NTS of dissimilar aluminum-based metal matrix composite MMC/AISI304 stainless steel friction joints. The effect of frictional pressure and rotational speed on NTS values have been found to be statistically significant.
- Balasubramanian and Guha [79] studied the fatigue endurance of flux cored arc welded (FCAW) cruciform joints using design of experiments. It was noted that ANOVA technique is the most convenient to identify the significance of the main effects and interaction effects of joint dimensions.
- Balasubramanian and Guha [80] continued their investigation by developing mathematical models using design of experiment to predict the fatigue life of shielded metal arc welding SMAW and FCAW cruciform joints failing from root and toe regions.
- Koganti et al. [81] have employed a full factorial design to define the optimum weld MIG process parameters for non-treatable 5754 aluminum alloys. The

effects of weld process parameters on lap joint failure load (tensile-shear strength) and weld penetration were investigated. Based on lap shear load to failure and weld penetration data two significant factors were identified which are power input and gas flow.

- Sampath [82] presented an innovative constraints-based approach that proved quite efficient in developing a specification for consumable solid-wire electrodes for GMAW of HSLA-80 and HSLA-100 steels that meet or exceed the US Navy requirements. Subsequently, a 2^3 factorial design was used to develop a batch of welding electrodes in order to evaluate their performance. It was concluded that the use of this approach greatly reduced the risk inherent in developing electrode specifications.
- Pine et al. [83] conducted an experimental and numerical study to find out torsional stiffness, elastic limit and ultimate strength of spot welded in adhesively bonded and weld-bonded box sections. They investigated various factors which includes design considerations, strength, thickness of sheet and technique for its joining. The effect on torsional properties of box sections have been determined using factorial design techniques. The author have concluded that the joining technique, section area and section thickness were the main factors which have the greatest effect on torsional stiffness of the box sections.

2.3.2 Response Surface Methodology

- Wang and Rasmussen [84] have investigated the inertia welding process of low carbon steels using RSM, with the purpose of establishing an empirical function relationship between the process parameters (the axial pressure, the initial

rubbing velocity and total moment of inertia) and breaking strength of the joint. It was observed that while using wide range of operating conditions the welds produced are more successful. Also, they observed that the average micro-hardness at the weld was about 27 percent higher than the base material and the ideal weld should be made with the least possible amount of kinetic energy as long as full penetration at the interface is achieved.

- Yamaguchi et al. [85] investigated the friction stir welding process of 5056 aluminum alloy using RSM. Their study was aimed to find best optimum welding conditions that would result in achieving higher tensile strength in the fusion zone. It was reported that the successful welds shows 89.2% joint efficiency in tensile strength.
- Koichi et al. [86] studied the combination of welding conditions that provide maximum notched tensile strength of friction welded joints of carbon steel using RSM. They managed to correlate the process parameters to the tensile strength of the weld joint. Successful weld strength was obtained using the optimal welding condition predicted by empirical equation.
- Benyounis et al. [87] proposed models using RSM to investigate the effect of welding parameters in SAW on the impact strength at two testing temperatures of 50 °C and 27 °C. The aim was to improve the impact strength of the spiral-welded joints by predicting and optimizing the process parameters. It was observed that welding current was the most significant factor which effects impact strength rather than the welding speed and voltage.
- Ege et al. [88] studied the production of strong and stiff, aluminum-titanium, multi-layered composites by explosive welding. The study was performed using

RSM to investigate the mechanical behavior of the laminates with changes in two characteristics variables; abundance of interfaces and volume percentage of the more ductile component. It was reported that the mechanical properties of the laminates depend strongly on the relative amounts of the components, but only weakly on the abundance of the interface within selected operability region.

- Allen et al. [89] proposed a RSM model based on central composite design for robotic gas metal arc welding of the sheet metal of 409-gauge, stainless steel. The objective was to minimize the weld cycle time by maximizing welding speed, while maintaining predictable weld quality over a range of worst-case processing conditions. The optimal welding conditions for this type of material with a lap joint were reported and confirmed by experimental tests.
- Raghukandan [90] conducted the experiments to clad low carbon steel and copper plates using nitroglycerine explosive (2500 m/s detonation velocity). The aim was to adopt RSM to relate the bond and shear strength of the clad to factors. Mathematical models were developed and the effect of process parameters on responses was discussed. It was found that flyer thickness, the loading ratio and the angle of the inclination have significant contribution to the interfacial morphology of explosive clad.
- V. Murugan and Gunaraj [91] implemented RSM to correlate the angular distortion in GMAW of structural steel plate (IS: 2062) to process parameters. The main and interaction effects of the process parameters were analyzed and presented. It was found that the number of passes had strong effect on the

response, therefore to control the angular distortion in practice the number of passes has to be monitored carefully.

- Benyounis et al. [92] carried out the investigation to study the various effect of CO₂ laser welding parameters on mechanical properties especially the impact strength and NTS of butt joints made of medium carbon steels. The influence of process parameters on two responses were described from mathematical models developed using RSM. The determination of main, quadratic and interaction effects of the process parameters on the two responses were found quantitatively and presented graphically. Welding speed is found to be the most influential factor affecting response. From the results it was observed that decrease in the welding speed increases the responses by 89.3% and 76.45% respectively.
- Benyounis et al. [93] have done another work to predict the residual stress for CO₂ laser butt-welding joints of AISI 304 stainless steel plates. The investigation is carried out using RSM to develop models in terms of the process input parameters to predict the principal residual stress and its direction. It was observed that travel speed and laser power were the main factors affecting the behaviour of maximum residual stress.
- Olabi et al. [94] established the relationship between the CO₂ laser welding parameters and the residual stress magnitude and distribution using RSM for butt joint welded components. The base material was AISI 304 stainless steel plates with 3 mm thickness. A procedure of four steps was presented to use the developed models in order to predict the residual stress magnitude at the proposed welding conditions and at a given position. Also, the effect of process

parameters on the residual stress behavior has been determined quantitatively and presented graphically.

- Benyounis et al. [95] developed a mathematical model using RSM to relate the failure load to laser welding parameters. The effect of process parameters on the failure load and tensile-shear strength of the lap joint made of AISI 304 with 1 mm thickness have been investigated. It was found that the main factor affecting the joint strength is the welding speed and the other two factors are slightly affecting the joint strength.

2.4 Gaps in Research Work

- i. Most of the researchers have investigated the pulse TIG welding parameters separately on AA6061 or on AA5083. The investigations have been hardly found on butt welding of both these alloys using pulse TIG welding parameters.
- ii. The work in literature is limited to testing of tensile properties. The micro-hardness, and microstructural characterization study has been rarely found in the literature.
- iii. In addition to this impact toughness test as a response has been hardly studied till now.
- iv. Most of the work has been done on 5xxx series alloys like 5456, 5182 and in 6xxx series alloys 6082, 6111 but work on 5083 and 6061 aluminum alloy has been scarcely found
- v. Limited studies have been done in analyzing the effect of weld speed on mechanical and metallurgical properties of the dissimilar weld joint of aluminum alloy AA5083 and AA6061

2.5 Research Objectives

The following objectives for the present work have been framed.

1. Development of Experimental set-up
2. Selection of welding consumable using Multi-Attribute Decision making approach (MADM)

3.A) *Experimental study*

- Identifying the important Pulse TIG welding parameters which are having the influence on fusion zone grain refinement and mechanical properties.
- Finding the upper and lower limits of the identified parameters by visually inspecting the weld bead shape and subsequently deciding the levels of parameters.
- Development of experimental design matrix
- Conducting the experiments as per design matrix.

B. *Study of mechanical properties*

- Deciding the mechanical responses under study
- Making of specimen for tensile testing, micro-hardness testing and impact testing.
- Recording the quality characteristics or responses (i.e mechanical properties)

C. *Mathematical modeling*

- Developing the regression models to predict the mechanical properties within selected range.

- Identifying the significant factors
- Checking the adequacy of developed models
- Conducting the confirmation test to validate the model.

4. Metallurgical testing of welds

2.6 Benefits of Research

The outcome of the research proposed will have strong bearing and usefulness for the development of new aluminum alloy products not only in the industrial application but also in home appliances. Considered as most abundance element in the earth crust, success in joining of aluminum alloy will increase its marine, aerospace and automobile application.

Chapter 3
Development of Experimental Set-Up

DEVELOPMENT OF EXPERIMENTAL SET-UP

3.1 Introduction

Pulse TIG welding continues its apex position due to its versatility and flexibility in adaptation. The superior weld quality obtained in TIG weldments differentiates the TIG process in comparison with other competing and emerging joining process. Pulse TIG welding is often considered the most difficult of all the welding processes commonly used in industry. Because the welder must maintain a short arc length, great care and skill are required to prevent contact between the electrode and the workpiece. Pulse TIG welding is most commonly used to weld thin sections of stainless steel, non-ferrous metals such as aluminum, magnesium and copper alloys. It is significantly slower than most other welding techniques and comparatively more complex and difficult to master as it requires greater welder dexterity than MIG or stick welding.

3.2 Problems Associated with Manual TIG Welding

The problems associated with manual TIG welding includes

- Undercutting
- Tungsten inclusions
- Porosity
- Heat affected zone cracks and
- Adverse effect on health of welding gun operator due to amount of tungsten fumes produced during the welding process.

3.3 Necessity for Automation in Pulse TIG Welding

To improve the quality of weld joint, automation is essential especially where thickness of welding sections are greater than $t > 5$ [96]. Also adverse effect on operator health due to amount of tungsten fumes, safety of operator and costly availability of SPM in the market are some of the reasons which urged to make automation in TIG welding process. Hence, an automated setup of Pulse TIG welding process has been built which decreases the defects and increases the weld mechanical properties.

3.4 Advantages of Automation in Pulse TIG Welding

They have several benefits which includes

- Consistency in quality welds
- Greater repeatability
- Lowered production costs
- Fewer scrapped parts
- Increases return on investment
- Faster speed per cycle.

3.5 Automation in Pulse TIG Welding Machine

Many researchers have built customerize TIG automatic set-up according to the applications. karpagaraj et al. [97] used automatic setup for welding titanium alloy in which torch movement is automated using single axis mechanism. Tadayuki suggested to have built the automatic setup built having torch position specifically kept at 40° to yield good results [98]. Roshan et al. [99] uses single axis movement of torch using lead screw for welding carburetor components of sheet metal thickness of

1.2 mm. After literature survey, It was found out that the set-up will comprise two things, one is automatic torch movement or automatic manipulator movement as shown in figure 3.1 and second is wire feed system. After discussion with various manufacturers and suppliers of industries, automatic manipulator movement as option was turning out to be costly mechanism. So, it was decided to make the torch movement automatic while keeping the welding workpiece stationary. Second thing was wire feed system. The cost of automatic wire feed system was coming out to be around 1000 USD. It was huge amount. So it was decided to build the customerize set-up by assembling the different components. After considering all these factors, market survey was conducted to find out how the setup will built and what will be the estimated cost of set-up. A automatic set-up was built and the cost associated for making of automated TIG is found to be low around 300 USD as compared to SPM (Special Purpose machines) available in the market.

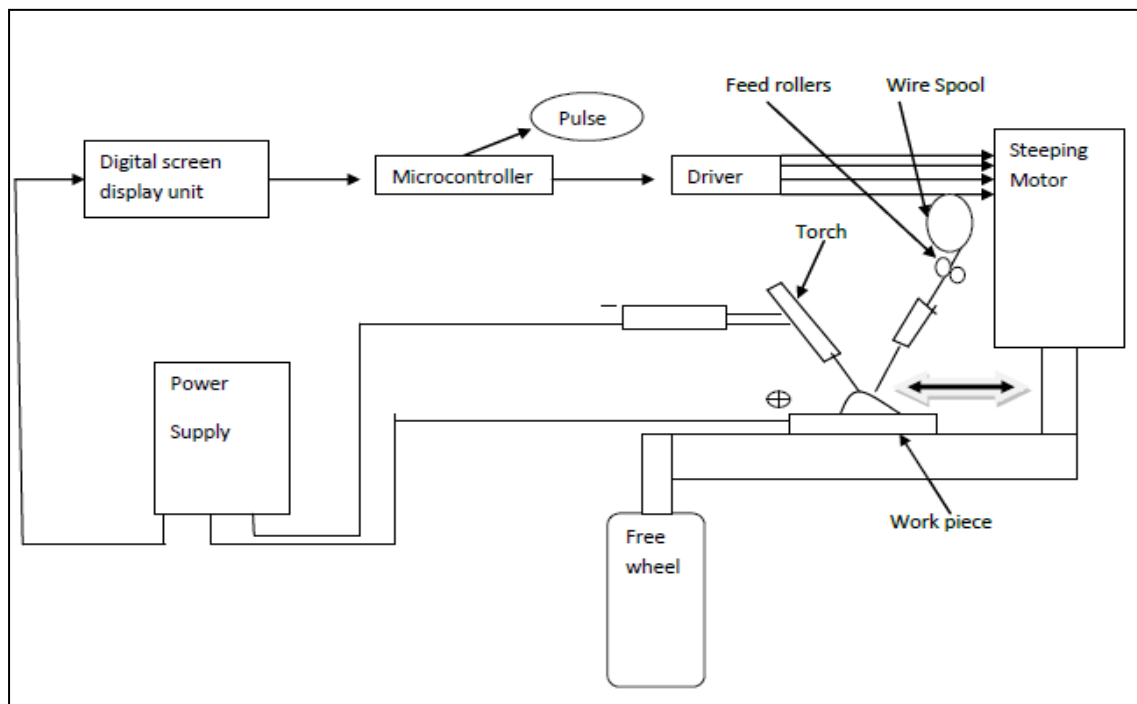


Figure 3.1: Automatic TIG Set-Up

The automatic set-up has been described in subsequent section

3.5.1 Automatic Torch Movement

Automating the torch motions decreases the error potential which means decreased scrap and rework. The setup consist of trolley, pencil torch (air cooled) (figure 3.2), track, fixture for holding pencil torch. The set up with torch movement is shown in figure. 3.3



Figure 3.2: Air Cooled Torch



Figure 3.3: Torch Mounted on Trolley Moving on Dedicated Track

3.5.2 Custom Built Wire Feed System

The custom built wire feeder system comprises of feeder casing, feeder motor (5A, 24V), MIG Torch, Teflon liner, Copper wire Transformer (5A, 12V), Silicon bridge

rectifier (406KBL), Voltage variac (4A). First the 220V, 50 Hz power supply was given to voltage variac or dimmer to vary the voltage which leads to change in wire feed rate, then output of voltage variac is given in step down transformer which decreases the voltage as per its rating. The output of decreasing voltage is then given in silicon bridge rectifier which converts ac into dc and finally the dc output is given in the dc wire feed motor. The custom build wire feed system is shown in figure 3.4. The custom build wire feeder along with circuit diagram is shown in figure 3.5. The total expenditure occurred was around \$300 which is much lesser as compared to feeders available in the market.

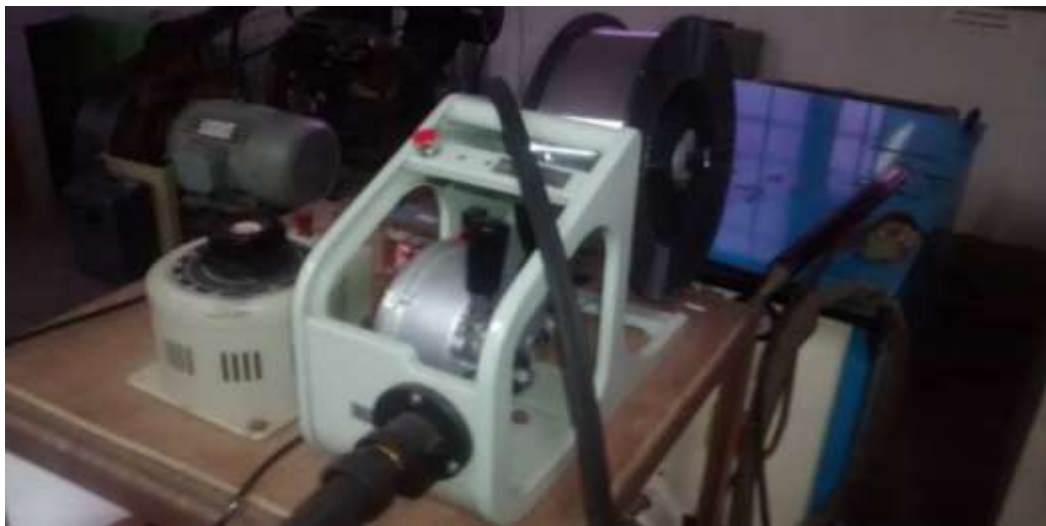


Figure 3.4: Custom Build Wire Feed System

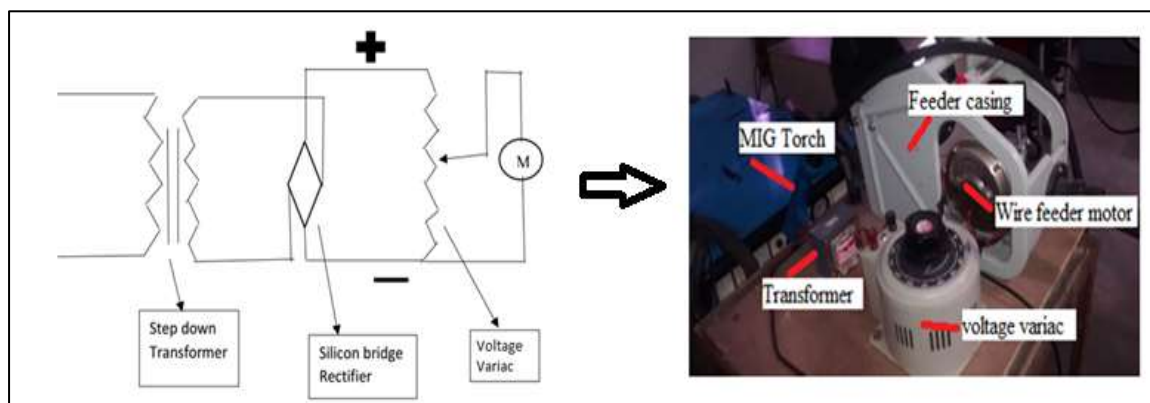


Figure 3.5: Circuit Diagram of Custom Built Wire Feeder and Custom Build Wire Feeder for Pulse TIG Welding

3.6 Design and Fabrication of Fixture

The main function of fixture is to hold the plates in position while the welding is being performed. Careful design selection of fixture is essential part of welding. Fixture should be such that it should withstand the forces and rising temperature during welding process without distortion in shape. The stability during the process is important since any deflection or major vibration would affect the quality of the weld. So, Certain features were kept in mind while designing the fixture.

- a) The design should be such that it accommodate both the plate to be welded.
- b) Clamp strips are also required for fixing the plates so that plates do not get displayed from their original position while performing welding.
- c) Grooving at the centre is also required, so that temperature can be spread uniformly around the edges to be welded.
- d) Two holes at the centre line should also be required so that temperature during welding can be measured using the thermocouple.

Considering the above versatile features, the design of fixture was prepared using SOLIDWORKS 2017. Design as shown in figure 3.6 was prepared considering the dimensions of plates to be welded.

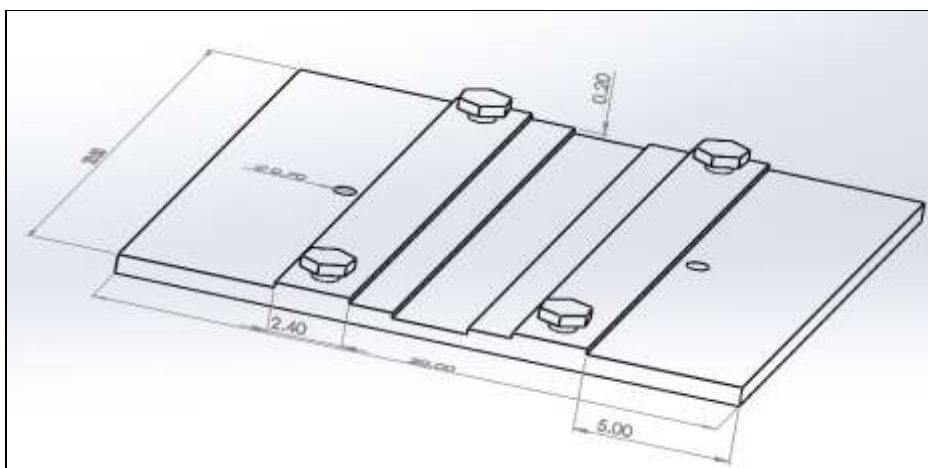


Figure 3.6: Dimensional Drawing of Fixture

Mild steel is the material used for manufacturing the fixture, clamps strips. Since mild steel has high strength and toughness which is required to withstand unbalanced force and pressure during TIG welding operation.

After designing the fixture, its manufacturing was done that involved following operations.

i. Milling operation on horizontal milling machine.

The Milling operation was done to produce the sharp edges of right angle at four corners of the workpiece to be manufactured. After developing equal edges of right angle produced by the machining, the measurement using scale and the marking using red chalk was done according to the dimensions given in the drawing. Climb milling process was used for milling. The tool used was high speed steel cutter

ii. Shaping operation on shaper machine.

In the shaping operation, shaper machine was used for creating the grooves on two positions separating with equal distances. The tool used was high speed steel tool.

iii. Drilling operation on drilling machine

Drilling operation was done using tool bits of different sizes as per the design specification. Four holes at centre were drilled using 7mm drill bit.

iv. Surface finishing is done using grinding operations

Surface finish using surface grinder was used for removing the roughness and providing the desired tolerance.

After performing all these operations finally fixture is produced as shown in figure.3.7



Figure 3.7: Fabricated Fixture

3.7 Design and Fabrication of Welding Torch Holder

The welding torch holder has two functions. First to hold the torch straight in the vertical position and second to provide support to MIG wire feeder gun. Certain features were kept in mind while designing the welding torch holder.

- i. The torch should be such that it supports the weight of the welding torch by clamping it from two sides with help of bolts

- ii. A metal strip is required which make the angle of 40° with the torch as wire feeding during the welding is required from MIG wire feeder gun at a certain angle .

So considering the above features the welding torch holder was designed using SOLIDWORKS 2017. Design as shown in figure.3.8 was made considering the dimensions of welding torch and MIG wire feeder gun. Stainless steel is the material used to make welding torch holder. Since stainless steel has high strength to weight ratio and good resistance to heat which are essential properties as required during welding operation.

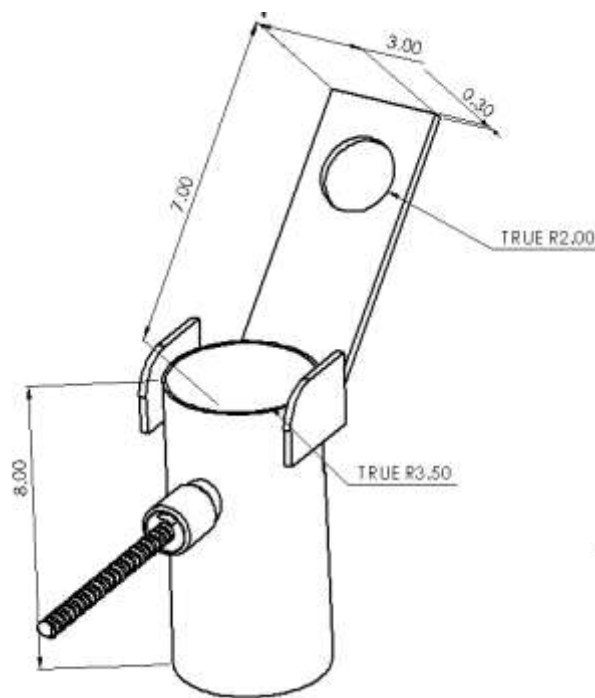


Figure 3.8: Dimensional Drawing of Welding Torch Holder

After designing the welding torch holder, its manufacturing was done using different operations. First, the drilling operation was performed on drilling machine. Two holes of equal size were drilled to allow the bolts to screw inside and hold the torch.

Secondly, the welding operation was performed using Shielded metal arc welding (SMAW). The metals strip was welded at an angle and hole within the strip was drilled to support the MIG wire feeder gun. At last surface finishing operation was done using hand grinder.

After performing all these operations welding torch holder was fabricated as shown in figure. 3.9



Figure.3.9: Fabricated Welding Torch Holder

Chapter 4
Selection of Welding Consumable
Multi-Attribute Decision Making
Approach (MADM)

SELECTION OF WELDING CONSUMABLE USING MULTI-ATTRIBUTE DECISION MAKING APPROACH (MADM).

4.1 Introduction

Pulse TIG is most commonly used arc welding technique for joining aluminum [1]. Due to its pin point control of heat input (narrow heat affected zone) and eco-friendly nature (no spatter and smoke) it has found various applications in joining not only similar aluminum alloys but also dissimilar aluminum alloys [2]. Dissimilar aluminum alloy joint of 5083-O and 6061-T651 is used in number of structural and load bearing applications like building's rooftops, multiple hull high speed ferries, diesel engine bases, pressure vessels or cargo oil tanks (for storage of liquefied petroleum gas along with piping system for transfer of gas or oil), chemicals in ships, cars body frame, valve stem and head, gun mount bases [2, 3]. These application requires the weld joint to withstand: direct mechanical loading, stresses caused by thermal gradients and thermal cycling. If the joint fails during service of these application, disastrous situation could arise which could lead to catastrophic consequences. In order to increase the service life of weld joint, it should have improved mechanical and chemical properties like impact toughness, strength, ductility, corrosion resistance. These desirable mechanical and chemical properties can be achieved by 1) Proper material selection like Filler Alloy, electrode, Shielding Gas from set of alternates and 2) Welding process parameter selection. Traditionally, when choosing a filler alloy, electrode and shielding gas experts usually use previous experimentation experience or test each alternates of filler alloy, electrode, shielding

gas separately. This not only increases the cost of experimentation but also becomes time taking process. This shortcoming can be overcome by adopting a multi-attribute decision making (MADM) model. The MADM approach usually employed in evaluation and selection problems where decisions involve set of alternatives and set of attributes. Various MADM approaches have been used for material selection problems. Although some researchers have used MADM approaches for selection of welding process and its consumables [100, 101] the literature available for material selection is very scant. Multi Criteria Decision Making (MCDM) methods are frequently used to find solution of uncertainty problems.

MCDM is a sub-discipline and full-developed branch of operations research that deals with designing mathematical and computational tools to support the subjective evaluation of a finite number of decision alternatives under a finite number of performance criteria by a single decision maker or by group. MCDM uses knowledge from many fields, including mathematics, behavioural decision theory, economics, and computer technology, and software engineering and information systems. Khrais et al. [102] uses MCDM tool to find suitable shielding gas for improved efficiency of weld joint.

These methods are classified into Multi-Objective Decision Making (MODM) and Multiple Attribute Decision Making (MADM) techniques. In MODM an alternative is optimized on the basis of prioritized objectives while in MADM technique the selection of best alternative is made from the available alternatives based on their prioritized attributes.

Various methods are developed based on MADM approach such as, Technique for order preference by similarity to ideal solution (TOPSIS) [103-105], Vlse

Kriterijumska Optimizacija I Kompromisno Resenje (VIKOR) [106-109], Elimination Et Choix Traduisant la REalite (ELECTRE) [110-112], Preference Ranking Organization Method for Enrichment Evaluation (PROMETHEE) [113], complex proportional assessment (COPRAS) [114, 115] and COPRAS-G [116], graph theory and matrix approach [117], preference selection index (PSI) method [118] and linear assignment method [119].

4.2 Methodology Adopted

Integrated AHP-TOPSIS method has been used to find best alternate from available alternates from each material (filler alloy, electrode and shield gas). AHP is used for assigning weights to each attribute and then these weights are used in TOPSIS process to determine the final ranking of best alternate from available alternates.

Analytical Hierarchy Process (AHP) method

It was developed by satty [120] to handle complex problems based on multiple criteria. AHP is a useful systematic tool with scale applicability in the field of science and technology [121]. The advantage of AHP over other methods is its flexibility and intuitiveness. It supports group decision making by determining the geometric mean of the individual pair wise comparisons. But it has the disadvantage that the problem has to be decomposed into a number of subsystems for pair wise comparisons which is not always feasible.

Steps in AHP

To determine the relative importance of different factors with respect to the objective following steps are followed.

The multiple pair-wise comparisons are based on a standardized comparison scale of nine levels (Table 4.1)

Table 4.1 Nine Point Intensity of Importance Scale [122, 123]

Relative importance (a_{ij}) Description (i over j)	
1	Equal importance
3	Moderate importance
5	Strong importance
7	Very strong importance
9	Absolute importance
2, 4, 6, 8	Intermediate values

Let $C = \{C_j | j = 1, 2, \dots, n\}$ be the set of criteria.

The result of the pair-wise comparison on n criteria can be summarized in an $(n \times n)$ evaluation matrix A . The every element a_{ij} ($i, j = 1, 2, \dots, n$) denotes the relative importance of factor i with respect to factor j . A criteria compared with itself is always assigned the value 1 so the main diagonal entries of the pair-wise comparison matrix are all 1.

Square matrix A containing every element a_{ij} is shown in Eq. (4.1).

$$A = \begin{pmatrix} 1 & a_{12} & \dots & a_{1m} \\ a_{21} & 1 & \dots & a_{2m} \\ \dots & \dots & \dots & \dots \\ a_{m1} & a_{m2} & \dots & 1 \end{pmatrix}, a_{ij} = 1/a_{ji}, a_{ji} \neq 0 \quad (4.1)$$

- The relative normalized weight (W_i) of each factor is evaluated by finding the geometric mean of i th row and normalizing the geometric means of rows in the comparison matrix.

$$GM_i = \{a_{i1} \times a_{i2} \times a_{i3} \times \dots \times a_{in}\}^{1/n}$$

And

$$W_i = \frac{GM_i}{\sum_{j=1}^n GM_j}$$

Matrix X is obtained to denote an n -dimensional column vector. The sum of the weighted values is computed for the importance degrees of alternatives, then $X=A*W$, where:

$$W = [W_1, W_2, W_3, \dots, W_n]^T$$

$$X = A * W = \begin{bmatrix} 1 & a_{12} & \dots & a_{1n} \\ a_{21} & 1 & \dots & a_{2n} \\ \dots & \dots & \dots & \dots \\ a_{n1} & a_{n2} & \dots & 1 \end{bmatrix} \begin{bmatrix} W_1 \\ W_2 \\ \dots \\ W_n \end{bmatrix} = \begin{bmatrix} C_1 \\ C_2 \\ \dots \\ C_n \end{bmatrix} \quad (4.2)$$

- The consistency values (CV) are calculated for the cluster of alternatives represented by the vector.

$$CV_i = \frac{C_i}{W_i}$$

- The largest eigen value λ_{max} is obtained which is the mean of the consistency values.
- The consistency index (CI) is calculated by

$$CI = \frac{\lambda_{max} - n}{n - 1}$$

The AHP output quality is strictly related to the consistency of the pair wise comparison judgements.

- The random index (*RI*) is obtained for the number of factors being used in decision making (Table 4.2)

Table 4.2: Random Index (*RI*) Values [124]

Criteria	RI	Criteria	RI
3	0.52	7	1.35
4	0.89	8	1.40
5	1.11	9	1.45
6	1.25	10	1.49

- The final consistency ratio (*CR*) is calculated as the ratio of the *CI* and *RI*

$$CR = \frac{CI}{RI} \quad (4.3)$$

The acceptable upper limit for *CR* is 0.1. The evaluation process has to be repeated to improve the consistency, if the final consistency ratio exceeds this value.

This consistency check is essential to establish the validity of the pair wise comparison matrix evaluation.

TOPSIS method

TOPSIS method has received lot of attention in the field of material selection. Khorshidi et al. [125] used TOPSIS for selecting the optimal refinement condition to achieve maximum tensile property in Al-15%Mg₂Si composite. Mirhedayatian et al. [126] used TOPSIS approach and integrated fuzzy data envelopment analysis in

welding process selection for repairing nodular cast iron engine block. Jafarian and Vahdat [101] used fuzzy AHP-TOPSIS for selection of welding process for high pressure vessel manufacturing. Chatterjee et al. [127] used VIKOR and ELECTRE methods to find the relative ranking of candidate materials by simultaneously considering their respective properties. Although ELECTRE methods generate good output, they still have certain drawbacks. As the number of alternatives increases, the computational procedure becomes more complex and elaborate. Also, ELECTRE methods only provide rank of each material but do not give any numerical value.

The VIKOR and TOPSIS method use different aggregation functions and normalization process. VIKOR method uses linear normalization whereas TOPSIS method uses vector normalization. Finding the optimal point in the VIKOR is based on the measure of closeness to positive ideal solution. Therefore it is more suitable in the circumstances in which the risk of the decisions is less important to the decision maker and maximum profit is the priority.

TOPSIS is a good choice for material selection as it is a relatively more systematic process. It is useful for both qualitative and quantitative data. It gives the output with a numerical value that provides the better understanding of differences and similarities among the alternatives.

TOPSIS method is employed to find the best alternative in the present work. It was first proposed by Hwang and Yoon [103].

The methodology comprises of calculating the Euclidean distance of the given alternative from the positive and the negative ideal solution respectively. The concept

is that the best possible alternative will be the one which is closest to the positive ideal solution and the farthest from the negative ideal solution.

Steps in TOPSIS

TOPSIS method consists of the following steps as shown in figure 4.1

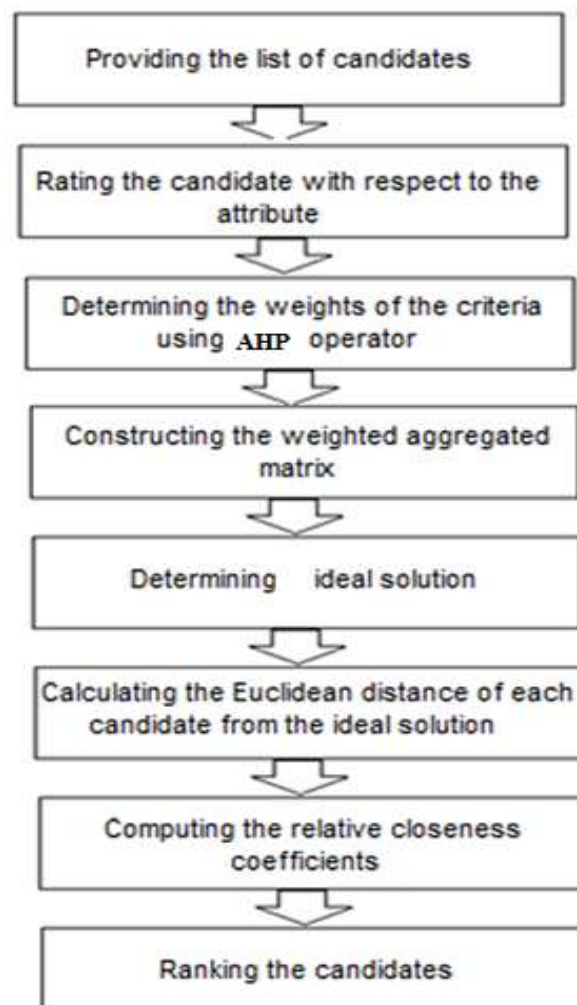


Figure 4.1: TOPSIS Method [103]

Step 1: Construction of the normalized decision matrix

The Euclidean length of a vector, the element r_{ij} of the normalized decision matrix R is evaluated using the following transformation

$$r_{ij} = \frac{X_{ij}}{\sqrt{\sum_{i=1}^m (X_{ij})^2}}$$

$$j = 1, 2, \dots, n; i = 1, 2, \dots, m; \quad (4.4)$$

Here, r_{ij} is the normalized preference measure of the i th alternative. ‘ m ’ is the number of alternatives, ‘ n ’ is the number of criteria

Step 2: Construction of the weighted normalized decision matrix

Multiply the columns of the normalized decision matrix with the set of weights

$W = (w_1, w_2, w_3, \dots, w_n)$ to obtain weighted normalized decision matrix:

$$V = RW = \begin{pmatrix} w_1 \cdot r_{11} & w_2 \cdot r_{12} & \dots & w_n \cdot r_{1n} \\ w_1 \cdot r_{21} & w_2 \cdot r_{22} & \dots & w_n \cdot r_{2n} \\ \cdot & \cdot & & \cdot \\ \cdot & \cdot & & \cdot \\ w_1 \cdot r_{m1} & w_2 \cdot r_{m2} & \dots & w_n \cdot r_{mn} \end{pmatrix} \quad (4.5)$$

Step 3: Determination of the ideal and negative- ideal solutions

The ideal solution and negative ideal solution value sets are determined, respectively as follows:

$$\{V_1^+, V_2^+, \dots, V_n^+\} = \left\{ \left(\max_i V_{ij} \mid J \in K \right), \left(\min_i V_{ij} \mid J \in K' \right) \mid i = 1, 2, \dots, m \right\} \quad (4.6)$$

$$\{V_1^-, V_2^-, \dots, V_n^-\} = \left\{ \left(\min_i V_{ij} \mid J \in K \right), \left(\max_i V_{ij} \mid J \in K' \right) \mid i = 1, 2, \dots, m \right\} \quad (4.7)$$

Where,

$$K = \{j = 1, 2, 3, \dots, n \text{ and } j \text{ is associated with benefit criteria}\}$$

$$K' = \{j = 1, 2, 3, \dots, n \text{ and } j \text{ is associated with cost criteria}\}$$

Step 4: Measurement of separation distances from ideal and negative ideal solutions.

Euclidean distances for each alternative are, respectively calculated as:

$$S_i^+ = \left\{ \sum_{j=1}^n (V_{ij} - V_j^+)^2 \right\}^{1/2}, i = 1, 2, \dots, m \quad (4.8)$$

$$S_i^- = \left\{ \sum_{j=1}^n (V_{ij} - V_j^-)^2 \right\}^{1/2}, i = 1, 2, \dots, m \quad (4.9)$$

Step 5: Calculation of the relative closeness to the idea solution. The relative closeness to the ideal solution can be defined as:

$$C_i = \frac{S_i^-}{S_i^+ + S_i^-}, i = 1, 2, \dots, m; 0 \leq C_i \leq 1 \quad (4.10)$$

The higher the closeness means better the rank.

Step 6: Ranking of the preference order

The preference order is ranked on the basis of the order of C_i . Hence, the best alternative is the one which is nearer to the ideal solution and farther to the negative ideal solution

Figure 4.2 below shows flow chart depicting integrated AHP-TOPSIS methodology for consumable material selection

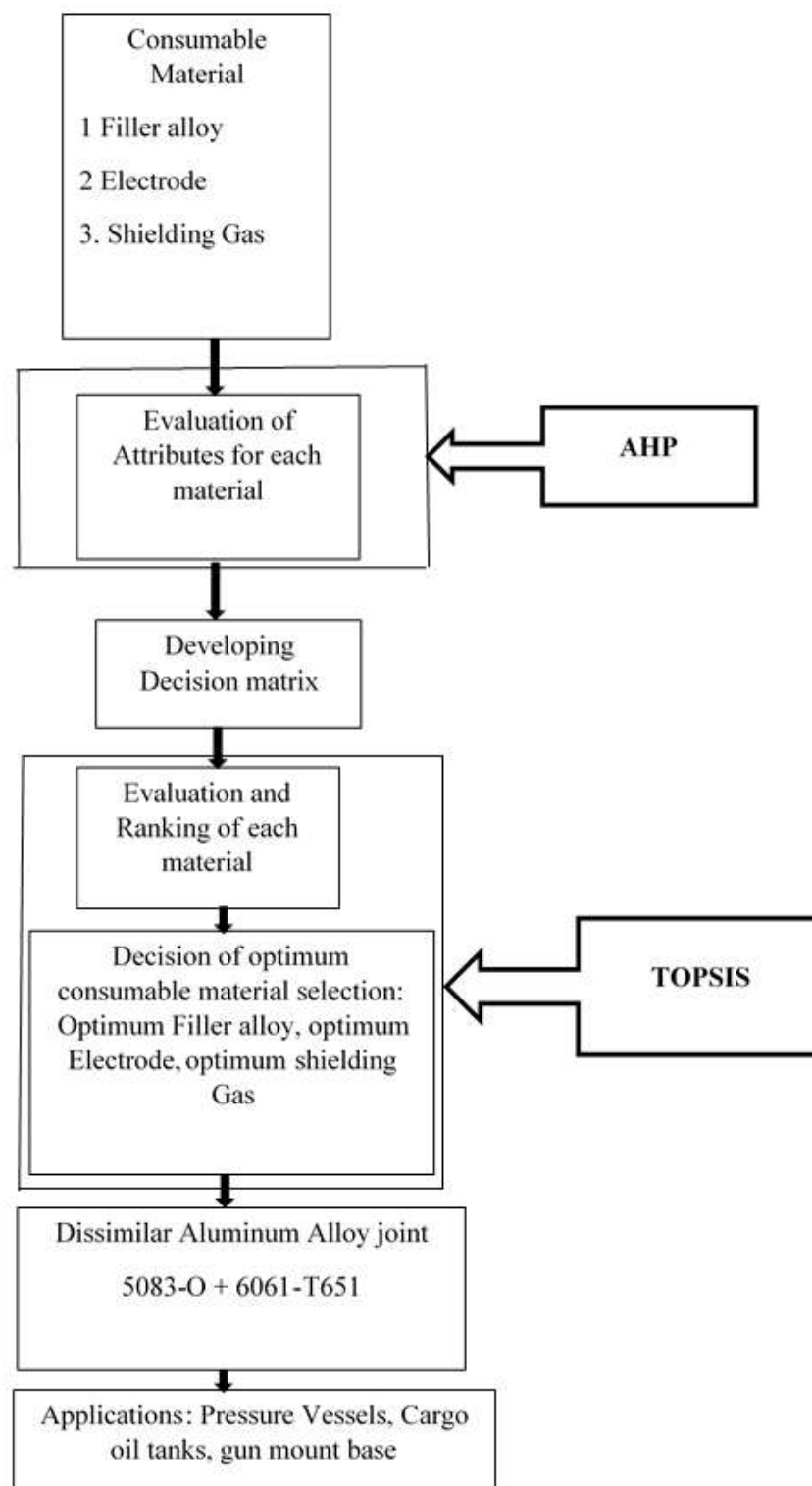


Figure 4.2: Flow Chart Depicting Integrated AHP-TOPSIS Methodology for Material Selection

4.3 Filler Alloy

Selection of appropriate filler is an important aspect for arc joining of not only for similar aluminum alloys but also for dissimilar aluminum alloys [70]. Welding consumable like filler alloy used has to be appropriate and matching with the base alloy chemical composition. The need for matching filler metals is dependent upon joint type and loading condition. Most of the defects like porosity, solidification cracking in fusion welding process especially in Pulse TIG occurs due to improper filler alloy selection. Selection of suitable filler not only depends on mechanical properties but also on the microstructural characteristics required in the weldment for particular application. When welding dissimilar combination of 5xxx and 6xxx such careful selection becomes more important as the formation of intermetallic compound formed indicate brittle behavior resulting lower ductility [71-73, 128]. The required strength, toughness, ductility, corrosion resistance, sensitivity to cracking, low temperature service capability or colour match for anodising are dominant factor in deciding which filler to use for particular application. Various charts [129-133] are used for selection of filler alloy for different aluminum alloy combinations even they recommend various filler options (alternates) for joining same combination of aluminum alloy. As per the claim, they have made chart according to the common understanding that tensile strength of filler used should be matching as that of base metal. This is practically not possible, matching tensile strengths often do not result in matching yield strength because the yield-to-tensile ratio for most aluminum is lower than that of as deposited welds. This could lead to either overmatching or undermatching properties of weld and base metal. While overmatching properties may not be the economical choice, undermatching properties could lead to failure of

components where higher yield to tensile ratio is expected, examples include components in buildings subject to inelastic deformations in large earthquakes, roll over protection devices on construction equipment [134]. Under these conditions where yielding is expected, it is preferred that such deformations be distributed throughout the base metal. For that to happen the properties of as deposited weld should match base metal properties. Filler alloy selected should be such that it should have properties which is according to the required properties for particular application and it should also have the properties so that as deposited weld properties should match with the base metal properties , so that uniform distribution of properties throughout the weldment. MADM is the technique used to select best filler alloy based on closely distinguished properties (attributes).

Available material and their relevant properties

Though different application demands different properties, but type of joint and loading condition determines choice of filler material and ultimately weld strength. Generally most of the applications require mechanical properties of filler to be passed to required weld joint applications. Absence of any one of these properties could lead to weld failure. Selection of suitable filler for structural applications depends upon following properties.

➤ **Yield Strength:** Yield point generally represents upper limit of load in designs, its knowledge is vital for designing the components of weld joint in structures. High yield strength is required for applications where inelastic deformation could lead to failure. Filler alloy selected should have higher yield strength than base metal so that properly executed weld will become stronger relatively to base metal. Structural designs of ships, stadium roof tops, car bodies of Audi 8, Jaguar have required yield strength [1, 2].

- **Tensile Strength:** It is also known as permanent deformity strength. In applications where groove weld joint is required, the tensile strength of the weld is critical as the weld is usually stressed in tension. When welding aluminum, fabricators rarely obtain a weld that is as strong as the base metal. Carefull selection of filler alloy is required which have minimum tensile strength in groove welds that will meet the as-welded strength of base metal.
- **Percent Elongation:** It represents the ductile behaviour of weldment. Buildings subject to inelastic deformation during large earthquake requires ductile property. Increased ductility rating of filler alloy indicate greater ability to deform plastically and redistribute load and thereby decrease the crack propagation sensitivity. This characteristics also be considered when forming operations are to be used on completed weldment.
- **Brinell Hardness:** Higher hardness leads to higher resistance to plastic deformation. This property is required in structural pipe and tubes. Aluminum hardness can be improved by addition of magnesium as alloying element required specially in of aircraft body structure. Careful selection of 5xxx series filler alloy should be done to maintain the magnesium content less than 3 % so that weld failure due to stress corrosion cracking (SSC) do not take place when exposed to prolonged elevated temperature; (150°F to 350°F).
- **Cost:** The goal of fabrication of weld is to produce the weldment at low cost. The economics of weldment should be lower for low cost structural manufacturing. Therefore selection of filler alloy for required applications should have low cost, so that more economical fabrication of weld joint could be done of course without compromising on properties required by application.
- **Longitudinal Shear Strength:** It is the shear strength of weld which is required when weld usually stressed in parallel direction to the longitudinal axis of the weld. In

case of I-beam section joints in bridge structures, fillet welds are usually not diluted significantly by the base metal as heat affected zone in groove welds therefore, filler alloy used mainly determines shear strength of as welded joint.

➤ **Transverse Shear Strength:** In lap or fillet welds, shear strength of weld is critical since the weld usually stressed in shear in direction perpendicular to the longitudinal axis. Honey comb structures is the application where fillet weld is loading conditions are in transverse direction of joint.

➤ **Impact Strength:** This rating applies to the ability of an aluminum weldment to deform plastically in the presence of stress raisers without low-energy initiation and propagation of cracks therefore filler alloy selected should contain excellent impact toughness as required in structural designs in cryogenic process plants, gun mount bases, diesel engine bases, LPG storage tanks, oil tanks, pressure vessels where protection against cracking of weld is prime consideration.

Table 4.3 shows the list of attributes

Table 4.3: List of Attributes for Selection of Filler Alloy

Attributes	
A ₁	Yield Strength
A ₂	Tensile Strength
A ₃	Percentage Elongation
A ₄	Brinell Hardness
A ₅	Cost
A ₆	Longitudinal Shear Strength
A ₇	Transverse Shear Strength
A ₈	Impact Strength

Some researchers [142] have used different filler alloys like ER 5356, ER 5556, ER 5183, ER 5654, ER4043 for dissimilar aluminum alloy combination 5083-O and 6061-T651 where the application demands low temperature service duty i.e less than 150 °F. Filler Charts [143-146] indicates use of filler alloys ER 5356, ER 5556, ER 5183, ER 5654, ER

5554 for joining of dissimilar aluminum alloy combination of 5083 and 6061 aluminum alloys for extrusion applications. Mutombo [135] has used three filler alloys namely 4043, 5356, 5183 for joining dissimilar combination of 5083 and 6061 aluminum alloy to study the corrosion fatigue behavior in saline environment created by 3.5 % NaCl solution. Table 4.4 welding filler alloys which are identified from literature for joining dissimilar aluminum alloy 5083-O and 6061-T651.

Table 4.4: Welding Filler Alloys Identified (from literature) for Joining Dissimilar Aluminum Alloy 5083-O and 6061-T651

Candidates	Welding filler alloys
C ₁	ER 5356
C ₂	ER 5556
C ₃	ER 5183
C ₄	ER 5654
C ₅	ER 5554

Figure 4.3 depicts hierarchical structure for suitable filler selection

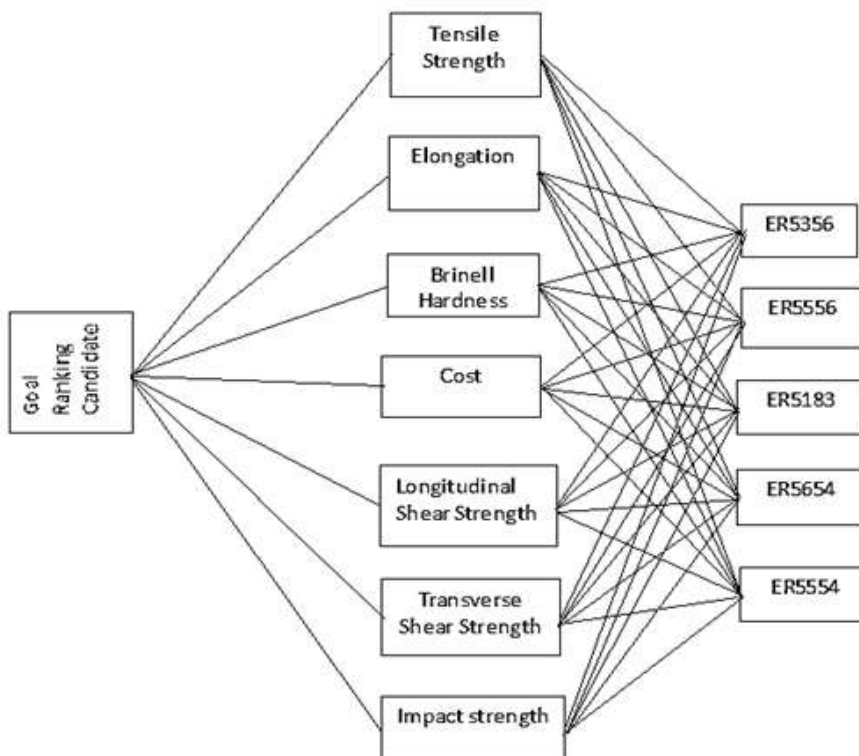


Figure 4.3: Hierarchical Structure for Suitable Filler Selection

4.4 Electrode

There are several variables in electrode to consider in a welding procedure which affects the weld quality. Electrode geometry which affects the arc shape (thereby affecting the weld bead size and shape), the weld penetration, and point longevity of the electrode and composition of electrode which affecting arc start ability, electrode life, and contamination resistance. Different electrode material (percentage of other material oxide by weight in tungsten electrode composition) possess different characteristics which determines welding performance [136]. The proper electrode material to use for an application depends on many variables, including type of weld, the composition of material being welded, the amperage level, among other factors. However, because of many variables present the best way to determine which material is best suited for particular application is through testing which is often the method suggested and followed by many researchers [137], but it is not possible in case of large welded structures where testing each electrode material will have large bearing on cost of manufacturing. MADM approach is used to select suitable arc electrode material best suited for certain applications.

Available materials and properties

In structural application of chemical process plants (orbital tube and pipe welding), roof tops of stadiums and buildings where slight initiation of crack could lead to its propagation on complete structure that could result in catastrophic failure, so such should be the quality of weld joint that it could bear stresses under heavy loading also. Electrode material (oxides) plays an important role in quality fabrication of joint [73] as it improves arc stability and arc starting, which ultimately results in improved mechanical properties of joint. Selection of oxide material of Electrode becomes important as each oxide has unique

characteristics (attributes) that effect electrode performance and hence joint mechanical properties. According to application each characteristics value decide which arc electrode to be selected for which applications. These attributes are:

- **Electrode Work function:** It is measured in electron volts (eV). More the oxide added to electrode, lower will be the work function and lower the voltage necessary to strike an arc, thus easier arc starts. Lower work function decreases grain growth and provide constant flow of oxides and thus increases service life.
- **Density:** Higher the density of grains in electrode, smaller will be the grain size, the better the oxide migrate to the tip. Smaller grains produce more paths and due to this oxides can more easily migrate to the tip thus increases current capacity. Each arc oxide of electrode material have different densities which depend upon the required joints in particular applications.
- **Volume % of 2 % weight of electrode:** 2 % by weight of electrode material means, it will have different amount of oxides by volume in electrode. Amount of oxide in given area should remain same which depends upon effective size of grains same while maximizing the homogeneity of oxide distribution and maintaining the proper quantity of oxide throughout the arc electrode. Uneven distribution results in poor performance as areas with little or no oxides will tend to suffer from grain growth, whereas areas with too much oxide will tend to create hindrance and thus decreases mobility.
- **Melting point:** At elevated temperature during welding, the rate of melting of electrode increases which accelerates its consumption. Higher melting point of electrode material lesser will be burn-off rate thus increases service life.
- **Electron Negativity:** Higher the electronegativity of atom of oxide material in electrode, lesser will be the force of attraction between electron and nucleus of atom of oxide, least will be the tendency of atom of oxide to attract electrons

towards its nucleus, easier for the electron move itself, which increases electron mobility thus higher electron emission easier will be arc starting.

- **Cost:** The foremost purpose of fabrication is to produce the joint with low expenditure. Selection of electrode material which is a part of weld joint fabrication procedure makes the weld more economical by selecting electrode material which is well suited for most applications.
- **Particle size:** Particle size or grain size determines migration and evaporation rate. Smaller size grains increases migration rate as large paths are created for oxide to move to the tip. Slower migration than evaporation rate lowers the mobility of oxide at the tip of electrode to maintain consistent arc resulting in lower performance whereas slower evaporation rate than migration rate triggers the oxide accumulation at a point thus blocking passage for other oxides to move to the tip decreasing performance of electrode. Thus optimum good migration and evaporation rate values of electrode material should be selected to have good performance and increased service life of electrode.

Table 4.5 contains the list of attributes

Table 4.5: List of Attributes for Electrode Selection

	Attributes
A ₁	Electrode Work function
A ₂	Density
A ₃	Volume % of 2 % by weight of electrode
A ₄	Melting point
A ₅	Electron Negativity
A ₆	Cost
A ₇	Particle size

Various electrode material like ceriated ,lanthanated, thoriated, zirconiased around 2 % are used in TIG welding of similar and dissimilar aluminum alloys [138, 139]. The

Table 4.6 shows the electrode for pulse TIG welding of dissimilar aluminum alloy 5083-O and 6061-T651.

Table 4.6: Electrode for Pulse TIG Welding of Dissimilar Aluminum Alloys 5083-O and 6061-T651

Candidates	Welding Electrode
C ₁	Pure Tungsten
C ₂	2 % Thoriated
C ₃	2 % Ceriated
C ₄	1.5 % Lathanated
C ₅	0.8 % Zirconiated

Figure 4.4 represents hierarchical structure for electrode selection

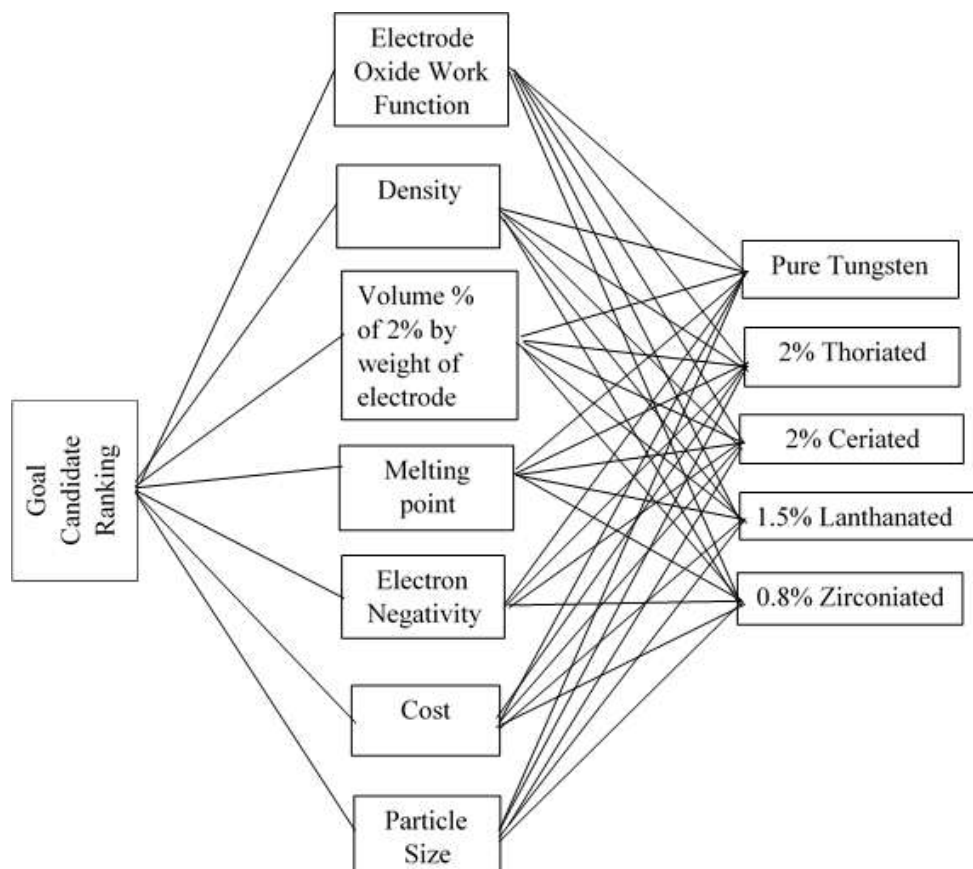


Figure 4.4: Hierarchical Structure for Electrode Selection

4.5 Shielding Gas

The main function of shielding gas is to protect the molten weld metal from atmospheric contamination. In addition to its shielding function, each gas mixture has unique physical properties [140] that can have major effect on welding speed, penetration, weld appearance and shape which ultimately effects the mechanical properties [141]. The change in shielding gas composition is usually considered an essential variables in most qualified welding procedures. The composition of gas is tailored to meet the process, material and application requirement. Therefore the selection of shielding gas becomes quite complex due to many combination available for most common structural applications. Selection of shielding gas composition must be based on knowledge of physical, thermal, chemical properties on which characteristics of suitable shielding gas depends which is required in accordance with welding procedures for certain specific applications .

Available material and properties

Weld metal properties according to application are primarily controlled by the composition of the gas. Selection of suitable composition or gas blend depends upon the properties (attributes) which effects the effectiveness of gas. These attributes effects metal transfer, wetting behavior, penetration, travel speed, arc starting which effects the mechanical properties of weldment in most application [142]. These attributes are:

- **Thermal Conductivity:** Thermal conductivity of a gas is its ability to conduct heat. Thermal properties considerably influences travel speed [143] which effects weld penetration profile in weld fusion area. It influences the radial heat

loss from the center to the periphery of the arc column. Gas with low thermal conductivity, produces an arc which has two zones a narrow hot core and considerably cooler outer zone creating narrow weld root and wider top. On other hand, a gas which has a high thermal conductivity conducts more of the heat outward from the core, resulting in a wider, hotter arc core.

- **Gas Density:** Gas density is one of the chief factors influencing effectiveness of shielding gas. Flow rate of gas which have considerable effect on weld metal properties [144, 145] depends on gas density. Gases heavier than air blanket the weld and require lower flow rates than gases lighter than air.
- **Specific Gravity:** It determines the heat content of gas. Specific gravity influences metal transfer modes which effected by interfacial energy (surface tension) of molten metal and inert atmosphere and ultimately effecting mechanical properties of weld.
- **Ionization Potential:** It is the energy (eV) necessary to remove an electron from a gas atom. Arc starting and arc stability are largely depend on the ionization potential of the shielding gas selected [146]. Gases with relatively low ionization potential give up electrons more easily, helping to initiate and maintain the arc in a stable operating condition.
- **Cost:** Decision for selection of shielding gas is made on the cost of best suited gas, It is the goal of fabrication to achieve economics in weld, as to decrease the overhead cost per unit weld, shielding gas which is the part of welding procedure to fabricate the weld joint needed to be at lower cost [147-148].
- **Specific Heat Capacity:** Heat capacity of the gas is greater if the heat is supplied at constant pressure. Specific heat capacity has significant effect on metallurgical structure, properties, soundness of weld and heat treatment response [149].

List of attributes are shown in table 4.7

Table 4.7: List of Attributes for Selection of Shielding Gas

Attributes	
A ₁	Thermal Conductivity
A ₂	Gas Density
A ₃	Specific Gravity
A ₄	Ionization Potential
A ₅	Cost
A ₆	Specific Heat Capacity

Researchers [154] have used different chemical composition of argon and helium mixture. Alternating shielding gas has been applied to used in TIG welding process of joining similar and dissimilar aluminum alloys [153, 160]. Table 4.8 shows shielding gas alternates used for pulse TIG welding of 5083-O and 6061-T651 aluminum alloy.

Table 4.8: Shielding Gas Alternates used for Pulse TIG Welding of 5083-O and 6061-T651 Aluminum Alloy

Candidate	Shielding gas
C ₁	Pure Argon
C ₂	Pure Helium
C ₃	25 % Argon + 75 % Helium
C ₄	75 % Argon + 25 % Helium
C ₅	50 % Argon + 50 % Helium

Figure 4.5 represents the hierarchical structure for selection of shielding gas

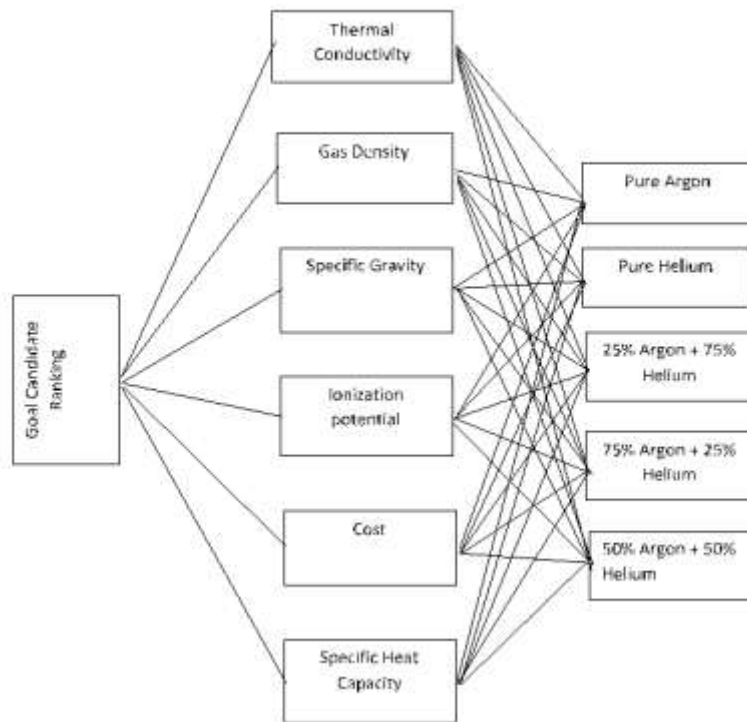


Figure 4.5: Hierarchical Structure for Selection of Shielding Gas

4.6 Result

These weights of all attributes of respective consumables are evaluated using AHP method and the results are presented in Table 4.9

Table 4.9: Consumable Material Weights

Attributes	Filler Alloy Weights	Electrode Weights	Shielding Gas Weights
A ₁	0.0326	0.0311	0.0428
A ₂	0.0235	0.0447	0.1006
A ₃	0.0476	0.1586	0.1595
A ₄	0.1059	0.1036	0.0640
A ₅	0.3313	0.2399	0.2504
A ₆	0.1572	0.3542	0.3824
A ₇	0.2306	0.0675	
A ₈	0.0709		

4.6.1 Computational Results for Selection of Filler Alloy

Table 4.10 shows alternates of filler alloy and their attributes

Table 4.10 Alternates of Filler Alloy and their Properties (Attributes)[1,2, 142,144-146]

Properties	ER5356	ER5556	ER5183	ER5654	ER5554
1. Yield Strength (MPa)	268.89	158.579	296.47	227.52	124.10
2. Tensile Strength (MPa)	240	317.15	275	220.63	186
3. Elongation 2%	17	14	17	17	8
4. Brinell Hardness (HB) (@load 500 Kg; thickness 10:ohm)	105	65	99	83	39
5. Cost (\$)	13.5	16	15.5	17.2	13
5. Longitudinal Shear Strength (MPa)	117.21	137.89	127.55	82.73	79.289
7. Transverse Shear Strength (MPa)	179.26	206.84	193.05	124.10	103.42
8. Impact Strength (J)	18.2	15.7	16	13	10

The normalized decision matrix for filler alloy, electrode, shielding gas is calculated using Equation (4.1) as shown in matrices (4.11)

$$\begin{bmatrix} 0.5351 & 0.4262 & 0.5064 & 0.5740 & 0.3994 & 0.4702 & 0.4821 & 0.5401 \\ 0.3156 & 0.5632 & 0.4170 & 0.3553 & 0.4734 & 0.5531 & 0.5562 & 0.4659 \\ 0.5900 & 0.4884 & 0.5064 & 0.5412 & 0.4586 & 0.5116 & 0.5191 & 0.4748 \\ 0.4528 & 0.3918 & 0.5064 & 0.4538 & 0.5089 & 0.3318 & 0.3337 & 0.3858 \\ 0.2470 & 0.3303 & 0.2383 & 0.2132 & 0.3846 & 0.3180 & 0.2781 & 0.2967 \end{bmatrix} \quad (4.11)$$

A weighted normalized decision matrix for filler alloy is presented in matrices (4.12)

$$\begin{bmatrix} 0.0174 & 0.0100 & 0.0241 & 0.0608 & 0.1323 & 0.0739 & 0.1112 & 0.0427 \\ 0.0103 & 0.0132 & 0.0199 & 0.0376 & 0.1568 & 0.0869 & 0.1283 & 0.0368 \\ 0.0192 & 0.0115 & 0.0241 & 0.0573 & 0.1519 & 0.0804 & 0.1197 & 0.0375 \\ 0.0148 & 0.0092 & 0.0241 & 0.0481 & 0.1686 & 0.0522 & 0.0770 & 0.0305 \\ 0.0081 & 0.0078 & 0.0113 & 0.0226 & 0.1274 & 0.0500 & 0.0641 & 0.0234 \end{bmatrix} \quad (4.12)$$

Ranking Results

Figure 4.6 depicts histogram which shows ranking of alternates of filler alloy

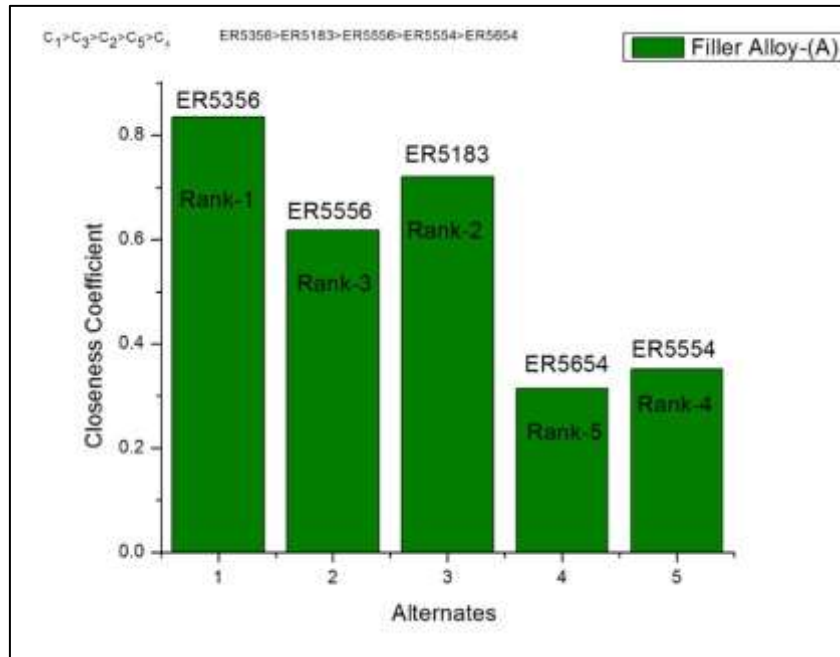


Figure 4.6: Histogram Depicting Ranking of Alternates of Filler Alloy

Figure 4.7 depicts Pie-chart which shows ranking percentage of alternates of filler alloy

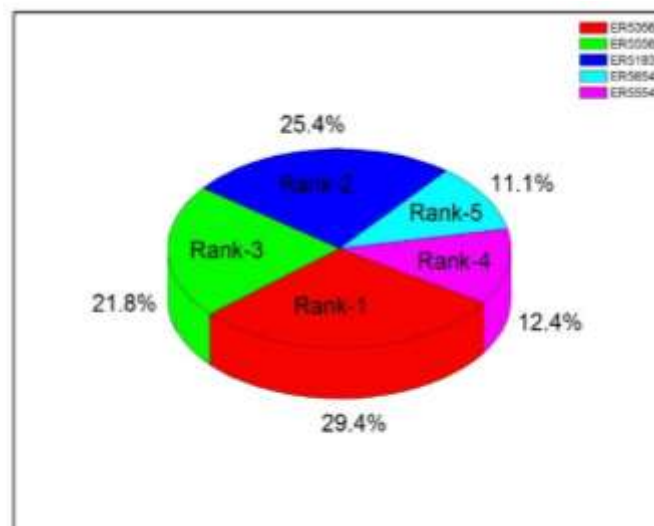


Figure 4.7: Pie-chart Depicting Ranking Percentage of Alternates of Filler Alloy

4.6.2 Computational Results for Electrode

Table 4.11: Alternates of Electrode and their Properties (Attributes)[149-151]

Properties	Pure Tungsten	2%Thoriated	2%Ceriated	1.5% Lanthanated	0.8%Zirconiated
1. Electrode Oxide Work Function (eV)	0.01	2.6	3.2	2.5	0.3
2. Density (g/cm ³)	19.25	11.72	6.65	5.7	6.49
3. Volume% of 2% weight of electrode	6	3.8	5.2	5.7	6.9
4. Melting Point (°C)	3410	1750	795	826	1852
5. Electron negativity (according to pauling)	1.7	1.3	1.0	1.1	1.2
6. Cost (\$)	23.99	14.99	18.4	23.99	20.3
7. Particle Size (Nm)	30	50	40	20	30

The normalized decision matrix for electrode is calculated using Equation (4.2) as shown in matrices (4.13)

$$\begin{bmatrix} 0.0021 & 0.7691 & 0.4781 & 0.7735 & 0.5927 & 0.5203 & 0.3780 & 0.5401 \\ 0.5383 & 0.4682 & 0.3028 & 0.3970 & 0.4533 & 0.3251 & 0.6300 & 0.4659 \\ 0.6625 & 0.2657 & 0.4143 & 0.1803 & 0.3487 & 0.3990 & 0.5040 & 0.4748 \\ 0.5176 & 0.2277 & 0.4542 & 0.1874 & 0.3835 & 0.5203 & 0.2520 & 0.3858 \\ 0.0621 & 0.2593 & 0.5498 & 0.4201 & 0.4184 & 0.4403 & 0.3780 & 0.2967 \end{bmatrix} \quad (4.13)$$

A weighted normalized decision matrix for filler alloy, electrode, shielding gas is presented in matrices (4.14)

$$\begin{bmatrix} 0.0001 & 0.0344 & 0.0755 & 0.0797 & 0.1417 & 0.1842 & 0.0255 & 0.0427 \\ 0.0167 & 0.0209 & 0.0478 & 0.0409 & 0.1083 & 0.1151 & 0.0425 & 0.0368 \\ 0.0206 & 0.0119 & 0.0655 & 0.0186 & 0.0833 & 0.1413 & 0.0340 & 0.0375 \\ 0.0161 & 0.0102 & 0.0718 & 0.0193 & 0.0917 & 0.1842 & 0.0170 & 0.0305 \\ 0.0019 & 0.0116 & 0.0869 & 0.0433 & 0.1000 & 0.1558 & 0.0255 & 0.0234 \end{bmatrix} \quad (4.14)$$

Ranking Results

Figure 4.8 represents histogram which depicts the ranking of alternates of electrode

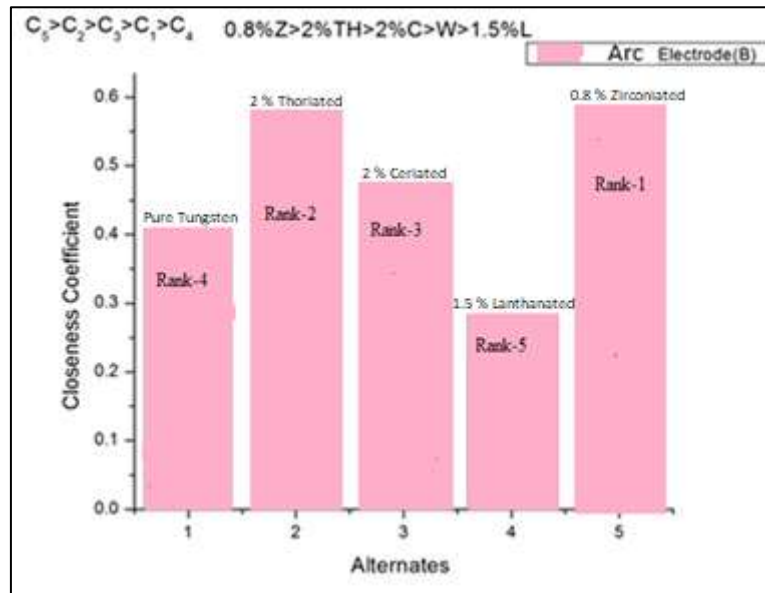


Figure 4.8: Histogram Depicting Ranking of Alternates of Electrode

Figure 4.9 shows the pie-chart which depicting the ranking percentage of alternates of electrode

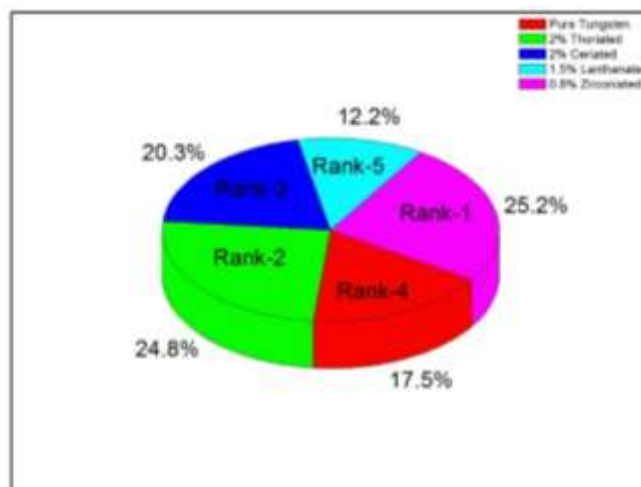


Figure 4.9: Pie-chart Depicting Ranking Percentage of Alternates of Electrode

4.6.3 Computational Results for Shielding Gas

Table 4.12 depicts alternates of shielding gas and their properties

Table 4.12: Alternates of Shielding Gas and their Properties (Attributes)[153-160]

Properties	Pure Argon	Pure Helium	25%Argon+75%Helium	75%Argon+25%Helium	50%Argon+50%Helium
1. Thermal Conductivity W/mK at (1.013 bar at 0°C)	0.016	0.1513	0.1174	0.0498	0.0836
2. Gas density (lb/wft) at 0°C, 1 atm	0.1114	0.0111	0.0361	0.0863	0.0612
3. Specific gravity (g/cm ³) Air=1	1.38	0.1368	0.4476	1.0692	0.7584
4. Ionization potential (eV)	15.7	24.5	22.3	17.9	20.1
5. Cost (per100g) (\$)	0.5	5.2	4.025	1.675	4.15
6. Specific Heat capacity at (kJ/Kg.K C _p (1.013 bar and 25°C)	0.520	5.19	4.0225	1.6875	2.855

The normalized decision matrix for shielding gas is calculated using Equation (4.2) as shown in matrices (4.15) respectively

$$\begin{bmatrix} 0.0743 & 0.7042 & 0.7041 & 0.3452 & 0.0705 & 0.0627 \\ 0.7024 & 0.0702 & 0.0698 & 0.5387 & 0.7038 & 0.6525 \\ 0.5450 & 0.2282 & 0.2284 & 0.4903 & 0.5455 & 0.5050 \\ 0.2312 & 0.5455 & 0.5455 & 0.3936 & 0.2288 & 0.2102 \\ 0.3881 & 0.3869 & 0.3869 & 0.4420 & 0.3871 & 0.5207 \end{bmatrix} \quad (4.15)$$

A weighted normalized decision matrix for shielding gas is presented in matrices (4.16)

$$\begin{bmatrix} 0.0032 & 0.0708 & 0.1123 & 0.0221 & 0.0177 & 0.0240 \\ 0.0301 & 0.0071 & 0.0111 & 0.0345 & 0.1762 & 0.2495 \\ 0.0233 & 0.0230 & 0.0364 & 0.0314 & 0.1366 & 0.1931 \\ 0.0099 & 0.0549 & 0.0870 & 0.0252 & 0.0573 & 0.0804 \\ 0.0166 & 0.0389 & 0.0617 & 0.0283 & 0.0969 & 0.1991 \end{bmatrix} \quad (4.16)$$

Ranking results

Figure 4.10 depicts histogram which shows ranking of alternates of shielding gas

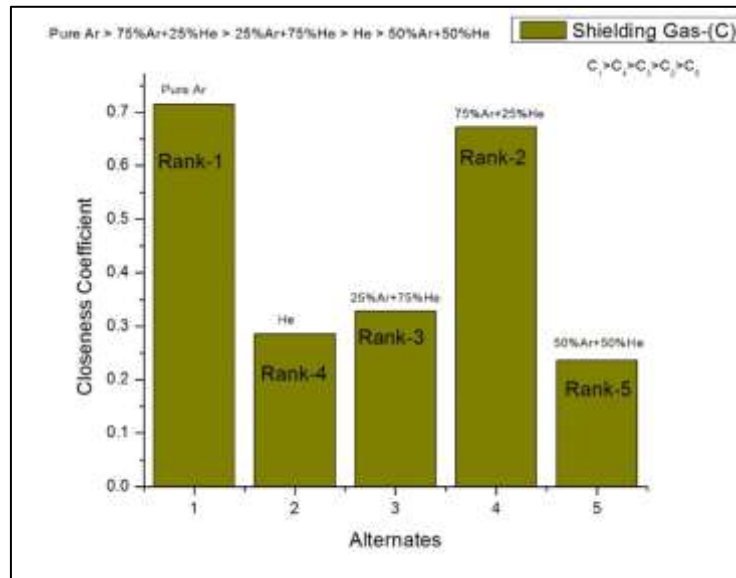


Figure 4.10: Histogram Depicting Ranking of Alternates of Shielding Gas

Figure 4.11 depicts pie-chart which shows percentage ranking of alternates of shielding gas

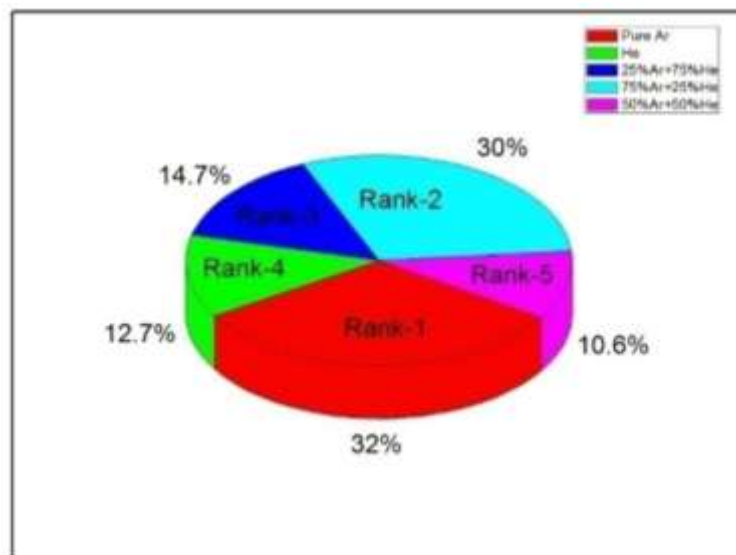


Figure 4.11: Pie-chart Depicting Percentage Ranking of Alternates of Shielding Gas

4.6.4 Analysis of Ranking Results

The relative closeness to the ideal solution hence can be found using equation (4.7).

The ranks are assigned based on their 'C' values and are given in Table 4.13. The larger the value of closeness the better is the rank

Table 4.13 Ranks Based on C Values

Filler Alloy	Electrode			Shielding gas		
	Alternates	C _i	Rank	Alternates	C _i	Rank
ER 5356 (C ₁)	Pure Tungsten (C ₁)	0.8358	1	Pure Argon (C ₁)	0.7149	1
	2% Thoriated (C ₂)	0.6184	3	Pure Helium (C ₂)	0.2850	4
	2% Ceriated (C ₃)	0.7205	2	25% Argon+75% Helium (C ₃)	0.3280	3
ER 5654 (C ₄)	1.5% Lanthanated (C ₄)	0.3142	5	75% Argon+25% Helium (C ₄)	0.6719	2
	0.8% Zirconiated (C ₅)	0.3516	4	50% Argon+50% Helium (C ₅)	0.2363	5

It can be concluded from Table 4.13, filler alloy; ER5356 has the highest ranking followed by ER 5183 while ER 5654 is the least ranked material. In arc electrode selection problem the optimum arc electrode is 0.8 % Zirconiated electrode is best alternate as it has slightly higher “C” value than 2% thoriated electrode. Shielding gas analysis results indicate pure Argon as the optimum consumable component closely followed by Ar-He gas blend as second best alternative.

Figure 4.12 shows the plots for best consumable material selection

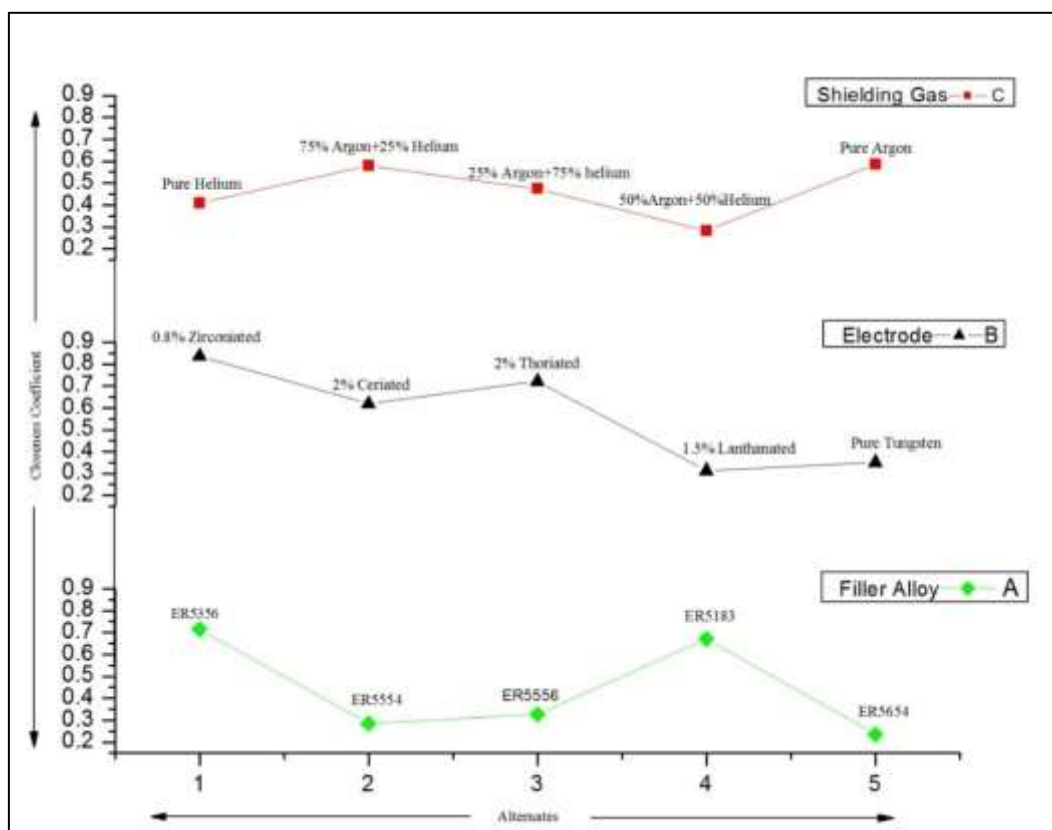


Figure 4.12: Plots for Best Consumable Material Selection

Chapter 5
Methodology and Experimentation

METHODOLOGY AND EXPERIMENTATION

5.1 Introduction

Welding joints of similar and dissimilar aluminum alloys have become important due to increased engineering applications, mainly in aerospace, automotive and defense industries [1, 70, 73, 150-153]. This is attributed to their high corrosion resistant properties, high specific strength coupled with greater toughness and formability. The weldability characteristics of dissimilar aluminum alloys largely depend on their thermal conductivities. Material with larger thermal conductivity has the more easy inflow of heat. This can result in lack of fusion as excessive melting takes place on material with lower thermal conductivity. Another important factor, governing weldability of dissimilar aluminum alloy, is hot cracking or solidification cracking tendency. The susceptibility to solidification cracking is highly influenced by the composition of the weld metal, which makes the proper choice of filler material necessary [154, 155]. When welding dissimilar combination of 5083-O and 6061-T651, such careful selection becomes more important as filler material with more than 3% Mg at an elevated temperature of 150°F can induce hot cracking.

In conventional welding, structure of grains in fusion zones typically exhibit the coarse columnar structure, this often results in reduced weld mechanical properties and poor resistance to hot cracking [156, 157]. TIG and gas metal arc welding (GMAW) processes are most commonly used for welding of aluminum alloys. However, TIG process is generally preferred because it produces high quality welds. Welded parts exhibit greater tolerance to heat sink variations, lower heat input

requirements, low residual stresses and distortion [158]. The research work in welding of dissimilar aluminum alloy in relation with pulse current parameters and mechanical properties are scant with no systematic study reported so far to correlate the pulse current parameters and mechanical properties. Statistical tools have been used by many investigators [159-161], which have gained wide approval.

5.2 Base Metal Grade Selection

The base metal used in this investigation is a two dissimilar aluminum alloy. One is annealed aluminum alloy 5083-O plate of thickness 6.35 mm and other solution heat treated and artificially aged aluminum alloy 6061-T651 of same thickness. They are selected because of their wide application in marine and chemical industries. The filler alloy ER5356 of thickness 1.6 mm is used which is selected using MADM approach as described in chapter 3. The chemical composition, mechanical properties and physical properties of base metals along with filler metal is given in Table 5.1, Table 5.2 and Table 5.3.

Table 5.1: Chemical Composition (wt. %) of Base Metal and Filler Metal.

Composition	Si	Mg	Fe	Cu	Mn	Cr	Zn	Ti	Al
AA 5083-O	0.15	4.2	0.21	0.01	0.71	0.12	0.01	0.02	Balance
AA6061-T651	0.53	0.68	0.23	0.30	0.33	0.06	0.07	0.05	Balance
ER 5356	0.23	5.0	-	0.05	0.12	0.9	-	0.13	Balance

Table 5.2: Mechanical Properties of Base Metal and Filler Metal

Mechanical property	Yield strength (MPa)	Ultimate tensile strength (MPa)	Elongation (%)	Vickers Microhardness (HV)	Charpy Impact toughness (J)
AA 5083-O	228	317	17	95	24
AA 6061-T651	276	310	12	107	105
ER 5356	240	270	17	105	22

Table 5.3: Physical Properties of Base Metal and Filler Metal [1, 2]

Physical properties	Density (g/cm ³)	Melting Point (°C)	Modulus of Elasticity (GPa)	Electrical Resistivity (Ω.cm)	Thermal Conductivity (W/m.K)	Thermal Expansion (20°C-100°C)
5083-O	2.65	570	72	0.058×10^{-6}	121	25×10^{-6}
6061-T651	2.70	580	75	4.0×10^{-6}	173	23.5×10^{-6}
ER 5356	2.64	571	76	0.059×10^{-6}	116	23.8×10^{-6}

5.3 Welding Machine

In this work, Pulse TIG welding machine TRITON 220 AC/DC is employed in which the welding current can be varied from 5 Amp to 220 Amp, voltage can be varied from 10.1 V – 18.8 V, frequency can be varied from 50 – 200 Hz, Pulse Time can be varied from 0.01-10.0s with 0.01s increment, Secondary current can be varied from 0-100% of main current with 1% increment. The image of the TRITON 220 AC/DC pulse TIG welding machine is shown in figure 5.1

**Figure 5.1: TRITON 220 AC/DC (Pulse TIG Welding Machine)**

5.4 Process Parameters of Pulse TIG welding which are affecting the Mechanical Properties of Weld

The parameters of Pulsed TIG welding that are affecting the mechanical properties of the weld: (1) Peak current, (2) Base current, (3) Pulse Frequency, (4) Pulse On Time, (5) welding speed, (6) Wire feed rate, (7) Gas flow rate. Figure 5.2 shows the schematic representation of current-time diagram during pulse power welding

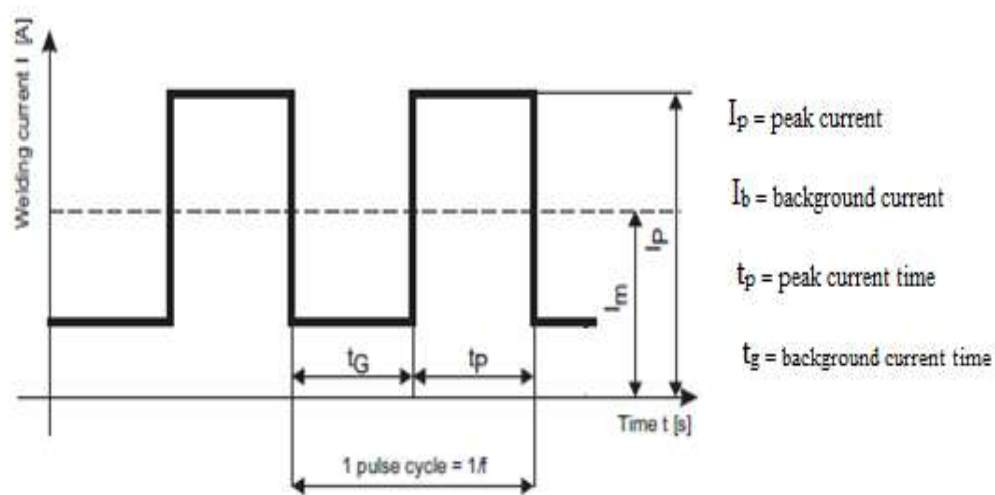


Figure 5.2: Current-Time Diagram during Pulse TIG Welding

- **Peak Current (I_p):** It is the current level at which welding take place. This value is usually set somewhat higher than it would be set for a non-pulse TIG welding. Peak current controls the amount of heating and fusion taking place in the weldment
- **Base Current (I_b):** This is the current required for maintaining the arc. The base current would be set lower than peak current. Base current controls the amount of cooling and solidification in the weldment.

- **Pulse Frequency:** It is the number of peak current pulses, which occur in one second of time and it is given by the inverse of the cycle time, T in seconds. A pulse cycle time (T) is defined as the period from the start of a pulse to the end of the base time just before the next pulse.
- **Pulse On Time:** It is the pulse peak duration as a percentage of total time. It controls how long the peak amperage level is maintained before it drops to the base value.
- **Welding Speed:** The welding speed is proved significant parameter in controlling weld bead characteristics and ultimately mechanical properties. Faster the welding speed, faster the cooling rate, smaller the grains formed resulting in maximum tensile properties [162, 163].
- **Wire Feed rate:** Controlling the wire feed rate is essential parameter as it influences cooling rate of weld which effects the grain size and ultimately influences weld metal properties.
- **Gas flow rate:** When rate of gas flow varies transfer of filler metal drops, stability of the welding process, as well as chemical composition of weld metal, thermal and other processes in consumable electrode welding can be controlled, and required properties of joint weld can be achieved [2, 164-167].

5.5 Design of Experiment (DOE)-An Overview

The design of experiment is a test or a series of tests conducted in which the changes are made in the input process parameters to observe and find the reasons for the observed changes in the output response. The experimentation procedure extensively adopted in use is the one-factor-at-a-time approach. In this method, each factor is

varied over its range while the other factors are held at the baseline level. The Analysis of Variance (ANOVA) is a collection of statistical model and related procedures, in which the examined variance is partitioned into components due to different explanatory variables. The technique is demarcation of the total sum of squares into components related to the effects used in the model.

5.5.1 Types of DOE

Depending on the factors and different factor levels, the DOE are classified as

- One Factor Design
- Factorial Design
- Response Surface Design

5.5.1.1 One Factor Design

These are the designs where only one factor is under investigation, and the objective is to determine whether the response is significantly different at different factor levels.

The factor can be qualitative or quantitative

5.5.1.2 Factorial Design

Factorial design is a standard statistical tool to conduct the experiment in an optimum and effective way to investigate the effects of process parameters on the response or output parameter [168]. The important advantage of the design was that simultaneously two or more number of parameters could be studied for a deeper insight to the combined effects of the parameters on the response, which is not possible with a conventional experimental approach since only one parameter was considered at a time for the one investigation and all other parameters were held

constant. A $3^2 \times 2^3$ factorial design requires running all 72 combinations of two variables with three levels each (3^2) and three variables with two levels each (2^3). In such designs, all possible combinations of levels of factors were tedious. The simplest and the most economical factorial design is a two level factorial experiment consisting of 2^k experimental runs in which every factor is fixed at two levels and all combinations of k factors are used. The chief reasons for its importance are [169]

- i. It forms the basis for two level fractional design
- ii. It can be suitably augmented to form composite designs if a more thorough local exploration is needed, and
- iii. The interpretation of the results produced by the design can proceed largely by using common sense and elementary arithmetic.

However, the number of runs required for full 2^k factorial design increases geometrically as K is increased. The large increase in the number of trails called for primarily to provide for estimates of the increasing number of higher order interactions, which most likely do not exist. In other words, such a factorial experiment has a great surplus number of trails involving wastage of money and time. Under such conditions it is possible and advantageous to use only part of the full factorial design for reducing the number of experiments runs, i.e., fractional factorial design. This would be at the expense of information such as the effect of combined interaction of all factors that is not very significant in constructing linear models. The other draw back of this technique is that information on quadratic terms for curvature estimate cannot be extracted from such a factorial experiment [170]

5.5.1.3 Response Surface Design

Response surface designs [171-174] are employed in the empirical study of relationships between one or more measured response variable and a number of independent or controllable variables of a process. This method has been successfully used since 1950 and for a wide variety of problems, for example, in chemical engineering, agriculture, chemistry and mechanical engineering.

Response surface designs were employed to investigate and predict the following important conditions of a process:

- The effect on a particular response by a given set of input variables over some specified region of interest.
- The required values of variables to obtain desirable or acceptable level of a response
- The required values of variables to achieve a minimum or maximum response and the nature of response surface near this minimal or maximal value.

The relationship between response and control variable is almost always polynomial of second order because second order designs are well devised. Besides, second order response surfaces designs lend themselves to detect optimal conditions with ease [168].

To describe the response surface by second-order polynomials, the factors in experimental design should have at least three to five levels. A three-level factorial experiment in which all-possible combinations of k factors at all levels are used is called a $3k$ full factorial design. Such a design involves a large number of

observations even when k is greater than 2, and the coefficients of the squared terms are estimated with relatively low precision [172].

Box and Wilson [175] developed new designs specifically for fitting second order response surface called central composite rotatable designs which were constructed by adding further treatment combinations to those obtained from a 2^k factorial. The total number of observations was reduced significantly by employing these designs. Each design consists of a two-level factorial box (2^k) augmented by replicated experiments at the center point and symmetrically located ‘star’ points. For 2 through 4 factors, the central box is a full factorial design; for five or more factors it becomes a half fractional design [168, 172], The center point is replicated to provide a measure of experimental error and hence in using second order rotatable designs no replication is needed in order to find error mean square. Rotatable designs means that the predicted response is capable of being estimated with equal variance regardless of the direction from the center of the design space.

5.6 Selection of Design

One of the main aims of present investigation was to study the main and interaction effects of welding process parameters on mechanical properties using developed models in predicting, controlling and optimizing the process parameter for high quality weld. It is therefore imperative to design the experiments based on factorial technique. As two level factorial techniques, either full or fractional type, have linear response surfaces and they do not estimate curvature, a five level, central composite rotatable design was selected for the present investigation.

5.7 Identifying the Important Process Parameters

Welding conditions being set by various process parameters influence the microstructure, mechanical and metallurgical properties of the weldment. Also, identification of correct welding conditions is of paramount importance in obtaining sound and leak proof welded joint free from weld defects such as hot cracking, porosity, stress corrosion cracking etc. Desired welding conditions may be achieved by properly selecting the independently controllable process variables or factors which influence the weld quality. Among the many independently controllable process variables or factors affecting mechanical properties [159-161], Peak current, Base current, Pulse frequency, Pulse on time, Welding speed were selected to carry out the experimental work and develop mathematical models.

5.8 Experimentation





A weld size of 120mm X 150mm X 6.35mm of each was used for fabrication of butt joined using Pulse TIG welding (Triton 220 AC/DC). Chamfering of material from 1mm distance above the base was done to make it 60° groove weld joint. Surface of the base plates were first wire brushed and cleaned with acetone to remove oil/grease, dust and oxides. Welding is performed using automatic set up. The 0.8% Zirconiated tungsten electrode and pure argon as shielding gas is used which is selected using MADM approach as described in chapter 3.

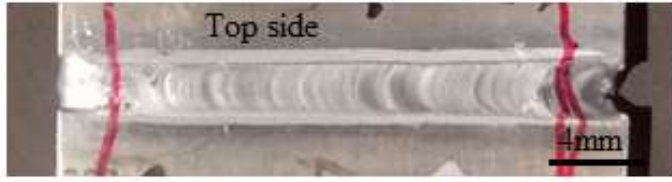

5.8.1 Experimental Trails and Determination of Working Limits of Parameters

Numerous trial runs have been carried out using 6.35 mm plates of AA5083-O and AA6061-T651 aluminum alloy to find out the feasible working limits of each process parameter. Various combinations of pulsed current parameters have been used to carryout

the trial runs as shown in Table 5.4. The weld quality based on bead contour, bead appearance have been inspected to identify the working limits of welding parameters.

Table 5.4: Trail Runs

Run	Parameters		Weld bead surface	Accepted(A) /Rejected (R)
	Name	Value		
1	Peak current (Amp)	150		Rejected
	Base current (Amp)	100		
	Pulse frequency (Hz)	2		
	Pulse on time (%)	30		
	Welding speed (mm/min)	WS1		
	Wire feed rate (cm/sec)	WF1		
2	Peak current (Amp)	155		Rejected
	Base current (Amp)	100		
	Pulse frequency (Hz)	2		
	Pulse on time (%)	30		
	Welding speed (mm/min)	WS1		
	Wire feed rate (cm/sec)	WF1		
3	Peak current (Amp)	160		Rejected
	Base current (Amp)	105		
	Pulse frequency (Hz)	2		
	Pulse on time (%)	30		
	Welding speed (mm/min)	WS1		
	Wire feed rate (cm/sec)	WF1		
4	Peak current (Amp)	175		Rejected
	Base current (Amp)	105		
	Pulse frequency (Hz)	2		
	Pulse on time (%)	40		
	Welding Speed (mm/min)	>WS1		
	Wire feed rate (cm/sec)	WF1		

Run	Parameters		Weld bead surface	Accepted(A) /Rejected (R)
	Name	Value		
5	Peak current (Amp)	175		Accepted
	Base current (Amp)	105		
	Pulse frequency (Hz)	2		
	Pulse on time (%)	40		
	Welding Speed (mm/min)	WS1		
	Wire feed rate (cm/sec)	WF1		
6	Peak current (Amp)	175		Accepted
	Base current (Amp)	105		
	Pulse frequency (Hz)	2		
	Pulse on time (%)	40		
	Welding Speed (mm/min)	WS1		
	Wire feed rate (cm/sec)	WF1		

From the above analysis certain observations have been listed here:

- (i) If peak current is less than 175 A, then incomplete penetration and lack of fusion were observed. At the same time, if peak current is greater than 215 A, then undercut, spatter and overheating were observed on weld bead surface.
- (ii) If the base current is lower than 105 A, then the arc length is found to be very short and addition of filler metal becomes inconvenient. On the other hand, if the background current is greater than 133 A, then arc becomes unstable and lengthy.
- (iii) If the pulse frequency is less than 2 Hz, then the bead appearance and bead contours were not of good quality. However, if the pulse frequency is greater than 10 Hz, then more arc glare and arc spatter have been experienced.

- (iv) If pulse on time is lower than 40 %, then weld nugget formation is not so smooth due insufficient heat input. On the contrary, if the pulse on time is greater than 60 %, then over melting of filler metal and overheating of tungsten electrode were observed.
- (v) If the welding speed is lower than 155 mm/min then large molten pool is formed that flows around the arc resulting in rough bead and burn through of the weld plate. On the other hand if welding speed is greater than 195 mm/min then uneven bead shape and cracking have been observed in the weld metal.

From the above observations .The upper limit of the factor was coded as (+2) and lower limit as (-2) which is listed in Table 5.5.

Table 5.5: Welding Parameters and their Upper and Lower Limits

Parameters	Unit	Notation	Factor levels	
			Lower limit (-2)	Upper limit (+2)
Peak current	A	P	175	215
Base current	A	B	105	133
Pulse frequency	Hz	F	2	10
Pulse on time	%	T	40	60
Welding speed	mm/min	S	155	195

The coded values for the intermediate ranges were then calculated from the following relation [176]

$$X_i = \frac{[2X - (X_{\max} + X_{\min})]}{(X_{\max} - X_{\min}) / 2} \quad (5.1)$$

Where X_i is the required coded value of a i^{th} variable X . X is any value of the variable from X_{\min} to X_{\max} . X_{\min} and X_{\max} are lower and upper limits of the variable X respectively.

The decided levels of the selected process parameter with their units and notations are given in Table 5.6

Table 5.6: Welding Parameters and their Levels

Parameters	Unit	Notation	Factor Levels				
			-2	-1	0	1	2
Peak current	A	P	175	185	195	205	215
Base current	A	B	105	112	119	126	133
Pulse frequency	Hz	F	2	4	6	8	10
Pulse on time	%	T	40	45	50	55	60
Welding Speed	mm/min	S	155	165	175	185	195

5.8.2 The Design of Experiments Matrix

Due to wide ranges of factors, it has been decided to use five factors, five levels, central composite rotatable design matrix. The design matrix comprises of full replication of 2^5 ($= 32$). All welding parameters in the intermediate levels (0) constitute the central points and combination of each welding parameters at either is highest value (+2) or lowest (-2) with other parameters of intermediate level s (0) constitute star points. 32 experimental trails were conducted that make the estimation of linear, quadratic and two way interactive effects of process parameters on tensile

strength, yield strength, elongation, impact strength and micro-hardness . The design matrix is depicted in Table 5.7

Table 5.7: The Design Matrix

Std order	P	B	F	T	S
1	-1	-1	-1	-1	1
2	1	-1	-1	-1	-1
3	-1	1	-1	-1	-1
4	1	1	-1	-1	1
5	-1	-1	1	-1	-1
6	1	-1	1	-1	1
7	-1	1	1	-1	1
8	1	1	1	-1	-1
9	-1	-1	-1	1	-1
10	1	-1	-1	1	1
11	-1	1	-1	1	1
12	1	1	-1	1	-1
13	-1	-1	1	1	1
14	1	-1	1	1	-1
15	-1	1	1	1	-1
16	1	1	1	1	1
17	-2	0	0	0	0
18	2	0	0	0	0
19	0	-2	0	0	0
20	0	2	0	0	0
21	0	0	-2	0	0
22	0	0	2	0	0
23	0	0	0	-2	0
24	0	0	0	2	0
25	0	0	0	0	-2
26	0	0	0	0	2
27	0	0	0	0	0
28	0	0	0	0	0
29	0	0	0	0	0
30	0	0	0	0	0
31	0	0	0	0	0
32	0	0	0	0	0

5.8.3 Conducting the Experiments

The 32 trails runs were conducted based on the design matrix. The plates were welded according to the design matrix. The parameters which were kept constant during experimentation is listed in Table 5.8

Table 5.8: Constant Parameters

Welding conditions	
Wire feed rate (cm/sec)	3.9
Filler wire diameter (mm)	1.6
Shielding gas	Pure Argon
Arc voltage (Volts)	13.2
Gas flow rate (L/min)	6
Electrode	W+0.8% zirconiated
Electrode diameter (mm)	2.4
Nozzle to plate distance (mm)	1.7
Torch position	vertical
Operation	Semi-Automatic
Polarity	AC
AC % Balance	0.00 (Sinusoidal)

5.9 Non-destructive Testing of Weld

Non-destructive testing (NDT) is essential to ensure that defects in the welds are detected prior to being put to use. Faulty welds could lead to problems, some of which could be disastrous depending on the items being welded (i.e., an oil or gas pipeline). Weld connections can encounter loads and suffer fatigue over the course of their lifetime, which could lead to failure unless they meet the proper specifications. That's where NDT plays a vital role. It can identify both surface and sub-surface deficiencies

in weldment. Some most conventional NDT methods used today are visual inspection, magnetic particle testing, liquid penetrant testing, ultrasonic testing, and radiography. Visual, magnetic particle, liquid penetrant testing is useful in detecting surface imperfections such as cracks, gaps, inconsistent weld bead profiles, undercut, and concave or convex welds. Ultrasonic and radiography are used to discover sub-surface flaws.

The welded plates were examined by visually examined to find out any surface defect, then the radiography X-ray was conducted to detect any sub-surface flaws

5.9.1 Visual Examination of the Weld

Visual inspection is often the most cost-effective method because it requires little equipment. A hand-held mirror, pocket rule, weld gauge. No visual defects were observed after thorough examination. The welded plate is shown in figure 5.3.



Figure 5.3: Welded Plate

After visual inspection the radiography X-ray was conducted to find out any sub-surface defects.

5.9.2 X-Ray Radiography of the Welds

Radiography test was performed as per ASME Sec – IX, 2013 to check lack of penetration. The X-Ray on Kodak- D4 (MX-125) film is thrown for development time of 4 minutes at temperature of 20°C. The radiographic film of weld with no sub-surface defect was obtained (figure 5.4). The weld samples was cut to study the microstructure and mechanical properties of weld, described in subsequent section

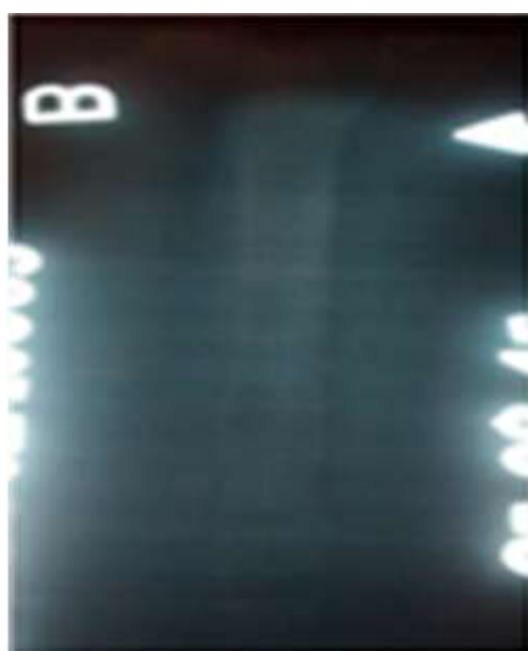


Figure 5.4: Radiography of Weld Joint 5083-O + 6061-T651

Preparation of test coupons

After performing welding according to the experimental design and subsequently performing NDT tests. The test specimen of tensile test, micro-hardness and impact toughness were prepared.

5.10 Mechanical Testing of Welds

AA5083 is a non heat-treatable aluminum alloy while AA6061alloy is heat treatable. These alloys exhibit higher strength to weight ratio, good ductility, and good corrosion

resistance [177-179]. The dissimilar joining of these two materials leads to the combined properties of both materials, which makes this combination useful in military applications such as light combat aircraft (LCA), gun mount bases, pressure vessels , cargo tanks, submarine torpedo etc. As the welded joint find applications in critical components (whose failure results could lead to catastrophe), the standards are continually rising. Acceptance standards represent the minimum weld quality and are based upon test of welded specimens. All types of welded structures which experience high pressure are expected to perform certain functions. The joints comprising these structures must possess certain service-related capabilities. To test that the required function will be met, different types of tests were conducted. The ideal test is the observance of the structure in actual practice. This is usually not possible. Therefore, some mechanical tests are performed on the standard specimens to assess the behavior of the structure in service.

5.10.1 Tensile Testing of Welds

Tensile tests were carried out to determine the ultimate tensile strength on the weld section that is heterogeneous in nature, containing base metal, weld metal and the welded joint. Various types of tensile tests carried out to evaluate the weldment include, all-weld metal test, longitudinal butt-weld test, transverse butt-weld test, transverse butt weld with notch test and tension-shear test. The transverse tensile test is a standard test for procedure qualification and is also used to indicate whether the weld strength equals that of the base metal tensile strength or less.

5.10.1.1 Transverse Tensile Testing of Weldments

The tensile samples were extracted from welded samples along the transverse welding direction and prepared as per ASTM E8 M04 standard. Tensile test was carried out in

50 KN electro-mechanical controlled universal testing machine (Tinius Olsen) with cross head speed of 2.5mm/min shown in figure 5.5. The 0.2 % offset of yield strength, ultimate tensile strength and percentage of elongation were evaluated from un-notched tensile sample. The standard drawing is shown in figure 5.6.

Tensile test is carried out by gripping the end of the specimen in a tensile testing machine and applying and increasing pull on to the specimen till it fractures. The tensile specimen is shown in figure 5.7

During the test, the tensile load as well as the elongation of a previously marked gauge length in specimen is measured with the help of load dial of the machine and extensometer respectively. After fracture, the two pieces of the broken specimen are placed as if fixed together and the distance between two gauge marks and the area at the place of fracture are noted. The fractured tensile specimen is shown in figure 5.8



Figure 5.5: Universal Tensile Testing Machine

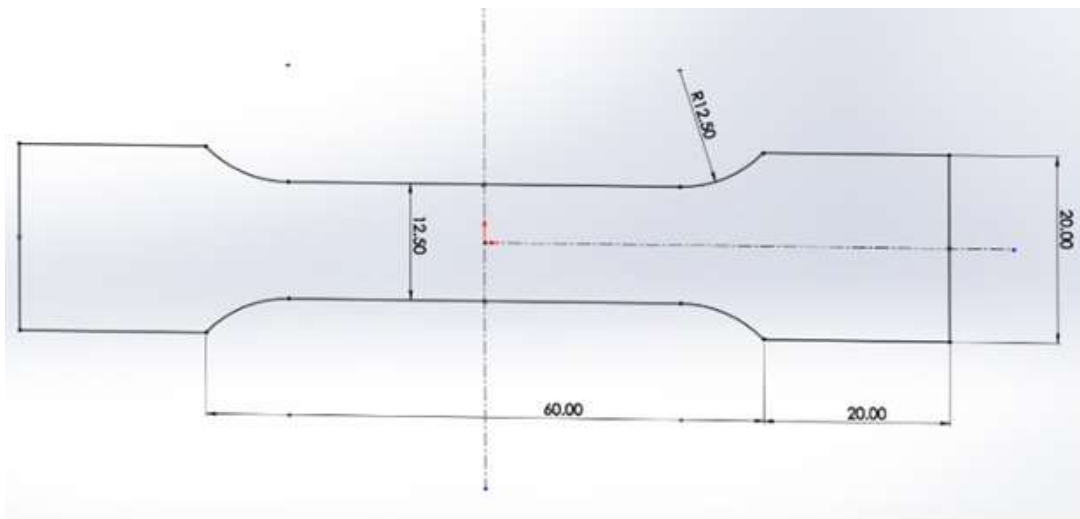


Figure 5.6: Drawing of Tensile Test Specimen according to ASTM E8 M04



Figure 5.7 Tensile Test Specimen as per Drawing



Figure 5.8: Fractured Tensile Specimen

The fractured tensile tested specimen are shown in figure 5.9



Figure 5.9: Tensile Tested Specimens Showing Location of Fracture

5.10.1.2 Analysis of Tensile Testing

As reported in studies of joining of dissimilar aluminum alloys, the TIG welded joints always fractured at locations in HAZ on the weaker material side [180]. However, those studies did not investigate the effect of material position on the tensile properties. The failure location in HAZ also indicate seamless bonding between dissimilar AA 5083-O and AA 6061-T651 alloys under all welding conditions. It is observed from the results that ultimate tensile strength of both base metal and welded specimen are higher which indicates considerable work hardening beyond the yield point. The strength of weld metal may also be increased due to solid solution strengthening by development of Mg_2Si particles in the fusion zone. It has been found that, there is no reduction in strength at the weld zone and the actual reduction in strength was occurred in the base metal region.

5.10.2 Micro-hardness Test

Micro-indentation hardness testing (or micro hardness testing) is a method for measuring the hardness of a material on a microscopic scale. A precision diamond indenter is impressed into the material at loads from a few grams to 1 kilogram. The impression length, measured microscopically, and the test load are used to calculate a hardness value. The hardness values obtained are useful indicators of a material's properties and expected service behaviour. Conversions from micro-indentation hardness values to tensile strength and other hardness scales (e.g., Rockwell) are available for many metals and alloys. The indentations are typically made using either a square-based pyramid indenter (Vickers hardness scale) or an elongated, rhombohedral-shaped indenter (Knoop hardness scale). The tester applies the selected

test load using dead weights. The length of the hardness impressions are precisely measured with a light microscope using either a filler eyepiece or a video image and computer software. A hardness number is then calculated using the test load, the impression length, and a shape factor for the indenter type used for the test

5.10.2.1 Vickers Micro-hardness Test

Preparation of the specimen for the micro-hardness test involves the following processes:

- i. Cutting and burring;
- ii. Mounting of specimen for handling during preparation;
- iii. Grinding;
- iv. Polishing; and
- v. Etching.

When the specimens are mounted and polished, consideration should be given to edge support if impressions are to be made near edges. If the edges are rounded off even slightly during metallographic preparation, due to soft mounting compounds, the micro-hardness levels at the interface of the welds. Micro-hardness measurements were covered out in all weld regions of the test specimens of size 10mm x 10mm x 55mm, cut from the weld coupon. These specimen were polished and mounted on micro-hardness tester. A Vickers micro-hardness tester (BLUE STAR, model no. MUK-H1) was employed for measuring the hardness across the transverse section of the joint with load of 1Kg and dwell time of 15 s was applied and reading was taken

as shown in figure 5.10. Figure 5.11 shown the reading taken in along with HAZ and FZ region in weldment.



Figure 5.10: Micro-hardness Tester Machine



Figure 5.11: Weldment Region of FZ and HAZ

5.10.2.2 Analysis of Micro-hardness Test

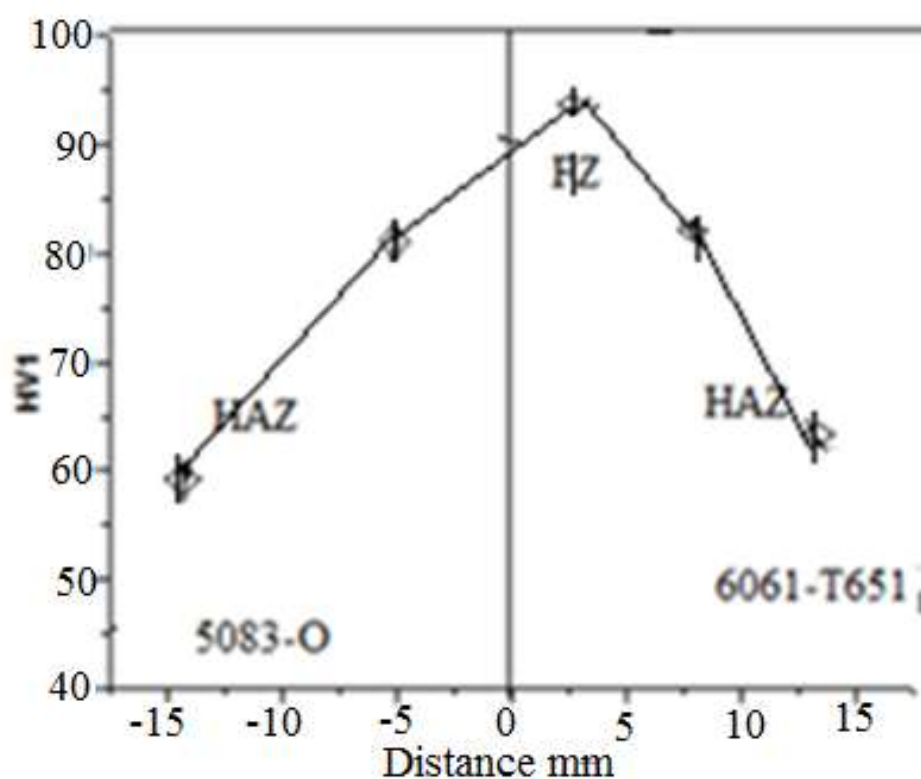


Figure 5.12: Micro-hardness Profile

In general, both AA6061 and AA5083 alloys have exhibited certain decrease in micro-hardness in the weld as compared to their corresponding base metals. This is mainly because of coarsening, dissolution and reprecipitation of strengthening precipitates caused by TIG thermal cycle [181, 182]. Hardness minima is observed in the HAZ on the AA6061 due to this joint failed on AA6061 side in HAZ regions very close to the FZ in tensile testing. Micro-hardness profile in figure 5.12 shows the hardness variations from the center of fusion zone to the end of HAZ. These hardness values have some fluctuations along the fusion zone to region adjacent to base metal. This is due to inhomogeneous grain growth and variations of beta phase particles in the microstructure of weldment of aluminum alloys AA5083 and AA6061. This

behavior is also due to slow cooling rate in TIG process. As compared to literature [183] the hardness value increases with increasing cooling rate (low heat input) due to the formation of an increasingly finer transformed structure. Increase in cooling rate directly effects solidification rate which has direct impact on formation of grains, shrinkage cavity and distribution of secondary and ternary phases.

5.10.3 Impact Testing of Welds

There are two forms of impact test, Izod and the charpy test. Both involve striking a standard specimen with a controlled weight pendulum travelling at a set speed. The amount of energy absorbed in fracturing the test piece is measured and this gives an indication of the notch toughness of the test material. These tests show that metals can be classified as being either brittle or ductile. A brittle metal will absorb a small amount of energy when impact tested, a tough ductile metal a large amount of energy. It should be emphasized that these tests are qualitative, the results can only be compared with each other or with a requirement in a specification - they cannot be used to calculate the fracture toughness of a weld or parent metal, such as would be needed to perform a fitness for service assessment. The Izod test is rarely used these days for weld testing having been replaced by the Charpy test. The Charpy specimen may be used with one of three different types of notch, a 'keyhole', a 'U' and a 'V'. The keyhole and U-notch are used for the testing of brittle materials such as cast iron and for the testing of plastics. The V-notch specimen is the specimen of choice for weld testing

5.10.3.1 Charpy Impact Test

The Charpy test measures the energy absorbed by a standard notched specimen while breaking under an impact load. Charpy Impact test (FIE, Model No – IT30) as

.shown in figure 5.13 was used to measure the sample impact toughness. The V-notch: 2mm deep, with 45° angle and 0.25mm radius along the base depicting in drawing shown in figure 5.14 has been made according to ASTM standard subsize E23. The standard Charpy Test specimen of size of 55mm \times 10mm \times 10mm having a V notch machined across one of the larger dimensions has been shown in figure 5.15 Impact testing was determined on the transverse cross section of the all-weld metal test assemblies at the Charpy V notch location using the Vickers 1000-g scale. Specimen was tested and the fractured specimen is shown in figure 5.16



Figure 5.13: Impact Testing Machine

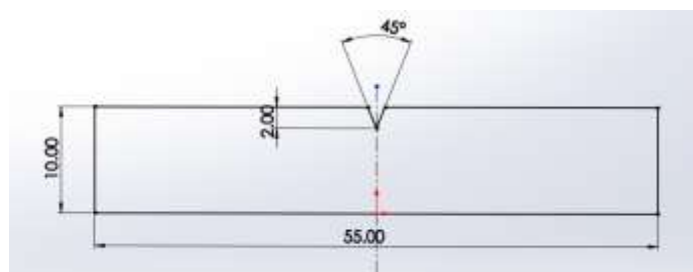


Figure 5.14: Drawing of Charpy Impact Test Specimen (Dimensions:mm) according to ASTM E23



Figure 5.15: Impact Test Specimen



Figure 5.16: Fractured Impact Test Specimen

5.10.3.2 Analysis of Charpy Impact Test

The specimen failed under impact loading because of decrease in temperature which lowered the ductility and toughness. The residual stress developed in multiaxial stress state makes the weld difficult to withstand the simultaneous elastic and plastic deformation in the various direction in regions in FZ. Loss of strength leads to brittle behavior in AA5083 leading to lower impact toughness

5.10.4 Fractography of Fractured Surface of Impact Test Specimen

Failure analyst usually investigate the fracture path to determine the fracture initiation and termination sites, as well as other fractographic features, Based on this information, the analyst can also identify various types of monotonic (single cycle) overload, fatigue (multiple cycle) cracking, and time-dependent (creep or corrosion) failure, or combinations thereof. Characterizing fracture surfaces and determining how a component fractured is sufficient to solve some problems for component designers. The specimen is etched slightly longer as compared to optical microscopy. The fractured surfaces were analyzed using SEM (Hitachi S3000N) as shown in figure 5.17



Figure 5.17: SEM Set up

5.10.4.1 Analysis of Fractography.

The fractured samples obtained from impact test shown in figure 5.18 are investigated under SEM. Figure 5.18 a) and b) show the fractured surface produced under the joints is characterized by large amount of equi-axed dimples with different sizes. As we know, In such dimple rupture mode, overload is the principal cause of fracture and failure is governed by continuous series of macro voids. Figure 5.18 c) and (d) show the formation of macro voids, which indicates that tested base metal has failed under ductile mode. The macrovoids may nucleate at regions adjacent to second phase particles, inclusions, grain boundaries, and dislocation pile-ups, consequently, the voids grow, coalesce, and eventually form a continuous fracture surface [184]. Second phase particles including incoherent β -Mg₂Si phase could effectively provide nucleation sites for macrovoids during fracture process. However, figure. 5.18 (c) indicates some examples of such nucleation sites at the bottom of dimples or at the top of ridges, but the counting and measurement of the amount of such second phase particles are usually hidden at the bottom of dimples and have similar color as the surrounding Al matrix on fractured surfaces under SEM.

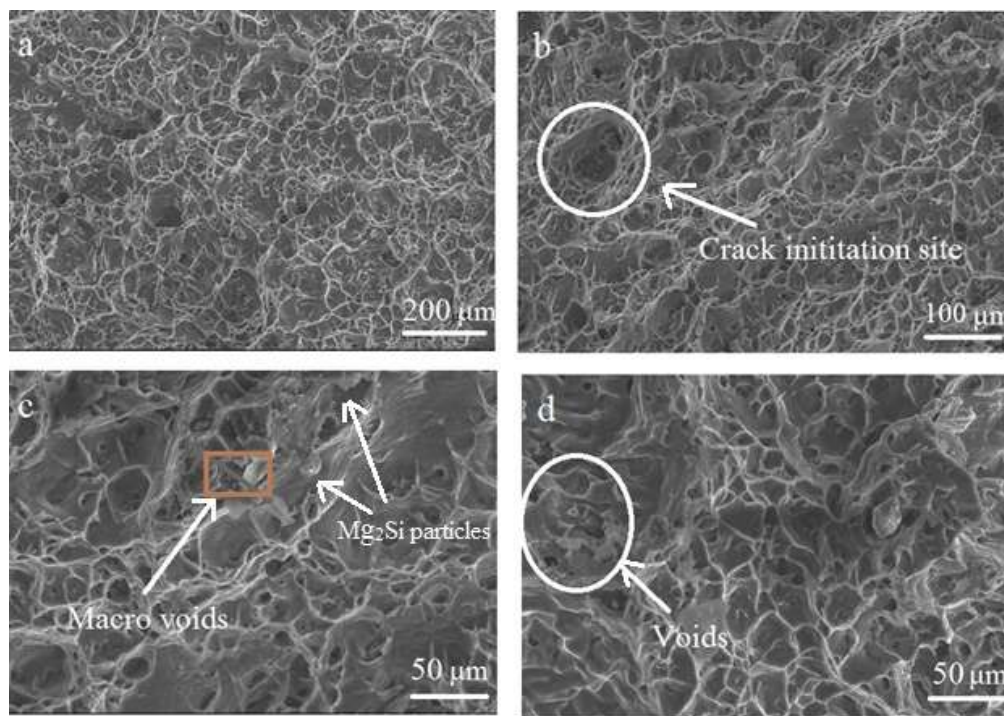


Figure 5.18: SEM Fractography of Impact Test Samples a) TIG joint at 200μm b) TIG Joint at 100 μm, c), d) TIG joint configuration at 50μm

SEM fractographs of failure surface of impact test specimen shown in figure 5.18

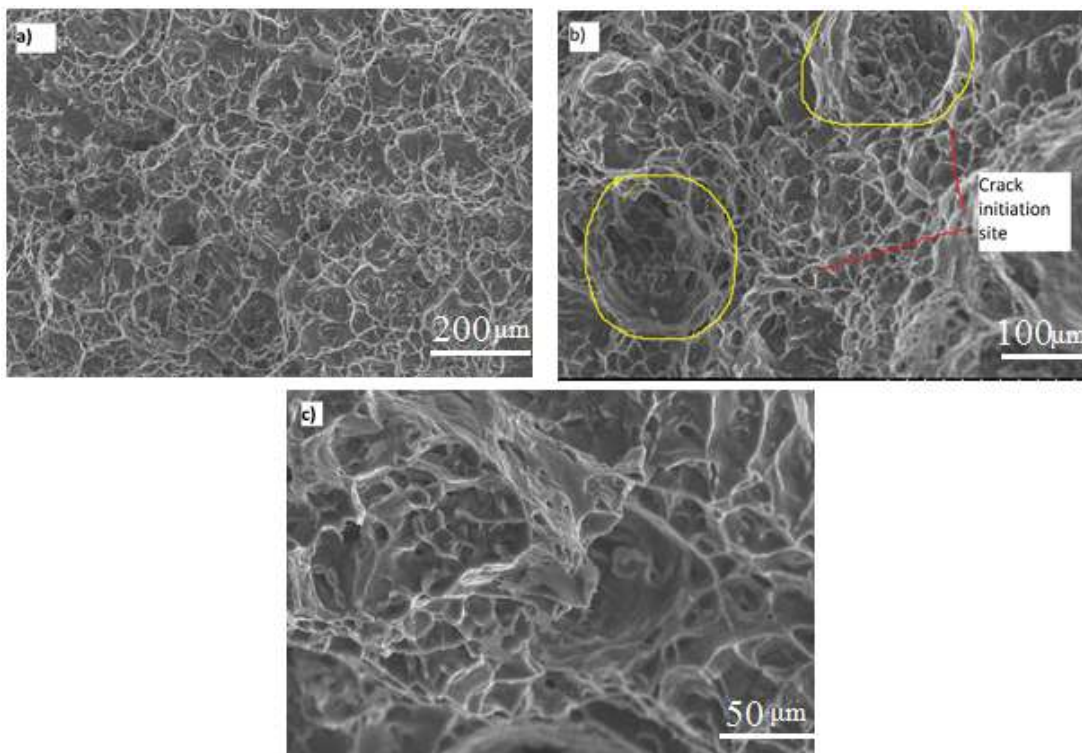


Figure 5.19: SEM Fractographs of Failure Surface of Impact Specimens at a) 200μm b) 100μm and c) 50μm

5.11 Recording of Responses

The measured response values along with design matrix has been listed in Table 5.9.

Table 5.9: Design Matrix and Measured Response Values

Std order	P	B	F	T	S	Tensile Strength (MPa)	Yield strength(MPa)	Percent Elongation(%EL)	Micro-hardness(HV)	Impact Toughness (J)
1	185	112	4	45	185	157.15	127	7.05	71	11
2	205	112	4	45	165	169	135.3	5.9	84.04	19.5
3	185	126	4	45	165	144.75	106.7	4.4	94.09	14
4	205	205	4	45	185	155.45	100.27	7.1	74.98	17
5	185	112	8	45	165	171	143.75	8.061	86.56	13.5
6	205	112	8	45	185	164.25	147.65	6.65	70.9	10.5
7	185	126	8	45	185	154.4	138.35	5.35	98.93	21.5
8	205	126	8	45	165	199.99	174.65	11.219	76.98	22.5
9	185	112	4	55	165	171.6	150.7	7.2	74.4	23
10	205	112	4	55	185	153.4	122.01	6.65	99.9	19.5
11	185	126	4	55	185	170.25	153.4	7.55	88.5	10
12	205	126	4	55	165	186.22	161.75	5.661	73.78	40.5
13	185	112	8	55	185	163.05	148.2	6.65	82	30
14	205	112	8	55	165	161.95	130.05	6.05	99.09	16
15	185	126	8	55	165	163.7	141.3	6.25	80.89	28.5
16	205	126	8	55	185	147.08	106.75	5.65	95.45	21.5
17	175	119	6	50	175	161.95	146.1	6.15	82.5	20.5
18	215	119	6	50	175	163.9	140.2	5.481	76.78	28.5
19	195	105	6	50	175	206.2	163.35	11.9	94.29	24.38
20	195	133	6	50	175	200.1	159.2	11.04	94.83	28.63
21	195	119	2	50	175	148.3	104.15	4.75	84.34	17
22	195	119	10	50	175	153	124.4	6.8	93.31	22.5
23	195	119	6	40	175	175.7	128.4	8.65	81.69	11.5
24	195	119	6	60	175	170.6	134.87	7.75	94.2	23
25	195	119	6	50	155	176.65	153.25	7.55	78.5	32
26	195	119	6	50	195	162.55	130.43	5.95	80.08	21
27	195	119	6	50	175	204.35	166.95	12.65	95.45	34
28	195	119	6	50	175	209.4	164.94	11.25	92.38	36.5
29	195	119	6	50	175	211.7	162.1	12.9	97.98	34
30	195	119	6	50	175	209.8	166.35	11.924	94.56	33
31	195	119	6	50	175	211	166.2	12.4	92.23	35
32	195	119	6	50	175	212.9	157.65	12.15	97.2	35.25

Values of responses are average of two trial runs

5.12 Development of Mathematical Model

Response Surface Methodology (RSM) is a collection of mathematical and statistical techniques that is useful for the modeling and analysis of problems in which a response of interest is influenced by several parameters and the objective is to optimize this response. The main aim of RSM model is to establish relationship between the process parameters and response. This relationship can be used to predict the response when the process parameters are varied within the selected ranges. This also brings out the relationship between the controllable input parameters and the obtained response surfaces. The above-mentioned regression model or the response surface model is represented as

The response function tensile strength (TS), yield strength (YS), percent elongation (%EL), micro-hardness (M) and impact toughness (IT). Representing Y as the response, the response function can be expressed as [185, 186].

$Y = f(\text{Peak current, base current, pulse frequency, pulse on time, welding speed})$

$$Y = f(P, B, F, T, S) \quad (5.2)$$

The second order polynomial (regression) equation used to represent the response surface 'Y' for five factors is given by

$$Y = \beta_0 + \sum_{i=1}^5 \beta_i X_i + \sum_{i=1}^5 \beta_{ii} X_i^2 + \sum_{i=1}^5 \sum_{j=1}^5 \beta_{ij} X_i X_j + \varepsilon \quad (5.3)$$

and for five factors the selected polynomial could be expressed as,

$$\begin{aligned} Y = & \beta_0 + \beta_1(P) + \beta_2(B) + \beta_3(F) + \beta_4(T) + \beta_5(S) + \beta_{11}(P^2) + \beta_{22}(B^2) + \beta_{33}(F^2) + \beta_{44}(T^2) + \\ & \beta_{55}(S^2) + \beta_{12}(PB) + \beta_{13}(PF) + \beta_{14}(PT) + \beta_{15}(PS) + \beta_{23}(BF) + \beta_{24}(BT) + \beta_{25}(BS) + \beta_{34}(FT) + \\ & \beta_{35}(FS) + \beta_{45}(TS) \end{aligned} \quad (5.4)$$

Where, β_0 is the free term of regression equation, the coefficient $\beta_1, \beta_2, \beta_3, \beta_4, \beta_5$ are linear terms, the coefficients $\beta_{11}, \beta_{22}, \beta_{33}, \beta_{44}, \beta_{55}$ are quadratic terms, and the

coefficients β_{12} , β_{13} , β_{14} , β_{15} etc are the interaction terms. All the coefficients were calculated for their significance at 95% confidence level by using Minitab 17 statistical software package. The calculated values of coefficients of five responses are provided in Table 5.10.

Table 5.10: Calculated Value of Coefficients for Five Responses

Term	Tensile strength			Yield strength			Percent Elongation			Micro-hardness			Impact Toughness		
	Coef	T-Value	P-Value	Coef	T-Value	P-Value	Coef	T-value	P-value	Coef	T-value	P-value	Coef	T-value	P-value
Const	209.46	133.83	0.000	163.18	104.24	0.000	12.165	55.17	0.000	94.849	112.48	0.000	34.637	56.07	0.000
P	1.889*	2.36	0.038	-1.782*	-2.22	0.048	0.043	0.38	0.711	-0.529	-1.23	0.246	1.313*	4.15	0.002
B	-0.073	-0.09	0.929	-1.241	-1.55	0.150	-0.115	-1.02	0.332	0.700	1.62	0.133	1.708*	5.40	0.000
F	1.125	1.40	0.188	4.753*	5.93	0.000	0.353*	3.13	0.010	2.002*	4.64	0.001	0.854*	2.70	0.021
T	-0.373	-0.47	0.651	2.226*	2.78	0.018	-0.245	-2.17	0.053	2.565*	5.94	0.000	3.437*	10.87	0.000
S	-5.474*	-6.83	0.000	-6.092*	-7.60	0.000	-0.220	-1.95	0.077	0.625	1.45	0.176	-2.438*	-7.71	0.000
P×P	-11.338*	-15.65	0.000	-4.365*	-6.02	0.000	-1.552*	-15.20	0.000	-3.714*	-9.52	0.000	-2.543*	-8.89	0.000
B×B	-1.282	-1.77	0.105	0.166	0.23	0.823	-0.138	-1.35	0.204	0.016	0.04	0.969	-2.042*	-7.14	0.000
F×F	-14.407*	-19.89	0.000	-11.584*	-15.99	0.000	-1.562*	-15.30	0.000	-1.418*	-3.63	0.004	-3.730*	-13.04	0.000
T×T	-8.782*	-12.12	0.000	-7.244*	-10.00	0.000	-0.955*	-9.36	0.000	-1.638*	-4.20	0.001	-4.355*	-15.23	0.000
S×S	-9.669*	-13.35	0.000	-4.693*	-6.48	0.000	-1.318*	-12.91	0.000	-3.802*	-9.74	0.000	-2.043*	-7.14	0.000
P×B	4.365*	4.45	0.001	2.394*	2.44	0.033	0.612*	4.43	0.001	-5.074*	-9.60	0.000	2.469*	6.38	0.000
P×F	0.050	0.05	0.960	0.373	0.38	0.711	0.259	1.88	0.088	-0.667	-1.26	0.233	-3.844*	-9.93	0.000
P×T	-5.084*	-5.18	0.000	-7.194*	-7.33	0.000	-0.603*	-4.36	0.001	5.382*	10.18	0.000	-0.219	-0.56	0.583
P×S	-5.674*	-5.78	0.000	-9.348*	-9.53	0.000	-0.217	-1.57	0.145	0.178	0.34	0.742	-1.469*	-3.79	0.003
B×F	-0.037	-0.04	0.970	0.268	0.27	0.790	0.197	1.42	0.182	0.731	1.38	0.194	0.969*	2.50	0.029
B×T	1.504	1.53	0.154	2.873*	2.93	0.014	-0.115	-0.84	0.421	-3.078*	-5.82	0.000	-0.531	-1.37	0.197
B×S	-1.986	-2.02	0.068	-4.418*	-4.50	0.001	-0.104	-0.75	0.466	3.276*	6.20	0.000	-2.156*	-5.57	0.000
F×T	-6.811*	-6.94	0.000	-12.293*	-12.53	0.000	-0.581*	-4.20	0.001	0.724	1.37	0.198	-0.219	-0.56	0.583
F×S	-2.034	-2.07	0.062	0.186	0.19	0.853	-0.779*	-5.64	0.000	-0.269	-0.51	0.620	2.656*	6.86	0.000
T×S	0.238	0.24	0.813	-0.394	-0.40	0.695	0.298	2.16	0.054	3.972*	7.52	0.000	-1.094*	-2.82	0.017

After determination of significant coefficients, mathematical models were developed by using these coefficients only after elimination of the insignificant coefficients. The final developed models for tensile properties, yield strength, percent elongation, micro-hardness and impact toughness are given as

i. Tensile strength

$$TS = 209.46 + 1.889P - 5.474S - 11.338P^2 - 14.407F^2 - 8.782T^2 - 9.669S^2 + 4.365PB - 5.084PT - 5.674PS - 6.811FT \quad (5.5)$$

ii. Yield strength

$$YS = 163.18 - 1.782P + 4.753F + 2.226T - 6.092S - 4.365P^2 - 11.584F^2 - 7.244T^2 - 4.693S^2 + 2.394PB - 7.194PT - 9.348PS + 2.873BT - 4.418BS - 12.293FT \quad (5.6)$$

iii. Percent Elongation

$$\%EL = 12.165 + 0.353F - 1.552P^2 - 1.562F^2 - 0.955T^2 - 1.318S^2 + 0.612PB - 0.603PT - 0.581FT - 0.779FS \quad (5.7)$$

iv. Micro-hardness

$$M = 94.849 + 2.002F + 2.565T - 3.714P^2 - 1.418F^2 - 1.638T^2 - 3.802S^2 - 5.074PB + 5.382PT - 3.078BT + 3.276BS + 3.972TS \quad (5.8)$$

v. Impact Toughness

$$IT = 34.637 + 1.313P + 1.708B + 0.854F + 3.437T - 2.438S - 2.543P^2 - 2.042B^2 - 3.730F^2 - 4.355T^2 - 2.043S^2 + 2.469PB - 3.844PF - 1.469PS + 0.969BF - 2.156BS + 2.656FS - 1.094TS \quad (5.9)$$

5.12.1 Checking the Adequacy of Developed Model

The adequacy of developed models was checked using analysis of variance technique.

This includes [187, 188]:

- i. The results of ANOVA (Table 5.11-5.15) show that regression is significant with linear, square and interaction terms for five models (P-value is less than 0.05).
- ii. The models are found to be adequate as F-value is significantly larger than F-table value of each model which shows models are highly significant.
- iii. Another evidence of the adequacy of models is insignificant lack of fit (P-value less than 0.05) which shows almost negligible lack of fitness of model.

Table 5.11: ANOVA Results for Testing Adequacy of the Tensile Strength Model

Source	Df	Seq SS	Adj SS	Adj MS	F-Value	P-Value
Regression	20	15112.4	15112.4	755.62	49.07	0.000
Linear	5	838.7	838.7	167.74	10.89	0.001
Square	5	12131.5	12131.5	2426.30	157.58	0.000
Interaction	10	2142.2	2142.2	214.22	13.91	0.001
Residual Error	11	169.4	169.4	15.40	-	-
Lack of Fit	6	124.9	124.9	20.81	2.34	0.185
Pure Error	5	44.5	44.5	8.90	-	-
Total	31	15281.7	-	-	-	-

Table 5.12: ANOVA Results for Testing Adequacy of the Yield Strength Model

Source	Df	Seq SS	Adj SS	Adj MS	F-Value	P-Value
Regression	20	12603.7	12603.7	630.18	40.91	0.000
Linear	5	1665.0	1665.0	333.01	21.62	0.000
Square	5	5751.8	5751.8	1150.36	74.68	0.000
Interaction	10	5186.8	5186.8	518.68	33.67	0.000
Residual Error	11	169.4	169.4	15.40	-	-
Lack of Fit	6	105.6	105.6	17.59	1.38	0.371
Pure Error	5	63.9	63.9	12.78	-	-
Total	31	12773.1	-	-	-	-

Table 5.13: ANOVA Results for Testing Adequacy of the Percent Elongation Model

Source	Df	Seq SS	Adj SS	Adj MS	F-Value	P-Value
Regression	20	216.550	216.55	10.8275	35.43	0.000
Linear	5	5.950	5.950	1.1900	3.89	0.028
Square	5	179.425	179.425	35.8850	117.43	0.000
Interaction	10	31.175	31.175	3.1175	10.20	0.000
Residual Error	11	3.362	3.362	0.3056	-	-
Lack of Fit	6	1.649	1.649	0.2748	0.80	0.608
Pure Error	5	1.713	1.713	0.3426	-	-
Total	31	219.912	-	-	-	-

Table 5.14: ANOVA Results for Testing Adequacy of the Micro-hardness Model

Source	Df	Seq SS	Adj SS	Adj MS	F-Value	P-Value
Regression	20	2590.09	2590.09	129.504	28.98	0.000
Linear	5	281.87	281.87	56.374	12.61	0.000
Square	5	831.39	831.39	166.278	37.20	0.000
Interaction	10	1476.83	1476.83	147.683	33.04	0.000
Residual Error	11	49.16	49.16	4.469	-	-
Lack of Fit	6	20.51	20.51	3.419	0.60	0.727
Pure Error	5	28.65	28.65	5.729	-	-
Total	31	2639.25	-	-	-	-

Table 5.15: ANOVA Results for Testing Adequacy of the Impact Toughness Model

Source	Df	Seq SS	Adj SS	Adj MS	F-Value	P-Value
Regression	20	2244.18	2244.18	112.209	46.78	0.000
Linear	5	555.08	555.08	111.017	46.28	0.000
Square	5	1093.19	1093.19	218.639	91.14	0.000
Interaction	10	595.91	595.91	59.591	24.84	0.000
Residual Error	11	26.39	26.39	2.399	-	-
Lack of Fit	6	18.92	18.92	3.153	2.11	0.215
Pure Error	5	7.47	7.47	1.494	-	-
Total	31	2270.57	-	-	-	-

Another evidence which indicates the high correlation between experimental and predicted values is R^2 , $R^2_{(adj)}$, $R^2_{(pred)}$. The values of R^2 and $R^2_{(adj)}$ of full models and reduced model as shown in Table 5.16 shows no significant difference, but $R^2_{(pred)}$ of reduced model is considerably higher than full models of all responses which show greater predictability of variation of experimental values in a new experiment. Therefore reduced models are preferred to full models

Table 5.16: Comparison of R^2 , $R^2_{(adj)}$, $R^2_{(pred)}$ Values

Response	R^2 (%)		$R^2_{(adj)}$ (%)		$R^2_{(pred)}$ (%)	
	Full model	Reduced model	Full model	Reduced model	Full model	Reduced model
Tensile strength	98.89	96.71	96.88	95.36	78.21	92.57
Yield strength	98.67	98.33	96.26	96.95	80.12	93.29
Percent Elongation	98.47	94.94	95.69	92.87	79.33	88.92
Micro-hardness	98.14	96.11	94.75	93.97	77.89	89.55
Impact Toughness	98.84	98.57	96.72	96.84	77.19	90.38

5.12.2 Comparison of Predicted and Experimentally Determined Mechanical Properties

The RSM was employed to predict the mechanical properties of pulse TIG welded AA5083-O and AA6061-T651 aluminum alloy welded joints by the established mathematical model. The predicted mechanical properties of AA5083-O and AA6061-T651 weldments by RSM and the experimentally determined mechanical properties are presented in Table 5.17.

Table 5.17: Predicted and Experimentally Determined Mechanical Properties

Std order	Tensile Strength (MPa)		Yield Strength (MPa)		Percent Elongation (%)		Micro hardness (HV)		Impact Toughness (J)	
	Exp	Pred	Exp	Pred	Exp	Pred	Exp	Pred	Exp	Pred
1	157.15	156.053	127	123.551	7.05	6.632	71	69.692	11	13.873
2	169	172.217	135.3	132.935	5.9	5.056	84.04	83.572	19.5	22.937
3	144.75	146.915	106.7	106.505	4.4	3.85	94.04	93.94	14	15.475
4	155.45	158.643	100.27	101.097	7.1	7.838	74.98	71.636	17	18.415
5	171	169.267	143.75	142.295	8.061	8.5	86.56	88.192	13.5	16.769
6	164.25	163.535	147.65	144.983	6.65	6.924	70.9	73.08	10.5	13.705
7	154.4	160.937	138.35	138.273	5.35	5.718	98.93	96.552	21.5	22.747
8	199.99	231.463	174.65	174.905	11.219	9.706	76.98	77.032	22.5	24.311
9	171.6	179.435	150.7	154.613	7.2	12.104	74.4	76.766	23	23.685
10	153.4	153.367	122.01	119.795	6.65	6.57	99.9	99.07	19.5	20.997
11	170.25	171.105	153.4	153.353	7.55	7.776	88.5	88.702	10	10.787
12	186.22	184.393	161.75	161.209	5.661	6.236	73.78	74.822	40.5	42.727
13	163.05	166.213	148.2	146.151	6.65	6.986	82	82.162	30	31.329
14	161.95	162.041	130.05	126.759	6.05	6.114	99.09	101.682	16	18.769
15	163.7	157.083	141.3	140.597	6.25	7.32	80.89	78.24	28.5	30.559
16	147.08	148.475	106.75	106.413	5.65	5.78	95.45	93.322	21.5	24.371
17	161.95	160.33	146.1	149.284	6.15	5.957	82.5	79.993	20.5	21.839
18	163.9	167.886	140.2	142.156	5.481	5.957	76.78	79.993	28.5	27.091
19	206.2	209.46	163.35	166.151	11.9	12.165	94.29	94.849	24.38	31.221
20	200.1	209.46	159.2	163.18	11.04	12.165	94.83	94.849	28.63	38.053
21	148.3	151.832	104.15	107.338	4.75	5.211	84.34	85.173	17	18.009
22	153	151.832	124.4	126.35	6.8	6.623	93.31	93.181	22.5	21.425
23	175.7	174.332	128.4	129.752	8.65	8.345	81.69	83.167	11.5	13.78
24	170.6	174.332	134.87	138.656	7.75	8.345	94.2	93.427	23	24.091
25	176.65	170.784	153.25	156.592	7.55	6.893	78.5	79.641	32	31.341
26	162.55	170.784	130.43	132.224	5.95	6.893	80.08	79.641	21	21.589
27	204.35	209.46	166.95	163.18	12.65	12.165	95.45	94.849	34	34.637
28	209.4	209.46	164.94	163.18	11.25	12.165	92.38	94.849	36.5	34.637
29	211.7	209.46	162.1	163.18	12.9	12.165	97.98	94.849	34	34.637
30	209.8	209.46	166.35	163.18	11.924	12.165	94.56	94.849	33	34.637
31	211	209.46	166.2	163.18	12.4	12.165	92.23	94.849	35	34.637
32	212.9	209.46	157.65	163.18	12.15	12.165	97.2	94.849	35.25	34.637

From the Table 5.16, it is observed that for all the mechanical properties, the experimental and predicted results are very close with minimum deviation. Therefore it is concluded that the RSM can able to predict the mechanical properties of welded joints with more accuracy.

Figure 5.20(a-e) shows scatter diagram between observed and predicted values of responses. The scatter diagram was drawn showing the degree of closeness between observed and predicted values of responses

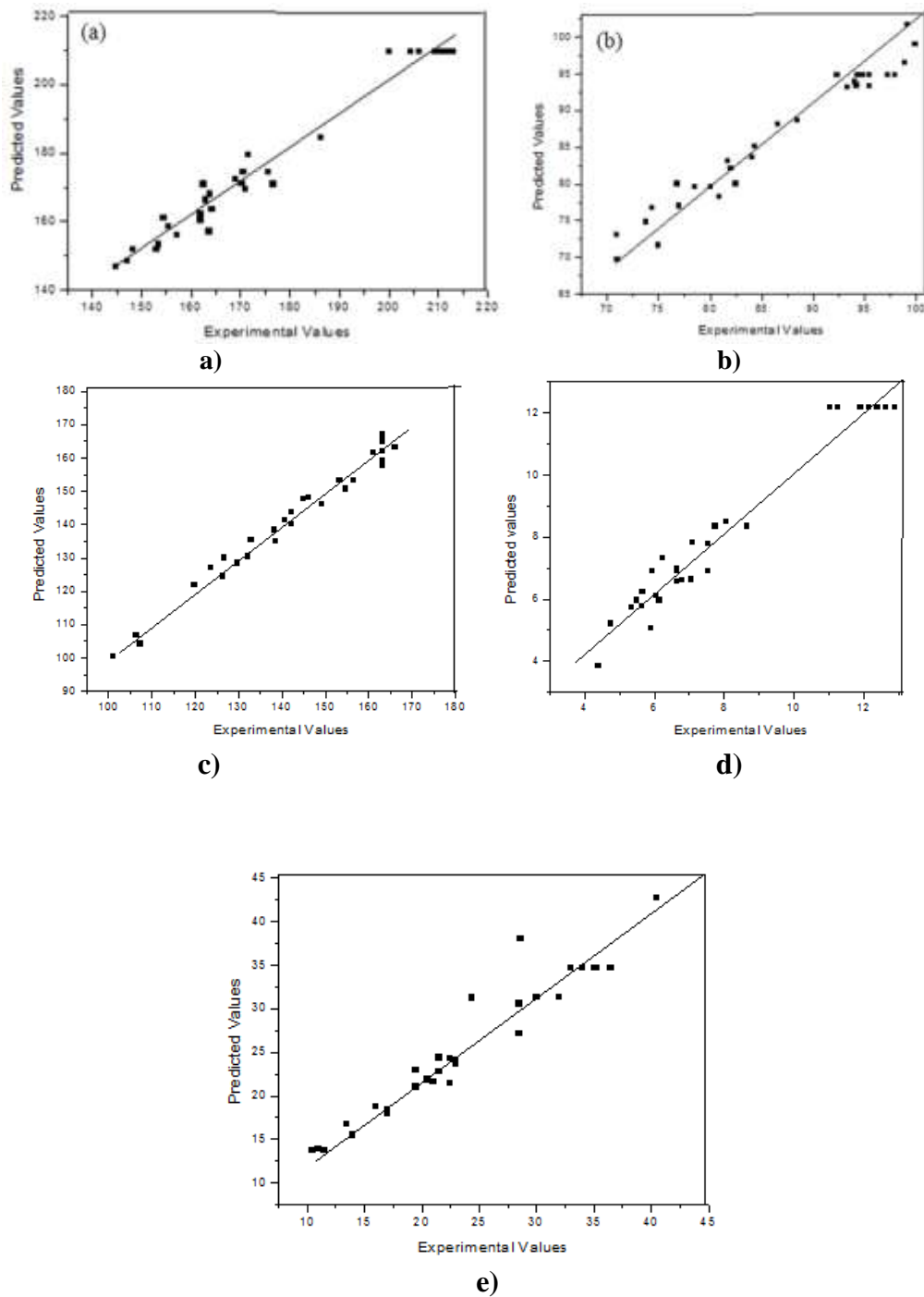


Figure 5.20: Scatter Diagram for Response a) Tensile Strength b) Micro-hardness c) Yield Strength d) Percent Elongation e) Impact Toughness

5.12.3 Conformity of Test to Declare Validity of Mathematical Models

To test the accuracy of the models in actual application, Conformity tests were conducted by assigning optimum values for the process variables within their working limits but different from design matrix. Specimens were cut for mechanical testing. The results of conformity test are presented in Table 5.18.

The error percentage was then calculated as:

$$\text{Error (\%)} = \frac{\text{Observed values} - \text{predicted values}}{\text{predicted values}}$$

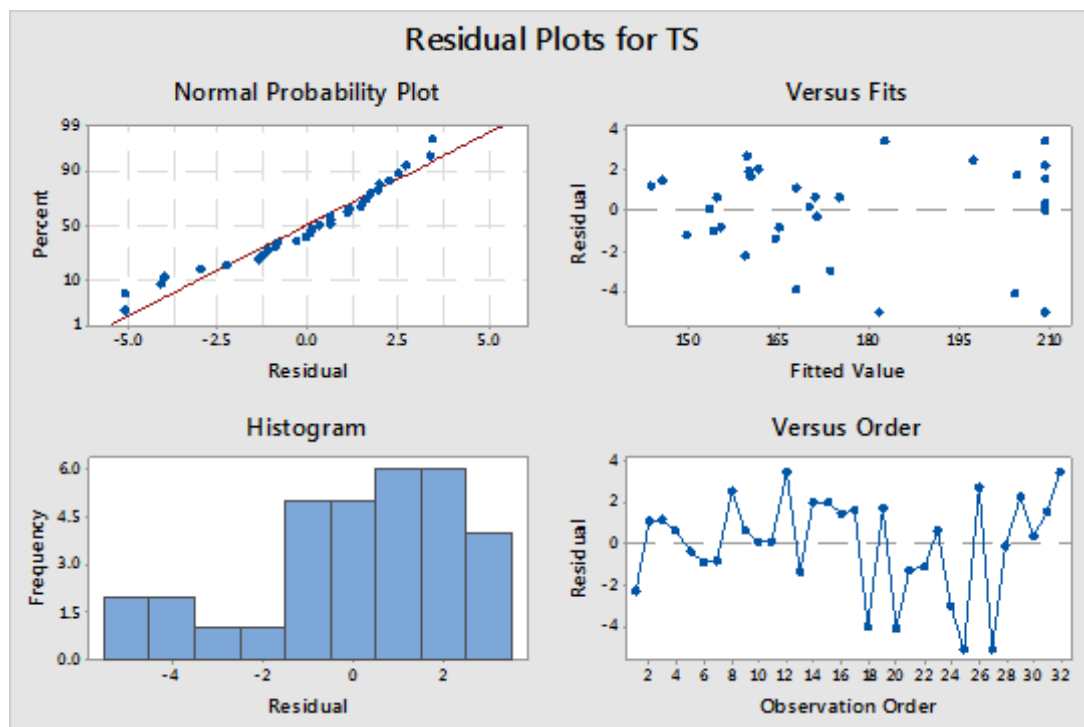
Table 5.18: Results of Conformity Test

Response	Process parameter					Experimental	Predicted	Error (%)
	P	B	F	T	S			
Tensile strength	196.81	133.0	6.04	49.9	171.16	202.50	201.85	0.32
	202	125	8.04	44	166	175.7	172.937	1.5
	212	118	5	48	174	168.2	170.636	-1.4
Yield strength						169.76	167.03	1.6
						172.67	169.03	2.1
						141.2	144.608	-2.3
Percent elongation						8.9	9.43	-5.6
						9.4	8.91	5.4
						7.1	8.1	-2.3
Micro-hardness						86.92	88.41	-1.6
						78.25	81.45	-3.9
						77.21	81.77	-5.5
Impact toughness						35.0	33.35	4.9
						21	19.95	5.2
						27.4	29.06	-5.7

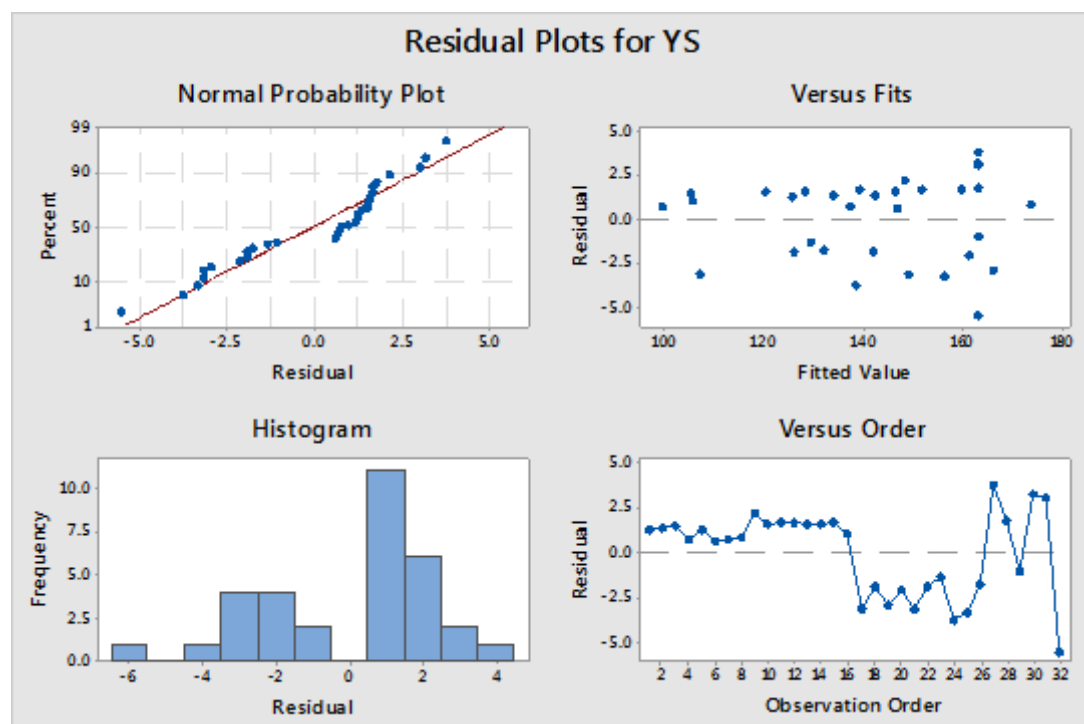
5.12.4 Residual Plots

The normal percentage probability versus residual plots for tensile strength, yield strength, percent elongation, micro-hardness and impact toughness are shown in figure.

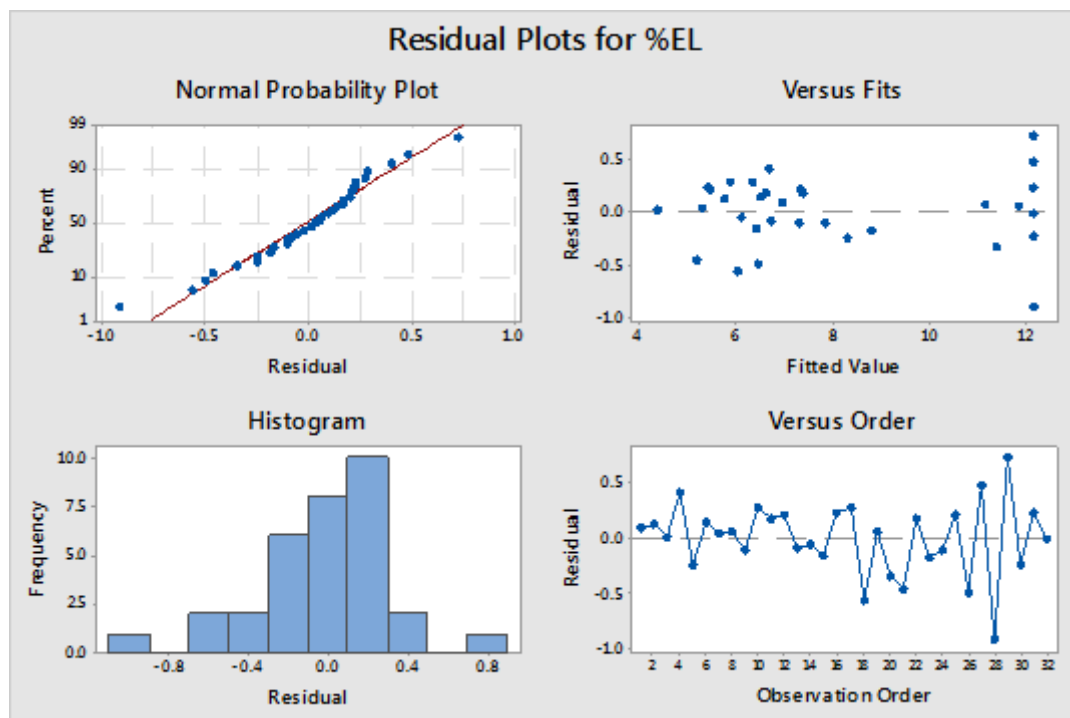
5.21 (a-e)



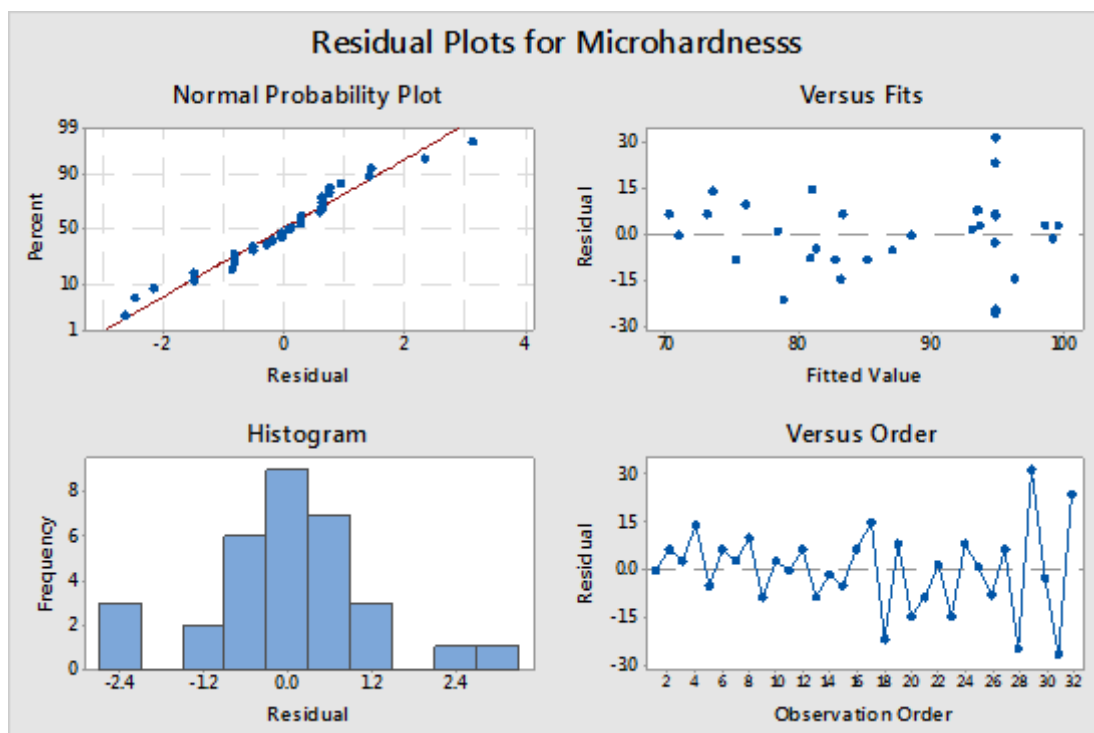
a)



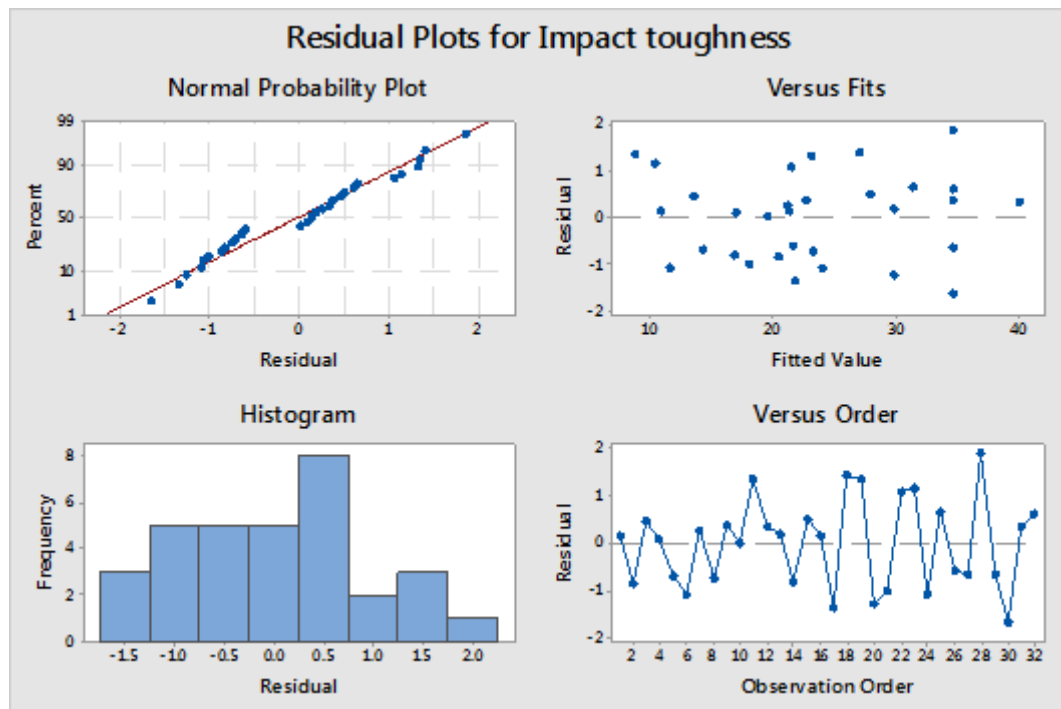
b)



c)



d)



e)

Figure 5.21: Plots for Checking Validity of a) Tensile Strength b) Yield Strength c) Percent Elongation d) Micro-hardness e) Impact Toughness

Figure 5.21 reveals that the residuals are falling on the straight line, which means the errors are normally distributed [189].

From the regression models, the effect of pulse TIG welding parameters viz peak current, base current, pulse frequency, pulse on time, welding speed on tensile strength, yield strength, percent elongation, micro-hardness, impact toughness of pulse TIG welding joints were evaluated. The five operating parameters considered directly affect heat input and bead geometry characteristics. The possible cause for the effects of different welding parameters on tensile strength, Yield strength, percent elongation, micro hardness and impact toughness has been interpreted as follows. The significant terms identified based on Eq. (5.5) are peak current (P), interaction effects of the pulse current and base current (PB). The negative coefficient of welding speed (S) indicates tensile strength decreases with increase in welding speed.

The significant terms identified based on Eq. (5.6) are pulse frequency (F), pulse on time (T), interaction effects of pulse current and base current (PB), base current and pulse on time. The negative coefficient of pulse current (P) and welding speed (S) indicates the decrease in yield strength as pulse current and welding speed increases.

The significant terms identified based on Eq. (5.7) are pulse frequency (F), interaction effects of the pulse current and base current (PB).

The significant terms identified based on Eq.(5.8) are pulse frequency (F), pulse on time (T), interaction effects of peak current and pulse on time (PT), base current and welding speed (BS), pulse on time and welding speed (TS).

The significant terms identified based on Eq.(5.9) are pulse current (P), base current (B), pulse frequency (F), pulse on time (T), interaction effects of pulse current and base current (PB), base current and pulse frequency (BF), pulse frequency and welding speed (FS)

Chapter 6
Results and Discussion

RESULT AND DISCUSSION

6.1 Introduction

Mathematical models developed in chapter 5 have been used to estimate the tensile strength, yield strength, percent elongation, micro-hardness and impact toughness of the pulsed current TIG welded AA5083-O and AA6061-T651 aluminum alloy joints for different combinations of process parameters. The plotted graphs can be effectively used to understand the direct effect of process parameter such as peak current, base current, pulse frequency, pulse on time and welding speed on mechanical and metallurgical properties of pulse TIG welded AA5083-O and AA6061-T651 Aluminum Alloy joints.

6.2 Tensile Strength

The study of effect of process parameters and their interaction on tensile strength is essential to understand the behavior of tensile strength. So subsequent sections describes the effect of peak current, base current, pulse frequency, pulse on time ,welding speed and their interaction on tensile strength.

6.2.1 Effect of Peak Current on Tensile Strength

Figure 6.1 depicts the effect of peak current on tensile strength of pulse TIG welded AA5083-O and AA6061-T651 Aluminum Alloy joint. At lower peak current (175 A), the tensile strength of pulse TIG welded joints is lower. When peak current is increased from 175 A to 195 A, likewise the tensile strength also increases and reaches a maximum at 195 A. If the peak current is increased above 195 A, the tensile

strength of the joint decreased. Higher peak current (215 A) usually resulting in higher heat input per unit length and slower cooling rate in the fusion zone causes excessive grain growth, which subsequently leads to lower tensile properties of the joints. A lower peak current (175, 185 A) results in lack of penetration due to lower heat input per unit length, which results in pores of the weld seam and this lower the tensile properties.

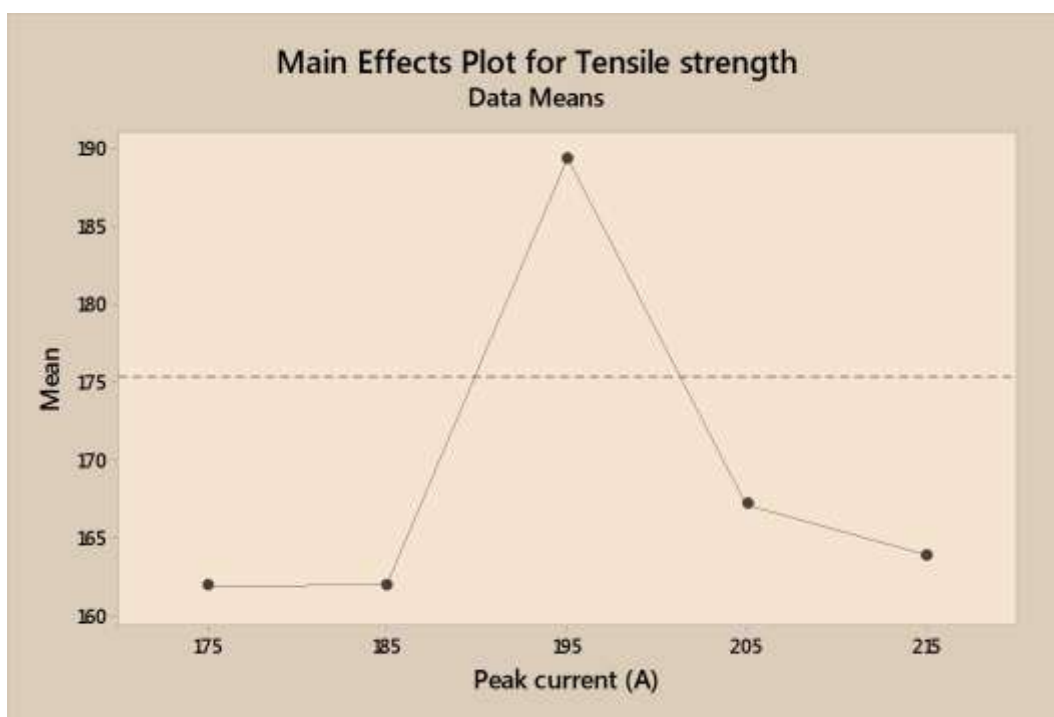


Figure 6.1: Effect of Peak Current on Tensile Strength

6.2.2 Effect of Base Current on Tensile Strength

Tensile strength of the joints fabricated using different levels of base current are presented in figure 6.2. The joints fabricated using base current of 105 A exhibited maximum tensile strength of 206 MPa. The joints fabricated using a base current of

126 A showed minimum tensile strength. The grain coarsening deteriorated the tensile properties of these joints.

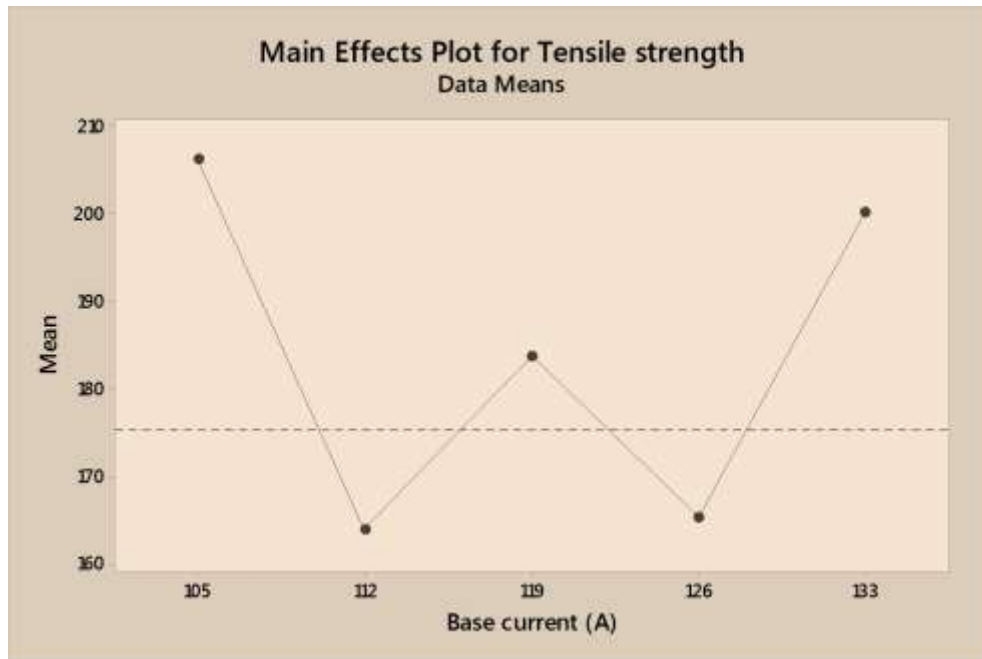


Figure 6.2: Effect of Base Current on Tensile Strength

6.2.3 Effect of Pulse Frequency on Tensile Strength

Figure 6.3 reveals the effect of pulse frequency on tensile strength of pulse TIG welded AA5083-O and AA6061-T651 Aluminum Alloy joints. At pulse frequency (2 Hz), the tensile strength of pulse TIG welded joints is lower. When lower pulse frequency is increased from 2 Hz, correspondingly tensile strength also increases and reaches a maximum at 6 Hz. If pulse frequency is increased above 6 Hz, the tensile strength of the joints decreased. At very low frequencies, the effect of pulsing on the weld bead is found to be very less. The mechanical and thermal disturbances to the weld pool at low frequency of pulsing are less intense. At high frequency values the molten pool is agitated more resulting in grain refinement in the weld region which in turn resulting in increased tensile strength.

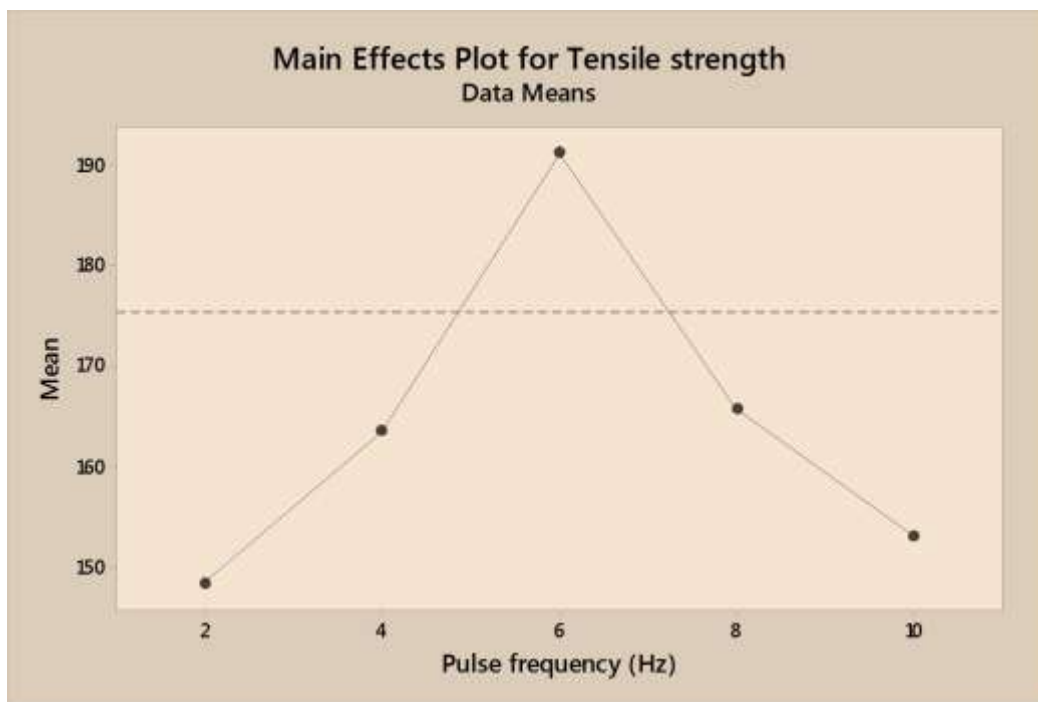


Figure 6.3: Effect of Pulse Frequency on Tensile Strength

6.2.4 Effect of Pulse On Time on Tensile Strength

Figure 6.4 reveals the effect of pulse on time on tensile strength of pulse TIG welded AA5083-O and AA6061-T651 Aluminum Alloy joints. As pulse on time increases from 40 to 45 %, the tensile strength decreases from 175 to 165 MPa. The tensile strength increases significantly from 165 to 190 MPa when pulse on time increases from 45 to 50 %. As pulse on time further increases from 50 to 55 %, there is significant decrease in tensile strength and then beyond 55 %, it is slightly increased. The pulse on time period decides the size of the weld pool. If the weld pool becomes too large the pulse time period is reduced. If the pulse on time was lower than 40 % weld nugget formation was not smooth due to incomplete melting of the base metal which resultantly lowers the tensile properties. On contrary, if the pulse on time was greater than 60 %, over melting of the base metal and overheating of the tungsten electrode were noticed, which leads to decrease in tensile strength.

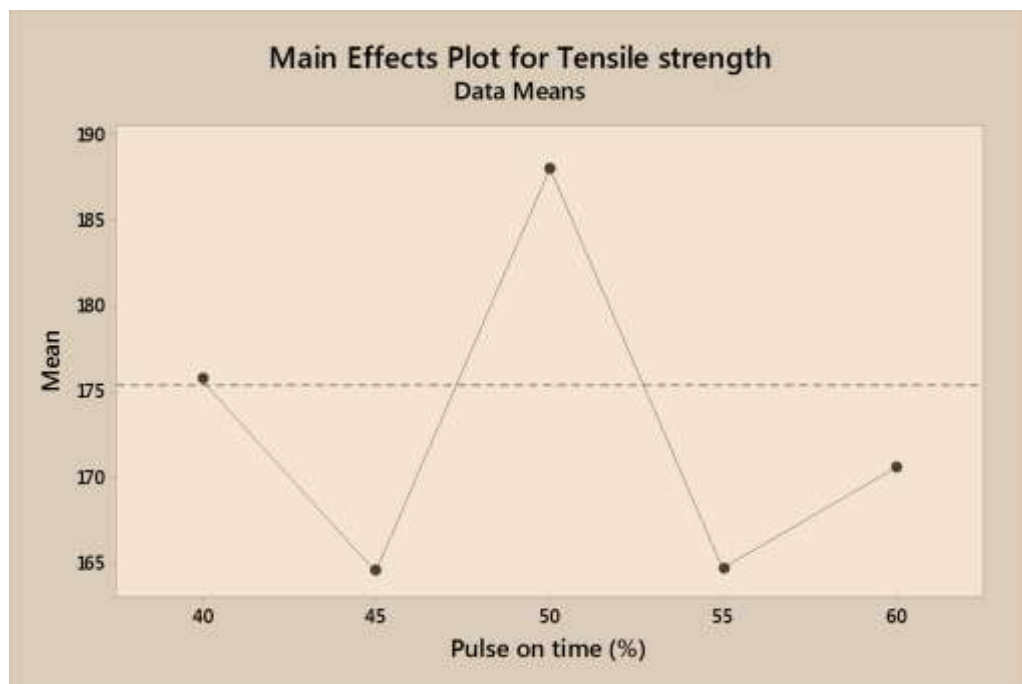


Figure 6.4: Effect of Pulse On Time on Tensile Strength

6.2.5 Effect of Welding Speed on Tensile Strength

Tensile strength of the joints fabricated using different levels of welding speed has been presented in figure 6.5. As welding speed increases from 155 to 165 mm/min, the tensile strength decreases slightly from 175 to 172 MPa. The tensile strength increases from 172 to 188 MPa when welding speed increases from 165 to 175 mm/min. As welding speed further increases from 175 to 185 mm/min, there is significant reduction in tensile strength and beyond 185 mm/min, there is slight increment in tensile strength. The increase in welding speed from 155 to 175 mm/min decreases the heat input per unit length of weld, due to this faster cooling takes place in the weldment which promotes equi-axed and homogeneous grain structure in weld zone which increases the tensile strength. On the contrary if welding speed is further increased that is from 175 to 195 mm/min, there is incomplete fusion and lack of penetration in the weldment which decreases the tensile strength.

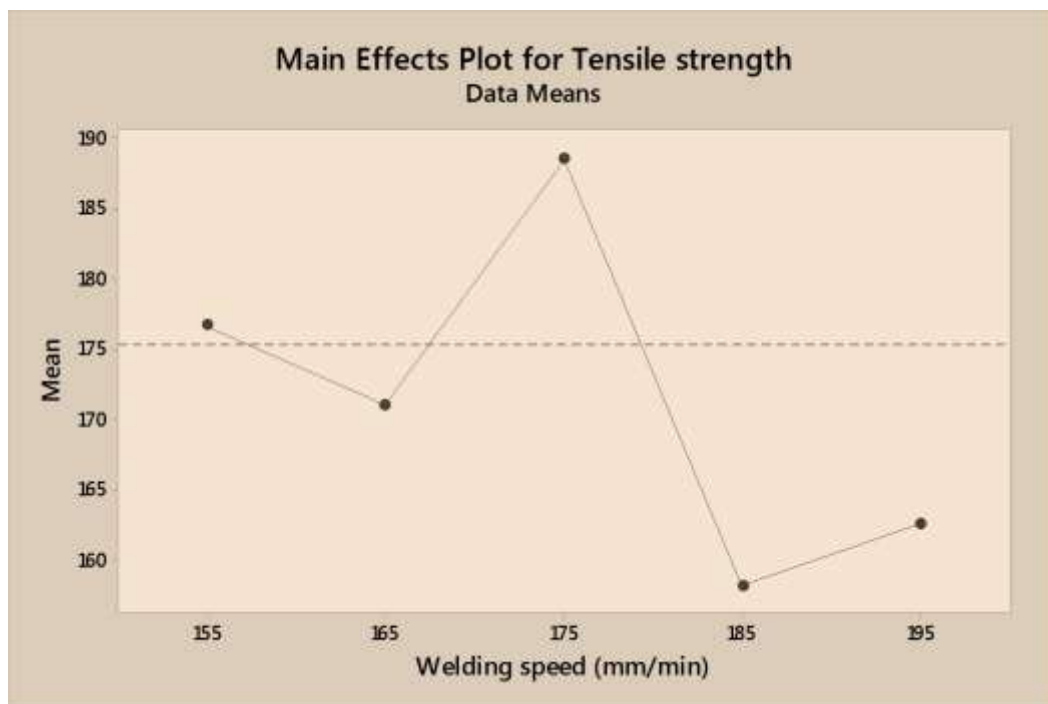


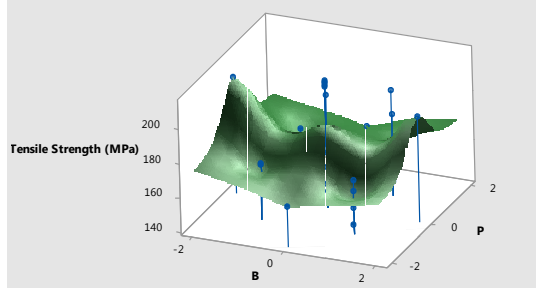
Figure 6.5: Effect of welding speed on tensile strength

6.2.6 Effect of Interactions of Parameters on Tensile Strength

From the figure 6.6 (ii), it is clear that peak current and pulse frequency has significant effect on tensile strength. The tensile strength increases when peak current and pulse frequency increases. Figure 6.6 (iii), shows peak current and pulse on time are significant parameter. Figure 6.6 (iv), indicates that peak current and welding speed are significant factors effecting tensile strength.

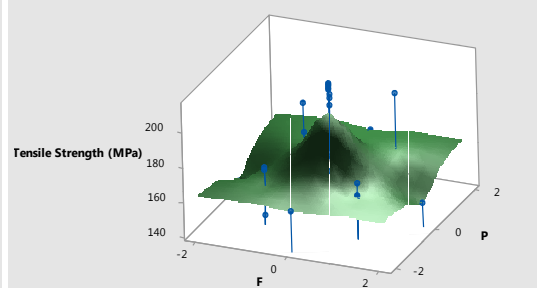
Figure 6.6 (viii), shows that pulse frequency and pulse on time has significant effect on tensile strength. Figure 6.6 (ix), indicates the significant effect of pulse frequency and welding speed. Figure 6.6 (x) pulse on time and welding speed are significant parameters affecting tensile strength. The tensile strength increases when all the above stated interaction parameters increases.

Surface Plot of Tensile Strength (MPa) vs P, B



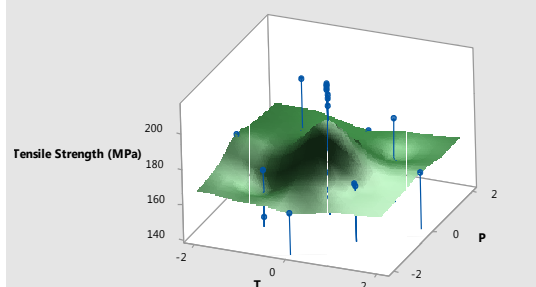
(i)

Surface Plot of Tensile Strength (MPa) vs P, F



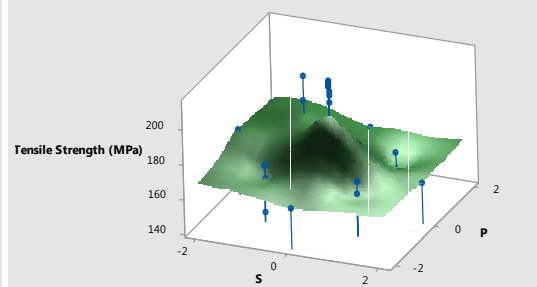
(ii)

Surface Plot of Tensile Strength (MPa) vs P, T



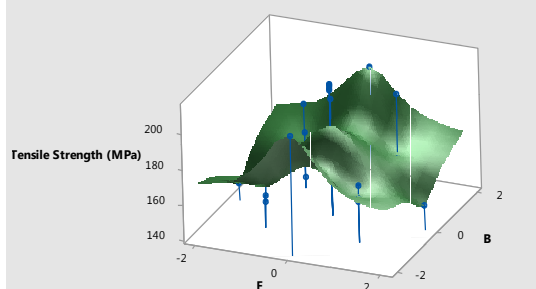
(iii)

Surface Plot of Tensile Strength (MPa) vs P, S



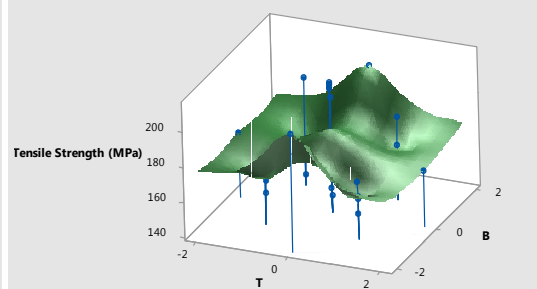
(iv)

Surface Plot of Tensile Strength (MPa) vs B, F



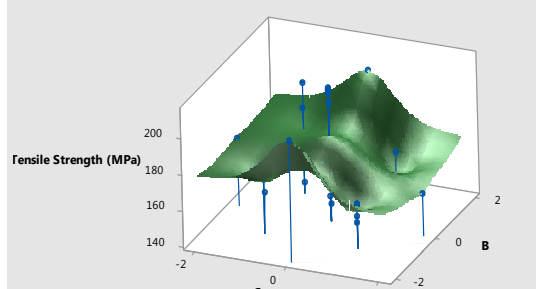
(v)

Surface Plot of Tensile Strength (MPa) vs B, T



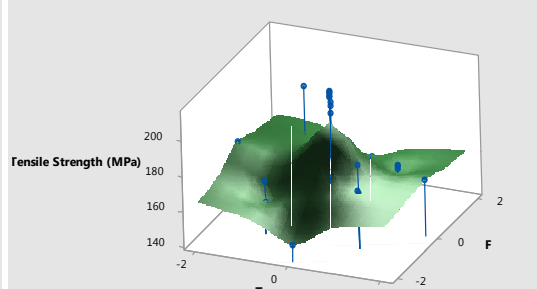
(vi)

Surface Plot of Tensile Strength (MPa) vs B, S



(vii)

Surface Plot of Tensile Strength (MPa) vs F, T



(viii)

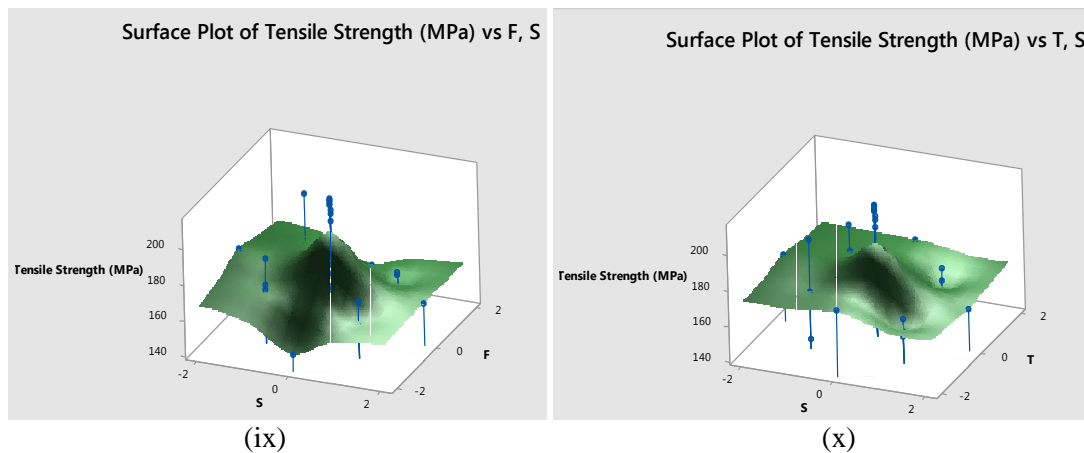


Figure 6.6: Interaction Effect of Parameters on Tensile Strength; i) P-B, ii) P-F, iii) P-T, iv) P-S, v) B-F, vi) B-T, vii) B-S, viii) F-T, ix) F-S, x) T-S

6.3 Yield Strength

The study of effect of process parameters and their interaction on yield strength is essential to understand the behavior of yield strength. So subsequent sections describes the effect of peak current, base current, pulse frequency, pulse on time, welding speed and their interaction on yield strength.

6.3.1 Effect of Peak Current on Yield Strength

Yield strength of the joints by using different levels of peak current has been presented in figure 6.7. As the peak current increases from 175 to 185 A, yield strength decreases slightly from 143 to 139 MPa. The yield strength increases significantly from 139 to 149 MPa when peak current increases from 185 to 195 A. As the peak current further increases from 195 to 205 A, there is significant reduction in yield strength and beyond 205 A, there is slight increase in yield strength.

It is evident that the peak current is important parameter which has significant influence on yield strength. It is considered crucial parameter and needs to monitored for yield strength properties of aluminum.

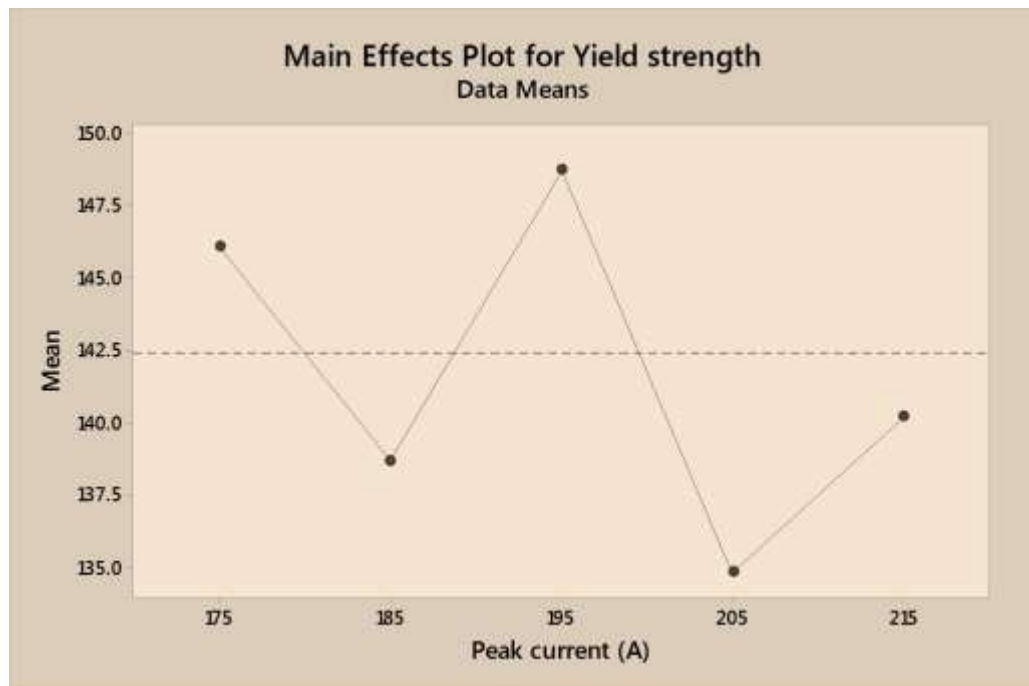


Figure 6.7: Effect of Peak Current on Yield Strength

6.3.2 Effect of Base Current on Yield Strength

Figure 6.8 reveals the effect of base current on yield strength of pulse TIG welded AA5083-O and AA6061-T651 Aluminum Alloy joints. As base current increases from 105 to 112 A, yield strength decreases significantly from 164 to 138 MPa.

The yield strength increases slightly from 138 to 145 MPa when base current increases from 112 to 119 A. As the base current further increases from 119 to 126 A, there is slight reduction in yield strength and beyond 133 A, there is significant increase in yield strength.

It is evident that the base current is important parameter which has significant influence on yield strength. It is considered crucial parameter and needs to be monitored for yield strength properties of aluminum.

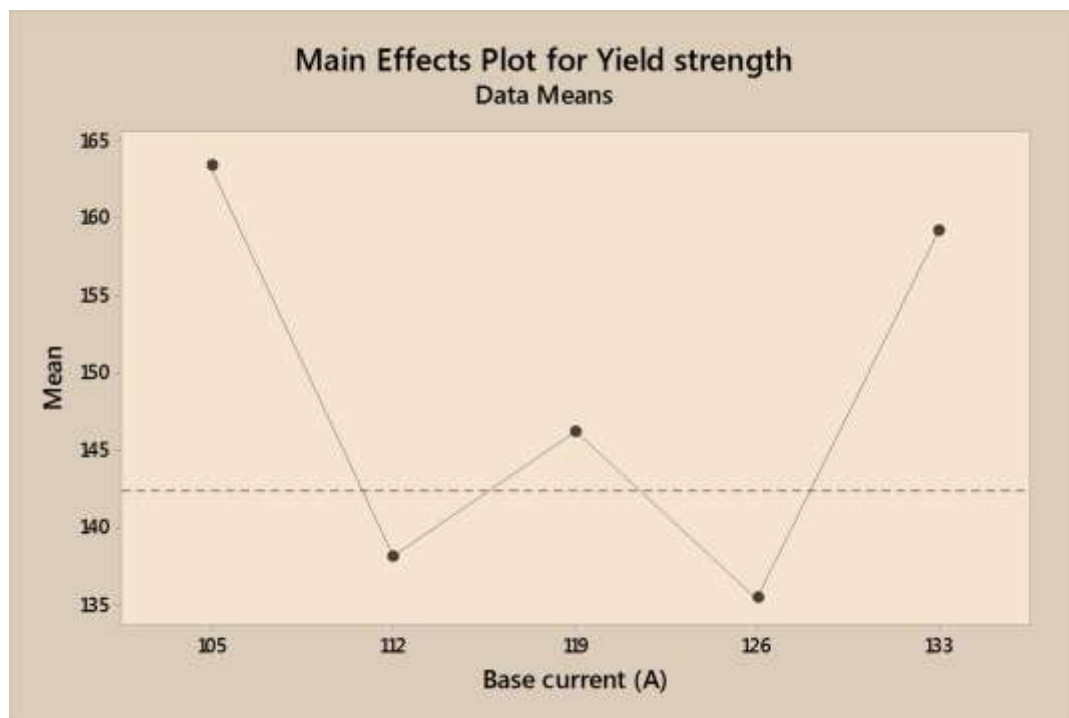


Figure 6.8: Effect of Base Current on Yield Strength

6.3.3 Effect of Pulse Frequency on Yield Strength

Figure 6.9 reveals the effect of pulse frequency on yield strength of pulse TIG welded AA5083-O and AA6061-T651 Aluminum Alloy joints. At pulse frequency (2 Hz), the yield strength of pulse TIG welded joints is lower.

When lower pulse frequency is increased from 2 Hz, correspondingly yield strength also increases and reaches a maximum at 6 Hz. If pulse frequency is increased above 6 Hz, the yield strength of the joints decreased.

It is evident that the pulse frequency is important parameter which has significant influence on yield strength. It is considered crucial parameter and needs to monitored for yield strength properties of aluminum

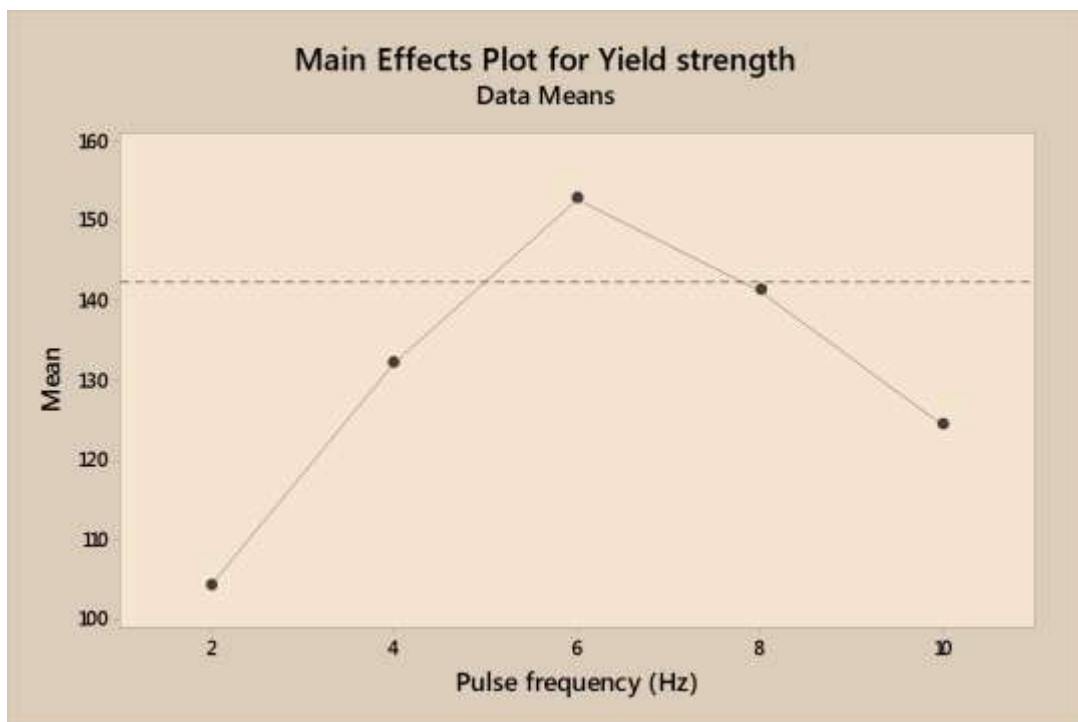


Figure 6.9: Effect of Pulse Frequency on Yield Strength

6.3.4 Effect of Pulse On Time on Yield Strength

Figure 6.10 reveals the effect of pulse frequency on yield strength of pulse TIG welded AA5083-O and AA6061-T651 Aluminum Alloy joints. At pulse on time (40 %), the yield strength of pulse TIG welded joints is lower.

When lower pulse on time is increased from 40 %, correspondingly yield strength also increases and reaches a maximum at 50 %. If pulse on time is increased above 50 %, the yield strength of the joints decreased

It is evident that the pulse on time is important parameter which has significant influence on yield strength. It is considered crucial parameter and needs to monitored for yield strength properties of aluminum

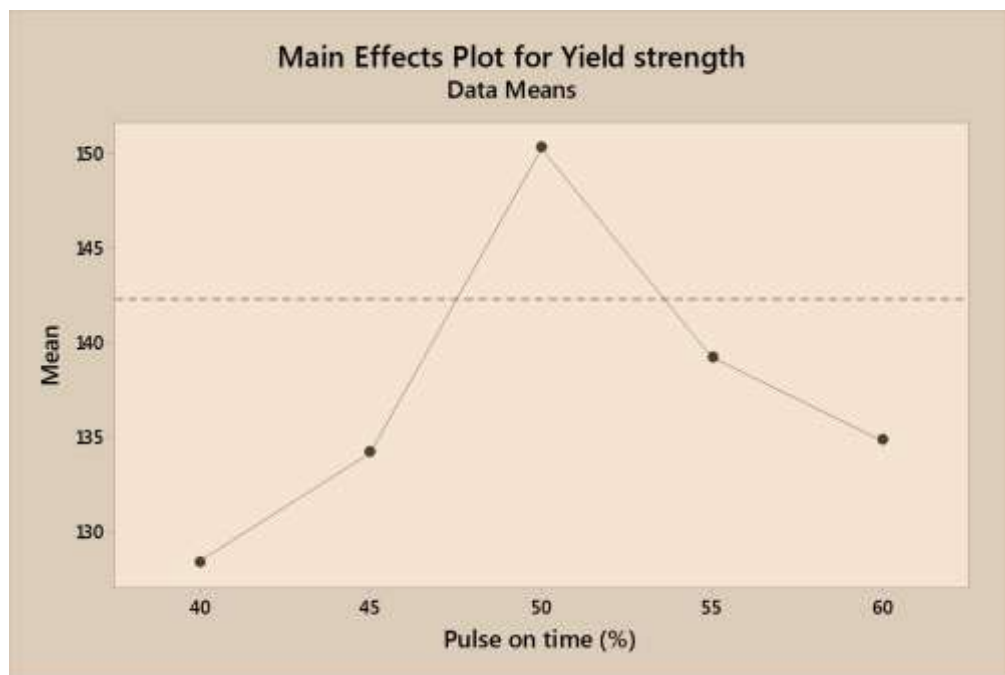


Figure 6.10: Effect of pulse on time on yield strength

6.3.5 Effect of Welding Speed on Yield Strength

Yield strength of the joints fabricated using different levels of welding speed has been presented in figure 6.11. As welding speed increases from 155 to 165 mm/min, the yield strength decreases from 154 to 143 MPa. The yield strength increases slightly from 143 to 148 MPa when welding speed increases from 165 to 175 mm/min.

As welding speed further increases from 175 to 185 mm/min, there is significant reduction in yield strength and beyond 185 mm/min, no change is seen value of yield strength.

It is evident that the welding speed is important parameter which has significant influence on yield strength. It is considered crucial parameter and needs to monitored for yield strength properties of aluminum

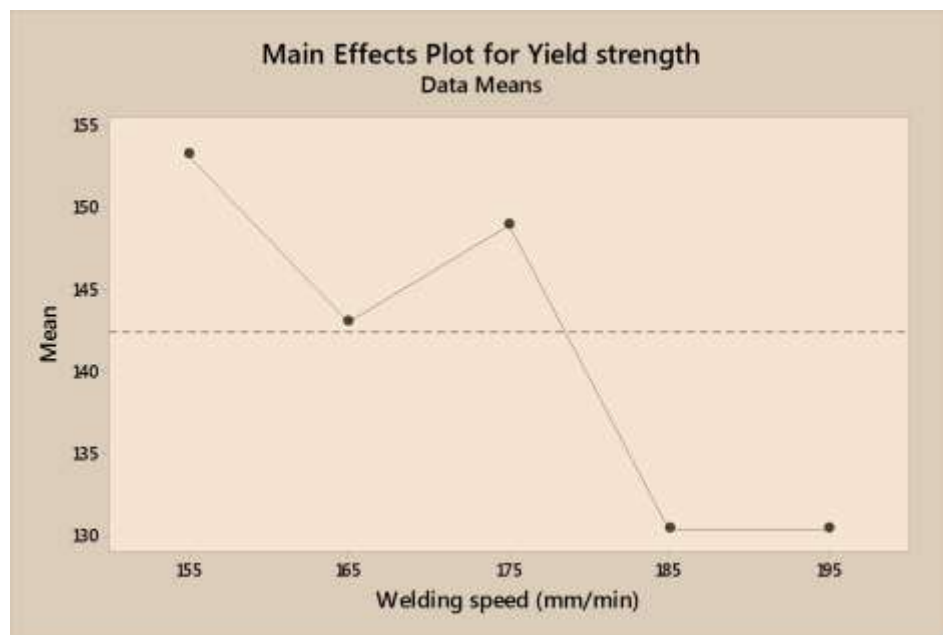


Figure 6.11: Effect of Welding Speed on Yield Strength

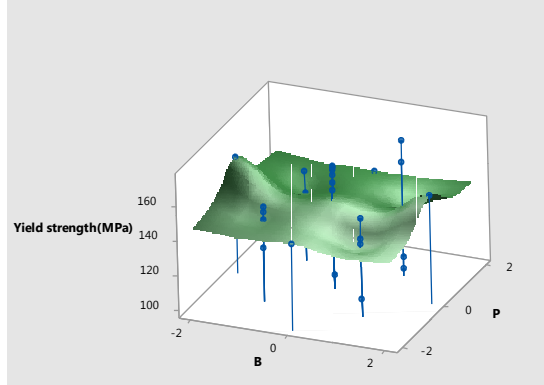
6.3.6 Effect of Interactions of Parameters on Yield Strength

Figure 6.12 (ii), shows the interaction effects of peak current and pulse frequency on yield strength, which indicates the increase in yield strength as peak current and pulse frequency increases.

Figure 6.12 (iii), indicates that peak current and pulse on time are significantly influencing yield strength. Figure 6.12 (viii), shows pulse frequency and pulse on time have considerable influence on yield strength. Figure 6.12 (ix), shows the pulse frequency and welding speed has significant effect on yield strength.

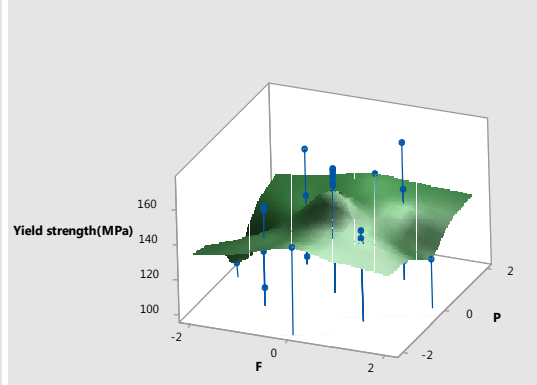
Figure 6.12 (x), indicates that pulse on time and welding speed are significantly effecting tensile strength. Yield strength increases when all the interaction combinations of parameters stated above increases

Surface Plot of Yield strength(MPa) vs P, B



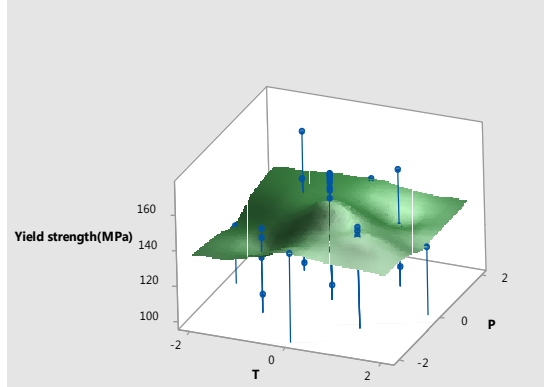
(i)

Surface Plot of Yield strength(MPa) vs P, F



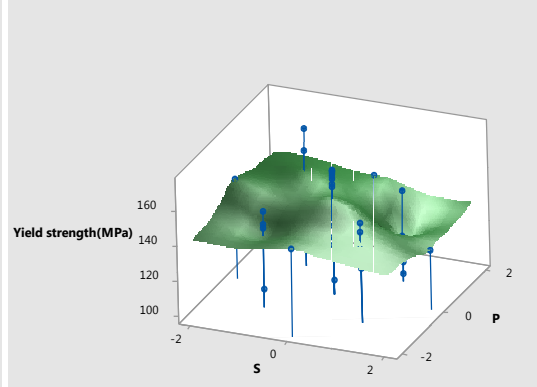
(ii)

Surface Plot of Yield strength(MPa) vs P, T



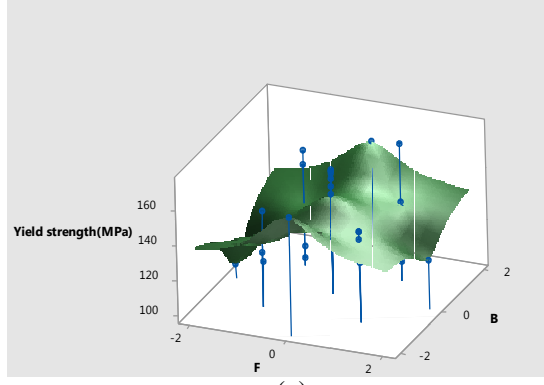
(iii)

Surface Plot of Yield strength(MPa) vs P, S



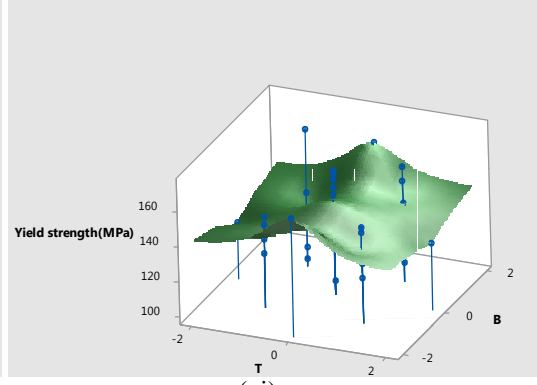
(iv)

Surface Plot of Yield strength(MPa) vs B, F



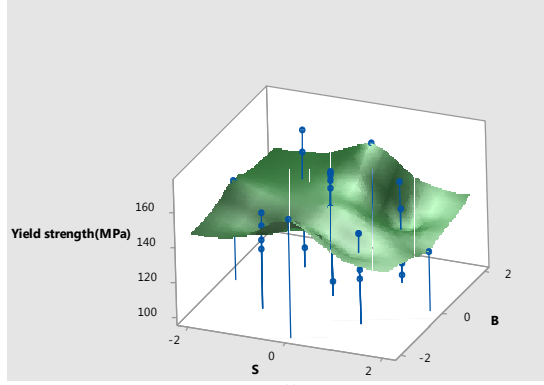
(v)

Surface Plot of Yield strength(MPa) vs B, T



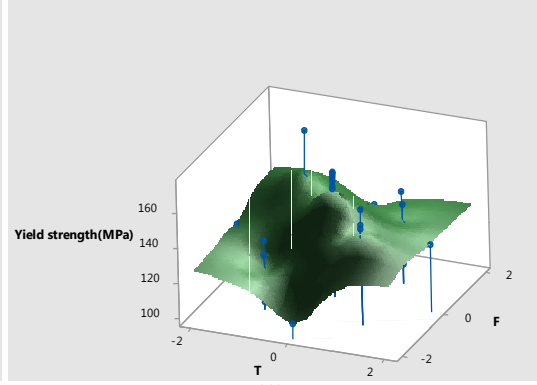
(vi)

Surface Plot of Yield strength(MPa) vs B, S



(vii)

Surface Plot of Yield strength(MPa) vs F, T



(viii)

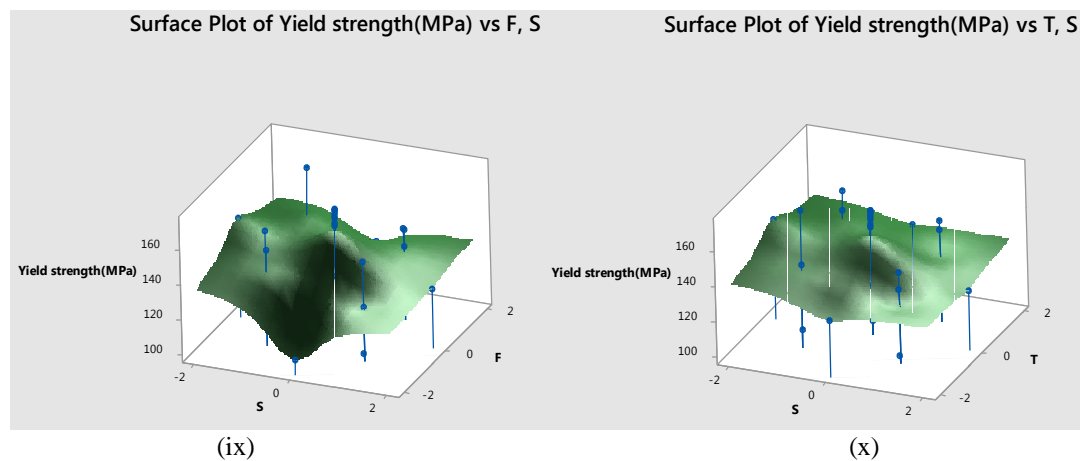


Figure 6.12: Interaction Effect of Parameters on Yield Strength; i) P-B, ii) P-F, iii) P-T, iv) P-S, v) B-F, vi) B-T, vii) B-S, viii) F-T, ix) F-S, x) T-S

6.4 Percent Elongation

The study of effect of process parameters and their interaction on percent elongation is essential to understand the behavior of percent elongation. So subsequent sections describes the effect of peak current, base current, pulse frequency, pulse on time, welding speed and their interaction on percent elongation.

6.4.1 Effect of Peak Current on Percent Elongation

Figure 6.13 reveals the effect of peak current on percent elongation of pulse TIG welded AA5083-O and AA6061-T651 Aluminum Alloy joints. At peak current (175 A), the percentage elongation of pulse TIG welded joints is lower.

When lower peak current is increased from 175 A, correspondingly percent elongation also increases and reaches a maximum at 195 A. If peak current is increased above 195 A, the percent elongation of the joints decreased.

It is evident that the peak current is important parameter which has significant influence on percent elongation. It is considered crucial parameter and needs to monitored for percent elongation properties of aluminum.

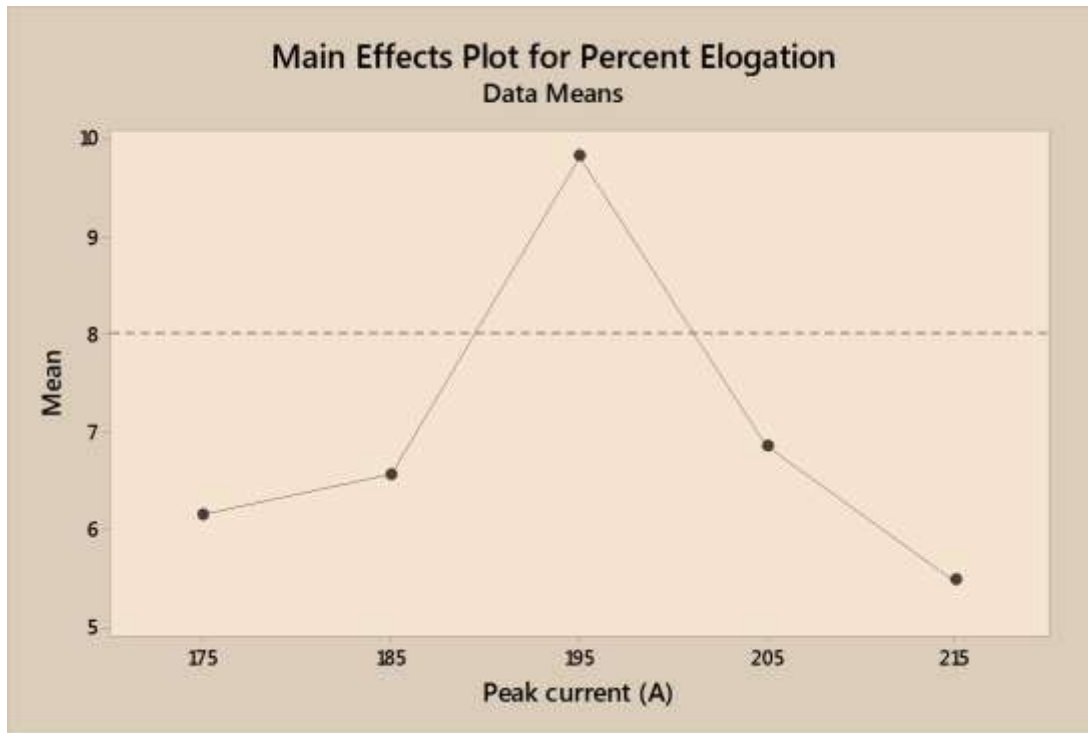


Figure 6.13: Effect of Peak Current on Percent Elongation

6.4.2 Effect of Base Current on Percent Elongation

Figure 6.14 reveals the effect of base current on percentage elongation of pulse TIG welded AA5083-O and AA6061-T651 Aluminum Alloy joints. As base current increases from 105 to 112 A, percent elongation decreases significantly from 12 to 7 %. The percent elongation increases slightly from 7 to 9 % when base current increases from 112 to 119 A. As the base current further increases from 119 to 126 A, there is slight reduction in percent elongation and beyond 133 A, there is significant increase in percent elongation.

It is evident that the base current is important parameter which has significant influence on percent elongation. It is considered crucial parameter and needs to be monitored for percent elongation properties of aluminum.

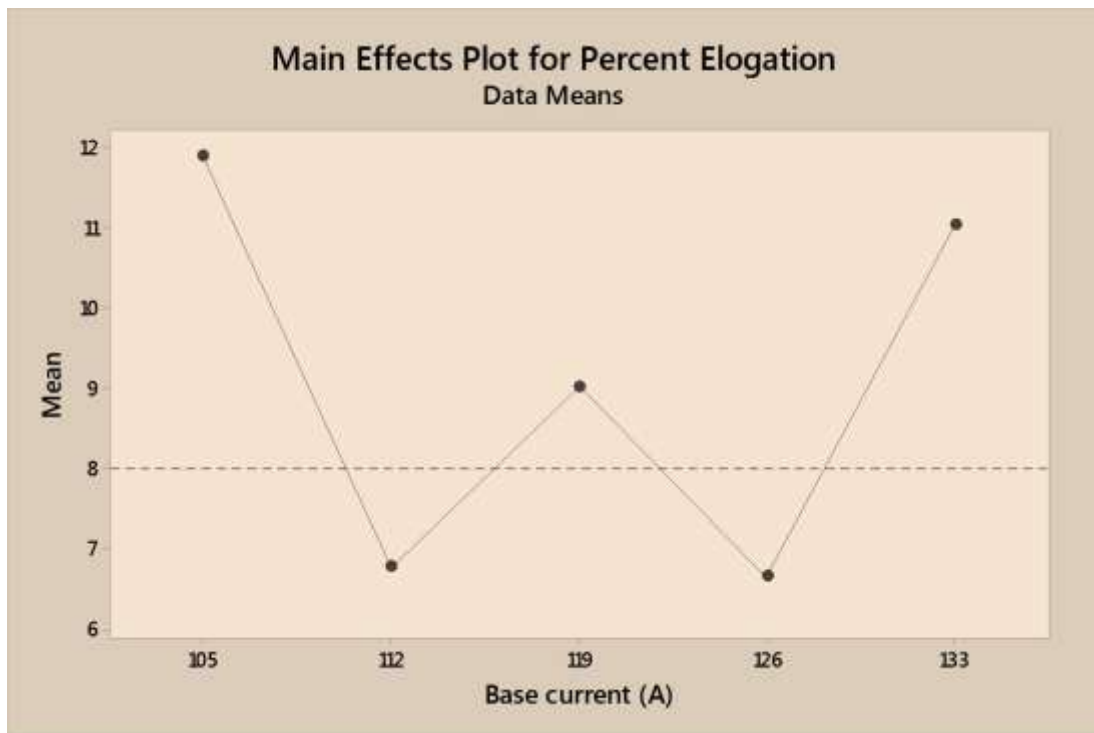


Figure 6.14: Effect of Base Current on Percent Elongation

6.4.3 Effect of Pulse Frequency on Percent Elongation

Figure 6.15 reveals the effect of pulse frequency on percent elongation of pulse TIG welded AA5083-O and AA6061-T651 Aluminum Alloy joints. At pulse frequency (2 Hz), the percentage elongation of pulse TIG welded joints is lower. When lower pulse frequency is increased from 2 Hz, correspondingly percent elongation also increases and reaches a maximum at 6 Hz. If pulse frequency is increased above 6 Hz, the percent elongation of the joints decreased.

It is evident that the pulse frequency is important parameter which has significant influence on percent elongation. It is considered crucial parameter and needs to be monitored for percent elongation properties of aluminum.

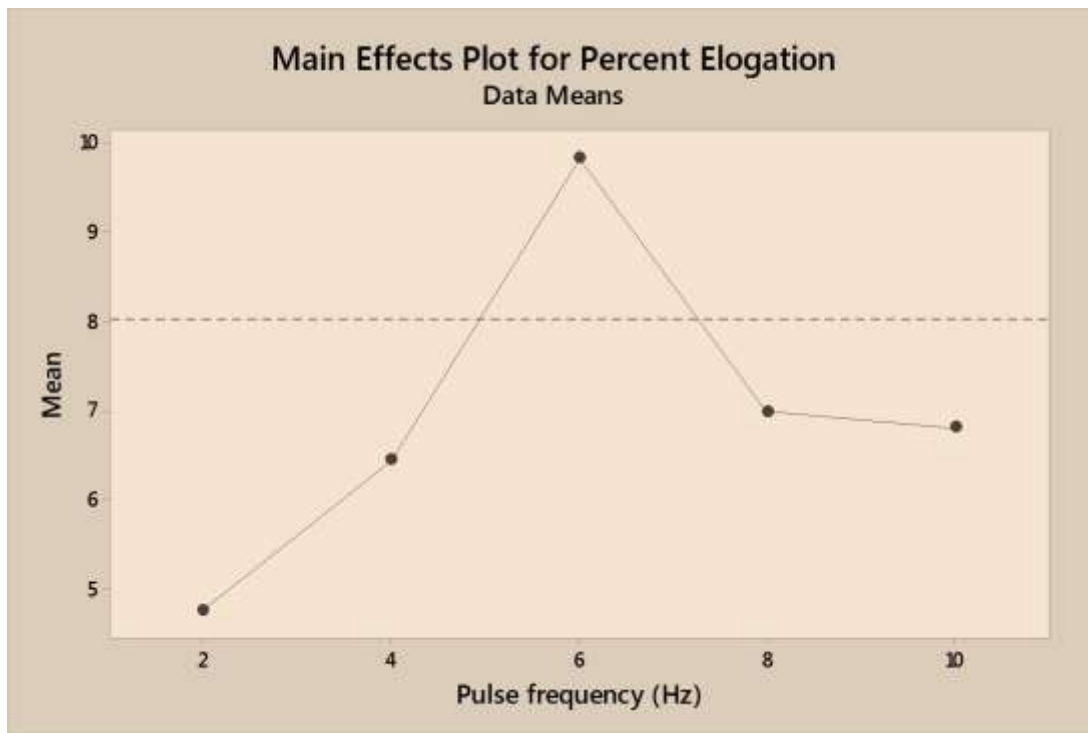


Figure 6.15: Effect of Pulse Frequency on Percent Elongation

6.4.4 Effect of Pulse On Time on Percent Elongation

Percent elongation of the joints by using different levels of pulse on time has been presented in figure 6.16. As the pulse on time increases from 40 to 45 %, percent elongation decreases slightly from 8.6 to 7 %. The percent elongation increases significantly from 7 to 9.5 % when pulse on time increases from 45 to 50 %. As the pulse on time further increases from 50 to 55 %, there is significant reduction in percent elongation and beyond 55 %, there is slight increase in percent elongation.

It is evident that the pulse on time is important parameter which has significant influence on percent elongation. It is considered crucial parameter and needs to be monitored for percent elongation properties of aluminum.

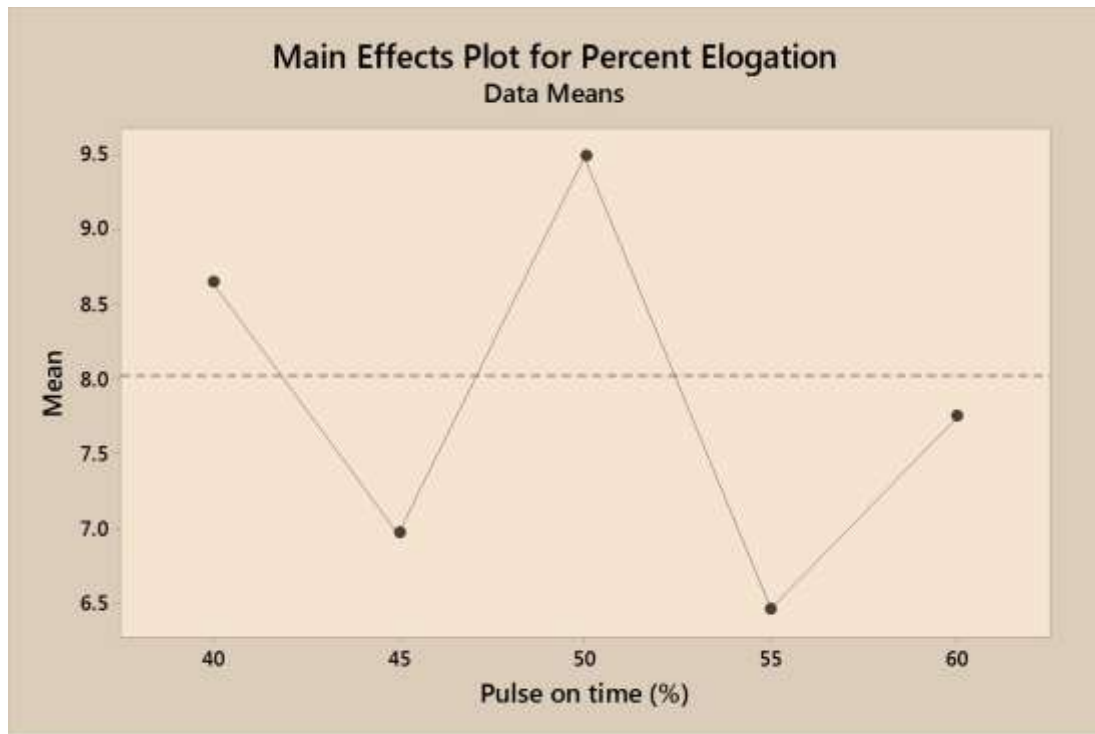


Figure 6.16: Effect of Pulse On Time on Percent Elongation

6.4.5 Effect of Welding Speed on Percent Elongation

Percent elongation of the joints by using different levels of welding speed has been presented in figure 6.17. As the welding speed increases from 155 to 165 mm/min, percent elongation decreases slightly from 7.5 to 7 %. The percent elongation increases significantly from 7 to 9.8 % when welding speed increases from 165 to 175 mm/min. As the welding speed further increases from 175 to 185 mm/min, there is significant reduction in percent elongation.

It is evident that the welding speed is important parameter which has significant influence on percent elongation. It is considered crucial parameter and needs to be monitored for percent elongation properties of aluminum.

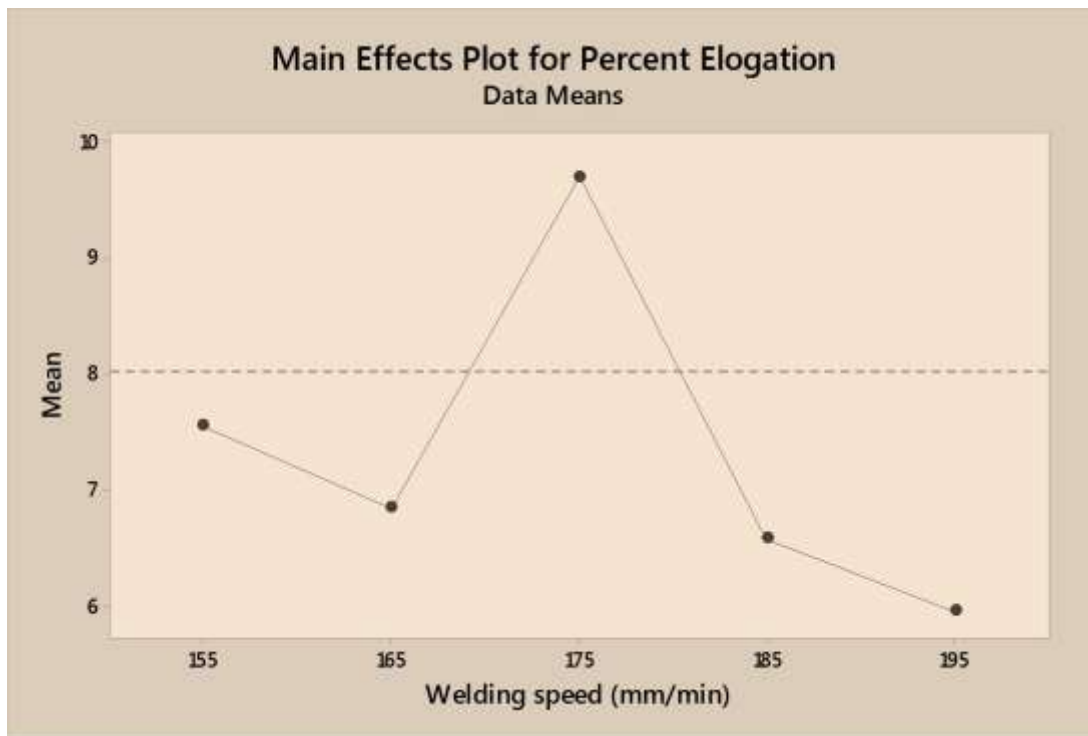


Figure 6.17: Effect of Welding Speed on Percent Elongation

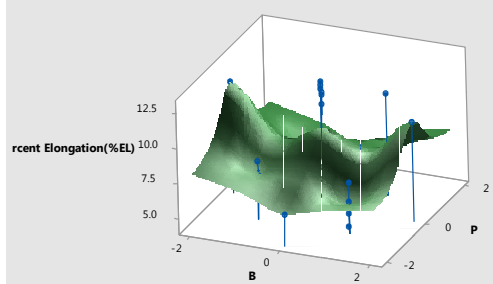
6.4.6 Effect of Interactions of Parameters on Percent Elongation

Figure 6.18 (ii), (iii), (iv), (viii), (ix), (x) indicates the significant interaction effect of peak current and pulse frequency, peak current and pulse on time, peak current and welding speed, pulse frequency and pulse on time, pulse frequency and welding speed, pulse on time and welding speed on percent elongation.

The percent elongation increases these above interaction parameter increases.

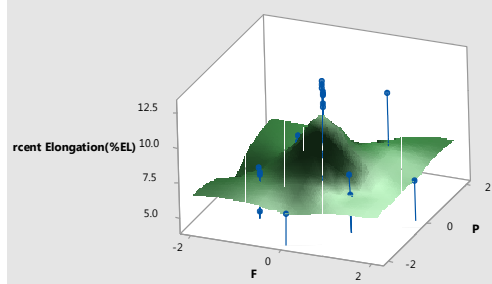
Study of interaction effects plays an important in deciding the significant interaction effect of parameters on percent elongation. It decides which combinations of parameter are important which significantly influences percent elongation

Surface Plot of Percent Elongation(%EL) vs P, B



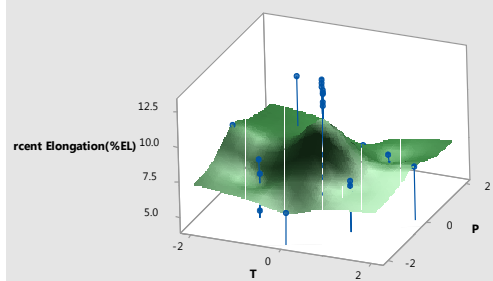
(i)

Surface Plot of Percent Elongation(%EL) vs P, F



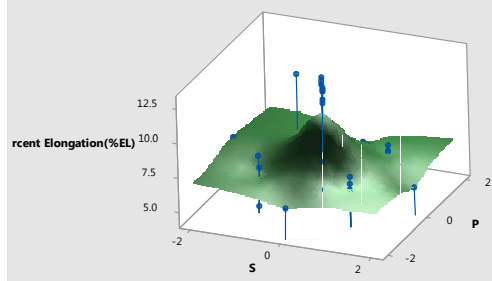
(ii)

Surface Plot of Percent Elongation(%EL) vs P, T



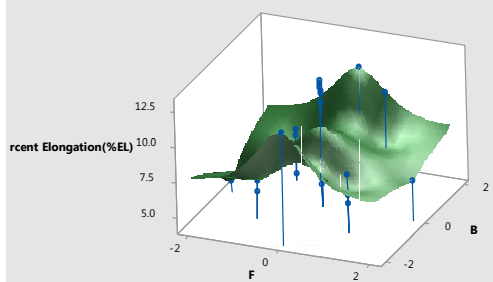
(iii)

Surface Plot of Percent Elongation(%EL) vs P, S



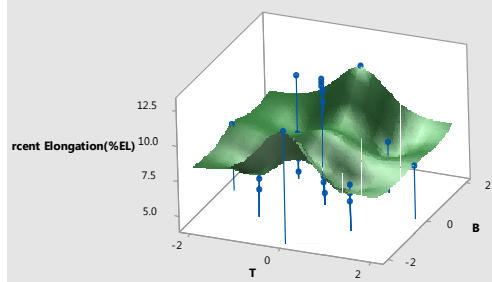
(iv)

Surface Plot of Percent Elongation(%EL) vs B, F



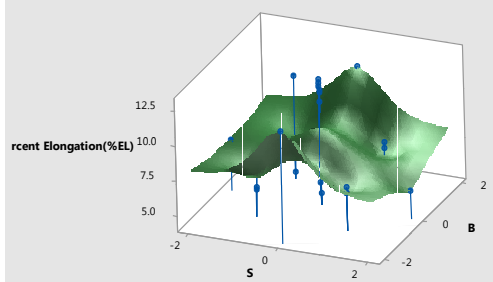
(v)

Surface Plot of Percent Elongation(%EL) vs B, T



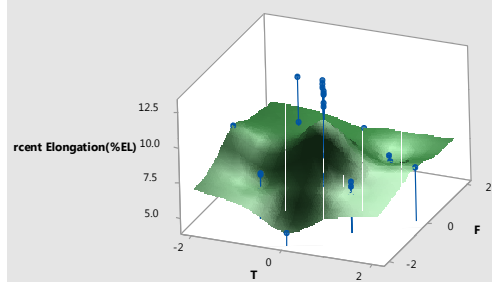
(vi)

Surface Plot of Percent Elongation(%EL) vs B, S



(vii)

Surface Plot of Percent Elongation(%EL) vs F, T



(viii)

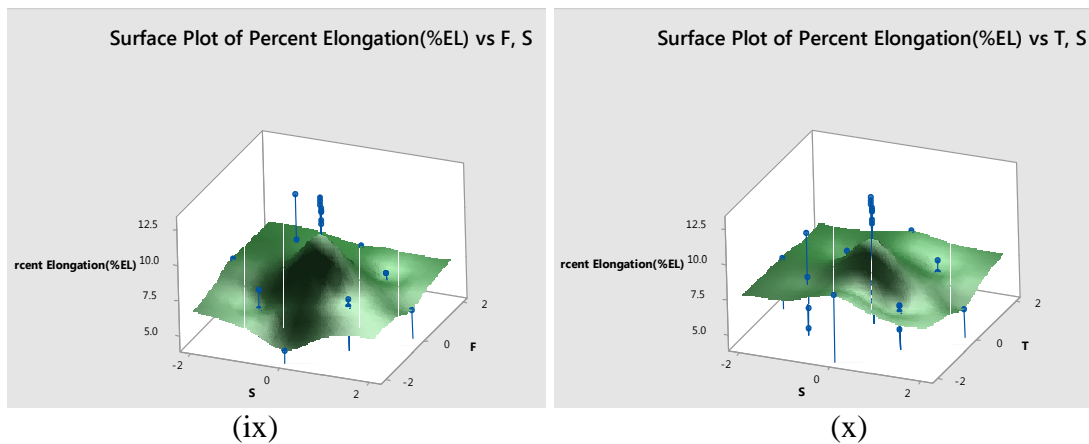


Figure 6.18: Interaction Effect of Parameters on Percent Elongation; i) P-B, ii) P-F, iii) P-T, iv) P-S, v) B-F, vi) B-T, vii) B-S, viii) F-T, ix) F-S, x) T-S

6.5 Micro-hardness

The study of effect of process parameters and their interaction on micro-hardness is essential to understand the behavior of micro-hardness. So subsequent sections describes the effect of peak current, base current, pulse frequency, pulse on time, welding speed and their interaction on micro-hardness.

6.5.1 Effect of Peak Current on Micro-hardness

Weld region micro-hardness was measured at the mid-thickness region of the welded joint and they are presented in figure 6.19. It can be seen that the maximum hardness of 91 Hv was recorded under peak current of 195 A.

This is mainly due to optimum heat input led to grain refinement. The lower hardness was recorded under peak current of 215 A. This is mainly due to higher heat input resulted in grain coarsening.

It is evident that the peak current is important parameter which has significant influence on micro-hardness. It is considered crucial parameter and needs to be monitored for micro-hardness properties of aluminum

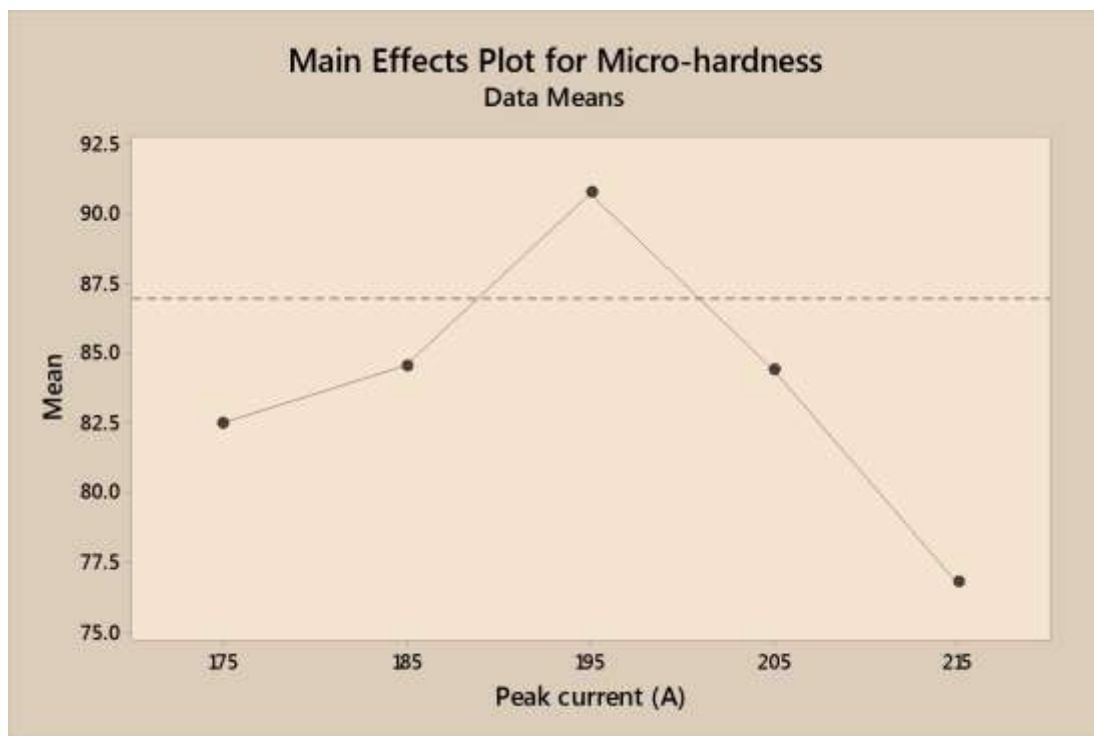


Figure 6.19: Effect of Peak Current on Micro-hardness

6.5.2 Effect of Base Current on Micro-hardness

Micro-hardness results of weld region of the joints fabricated using different levels of base current are displayed in figure 6.20. As base current increases from 105 to 112 A, micro-hardness decreases significantly from 94 to 82 Hv. The micro-hardness increases slightly from 82 to 89 Hv when base current increases from 112 to 119 A. As the base current further increases from 119 to 126 A, there is slight reduction in micro-hardness and beyond 133 A, there is significant increase in micro-hardness.

It is evident that the base current is important parameter which has significant influence on micro-hardness. It is considered crucial parameter and needs to be monitored for micro-hardness properties of aluminum.

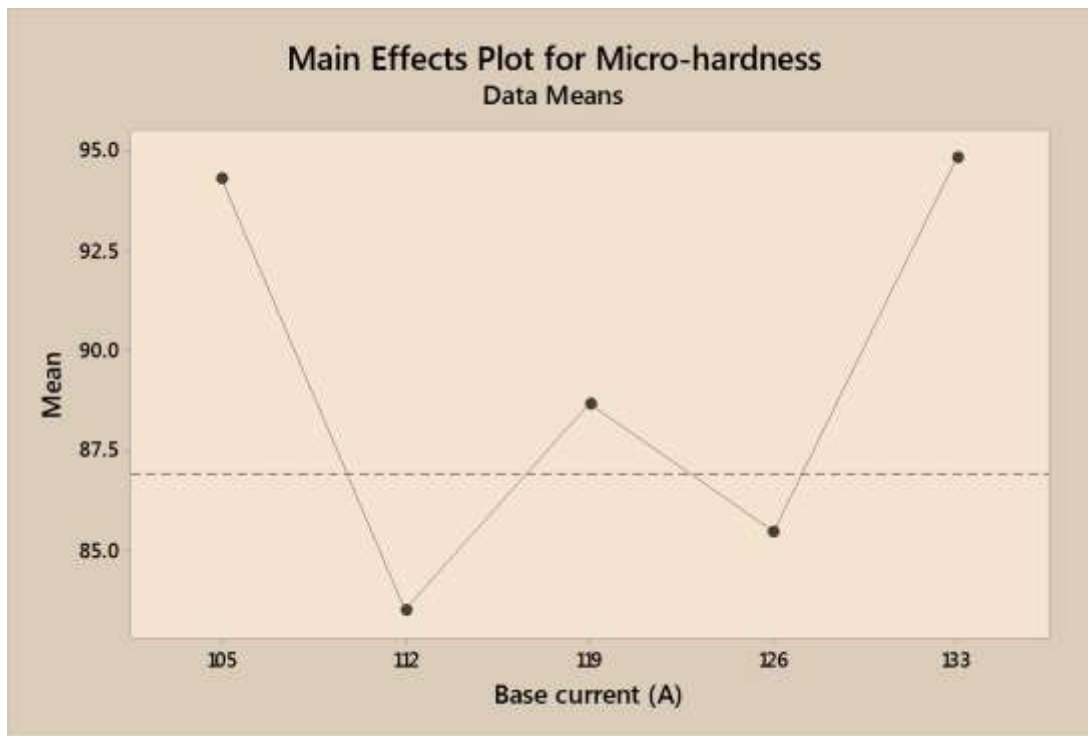


Figure 6.20: Effect of Base Current on Micro-hardness

6.5.3 Effect of Pulse Frequency on Micro-hardness

Micro-hardness of the weld joints fabricated using different levels of pulse frequencies are presented in figure 6.21. It can be seen that the maximum micro-hardness of 93 Hv was recorded when pulse frequency was 10 Hz. This is mainly because at high frequency, the molten pool is agitated more resulting in grain refinement in weld region. The minimum micro-hardness was recorded under the pulse frequency of 4 Hz.

It is evident that the pulse frequency is important parameter which has significant influence on micro-hardness. It is considered crucial parameter and needs to be monitored for micro-hardness properties of aluminum.

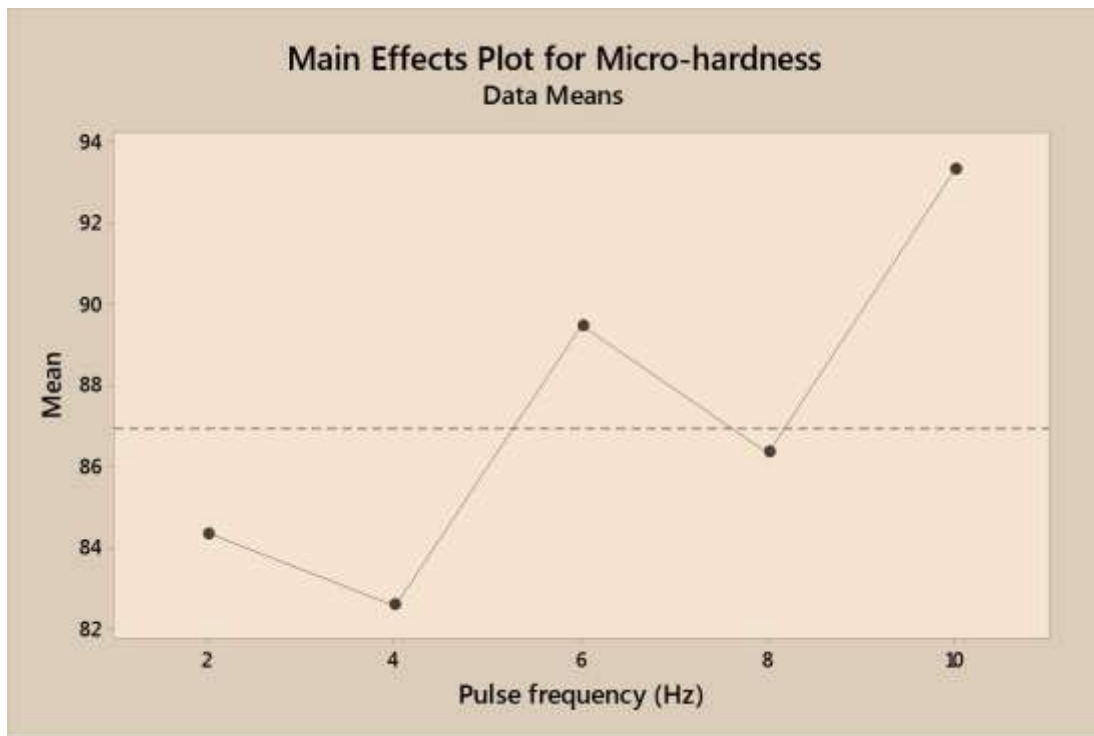


Figure 6.21: Effect of Pulse Frequency on Micro-hardness

6.5.4 Effect of Pulse On Time on Micro-hardness

Micro-hardness results of weld region of the joints fabricated using different levels of pulse on time are displayed in figure 6.22. As pulse on time increases from 40 to 45 %, micro-hardness increases slightly from 81 to 82 Hv. The micro-hardness increases significantly from 82 to 90 Hv when pulse on time increases from 45 to 50 %. As the pulse on time further increases from 50 to 55 %, there is slight reduction in micro-hardness and beyond 55 %, there is significant increase in micro-hardness.

It is evident that the pulse on time is important parameter which has significant influence on micro-hardness. It is considered crucial parameter and needs to be monitored for micro-hardness properties of aluminum.

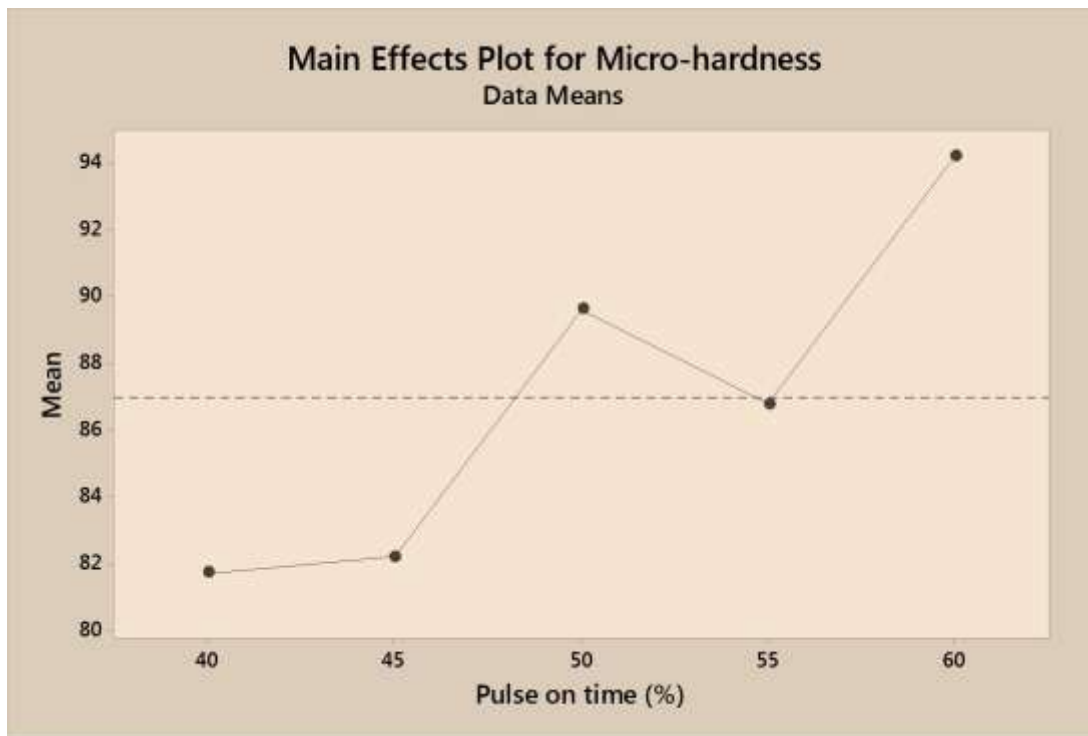


Figure 6.22: Effect of Pulse On Time on Micro-hardness

6.5.5 Effect of Welding Speed on Micro-hardness

Micro-hardness of the joints fabricated using different levels of welding speed has been presented in figure 6.23. At welding speed (155 mm/min) the micro-hardness of pulse TIG welded joints is lower. When welding speed is increased from 155 mm/min, correspondingly micro-hardness also increases and reaches a maximum at 175 mm/min. If pulse frequency is increased above 175 mm/min, the micro-hardness of the joints decreased.

The increase in welding speed from 155 to 175 mm/min decreases the heat input per unit length of weld, due to this faster cooling takes place in the weldment which promotes equi-axed and homogeneous grain structure in weld zone which increases the micro-hardness. On the contrary if welding speed is further increased that is from

175 to 195 mm/min, there is incomplete fusion and lack of penetration in the weldment which decreases the micro-hardness.

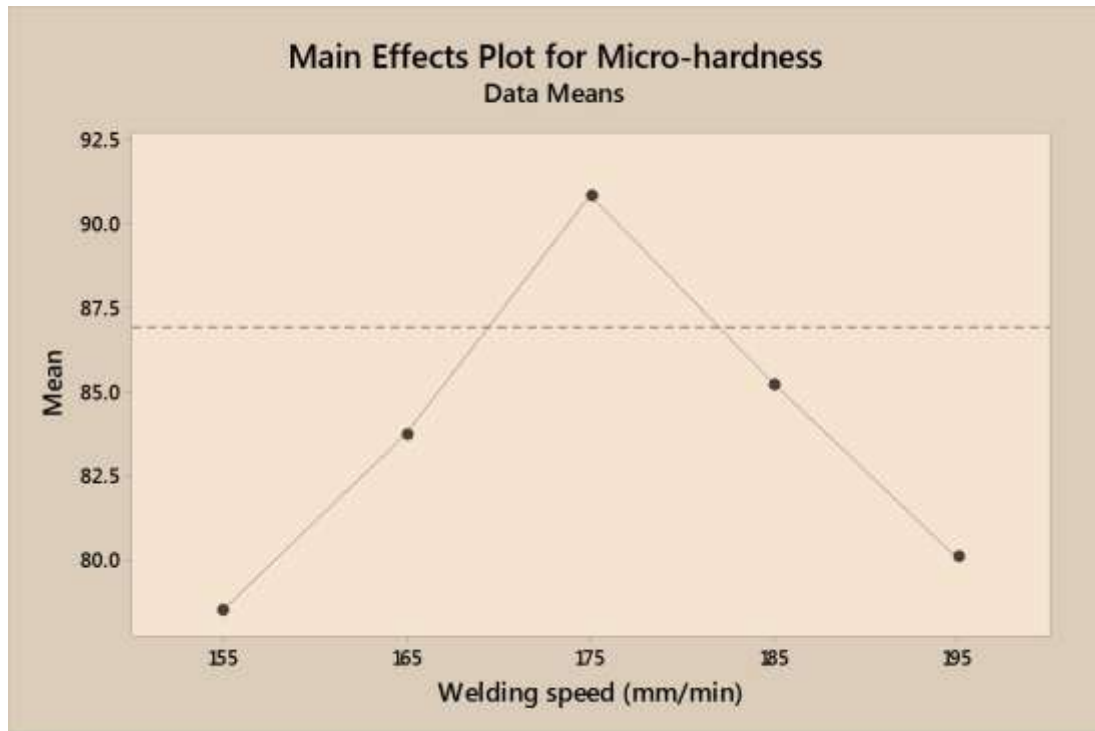
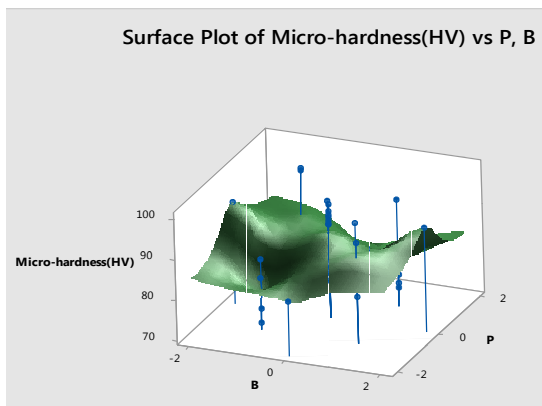


Figure 6.23: Effect of welding Speed on Micro-hardness

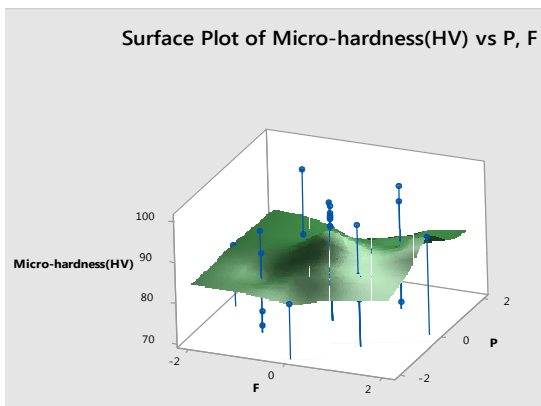
6.5.6 Effect of Interactions of Parameters on Micro-hardness

Figure 6.24 (ii), (iii), (iv) shows the significant effect of interaction between peak current and pulse frequency, peak current and pulse on time, peak current and welding speed on micro-hardness. The micro-hardness increases as there is simultaneous increase in parameters stated above.

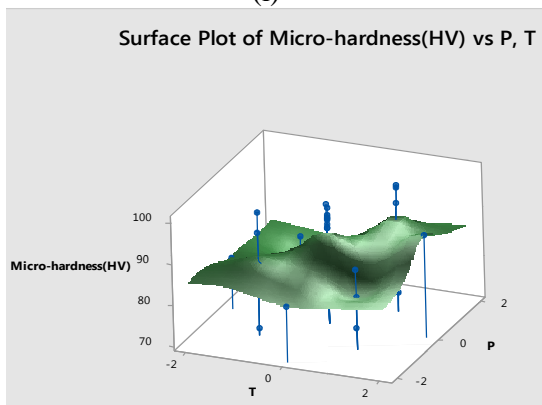
Study of interaction effects plays an important in deciding the significant interaction effect of parameters on micro-hardness. It decides which combinations of parameter are important which significantly influences micro-hardness



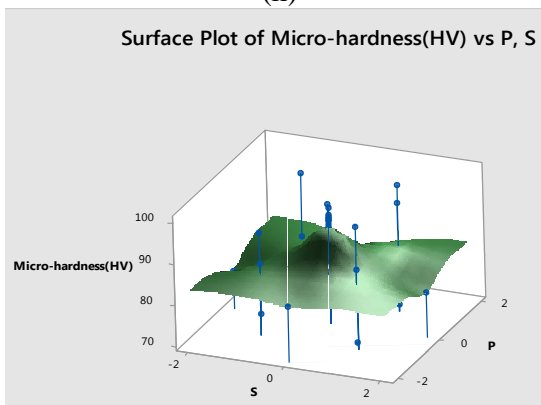
(i)



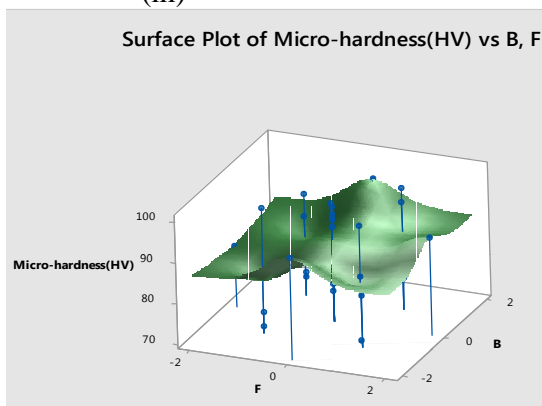
(ii)



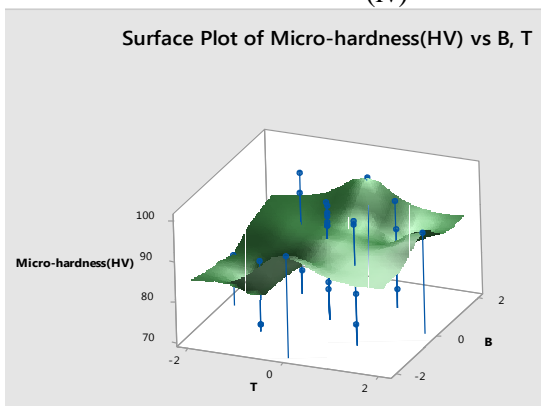
(iii)



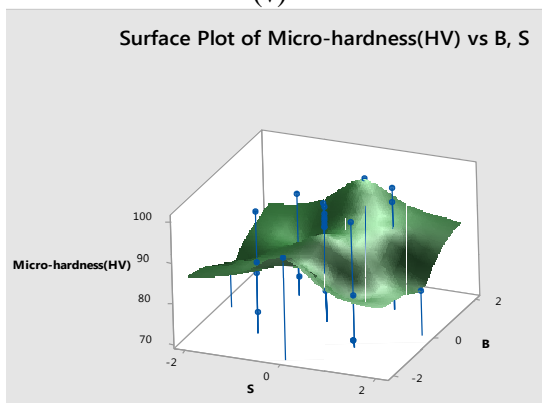
(iv)



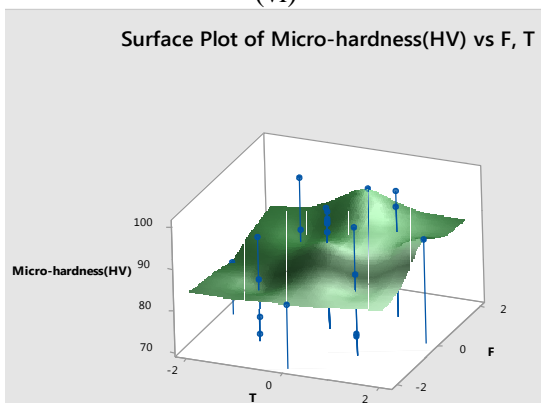
(v)



(vi)



(vii)



(viii)

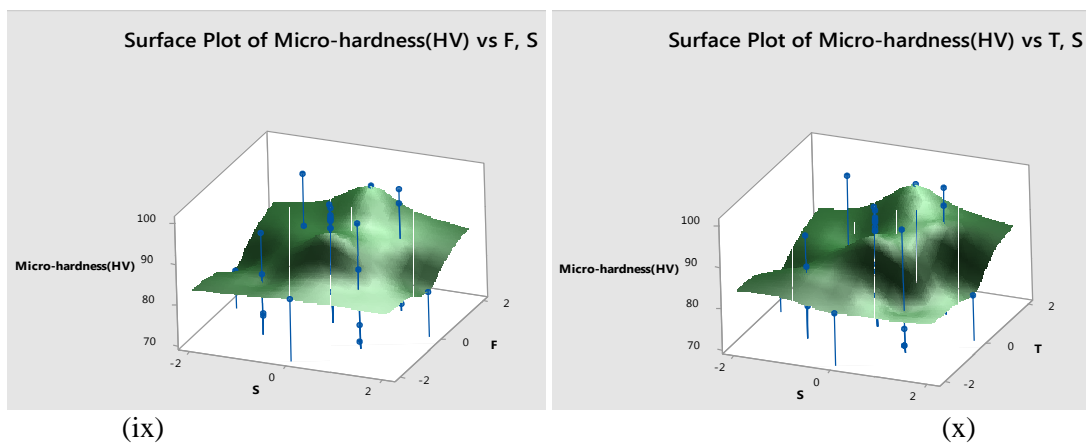


Figure 6.24: Interaction Effect of Parameters on Micro-hardness; i) P-B, ii) P-F, iii) P-T, iv) P-S, v) B-F, vi) B-T, vii) B-S, viii) F-T, ix) F-S, x) T-S

6.6 Impact toughness

The study of effect of process parameters and their interaction on impact toughness is essential to understand the behavior of impact toughness. So subsequent sections describes the effect of peak current, base current, pulse frequency, pulse on time, welding speed and their interaction on impact toughness.

6.6.1 Effect of Peak Current on Impact Toughness

Figure 6.25 depicts the effect of peak current on impact toughness of pulse TIG welded joints of 5083-O and 6061-T651. As the peak current increases from 175 to 185 A, impact toughness increases decreases from 21 to 18 J. The impact toughness increases significantly from 18 to 27 J when peak current increases from 185 to 195 A. As the peak current further increases from 195 to 205 A, there is significant reduction in impact toughness and beyond 205 A, there is significant increase in impact toughness. It is evident that the base current is important parameter which has significant influence on yield strength. It is considered crucial parameter and needs to be monitored for yield strength properties of aluminum

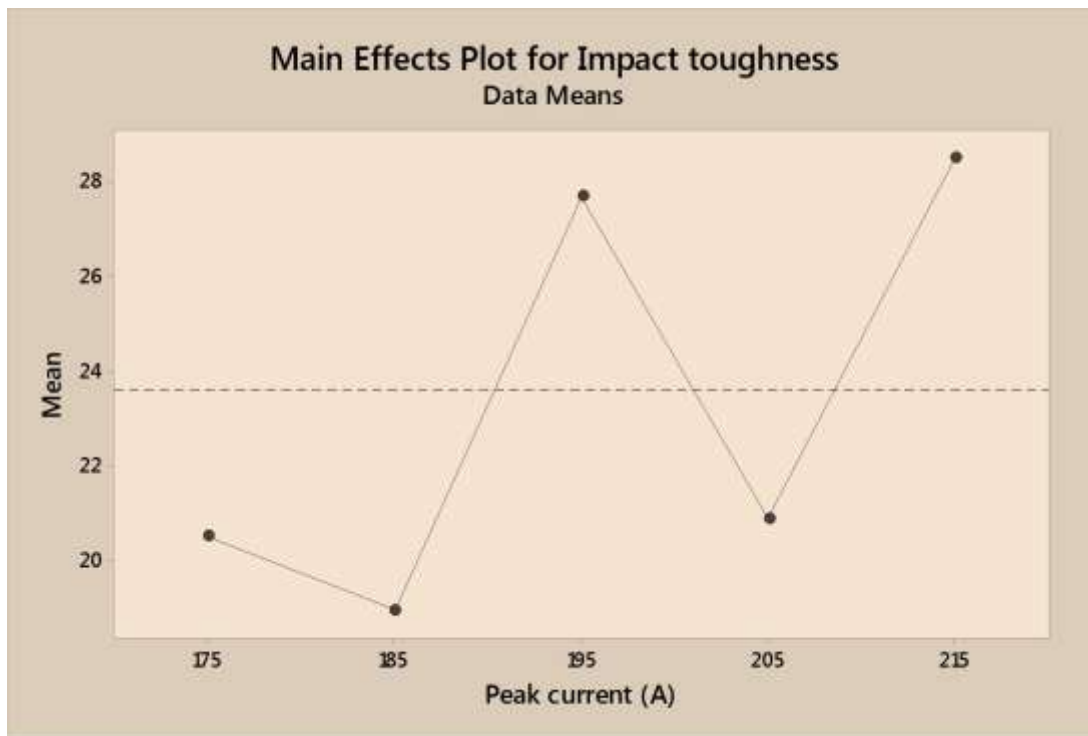


Figure 6.25: Effect of Peak Current on Impact Toughness

6.6.2 Effect of Base Current on Impact Toughness

Figure 6.26 depicts the effect of base current on impact toughness of pulse TIG welded joints of 5083-O and 6061-T651. As the base current increases from 105 to 112 A, impact toughness decreases from 24 to 18 J.

The impact toughness increases significantly from 18 to 28 J when base current increases from 112 to 119 A. As the base current further increases from 119 to 126 A, there is significant reduction in impact toughness and beyond 126 A, there is increase in impact toughness.

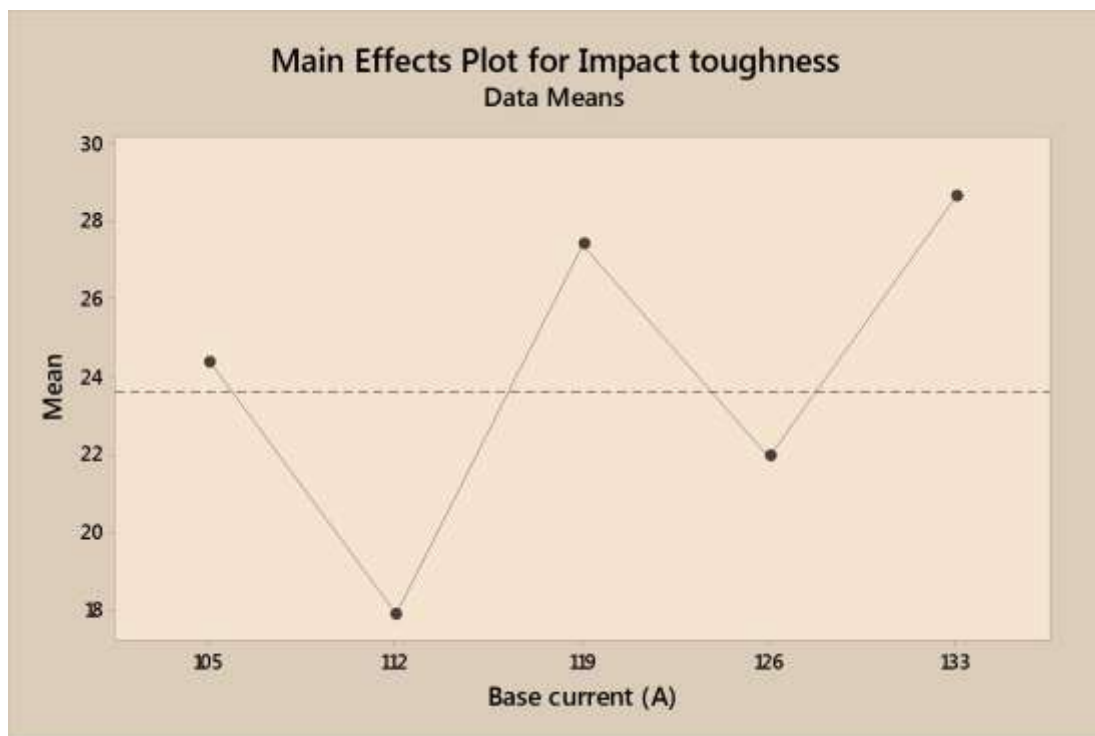


Figure 6.26: Effect of Base Current on Impact Toughness

6.6.3 Effect of Pulse Frequency on Impact Toughness

Figure 6.27 depicts the effect of pulse frequency on impact toughness of pulse TIG welded joints of 5083-O and 6061-T651. As the pulse frequency increases from 2 to 4 Hz, impact toughness increases from 15 to 19 J. The impact toughness increases significantly from 19 to 28 J when pulse frequency increases from 4 to 6 Hz. As the pulse frequency further increases from 6 to 8 Hz, there is significant reduction in impact toughness and beyond 8 Hz, there is slight increase in impact toughness.

It is evident that the pulse frequency is important parameter which has significant influence on impact toughness. It is considered crucial parameter and needs to be monitored for impact toughness properties of aluminum.

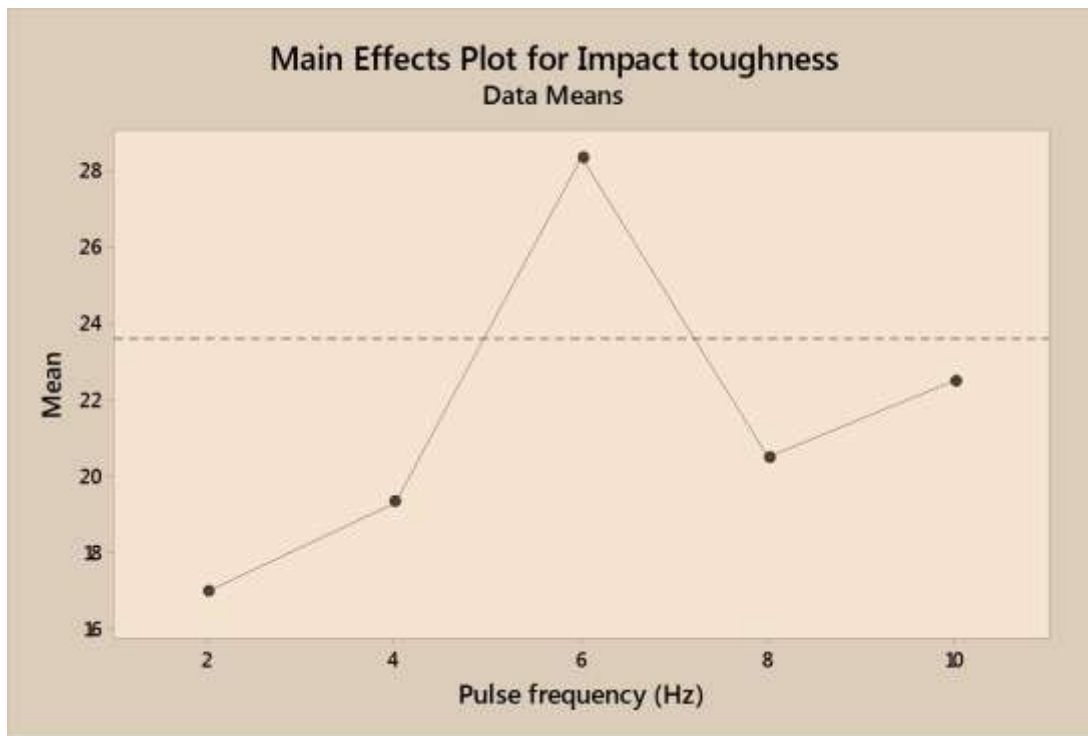


Figure 6.27: Effect of Pulse Frequency on Impact Toughness

6.6.4 Effect of Pulse On Time on Impact Toughness

Figure 6.28 depicts the effect of pulse on time on impact toughness of pulse TIG welded joints of 5083-O and 6061-T651. As the pulse on time increases from 40 to 50 %, impact toughness significantly increases from 11 to 28 J. The impact toughness decreases significantly from 28 to 24 J when pulse on time increases from 50 to 60 %.

It is evident that the pulse on time is important parameter which has significant influence on impact toughness. It is considered crucial parameter and needs to monitored for impact toughness properties of aluminum

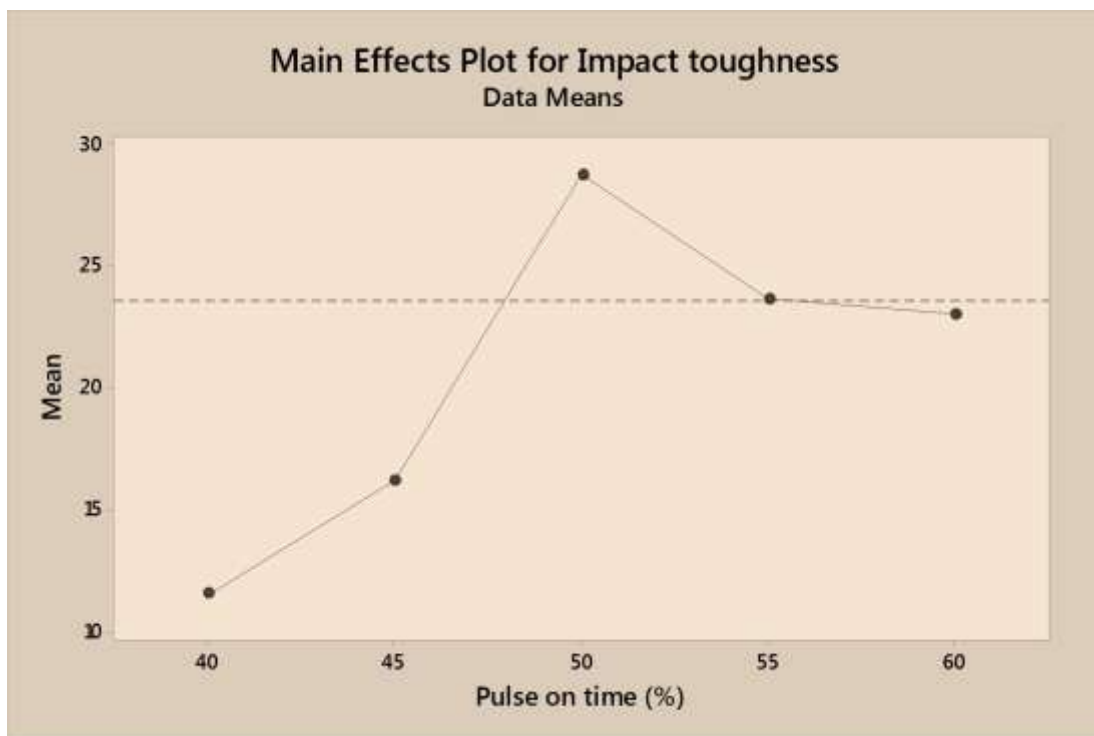


Figure 6.28: Effect of Pulse On Time on Impact Toughness

6.6.5 Effect of Welding Speed on Impact Toughness

Figure 6.29 depicts the effect of welding speed on impact toughness of pulse TIG welded joints of 5083-O and 6061-T651. As the welding speed increases from 155 to 165 mm/min, impact toughness decreases from 32 to 22 J. The impact toughness increases from 22 to 28 J when the welding speed increases from 165 to 175 mm/min. As the welding speed further increases from 175 to 185 mm/min, there is significant reduction in impact toughness and beyond 185 mm/min, there is slight increase in impact toughness.

It is evident that the welding speed is important parameter which has significant influence on impact toughness. It is considered crucial parameter and needs to be monitored for impact toughness properties of aluminum.

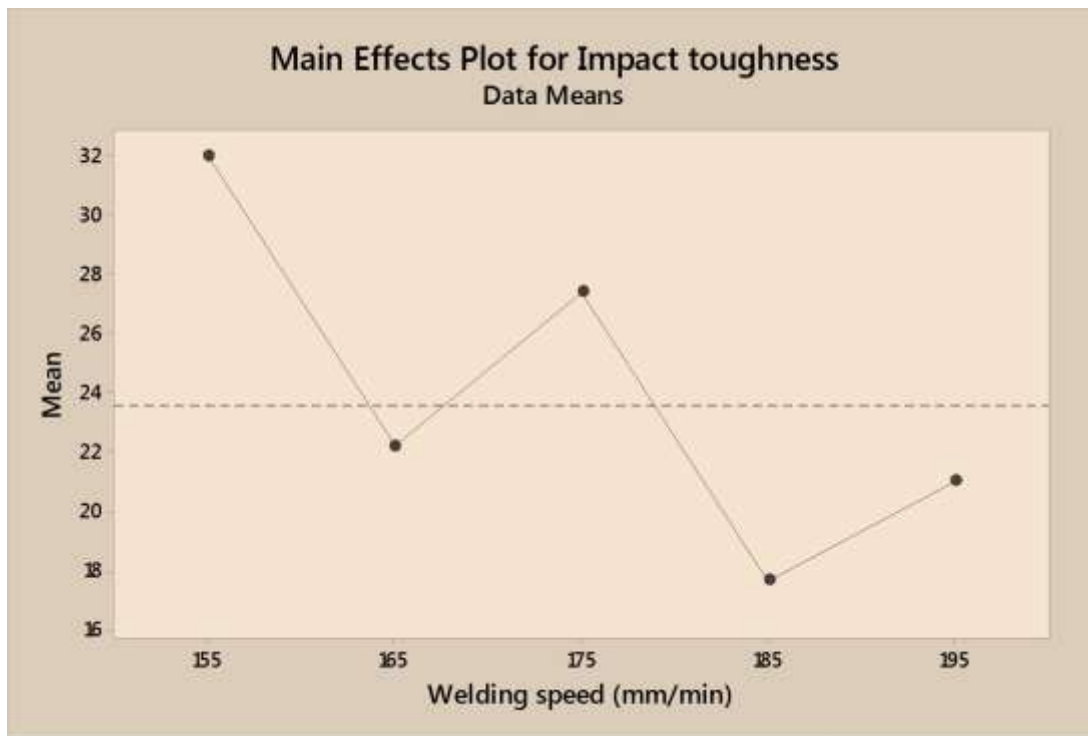


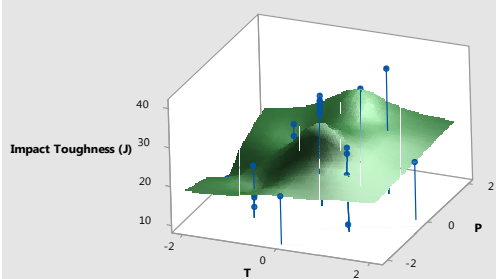
Figure 6.29: Effect of Welding Speed on Impact Toughness

6.6.6 Effect of Interactions of Parameters on Impact Toughness

Figure 6.30 (viii) indicated that interaction of pulse frequency and pulse on time have significant effect of impact toughness. The impact toughness increases as there is simultaneous increase in pulse frequency and pulse on time.

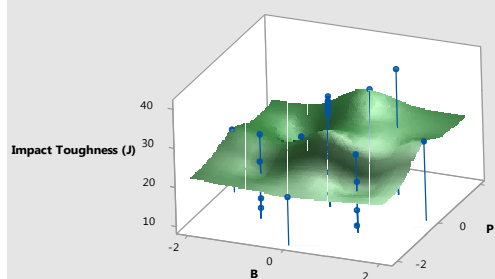
Study of interaction effects plays an important in deciding the significant interaction effect of parameters on impact toughness. It decides which combinations of parameter are important which significantly influences impact toughness.

Surface Plot of Impact Toughness (J) vs P, T



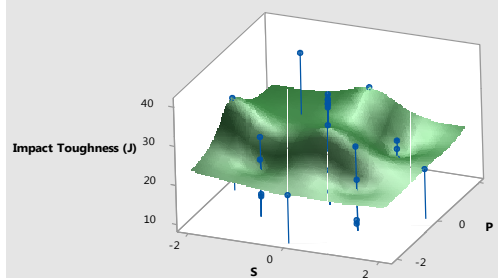
(i)

Surface Plot of Impact Toughness (J) vs P, B



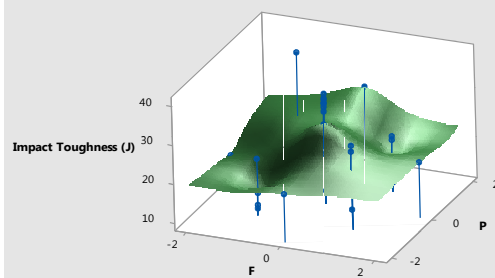
(ii)

Surface Plot of Impact Toughness (J) vs P, S



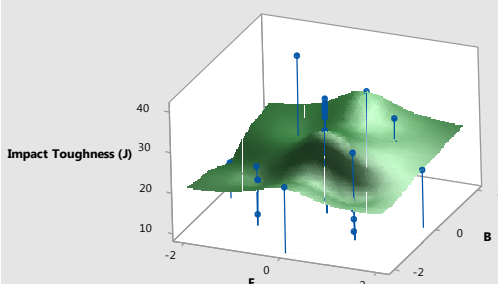
(iii)

Surface Plot of Impact Toughness (J) vs P, F



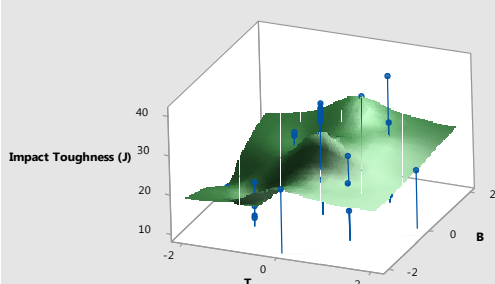
(iv)

Surface Plot of Impact Toughness (J) vs B, F



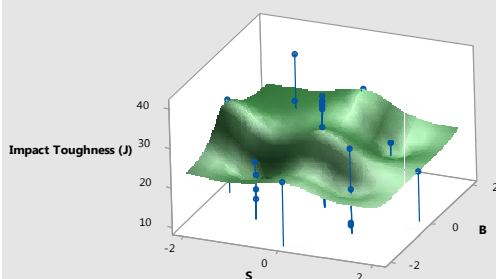
(v)

Surface Plot of Impact Toughness (J) vs B, T



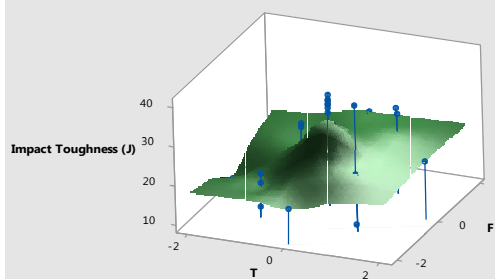
(vi)

Surface Plot of Impact Toughness (J) vs B, S



(vii)

Surface Plot of Impact Toughness (J) vs F, T



(viii)

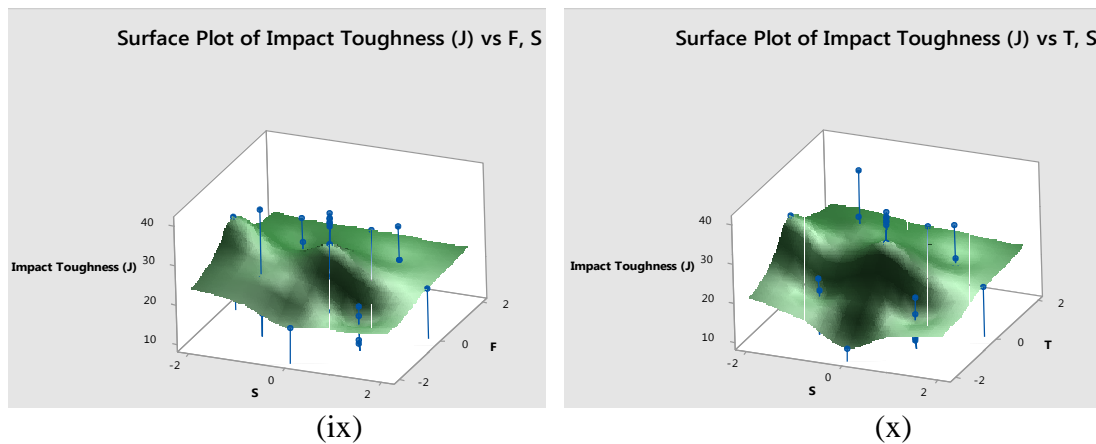


Figure 6.30: Interaction Effect of Parameters on Impact Toughness; i) P-B, ii) P-F, iii) P-T, iv) P-S, v) B-F, vi) B-T, vii) B-S, viii) F-T, ix) F-S, x) T-S

6.7 Summary

The summary of effect of parameters and their interaction has been depicted in subsequent section. The optimum combination of parameters at which mechanical properties are highest has been obtained.

6.7.1 Effect of Parameters on Mechanical Properties of Weld

1. Increase in peak current increases the tensile strength, impact toughness and decreases the yield strength, percentage elongation, micro-hardness
2. Increase in base current decreases the tensile strength, yield strength, percent elongation and increases the micro-hardness and impact toughness
3. Increase in pulse frequency increases the tensile strength, yield strength, percentage elongation, micro-hardness and impact toughness
4. Increase in pulse on time decreases the tensile strength, percent elongation and increases yield strength, micro-hardness, impact toughness
5. Increase in welding speed decreases the tensile strength, yield strength, percent elongation, impact toughness and increases the micro-hardness

Tensile strength is increased when peak current and pulse frequency is increased. Yield strength increases when pulse frequency and pulse on time increases. Percent elongation increases when pulse frequency increases. The tensile strength, yield strength and percent elongation increases at optimum level of parameters. The smaller dendrite sizes and large interdendritic spacing in fusion zone owing to low heat input increases the tensile strength of the joints. Beyond the optimum level, lower tensile properties is possessed by the joints at high heat input which are attributed to long dendrite sizes and large interdendritic spacing in the fusion zone. The optimum level of parameters are made to control the heat input and thereby controlling the grain size leading to increase in tensile properties. The results obtained here are similar to the work of other researchers.[190].

Impact toughness is increased when there is increase in pulse on time, pulse frequency, base current and peak current. The change in toughness is significantly influenced by the weld bead size. Due to lower heat input, refining of grains takes place which reduces the weld bead size which in turn increases the impact toughness. Impact toughness is decreased due to increase in welding speed. Due to higher heat input, there is increase in bead size due to coarse grains which in turn decreases the impact toughness. The optimum level of parameters are made to control heat input and thereby controlling the weld bead size leading to increase in impact toughness. The work obtained here are similar to the work of other researchers [190].

Micro –hardness increases when welding speed, pulse on time, pulse frequency and base current increased. The increase in welding speed, pulse on time, pulse frequency and base current decreases the heat input per unit length of weld, due to this faster

cooling takes place in the weldment which promotes equi-axed and homogeneous grain structure in weld zone therefore increases the micro-hardness. On the contrary, increase in peak current decreases micro-hardness, this is due to the fact that at high heat input, magnesium precipitates along grain boundaries leading to sensitized zone around the grain boundaries which coarsens the grain in the HAZ zone which results in reduced hardness around that area and finally the specimen undergoes brittle fracture under proper loading conditions. The optimum level of parameters are made to control heat input and thereby controlling the grain size leading to increase in micro-hardness.

6.7.2 Interaction Effect of Parameters on Mechanical Properties of Weld

In order to determine the process parameter values that give optimum response, surface plots were used. In surface plots, two parameters are shown on X, Y axes and the response is depicted in Z axis, which finally reveals the optimum point.

In figure 6.6, the interaction of various parameter indicates the optimum point at which maximum tensile strength is achieved. The surface plot for different parameter interaction and the response optimizer tool in MINITAB 17 software shows that the maximum tensile strength achieved is 201.85 MPa obtained at optimum level of peak current of 196.81 Amp, base current of 133.0 Amp, pulse frequency of 6.04 Hz, pulse on time of 49.9 % and welding speed of 171.16 mm/min.

Figure 6.12 depicts the surface plots of yield strength. The maximum yield strength achieved is 167.03 MPa which is obtained at the same optimum level as that of tensile strength.

The figure 6.18 depicts the surface plot of percent elongation. The maximum elongation achieved is 9.43 % which is obtained at same optimum level as that of tensile strength.

The figure 6.24 shows the surface plot of micro-hardness which indicates the maximum micro-hardness achieved at optimized level is 88.41 HV which is obtained at same optimum level as that of tensile strength.

The figure 6.30 shows the surface plot of impact toughness. The maximum impact toughness achieved is 33.35 J which is obtained at same combination of optimum levels as that of tensile strength.

The weld joint is then fabricated at optimum condition and metallurgical studies were done which is explained in next chapter

Chapter 7
Metallurgical Testing of Welds

METALLURGICAL TESTING OF WELDS

7.1 Introduction

Metallographic weld evaluations can take many forms. In most cases, a visual examination of weld is carried out for most common defects such as porosity and lack of fusion. On a micro scale, the examination is conducted to study the phase balance assessments from weld cap to weld root and to check the non-metallic or third phase precipitates in fusion zone. Examination related to grain size and grains structure and its growth patterns owing to various degrees of heat input determine the reasons for varying mechanical test results. For example, an extensive central columnar grain pattern can cause a plane of weakness giving poor tensile properties and impact test results.

7.2 Energy Dispersive X-Ray Spectroscopy (EDS) Analysis

EDS was performed to reveal the chemical composition of Fusion zone (FZ) at region adjacent to Heat Affected Zone (HAZ) on AA5083 and on AA6061 side and at Centre at Acc voltage 15 KV, take off angle 74.7 as shown in figure 7.1. The region adjacent to the HAZ on AA6061 side reveals oxygen weight of 1.38 % which indicates the loss of magnesium due to oxidation during welding which in turn caused due to insufficient shielding. The regions adjacent to the HAZ on AA5083 side shows magnesium weight of 3.29 % and oxygen weight of 0.70% which indicate less oxidation and higher retainment of magnesium content which is due to addition of ER 5356 filler alloy. Region at centre shows magnesium weight of 3.86%, manganese

weight of 0.45% and 0% silicon, this indicates the formation of intermetallic phase Mg_2Si in the FZ region due to rich magnesium content. Since the formation of intermetallic phase Mg_2Si and its precipitation at grain boundaries results in increasing the mechanical and metallurgical properties, formation of this phase is advantageous. However this also reduces the ductility.

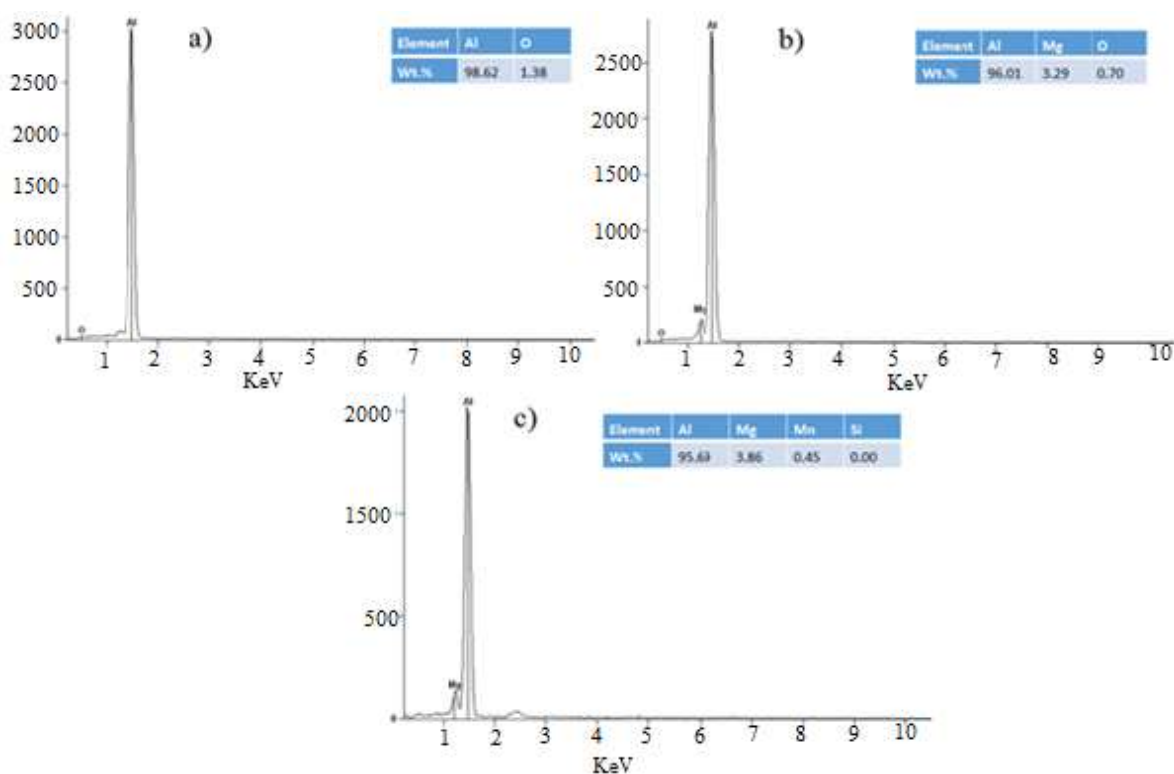


Figure 7.1: EDS Analysis at Three Regions a) Regions adjacent to HAZ on AA6061 side b) Regions adjacent to HAZ on AA5083 side c) Fusion Zone

7.3 Microstructural Examination of Weld

Microstructural examination is performed on samples that are cut according to the size required to be able to be mounted in a resin mold. The samples are polished to a fine finish, normally one micron diamond paste, and usually etched in an appropriate chemical solution prior to examination on a metallurgical microscope. Micro-examination is performed for many purposes and one of the main reasons is to study

the structure of material. It is also common to examine for metallurgical anomalies such as third phase precipitates, excessive grain growth, etc. Test to determination of grains size and counting of phases are done as a routine in conjunction with micro-examinations.

7.3.1 Procedure of Microstructural Examination

Microstructure characterization was performed using an optical microscope (OM) (VERSAMET UNITRON) to reveal the grain structure as shown in figure 7.2. The samples for metallographic examination were polished using various grades of emery paper. Final polishing was done using alumina powder in the disc polishing machine. Micro-etching was carried out using kellers reagent as per ASTM standard E407.



Figure 7.2: Optical Microscope

7.4 Analysis of Microstructure and its Evolution

Microstructure Examination is one of the primary means of assessing alloys and products to determine the effects of various fabrication and heat treatments, studying

the effects of new methods, and analyze the cause of failures. Many of the changes that become apparent with the examination of aluminum macrostructure and microstructure occur simultaneously with the freezing, homogenization, preheat, hot or cold reduction, annealing, or solution or precipitation heat treatment of the aluminum alloy. Good interpretation of microstructure relies on having a complete history. Figure 7.3 shows sample after polishing and etching



Figure 7.3: Sample after Polishing and Etching

7.4.1 Microstructure of Base Metal

The weld metal microstructure of aluminum alloy 5083-O consists of columnar, epitaxial grains with a cellular or columnar-dendritic substructure that has interdendritic eutectic constituents primarily Al_3Mg_2 and the same intermetallics like a base metal $\text{Al}_6(\text{Fe}, \text{Mn})$ or Al_6Mn and Al_3Fe . The 6061-T651 aluminum alloy belongs to one kind of wrought aluminum alloy. The main chemical composition have elements such as Al, Mg, Si, Cu. The main strengthening phase is Mg_2Si and has small number of $(\text{FeMn})_3\text{Si}_2\text{Al}_{15}$ and CuAl_2 phase. In 6061 aluminum alloy there may be present some impurity phases such as AlMnFeSi , AlFeSi and AlCrFeSi .

7.4.1.1 Microstructure of Base Metal 5083-O

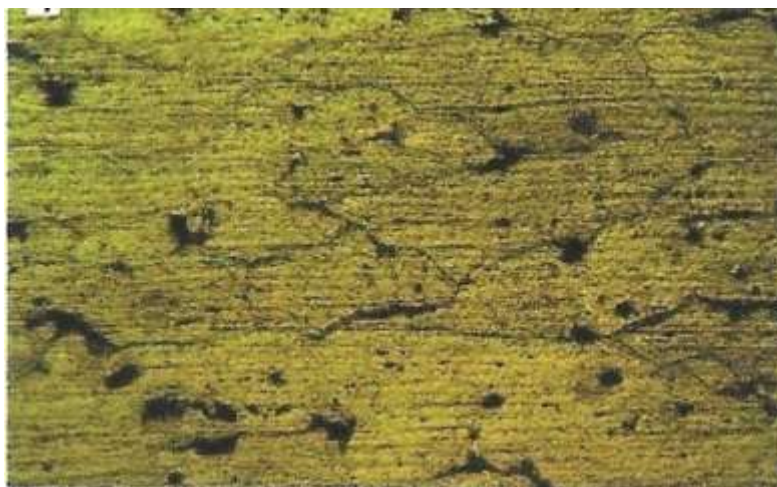


Figure 7.4: Microstructure of AA5083-O at 200X

Microstructure of base metal of AA5083-O as shown in figure 7.4 consists of coarse interdendritic network of Mg eutectic in the matrix of aluminum solid solution. The microstructure of 5083-O consists of dendritic segregation structure, though the initial microstructure consisted of equi-axed-grains with an average size of about 100 μm . It is worth noting that from inspection of the as-received sample, coarse precipitates of $(\text{Fe, Mn})_3\text{SiAl}_{12}$ and small Mg_2Si particles are present in the alloy as second-phase.

7.4.1.2 Microstructure of Base Metal 6061-T651

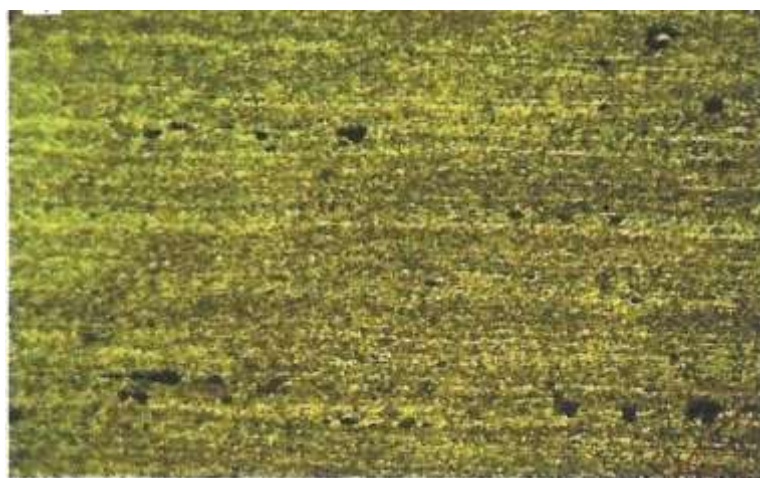


Figure 7.5: Microstructure of AA6061-T651 at 200X

Microstructure of base metal of AA6061–T651 as shown in figure 7.5 consists of Mg-Si in the aluminum solid solution. Microstructure analysis revealed a coarse, elongated grain structure with average grain dimensions of 141.1 μm in length and 29.2 μm in width. The coarse second-phase particles and boundary precipitates are evident.

7.4.2 Microstructure of Fusion Zone

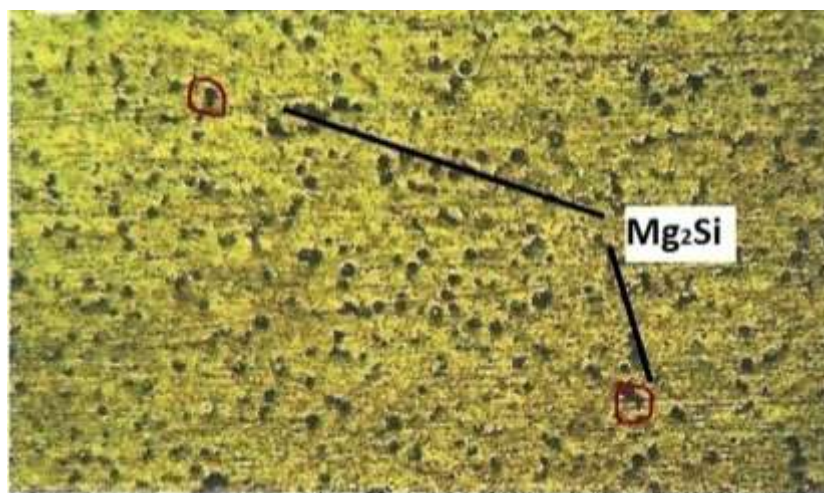


Figure 7.6 Microstructure of Fusion Zone at 200X

The microstructure of fusion zone within the welded joint of aluminum alloy of 5083-O and 6061-T651 is depicted in figure 7.6. Significant grain refining is noticed in FZ which consist of fine equi-axed grains of aluminum solid solution containing soluble phase consisting of Mg_2Si particles. Homogeneous growth of microstructure is obtained in FZ as compared to HAZ. This is because aluminum with its high conductivity dissipates heat quickly resulting in less heat availability for grain growth. The absence of increasing heat input availability leads to the formation of fine equi-axed grains which tend to reduce solidification cracking and improve the mechanical properties of welded joints. This is due to the fact that, in fine equi-axed grained materials, strains are more uniformly accommodated which permit easier transport of liquid between the grains. Thus result in

reduced cracking. The absence of solidification cracking or hot cracking in fusion zone promotes the strength of the weld joint obtained in TIG welding [191].

7.4.3 Microstructure of Heat Affected Zone

The HAZ is identified as the area between the weld or cut and the base metal. These areas can vary in size and severity depending on the properties of the materials involved, the intensity and concentration of heat, and the process employed. The exposure of sufficient heat for a long period of time enables the microstructural changes in this region. The change in microstructure results in difference in properties from the parent metal. These property changes are usually undesirable and ultimately serve as the weakest part of the component. For example, the change in microstructure could lead to increased residual stresses, reduced strength, higher brittleness, and decreased resistance to corrosion and/or cracking. As a result, many failures occur in the HAZ. HAZ has large columnar grains (columnar grains generally occur in directional solidification or cold worked elongated grains in metal) near fusion boundary and the size reduces towards the unaffected base metal. With the help of image analyzer system, HAZ width and ASTM grain size number were calculated from microstructures of samples.

7.4.3.1 Microstructure of Heat Affected Zone on 5083-O side



Figure 7.7: Microstructure of HAZ at 5083-O side at 200X

The microstructure of HAZ on AA5083-O side is shown in figure 7.7. The interface between base metal and fusion zone on aluminum 5083-O indicates the existence of thermal cycles during welding process leading to changes in the grain structure inside aluminum matrix. Due to this complex thermal cycle, the equi-axed grains had grown larger in size in HAZ

7.4.3.2 Microstructure of Heat Affected Zone on 6061-T651 side



Figure 7.8: Microstructure of HAZ at 6061-T651 side at 200X

Microstructural changes in the HAZ of Al-Mg-Si alloys have been examined by several investigators [192]. It is evident from Figure 7.8 for the alloy 6061-T6 that reversion of β'' precipitates occurs in the peak temperature range from 250 to 500°C which is associated with a continuous decrease in the HAZ hardness until the dissolution process is completed. The decrease in hardness in HAZ region is because of formation of columnar grains towards the fusion boundary. This is the result of epitaxial solidification, which grows toward the center in a direction along the maximum thermal gradient. However, close to the fusion boundary a large fraction of alloying elements will remain in solid solution at the end of the thermal cycle, thereby giving conditions for extensive precipitation hardening (age hardening) at room

temperature over a period of 5 to 7 days. Enhanced HAZ strength recovery can be achieved by the use of artificial aging in the temperature range from 150 to 180°C.

7.5 Immersion Test for Resistance to Pitting Corrosion

The problem of defects like stress corrosion cracking and stress fatigue cracking lies due to presence of intermetallic phase in aluminum alloy matrix as Mg_2Si particles are anodic with respect to the alloy matrix (5083 and 6061) joint. This promote rapid localized attack through galvanic interaction leading to the formation of pits which give rise to severe stress concentration at metal surface leading to crack initiation and propagation [193, 194]. To test the resistance of aluminum alloy against pitting corrosion, the immersion test was conducted

7.5.1 Procedure of Immersion Test

The immersion test according to ASTM G44-99 is conducted using neutral 3.5% NaCl solution. The specimen of size 55mm x 10mm x 6.35mm is made to test. The test duration was of 21 days. The test cycle was done on daily basis for 60 minutes which consists of alternate 10 minutes immersion in 3.5% NaCl solution and drying in air for rest 50 minutes. The test conditions are given in Table 7.1 as:

Table 7.1: Immersion Test for Testing Corrosion Resistance of Aluminum Alloy 5083-O and 6061-T651 Joint

Test condition	Values
Reagent grade	Sodium chloride
NaCl	3.5±0.1 parts
Distilled water	96.5 parts
pH of fresh solution	6.8
Temperature (°C)	27±1
Relative humidity (%)	45±10

7.5.2 Result of Immersion Test

The observations revealed very fine pits upto 10 μ diameter. The pits density was 3-4 per cm² and average depth of pit was 5 micron but the important things is no crack initiation sites were observed. The figure 7.9 reveals samples before and after test.

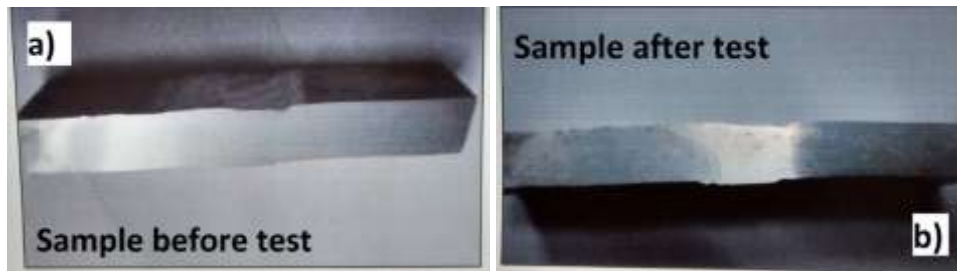


Figure 7.9: Samples of Immersion Test before and after Test of Pitting Corrosion

Chapter 8
Conclusion and Scope for Future Work

CONCLUSION AND SCOPE FOR FUTURE WORK

8.1 Conclusion

The present investigation have been carried out to assess the influences of pulse TIG parameters and to find the optimum combination of parameters to attain better mechanical and metallurgical properties of pulse TIG welded dissimilar aluminum alloys AA5083-O and AA6061-T651. From this study following conclusions can be obtained.

- i. Automatic setup has been developed to reduce the defects and problems associated with manual TIG. Also the setup is developed at very low cost around 300 USD as compared to setup available in the market which is around 1000 USD. This makes it a low cost automation of welding process.
- ii. Selection of welding consumable has been made using Multi- Attribute Decision Making Approach (MADM) to find out the optimum filler alloy, arc electrode and shielding gas. ER5356 as filler alloy, 0.8% Zirconiated electrode as arc electrode and pure argon as shielding gas has been found to be optimum welding consumables
- iii. Current pulsing leads to relatively finer and more equi-axed grain structure in pulse TIG welds. Grain refinement is accompanied by an increase in micro-hardness, tensile strength, yield strength, percent elongation and impact toughness.

- iv. Mathematical models using response surface methodology has been developed to predict the optimum pulse TIG welding parameters to attain a maximum grain refinement in fusion zone and maximum mechanical properties using statistical tools such as response graph, normal probability plot and analysis of variance techniques.
- v. Increase in peak current results in increase tensile strength and similar effect is observed when pulse frequency is increased.
- vi. Base current and pulse on time is having inversely proportional relationship with the tensile strength, i.e, if the base current is raised, then the tensile strength is decreasing and similar influence is noticed when pulse on time is increased.
- vii. Yield strength and percent elongation are directly proportional relationship with pulse frequency
- viii. Increase in peak current increases the impact toughness and similar effect is observed when pulse frequency is increased.
- ix. Micro-hardness has directly proportional relationship with welding speed, pulse on time, pulse frequency and base current increased.
- x. The optimum level of parameters obtained are peak current of 196.81 Amp, base current of 133.0 Amp, pulse frequency of 6.04 Hz, pulse on time of 49.9 % and welding speed of 171.16 mm/min. The maximum response value obtained for tensile strength is 201.85 MPa, yield strength is 167.03 MPa, elongation of 9.43 %, micro-hardness of 88.41 HV, impact toughness of 33.35 J
- xi. The microstructural examination conducted revealed refined grain structure in fusion zone.

- xii. The immersion test was conducted to study the resistance of welded joint against pitting corrosion. From the result it was noticed that no crack initiation sites were developed on the surface.

8.2 Scope for Future Work

Based on present investigation, following suggestions are made to explore further research in this area of dissimilar aluminum alloys welding.

- i. A wire feeding system with pulse control can be included in the system so that by using filler wire thicker plate can be welded.
- ii. Selection of optimum welding consumable can be explored using other techniques like Fuzzy AHP and Intuitionistic Fuzzy TOPSIS.
- iii. Studies of pulse TIG welding parameters on intergranular corrosion can be studied
- iv. Influence of pulse TIG welding parameters on fatigue life can be studied
- v. Development of mathematical model for pulsed TIG process parameter for welding of dissimilar aluminum alloys plates of various thickness can be made.

References

REFERENCES

- [1] Voyager E, (1990). Properties and Selection: Non-ferrous alloys-Purpose Materials, Metals Handbook, ASM International, Vol.2, 10th Ed, 958-983
- [2] Howard E. B., Timothy L., (1985). American society of Metals, Metal Park, Metals Handbook, Vol.5, 2nd Ed, 1123-1153.
- [3] Van L M. (1967). .Metallurgy of Aluminium Alloys, Chapman and Hall Ltd., London
- [4] Millers (2010). TIG welding Handbook, Vol.1, 4th Ed,1-86.
- [5] Min D, Shen J, Lai S, Chen J. (2009). Effect of heat input on the microstructure and mechanical properties of tungsten inert gas arc butt-welded AZ61 magnesium alloy plates. Materials Characterization, 60(12), 1583-1590.
- [6] Sudhakaran R, VeLMurugan V, Senthil Kumar KM, Jayaram R, Pushparaj A, Praveen C, VenkatPrabhu N.(2011). Effect of welding process parameters on weld bead geometry and optimization of process parameters to maximize depth to width ratio for stainless steel gas tungsten arc welded plates using genetic algorithm. European Journal of Scientific Research, 62(1), 76-94.
- [7] Balasubramanian M, Jayabalan V, Balasubramanian V. (2008).Developing mathematical models to predict grain size and hardness of argon tungsten pulse current arc welded titanium alloy. Journal of Materials Processing Technology, 196(1), 222-229
- [8] Yun SC, Kim JW.(2010). Selection of optimal welding condition for GTA pulse welding in root-pass of V-groove butt joint. Metals and Materials International, 16(6), 975-980.
- [9] Madadi F, Ashrafizadeh F, Shamanian M. Optimization of pulsed TIG cladding process of stellite alloy on carbon steel using RSM. (2012). Journal of Alloys and Compounds, 510(1), 71-77.
- [10] Lothongkum G, Chaumbai P, Bhandhubanyong P. (1999).TIG pulse welding of 304L austenitic stainless steel in flat, vertical and overhead positions. Journal of Materials Processing Technology, 89, 410-414.

- [11] Lothongkum G, Viyanit E, Bhandhubanyong P. (2001). Study on the effects of pulsed TIG welding parameters on delta-ferrite content, shape factor and bead quality in orbital welding of AISI 316L stainless steel plate. *Journal of Materials Processing Technology*, 110(2), 233-238.
- [12] Wang SH, Chiu PK, Yang JR, Fang J.(2006). Gamma (γ) phase transformation in pulsed GTAW weld metal of duplex stainless steel. *Materials Science and Engineering A* , 420(1), 26-33.
- [13] Reddy GM, Gokhale AA, Rao KP.(2002) Effect of the ratio of peak and background current durations on the fusion zone microstructure of pulsed current gas tungsten arc welded Al-Li alloy.*Journal of Material Science Letters* , 20(21), 1623-1625.
- [14] Balasubramanian M, Jayabalan V, Balasubramanian V. (2008).Process Parameter Optimization of the Pulsed Current Argon Tungsten Arc Welding of Titanium Alloy. *Journal of Material Science Technology*, 24(3), 423.
- [15] Traidia A, Roger F, Guyot E.(2010). Optimal parameters for pulsed gas tungsten arc welding in partially and fully penetrated weld pools. *International Journal of Thermal Sciences*, 49(7), 1197-1208.
- [16] Tsai CH, Hou KH, Chuang HT.(2006). Fuzzy control of pulsed GTA welds by using real-time root bead image feedback. *Journal of Materials Processing Technology*, 176(1), 158-167
- [17] Babu NK, Raman SGS, Mythili R, Saroja S. (2007). Correlation of microstructure with mechanical properties of TIG weldments of Ti-6Al-4V made with and without current pulsing. *Materials characterization*, 58(7), 581-587
- [18] Balasubramanian M, Jayabalan V, Balasubramanian V. (2009) Prediction and optimization of pulsed current gas tungsten arc welding process parameters to obtain sound weld pool geometry in titanium alloy using lexicographic method. *Journal of materials engineering and performance*, 18(7), 871-877.
- [19] Padmanaban G, Balasubramanian V, Reddy GM. (2011) Fatigue crack growth behaviour of pulsed current gas tungsten arc, friction stir and laser beam welded AZ31B magnesium alloy joints. *Journal of Materials Processing Technology*, 211(7), 1224-1233.

- [20] Babu SK, Natarajan S. (2007). Corrosion behavior of pulsed gas tungsten arc weldments in power plant carbon steel. *Journal of Materials Engineering and Performance*, 16(5), 620-625.
- [21] Balasubramanian M, Jayabalan V, Balasubramanian V. (2008). Effect of microstructure on impact toughness of pulsed current GTA welded α - β titanium alloy. *Materials Letters*, 62(6), 1102-1106.
- [22] Huang X, Shi F, Gu W, Chen S. (2009) SVM-based fuzzy rules acquisition system for pulsed GTAW process. *Engineering Applications of Artificial Intelligence*, 22(8), 1245-1255.
- [23] Huang X, Gu W, Shi F, Chen S. (2009). An adaptive inverse control method based on SVM-fuzzy rules acquisition system for pulsed GTAW process. *The International Journal of Advanced Manufacturing Technology*, 44(7-8), 686-694.
- [24] Tseng KH, Chou CP. (2002). The effect of pulsed GTA welding on the residual stress of a stainless steel weldment. *Journal of Materials Processing Technology*, 123(3), 346-353.
- [25] Balasubramanian M, Jayabalan V, Balasubramanian V. (2008). Optimizing pulsed current parameters to minimize corrosion rate in gas tungsten arc welded titanium alloy. *The International Journal of Advanced Manufacturing Technology*, 39(5-6), 474-481.
- [26] Swaminadhan P, Harkare G, Gawande SH. (2010). Experimental Investigations of weld characteristics for a single pass TIG welding with Stainless Steel 304. *International Journal of Engineering Science and Technology*, 2(8), 3676-3686.
- [27] Kumar S, Shahi AS. (2011). Effect of heat input on the microstructure and mechanical properties of gas tungsten arc welded AISI 304 stainless steel joints. *Materials & Design*, 32(6), 3617-3623.
- [28] Yan J, Gao M, Zeng X. (2010). Study on microstructure and mechanical properties of 304 stainless steel joints by TIG, laser and laser-TIG hybrid welding. *Optics and Lasers in Engineering*, 48(4), 512-517.

- [29] Padmanaban G, Balasubramanian V. (2011). Influences of pulsed current parameters on mechanical and metallurgical properties of gas tungsten arc welded AZ31B magnesium alloys. *Metals and materials international*, 17(5), 831-839.
- [30] Balasubramanian V, Jayabalan V, Balasubramanian M. (2008). Effect of current pulsing on tensile properties of titanium alloy. *Materials & Design*, 29(7), 1459-1466.
- [31] Balasubramanian M, Jayabalan V, Balasubramanian V. (2008). Effect of pulsed gas tungsten arc welding on corrosion behavior of Ti-6Al-4V titanium alloy. *Materials & Design*, 29(7), 1359-1363.
- [32] Balasubramanian M, Jayabalan V, Balasubramanian V. (2008). Developing mathematical models to predict tensile properties of pulsed current gas tungsten arc welded Ti-6Al-4V alloy. *Materials & Design*, 29(1), 92-97
- [33] Rose AR, Manisekar K, Balasubramanian V, Rajakumar S. (2012). Prediction and optimization of pulsed current tungsten inert gas welding parameters to attain maximum tensile strength in AZ61A magnesium alloy. *Materials & Design*, 37, 334-348.
- [34] Giridharan PK, Murugan N. (2009). Optimization of pulsed GTA welding process parameters for the welding of AISI 304L stainless steel sheets. *The International Journal of Advanced Manufacturing Technology*, 40(5-6), 478-489.
- [35] Mallaiah G, Kumar A, Reddy PR, Reddy GM. (2012). Influence of grain refining elements on mechanical properties of AISI 430 ferritic stainless steel weldments-Taguchi approach. *Materials & Design*, 36, 443-450
- [36] Rowe MD, Nelson TW, Lippold JC. (1999). Hydrogen-induced cracking along the fusion boundary of dissimilar metal welds. *Welding Journal- New York*, 78, 31-s
- [37] Chen J, Liu T, Lu L, Zhang Y, Zeng W. (2012). Microstructure and mechanical property of rolled weld magnesium alloy AZ31. *Materials & Design*, 36, 577-583.
- [38] Fujii H, Sato T, Lu S, Nogi K. (2008). Development of an advanced A-TIG (AA-TIG) welding method by control of Marangoni convection. *Materials Science and Engineering A*, 495(1), 296-303

-
- [39] Padmanaban G, Balasubramanian V. (2010). Fatigue performance of pulsed current gas tungsten arc, friction stir and laser beam welded AZ31B magnesium alloy joints. *Materials & Design*, 31(8), 3724-3732.
- [40] Munitz A, Cotler C, Stern A, Kohn G. (2001). Mechanical properties and microstructure of gas tungsten arc welded magnesium AZ91D plates. *Materials science and engineering A*, 302(1), 68-73.
- [41] Dong H, Yang L, Dong C, Kou S. (2012). Improving arc joining of Al to steel and Al to stainless steel. *Materials Science and Engineering A*, 534, 424-435.
- [42] Padmanaban G, Balasubramanian V. (2011). Optimization of pulsed current gas tungsten arc welding process parameters to attain maximum tensile strength in AZ31B magnesium alloy. *Transactions of Nonferrous metals society of China*, 21(3), 467-476.
- [43] Liu XH, Gu SH, Wu RZ, Leng XS, Yan JC, Zhang ML. (2011). Microstructure and mechanical properties of Mg-Li alloy after TIG welding. *Transactions of Nonferrous Metals Society of China*, 21(3), 477-481.
- [44] Madadi F, Shamanian M, Ashrafizadeh F. (2011). Effect of pulse current on microstructure and wear resistance of Stellite6/tungsten carbide claddings produced by tungsten inert gas process. *Surface and Coatings Technology*, 205(17), 4320-4328.
- [45] Juang SC, Tarng YS. (2002). Process parameter selection for optimizing the weld pool geometry in the tungsten inert gas welding of stainless steel. *Journal of materials processing technology*, 122(1), 33-37.
- [46] Li D, Lu S, Dong W, Li D, Li Y. (2012). Study of the law between the weld pool shape variations with the welding parameters under two TIG processes. *Journal of Materials Processing Technology*, 212(1), 128-136.
- [47] Shiri SG, Nazarzadeh M, Sharifitabar M, Afarani MS. (2012). Gas tungsten arc welding of CP-copper to 304 stainless steel using different filler materials. *Transactions of Nonferrous Metals Society of China*, 22(12), 2937-2942.
- [48] Yang D., Li X., He, D., Nie Z., & Huang H. (2012). Microstructural and mechanical property characterization of Er modified Al-Mg-Mn alloy Tungsten Inert Gas welds. *Materials & Design*, 34(6), 655-659
-

- [49] Temmar M., Hadji M., & Sahraoui T. (2011). Effect of post-weld aging treatment on mechanical properties of tungsten inert gas welded low thickness 7075 aluminium alloy joints. *Materials & Design*, 32(6), 3532-3536.
- [50] Kumar A., Shailesh P., & Sundarrajan S. (2008). Optimization of magnetic arc oscillation process parameters on mechanical properties of AA 5456 Aluminum alloy weldments. *Materials & Design*, 29(10), 1904-1913.
- [51] Malarvizhi S., & Balasubramanian V. (2011). Effect of welding processes on AA2219 aluminium alloy joint properties. *Transactions of Nonferrous Metals Society of China*, 21(5), 962-973.
- [52] Karunakaran N., & Balasubramanian V. (2011). Effect of pulsed current on temperature distribution, weld bead profiles and characteristics of gas tungsten arc welded aluminum alloy joints. *Transactions of Nonferrous Metals Society of China*, 21(2), 278-286.
- [53] Yarmuch MAR., & Patchett BM. (2007). Variable AC polarity GTAW fusion behavior in 5083 aluminum. *Welding Journal-New York*, 86(7), 196
- [54] Subbaiah K., Geetha M., Shanmugarajan B., & Rao, S. K. (2012). Comparative evaluation of tungsten inert gas and laser beam welding of AA5083-H321. *Sadhana*, 37(5), 587-593.
- [55] El-Shennawy M., Omar AA., & Masoud MI. (2005). Effect of Cu and Mg contents on similar and dissimilar welding of 7XXX series aluminum alloys. *AEJ-Alexandria Engineering Journal*, 44(5), 715-729.
- [56] Nair B., Phanikumar G., Prasad Rao K., & Sinha P. P. (2007). Improvement of mechanical properties of gas tungsten arc and electron beam welded AA2219 (Al-6 wt-% Cu) alloy. *Science and Technology of Welding & Joining*, 12(7), 579-585.
- [57] Shukla RK., & Shah PK. (2010). Comparative studies of friction stir welding and tungsten inert gas welding process. *Indian Journal of Science and Technology*, 3(6), 667-671.
- [58] Rao SR., Reddy GM., Rao KS., Rao PS., Kamaraj M., & Rao KP. (2004). Gas Tungsten Arc Welded AA 2219 Alloy Using Scandium Containing Fillers-Mechanical and Corrosion Behaviour. *Trans. Indian Inst. Met*, 57(5), 451-459.

- [59] Kumar A., & Sundarrajan S. (2009). Optimization of pulsed TIG welding process parameters on mechanical properties of AA 5456 aluminum alloy weldments. *Materials & Design*, 30(4), 1288-1297
- [60] Manti R., Dwivedi DK., & Agarwal A. (2008). Microstructure and hardness of Al-Mg-Si weldments produced by pulse GTA welding. *The International Journal of Advanced Manufacturing Technology*, 36(3-4), 263-269.
- [61] Kumar A., & Sundarrajan S. (2009). Effect of welding parameters on mechanical properties and optimization of pulsed TIG welding of Al-Mg-Si alloy. *The International Journal of Advanced Manufacturing Technology*, 42(1-2), 118-125
- [62] Manti R., Dwivedi DK., & Agarwal A. (2008). Pulse TIG welding of two Al-Mg-Si alloys. *Journal of Materials Engineering and Performance*, 17(5), 667-673.
- [63] Senthil Kumar T., Balasubramanian V., & Sanavullah MY. (2007). Influences of pulsed current tungsten inert gas welding parameters on the tensile properties of AA 6061 aluminium alloy. *Materials & design*, 28(7), 2080-2092.
- [64] Babu S., Kumar TS., & Balasubramanian V. (2008). Optimizing pulsed current gas tungsten arc welding parameters of AA6061 aluminium alloy using Hooke and Jeeves algorithm. *Transactions of Nonferrous Metals Society of China*, 18(5), 1028-1036.
- [65] Balasubramanian V., Ravisankar V., & Reddy G. M. (2008). Effect of pulsed current welding on mechanical properties of high strength aluminum alloy. *The International Journal of Advanced Manufacturing Technology*, 36(3-4), 254-262.
- [66] Wang B., Chen S. B., & Wang J. J. (2005). Rough set based knowledge modeling for the aluminum alloy pulsed GTAW process. *The International Journal of Advanced Manufacturing Technology*, 25(9-10), 902-908.
- [67] Balasubramanian V., Ravisankar V., & Reddy GM. (2008). Effect of postweld aging treatment on fatigue behavior of pulsed current welded AA7075 aluminum alloy joints. *Journal of Materials Engineering and Performance*, 17(2), 224-233.
- [68] Laiping L., Shanben C., & Tao L. (2005). The modeling of welding pool surface reflectance of aluminum alloy pulse GTAW. *Materials Science and Engineering: A*, 394(1), 320-326.

- [69] Sayer S., Yeni C., Ertugrul O. (2010). Comparison of mechanical and microstructural behavior of tungsten inert gas welded and friction stir welded dissimilar aluminum alloys AA2014 and AA5083, 49(2), 155 – 162.
- [70] Mossman MM., & Lippold JC. (2002). Weldability testing of dissimilar combinations of 5000-and 6000-series aluminum alloys. *Welding Journal New York*, 81(9), 188-S.
- [71] Menzemer CC., Lam PC., Wittel CF., & Srivatsan TS. (2001). A study of fusion zone microstructures of arc-welded joints made from dissimilar aluminum alloys. *Journal of materials engineering and performance*, 10(2), 173-177.
- [72] Okubo M., Kon T., & Abe N. (2007). Mechanical Properties of Aluminum-Based Dissimilar Alloy Joints by Power Beams, Arc and FSW Processes. *Journal of Material Engineering*, 33(4), 208-213.
- [73] Luijendijk T. (2000). Welding of dissimilar aluminium alloys. *Journal of Materials Processing Technology*, 103(1), 29-35
- [74] Jannet S, Mathews PK, Raja R (2013). Comparative investigation of friction stir welding and fusion welding of 6061-T6 and 5083-O aluminum alloy based on mechanical properties and microstructure, 61(2), 181-186.
- [75] Harris P. and. Smith B. L. (1983). Factorial techniques for weld quality prediction, *Journal of Metal Construction of Metal Construction*, 39(6), 661-666.
- [76] Murti KGK. and Sundaresan S. (1983). Parameter optimization in friction welded dissimilar materials. *Journal of Metal Construction*, 15(6), 331-335.
- [77] Arya SK., & Parma RS. (1986). Mathematical Models for Predicting Angular Distribution in CO sub 2--Shielded Flux Cored Arc Welding. In *JOM-3--Proceedings of the International Conference Joining of Metals*, 21(2), 240-245.
- [78] Huazhong O. (1995). Mechanical Properties of Particulate MMO/AISI304 Friction Joints. *Journal of Material Technology*, 34(7), 234-238
- [79] Balasubramanian V., & Guha B. (1999). Assessment of some factors affecting fatigue endurance of welded cruciform joints using statistical techniques. *International journal of fatigue*, 21(8), 873-877.

- [80] Balasubramanian V., & Guha B. (2004). Fatigue life prediction of load carrying cruciform joints of pressure vessel steel by statistical tools. *Materials & design*, 25(7), 615-623.
- [81] Koganti R., Karas C., Joaquin A., Henderson D., Zaluzec M., & Caliskan A. (2003). Metal inert gas (MIG) welding process optimization for joining aluminium sheet material using OTC/DAIHEN equipment. In *Proceedings of IMECE* 12(3), 15-21.
- [82] Sampath K. (2005). Constraints-based modeling enables successful development of a welding electrode specification for critical navy applications. *Welding journal*, 84(8), 131-138.
- [83] Pine T., Lee MMK., & Jones TB. (1998). Factors affecting torsional properties of box sections. *Iron making & steel making*, 25(3), 205-209.
- [84] Wang KK., & Rasmussen G. (1972). Optimization of inertia welding process by response surface methodology. *Journal of Engineering for Industry*, 94(5), 999-104.
- [85] Yamaguchi H., Ogawa K., & Sakaguchi K. (1991). Optimization of friction welding condition of 5056 aluminum alloy. *Japan Institute of Light Metals, Journal*, 41, 716-721.
- [86] Ogawa K., Yamaguchi H., Kaga S., & Sakaguchi K. (1993). Optimization of Friction Welding Condition for S45C Carbon Steel Using a Statistical Technique. *Transactions of the Japan Welding Society*, 24(2), 47-53.
- [87] Benyounis KY., Bettamer AH., Olabi AG., & Hashmi MSJ. (2004). Prediction the impact strength of spiral-welded pipe joints in Submerged arc welding of low carbon steel. *Proceedings of IMC*, 21(3), 1-3.
- [88] Ege ES., Inal OT., Zimmerly CA. (1998). Response surface study on production of explosively welded aluminium–titanium laminates. *J. Mater. Sci.*, 33(2), 5327-5332
- [89] Allen TT., Richardson RW., Tagliabue DP., & Mauz GP. (2002). Statistical process design for robotic GMA welding of sheet metal. *Welding Journal (USA)*, 81(5), 69-72.

- [90] Raghukandan K. (2003). Analysis of the explosive cladding of cu–low carbon steel plates. *Journal of materials processing technology*, 139(1), 573-577.
- [91] Murugan VV. & Gunaraj V. (2005). Effects of process parameters on angular distortion of gas metal arc welded structural steel plates. *Welding journal*, 84(11), 165-171.
- [92] Benyounis KY., Olabi AG., & Hashmi MSJ. (2005) Estimation of mechanical properties of laser welded joints using RSM. *Proceedings of IMC 22(7)*, 565-571.
- [93] Benyounis KY., Olabi AG., & Hashmi MSJ. (2005). Residual stresses prediction for CO₂ laser butt-welding of 304-stainless steel. *Applied Mechanics and Materials*, 3(1), 125-130.
- [94] Olabi AG., Benyounis KY., & Hashmi MSJ. (2007). Application of response surface methodology in describing the residual stress distribution in CO₂ laser welding of AISI304. *Strain*, 43(1), 37-46.
- [95] Benyounis KY. Olabi AG. and Hashmi MSJ. (2006). Effect of laser welding parameters on the tensile-shear strength of AISI304 sheet. *AMPT proceedings*, Ohio university, Athens, Ohio, USA, 22(4), 2345-2350.
- [96] Minnick WH. (1995). *Gas Tungsten Arc Welding*. GoodheartWillcox co
- [97] Karpagaraj A, Shanmugam NS, Sankaranarayananasamy K. (2015). Some studies on mechanical properties and microstructural characterization of automated TIG welding of thin commercially pure titanium sheets. *Material Science & Engineering A*, 640, 180-189.
- [98] Otani T. (2007). *Titanium Welding technology*. Nippon Steel Technical Report, 95, 88-92
- [99] Ttulankar RW, Dehankar SS. (2013). Automation in Sheet Metal TIG Welding Process: A Case Study, 7(4), 3077-3083.
- [100] Ravisankar V, Balasubramanian V, Muralidharan C. (2006). Selection of welding process to fabricate butt joints of high strength aluminum alloys using analytical hierarchic process. *Mater Des*, 27, 373-380.
- [101] Jafarian M, Vahdat SE. (2012). A fuzzy multi-attribute approach to select the welding process at high pressure vessel manufacturing. *J Manuf Proces*, 14, 250-256.

- [102] Khrais S, Al-Hawari T, Al-Shraideh M. (2013). Selection of shielding gas by adaptive AHP decision model. *Int. J. of computer Appl in Technol*, 46, 307-315
- [103] Hwang C, Yoon K, (1981). *Multiple attribute decision making methods and application survey*. Berlin: Springer.
- [104] Sen P, Yang JB. (1998). *Multiple criteria decision support in engineering design*. New York: Springer.
- [105]. Miani AS, Shanian A, Madoliat R, Nemes JA. (2005). The effect of normalisation norms in multiple attribute decision making models: a case study in gear material selection, *Struct. Multidisc. Optim*, 29, 312–8.
- [106] Wang TC, Liang JL, Ho. CY. (2006). Multi-criteria decision analysis by using fuzzy VIKOR. *Int Conf Serv Syst Serv Manage*, 25–7.
- [107] Opricovic S, Tzeng GH. (2007). Extended VIKOR method in comparison with outranking methods. *Eur J Oper Res.*, 178, 514–29.
- [108]. Datta S, Mahapatra S. (2010). Comparative study on application of utility concept and VIKOR method, for vendor selection. In: *Proceeding AIMS International Conference on value-based Management*.
- [109]. Cristobal JR. (2011). Multi-criteria decision-making in the selection of a renewable energy project in Spain: the VIKOR method. *J Renew. Energy*, 36, 498-502.
- [110] Rao. R. V (2008). A decision making methodology for material selection using an improved compromise ranking method. *Mater. Des*, 29, 49–54.
- [111]. Shanian A, Savadogo O. (2006). A material selection model based on the concept of multiple attribute decision making, *Mater. Des*, 27, 29–37.
- [112] Shanian A, Savadogo O. (2006). A non-compensatory compromised solution for material selection of bipolar plates for polymer electrolyte membrane fuel cell (PEMFC) using ELECTRE IV. *Electrochim Acta.*, 51, 7–15.
- [113] Chatterjee P, Chakraborty S. (2012). Material selection using preferential ranking methods, *Mater. Des.*, 35, 84–93

- [114]. Chatterjee P, Athawale VM, Chakraborty S. (2009). Selection of materials using compromise ranking and outranking methods, *Mater. Des.*, 30, 43–53.
- [115] Chatterjee P, Athawale VM, Chakraborty S. (2011). Materials selection using complex proportional assessment and evaluation of mixed data methods, *Mater. Des.*, 32, 51–60
- [116] Maity SR, Chatterjee P, Chakraborty S. (2012). Cutting tool material selection using grey complex proportional assessment method, *Mater. Des.* 36, 2-8.
- [117]. Rao. RV. (2006). A material selection model using graph theory and matrix approach, *Mater. Sci. Eng. A*, 431, 48-55
- [118] Maniya K., Bhatt MG. (2010). A selection of material using a novel type decision making method: preference selection index method, *Mater. Des.* 178, 5-9.
- [119] Jahan A., Ismail MY, Mustapha F, Sapuan SH. (2010). Material selection based on ordinal data, *Mater. Des.* 318, 0-7.
- [120]. Saaty TL. (2008). Decision making with the analytic hierarchy process, *Int. J. Services Sciences*, 1, 83-98
- [121] Vargas LG. (1990). An overview of the analytic hierarchy process and its applications. *Eur J Oper Res*, 48, 72-80.
- [122]. Wang TC, Chang TH. (2007). Application of TOPSIS in evaluating initial training aircraft under a fuzzy environment, *Exp. Syst. Appl.* 33, 870-80.
- [123] Rao RV. (2004). Evaluation of metal stamping layouts using an analytic hierarchy process method. *J. Mater. Process. Technol.*, 152, 71–6.
- [124]. Rathod MK , Kanzaria HK. (2011) A methodological concept for phase change material selection based on multiple criteria decision analysis with and without fuzzy environment, *J. Mater. Des.* 32, 3578-85
- [125] Khorshidi R, Hassani A, Rauof AH, Emamy M. (2013). Selection of an optimal refinement condition to achieve maximum tensile properties of Al-15%Mg₂Si composite based on TOPSIS method. *Mater Des*, 46, 442-450.
- [126] Mirhedayatian SM, Vahdat SE, Jelodar MJ, Saen RF.(2013). Welding process selection for repairing nodular cast iron engine block by integrated fuzzy data envelopment analysis and TOPSIS approaches. *Mater Des*, 43, 272-282.

- [127] Chatterjee P, Athawale SM, Chakraborty S. (2009). Selection of Materials Using Compromise Ranking and Outranking Methods. *Mater Des*, 30, 4043–4053.
- [128] Rowe M. D., Nelson T. W., & Lippold J. C. (1999). Hydrogen-induced cracking along the fusion boundary of dissimilar metal welds. *Welding Journal-New York*, 78(2), 31-35.
- [129] Hobart Brothers. (2013). Aluminum filler metal selection chart, 46-47
- [130] ESAB. Aluminum filler metal selection chart.
- [131] Alcotec. Filler Alloy selection chart. 1-2
- [132] Maxal. (2011). Filler metal selection chart, 1, 5-7
- [133] Miller. Filler selection chart for aluminum.
- [134] Funderburk RS. (1999). Key concepts in welding Engineering. *Welding Innovation* 16(2).
- [135] Mutombo FK. (2011). Corrosion fatigue behavior of 5083 H-111 and 6061-T651 aluminum alloy weld. Thesis: University of Pretoria.
- [136] Shirali, AA., Mills, KC. (1993). The effect of welding parameters on penetration in GTA welds, *Welding J.* 72(7), 347s-353s.
- [137] Tungsten guide book for proper selection and preparation of tungsten electrodes for arc welding .2015
- [138] Hichen GK, Gas-tungsten arc welding, *ASM Handbook, Welding, Brazing and Soldering*, 6, 190-194.
- [139] Chen Y, Nie ZR, Zhou ML, Zhang JX, Zuo TY. (2000). The research and development of tungsten electrodes without radioactivity, *International Symposium on Ecomaterials held in conjunction with the 39th Annual Conference on Metallurgists of CIM*, AUG 20-23, Environmental Concious Materials - Ecomaterials, 699-702,
- [140] Praxair (2010). Selection of shielding gas compositions.
- [141] Huang HY. (2009). Effects of shielding gas composition and activating flux on GTAW weldments. *Mater Des*, 30(7), 2404-2409.

- [142] Pires I, Quintino L, Miranda M. (2007). Analysis of influence of the shielding gas mixtures on the gas metal arc welding metal transfer modes and fume formation rate. *Mater Des*, 28(5), 1623-1631.
- [143] Campbell SW, Galloway AM, McPherson NA. (2012). Techno-economic evaluation of reducing shielding gas consumption in GMAW whilst maintaining weld quality. *Int J Adv Manuf Technol*, 18(8), 652-660.
- [144] Loxton industries. (2010). New welding gas innovation. *Australasian Weld J*, 55(1), 10-11.
- [145] Uttrachi GD. (2007). GMAW shielding gas flow control system. *Weld J*, 86(4), 22-23.
- [146] Armentani E, Esposito R, Sepe R. (2007). The effect of thermal properties and weld efficiency on residual stresses in welding. *J Achiev Mat Manuf Eng*, 20(1-2), 319-322.
- [147] Muralidharan C, Balasubramanian V, Anantharaman N, Deshmukh SG. (2000). Welding process selection. *J prod*, 41, 507-11.
- [148] Cooper R, Kaplan RS. Profit priorities form activity based costing. (1991). *Harvard Bus Rev*, (May-June), 23-30
- [149] Welding and brazing: ASM metals handbook; Vol.6; 8th edition: 37-38.
- [150] Srinivasa PB, DietzelZettler W, Dos Satos JF, Sivan V. (2005) Stress Corrosion Cracking Susceptibility of friction Stir Welded AA7075-AA6056 Dissimilar Joint, *Material and Engineering A*, 392, 292-300.
- [151] Somasekharan AC, Murr LE. (2004). Microstructures in Friction-Stir Welded Dissimilar magnesium alloys and magnesium alloys to 6061-T6 Aluminum Alloy, *Material Characterization*, 52, 49-64.
- [152] Gomez de Salazar JM, Barrena MI. (2003). Dissimilar Fusion Welding of AA7020/MMC Reinforced with Al₂O₃ particles, Microstructure and Mechanical properties, *Material Science and Engineering A*, 352, 162-168.
- [153] Menzmer C, Lam PC, Srivatsan TS, Wittel CF. (1999). An Investigation of Fusion Zone Microstructures of Welded Aluminum Alloy Joints, *Materials Letters*, 41, 192-197.

- [154] Kim HT, Nam SW. (1996). Solidification cracking susceptibility of high strength aluminum alloy weldment, *Scr Mater*, 1139-1145.
- [155] Janaki Ram GD, Mitra TK, Shankar V. (2003). Microstructural refinement through inoculation of type 7020 Al-Zn-Mg alloy welds and its effects on hot cracking and tensile property, *J Mater Process Technol*, 142, 174-181
- [156] Simpson RP. (1997). Controlled weld pool solidification and resultant properties with yttrium inoculation of Ti-6Al-6V-2Sn welds. *Welding J*, 56, 67-72.
- [157] Garland JG. (1974). *Metal Construct*, 6, 121-128.
- [158] Madhusudhan Reddy GR, Gokhale AA, Prasad KR. (1998). Optimization of pulse frequency in pulsed current gas tungsten arc welding of Al-lithium alloy steels. *J Mater Sci Technol*, 14, 61-66
- [159] kumar T.S, Balasubramanian V, Sanavullah MY. (2005). Effect of pulsed current TIG welding parameters on tensile properties of AA6061 aluminum alloy, *IWS*, 29-39.
- [160]. Balasubramanian M, Jayabalan V, Balasubramanian V. (2006) Optimizing the pulsed current gas tungsten arc welding parameters, *J Mater Sci Technol*, 22, 821-5.
- [161]. Balasubramanian M, Jayabalan V, Balasubramanian V. A mathematical model to predict impact toughness of pulsed current gas tungsten arc welded titanium alloy. *J Adv Manuf Technol*. in press
- [162] Yunga KCW, Ralph B, Lee WB, Fenn R. (1997). An investigation into welding parameters affecting the tensile properties of titanium welds. *Journal of Material Processing Technology*, 63(1-3), 759-764.
- [163] Meran C. (2006). Prediction of the optimized welding parameters for the joined brass plates using genetic algorithm. *Material Design*, 27(5), 356-363.
- [164] Chinakhov DA., Zuev AV. (2014) Filimonenko AG. Gas-dynamic Impact of a Shielding Gas Jet on the Drop Transfer When Welding with a Consumable Electrode. *Advanced Materials Research*, 1040(2), 850-853

- [165] Chinakhov DA. (2014). Gas Dynamic Control of Properties of Welded Joints from High Strength Alloyed Steels. *China Welding*. 23(3), 27-31.
- [166] Chinakhov DA., Chinakhova ED., Gotovschik YM., Grichin SV. (2016). Influence of welding with twojet gas shielding on the shaping of a welding joint. *IOP Conf. Series: Materials Science and Engineering* 125(1), 012-013.
- [167] Chinakhov DA., Grigorieva EG., Mayorova EI. (2013). Study of gas dynamic effect upon the weld geometry when consumable electrode welding. *IOP Conf. Series: Materials Science and Engineering* 127(1), 012-013.
- [168] Palani, P.K. and N. Murugan (2006). Selection of parameters of pulsed current gas metal arc welding, *J. Mater. Process. Tech.*, 172 (3), 1-10
- [169] Lothongkum, G., Chaumbai, P., Bhandhubanyong, P. (1999). TIG Pulse Welding of 304L Austenitic Stainless Steel in Flat, Vertical and Over Head Position, *Journal of Material Processing & Technology*, 89(4), 410 - 414
- [170] Needham, JC.(1972). Pulsed TIG Welding- Seminar Hand book, The Welding Institute, Abington Hall, Abington, Cambridge, U.K..
- [171] Jean C, (1988). *Advanced Welding System, TIG and Related Processes*, Springer Verlag, U.K.
- [172]. Gooch, TG, Jones, RL, and Woolin P. (1996). *Welding Process For Stainless Steels*, *Stainless Today*, 7-14.
- [173] Williams G. Cochran and Cox, GM. (1957). *Experimental Designs*, John Wiley & Sons Publications.
- [174] Murugan, N. (1993) *Some Studies on Metal Surfacing*, Ph.D. Thesis, Department of Mechanical Engineering, IIT, Delhi.
- [175] Box G. E. P, and Wilson K. B. (1951). On the experimental attainment of optimum conditions, *Journal of Royal Statistical Society, Series B*, 13, 1-45
- [176] Box G.E.P, Hunter W.H, Hunter J.S. (1978). *Statistics for experimenters*, New York, John Wileyand sons
- [177] Perez-Bergquist Sara J, Rusty Gray III GT, Cerreta EK, Trujillo CP, _erez-Bergquist AP. (2011). The dynamic and quasi-static mechanical response of three aluminum armor alloys: 5059, 5083 and 7039. *Mater Sci Eng A*, 528, 8733-41.

- [178] Katsas S, Nikolaou J, Papadimitriou G. (2006). Microstructural changes accompanying repair welding in 5xxx aluminium alloys and their effect on the mechanical properties. *Mater Des*, 27, 968-75.
- [179] Kumbhar NT, Bhanumurthy K. Friction stir welding of Al 6061 alloy. (2008). *Asian J ExpSci*, 22(2), 63-4.
- [180]. Jannet S, Mathews PK, Raja R. (2013), Comparative investigation of friction stir welding and fusion welding of 6061-T6 and 5083-O aluminum alloy based on mechanical properties and microstructure. *Journal of Achievement in Material Manufacturing Engineering*. 61(2), 181-186..
- [181] Sato YS, Kokawa H, Enomoto M, Jogan S. (1999), Microstructural evolution of 6063 aluminium during friction-stir welding'. *Metallurgical Material Transaction A*, 30, 2429–37.
- [182] Su J-Q, Nelson TW, Mishra R, Mahoney M. (2003). Microstructural investigation of friction stir welded 7050-T651 aluminium. *Acta Mater*, 51, 713–29
- [183]. Munoz C., Ruckert AG , Huneau B., Sauvageb, XS. (2008). Maryaa Comparison of TIG welded and friction stir welded Al-4.5Mg-0.26Sc alloy. *Journal of Materials Processing Technology*, 197, 337-343.
- [184] Kerlins V. (1991), Modes of fracture. In: ASM Handbook Committee Editors. *Fractography*. Materials Park, OH: ASM, International
- [185] Montgomery D.C. (1991) *Design and analysis of experiments*, New York, John Wiley.
- [186] Barker T.B, (1985). *Quality by experimental design*, ASQC Quality Press, Marcel Dekker.
- [187] Gunaraj V, Murugan N. (1999) *J Mater. Process. Technol*, 95, 246-261.
- [188] Murugan N, Parmar R.S. (1995) *Intern J Join Mater*, 7, 71-80.
- [189] Colligan J, Paul J, Konkol, James J, Fisher, Pickens Joseph R.(2003). Friction stir welding demonstrated for combat vehicle construction, *Weld J*, 82, 34-40

- [190] Kumar TS. (2005). Effect of Computer Controlled Pulsed Current Tig Welding Parameters on Mechanical Properties Of Aa6061 Aluminium Alloy, PhD Thesis, V.M.K.V. Engineering College, Periyar University, Salem-Tamil Nadu, India.
- [191] Jiang QC, Wang HY, Ma BX, Wang JG. (2005), Modification of Mg_2Si in Mg-Si alloys with yttrium. *Material Design.*, 392A, 130-135
- [192] Tsirkas, S.A., Papanikos, P., Kermanidis, T. (2003) .Numerical Simulation of the Laser Welding Process in Butt-joint specimens. *Journal of Materials Processing Technology*, 134(1), 59-69
- [193]. Enos G. D. The Potentiodynamic polarization scan. Technical Report 33. University of Virgin.
- [194] N. B. Z. and. Buchheit R. G. Electrochemical characteristics of intermetallics phases in aluminum alloys an experimental survey and discussion. *J. Electrochem. Soc.*, Fontana corrosion center.